Přírodovědecká fakulta
UNIVERZITY KARLOVY V PRAZE

Department of Physical and Macromolecular Chemistry

Doctoral Thesis

NOVEL AVENUES FOR THE PREPARATION OF ANTIFOULING SCAFFOLDS FOR TISSUE ENGINEERING

Ing. Nina Kostina

INSTITUTE OF MACROMOLECULAR CHEMISTRY AS CR, V.V.I.
Department of Polymer Networks and Gels

Supervisor: **Ing. Jiří Michálek, CSc.**

PRAGUE 2015

Přírodovědecká fakulta
UNIVERZITY KARLOVY V PRAZE

Katedra Fyzikální a Makromolekulární Chemie

Disertační Práce

NOVÉ PŘÍSTUPY K PŘÍPRAVĚ SCAFFOLDŮ PRO TKÁŇOVÉ INŽENÝRSTVÍ ODOLNÝCH PROTI NESPECIFICKÉ ADSORPCI PROTEINŮ A ADHEZI BUNĚK

Ing. Nina Kostina

ÚSTAV MAKROMOLEKULÁRNÍ CHEMIE AV ČR, V.V.I.
Oddělení Polymerních sítí a gelů

Školitel: **Ing. Jiří Michálek, CSc.**

PRAHA 2015

Prohlášení:

Prohlašuji, že jsem závěrečnou práci zpracovala samostatně a že jsem uvedla všechny použité informační zdroje a literaturu. Tato práce ani její podstatná část nebyla předložena k získání jiného nebo stejného akademického titulu.

Declaration:

Hereby I declare that I have worked out this doctoral thesis independently, and I have fully cited all sources used. This work has not been used in order to gain any other academic degree.

Prague, 08.12.2015

Nina Kostina

Acknowledgements

I would like to express the gratitude to my supervisor Dr. Jiří Michálek for providing me with the freedom to attain challenging goals in a self-directed manner and for his support and help every time I needed.

I am especially grateful to Dr. César Rodríguez Emmenegger for his inexhaustible source of advice, motivation, immense knowledge, and help. His guidance helped me in all the time of research and writing of this thesis. His exquisite way and passion to do science will always be a model for me.

I also would like to thank colleagues from the group of Dr. Rodríguez Emmenegger: Andrés de los Santos, Mariia Vorobii and František Surman, for their help and collaboration. In particular I am grateful to Andrés. During the time in Prague he was not only a bright colleague, but also he became a good friend. A special thanks for extensive proof-reading of my thesis.

My sincere gratitude goes to Prof. Dirk W. Grijpma from University of Twente and Prof. Christopher Barner-Kowollik from Karlsruhe Institute of Technology for giving me opportunity to work in their groups. My stays in these groups allowed me to work on very exciting projects and helped me to make quantitative advancements in my research.

I am equally thankful to my advisor during my studies and work in Moscow, Dr. Marina Gorshkova who introduced me to a science back to 2005. I am very grateful to her for teaching, keeping me motivated and interested in everything I did, for her support even in the hardest time, and for being so good friend.

I would like to acknowledge my office and lab mates, Dr. Radka Hobzová and Dr. Jakub Širc, who have helped me with many things and questions especially during the first days in Prague.

I want to thank all people who became my friends during this time; Andrés, Tomaš and Zuzana, Ognen and Neda, Alessandro and Alga, Kim and Tanja, Corinna, Anja, Eliezer, Frank. Thank all of you for great friendship. It was very enjoyable to spend time with you. A special note of gratitude goes to my dearest Marina Davydova who became a true friend during so short time. Thank you for your kindness, help, support and sharing with me the best and not always the best moments of my life.

I also would like to thank my dearest mother and granny for their infinite love, care, and support. Thank you for everything you have done for me, I will always be grateful to you. Additionally, I thank my granddaddy who gave me so much love. You will always stay in my heart.

Finally, I thank my beloved husband César who is a tremendous source of love and care. I could not have reached my goals without your help, support and encouragement at all times. I feel blessed be married to the most kind-hearted and generous man. I love you more than ever before!

Abstract

Non-specific protein adsorption –protein fouling– is an adverse effect occurring at the surface of most artificial materials which come into contact with biological fluids, affecting various biomedical devices and tissue engineering scaffolds. In order to address this ubiquitous problem the preparation of scaffolds resistant to protein fouling (antifouling) was proposed.

The main goal of this Thesis was the development of strategies for the preparation of antifouling scaffolds for tissue engineering. The work consisted of three steps: (i) the selection of monomers leading to antifouling properties by utilizing model system based on polymer brushes; (ii) preparation of antifouling hydrogels of different properties and architecture by copolymerization with zwitterionic carboxybetaine monomers, selected from model experiment; and (iii) modification of the surface of poly(ε-caprolactone) (PCL) nanofibers by growing four types of polymer brushes resistant to protein fouling.

The scaffolds presented in this work showed variety of unique properties, such as hydration (up to 30000%), elongation (up to 1800%), self-healing, biodegradation, availability of functional groups and complex pore structure. Importantly, all scaffolds showed significant reduction of protein fouling and non-specific cell adhesion and can be exploited as a platform for further functionalization with biological cues and signaling molecules for specific cell-matrix interaction. The methods applied for the preparation of antifouling scaffolds are universal and can be extended for different types of material in order to achieve specific property for the scaffold. The combination of these properties makes the presented scaffolds a highly promising material for tissue engineering applications.

Keywords: antifouling properties, hydrogels, nanofibers, polymer brushes, scaffold for tissue engineering.

Abstrakt

Nespecifická adsorpce proteinů (angl. protein fouling) je velmi nežádoucí efekt odehrávající se prakticky na každém umělém povrchu, který přichází do kontaktu s biologickými tekutinami, a má fatální vliv na aplikaci různých biomedicínských přípravků a nosičů určených pro tkáňové inženýrství (scaffold). Aby se předešlo tomuto všudypřítomnému problému, byly navrženy buněčné nosiče odolávající nespecifickým adsorpcím proteinů (tzv. „antifouling" povrchy).

Hlavním cílem této disertační práce byl vývoj strategie přípravy povrchů pro tkáňové inženýrství odolávajících nespecifickým adsorpcím proteinů. Práce se skládala ze tří hlavních částí: (i) výběr monomerů vedoucích k „antifouling" povrchům pro modelový systém založený na polymerních kartáčích; (ii) příprava „antifouling" hydrogelů s různými vlastnostmi a architekturou pomocí kopolymerizace zwitterionových karboxybetainových monomerů vybraných z modelových experimentů; (iii) modifikace povrchu poly(ε-karpolaktonových) nanovláken čtyřmi typy „antifouling" polymerních kartáčů.

Hydrogely připravené v této práci vykazují širokou škálu jedinečných vlastností, jako např. hydratace dosahující až 30000 %, tažnost až 1800 %, schopnost regenerace, biodegradovatelnost, struktura komunikujících pórů a přítomnost funkčních skupin. Navíc, všechny nosiče signifikantně potlačovaly nespecifické adsorpce proteinů a nespecifickou adhezi buněk a zároveň mohly být využity jako platformy pro další funkcionalizaci biologickými elementy a signálními molekulami pro specifickou interakci buněk s nosičem. Metodika přípravy „antifouling" nosičů je universální a může být rozšířena o různé typy materiálů za účelem dosažení specifických vlastností tkáňových nosičů. Kombinace těchto vlastností dělá z prezentovaných nosičů velmi slibné materiály pro aplikace ve tkáňovém inženýrství.

Klíčová slova: hydrogely, polymerní kartáče, „antifouling" vlastnosti, nespecifická adsorpce, nanovlákna, nosiče pro tkáňové inženýrství.

Publications Arising from the Thesis

[1] ***Non-fouling hydrogels of 2-hydroxyethyl methacrylate and zwitterionic carboxybetaine (meth)acrylamides***

Kostina, N. Yu.; Rodriguez-Emmenegger, C.; Houska, M.; Brynda, E.; Michalek, J. ***Biomacromolecules***, 2012, 13 (12), 4164-4170.

[2] ***Novel antifouling self-healing poly(carboxybetaine methacrylamide-co-HEMA) nanocomposite hydrogels with superior mechanical properties***

Kostina, N. Yu.; Sharifi, S.; de los Santos Pereira, A.; Michálek, J.; Grijpma, D. W.; Rodriguez-Emmenegger, C. ***Journal of Materials Chemistry B***, 2013, 1 (41), 5644-5650.

[3] ***Polymer brushes interfacing blood as a route toward high performance blood contacting devices***[‡]

Surman, F.; Riedel, T.; Bruns, M.; Kostina, N. Yu.; Sedláková, Z.; Rodriguez-Emmenegger, C. ***Macromolecular Bioscience***, 2015, 15(5), 636-646.

[4] ***Photo-triggered functionalization of hierarchically structured brushes*** [*]

de los Santos Pereira, A.; Kostina, N. Yu.; Bruns, M.; Rodriguez-Emmenegger, C.; Barner-Kowollik, C. ***Langmuir***, 2015, 31(21), 5899-5907.

[‡] Author.Kostina N. Yu contributed to the publication by performing AFM measurements for the characterization of surface topography.

[*] Author Kostina N. Yu.contributed to the publication by performing part of the syntheses of polymer brushes, streptavidin immobilization and preparation of manuscript.

[5] ***Non-fouling biodegradable poly(ε-caprolactone) nanofibers for tissue engineering***

Kostina, N. Yu.; Pop-Georgievski, O.; Bachmann, M.; Neykova, N.; Bruns, M.; Michálek, J.; Bastmeyer, M.; Rodriguez-Emmenegger, C. ***Macromolecular Bioscience***, 2015, DOI: 10.1002/mabi.201500252.

[6] ***Biodegradable zwitterionic functionalizable scaffolds with gyroid pore architecture for tissue engineering***

Kostina, N. Yu.; Blanquer, S.; Pop-Georgievski, O.; Höcherl, A.; Grijpma, D. W.; Michálek, J.; Rodriguez-Emmenegger, C. ***Macromolecular Bioscience,*** (under review).

Additional Publications

[7] ***Water-soluble polyplexes of modified chitosan***[†]

Kostina, N.; Gorshkova, M.; Izumrudov, V. Polymer Science Series A, 2011, 53, (10), 947-954.

[8] ***Synthesis of non-fouling poly[N-(2-hydroxypropyl)methacrylamide] brushes by photoinduced SET-LRP***[‡]

Vorobii, M.; de los Santos Pereira, A.; Pop-Georgievski, O.; Kostina, N. Yu.; Rodriguez-Emmenegger, C.; Percec, V. Polymer Chemistry, 2015, 6, 4210-4220.

[9] ***Designing molecular printboards: A photolithographic platform for recodable surfaces***[*]

Abt, D.; Schmidt, B. V. K. J.; Pop-Georgievski, O.; Quick, A. S.; Danilov, D.; Kostina, N. Yu.; Bruns, M.; Wenzel, W.; Wegener, M.; Rodriguez-Emmenegger, C.; Barner-Kowollik, C. Chemistry – A European Journal, 2015, 21, 13186-13190

[10] ***Grafting of methacrylate polymers brushes by photoinduced SET-LRP***[‡]

Vorobii, M.; Pop-Georgievski, O.; de los Santos Pereira, A.; Kostina, N. Yu.; Jezorek, R.; Sedláková, Z.; Percec, V.; Rodriguez-Emmenegger, C. Polymer Chemistry, (under review).

[†] Publication resulting from the Diploma thesis.

[‡] Author Kostina N. Yu. contributed to the publication by performing AFM measurements for the characterization of surface topography.

[*] Author Kostina N. Yu. contributed to the publication by performing AFM measurements for characterization of surface topography, printboard reversibility experiments, and measuring water drop contact angle.

Contents

Introduction

1 Evolution of Tissue Engineering

The evolution of technology, science and medicine in the last two centuries has led to important improvements of life quality and health management. This has, concomitantly, led to an important increase in the life span. However, while treatments for many diseases have been found, other problems have arised. Longer life spans mean that more people suffer from organ failure. In addition, many individuals suffer from dysfunctions involving the damage of tissues or organs even at an early age caused by new diseases as well as accidents.[1]

Artificial or prosthetic materials for the replacement of limbs, teeth, and other tissues have resulted in the partial restoration of lost functions. The use of artificial materials has long been applied dating back to thousands years ago. With the advent of biology and medicine new avenues have evolved. In the 16th century Tagliacozzi reported the nose replacement constructed from forearm flap. Modern surgery emerged with an improved understanding of the germ theory, the sterile technique and anesthesia, enabling surgeons to treat internal areas of the body, *i.e.* thorax, abdomen, brain and heart. At the same time this has led to a better understanding of the functions of the human body and its physiology, which concomitantly enables not only extirpative surgical procedures but also reconstruction of organs.[2-4]

Transplantation of organs and tissues can be pictured as an extreme case of reconstructive surgery. Currently, transplantation of organs and tissues has been the ideal and in many cases the only way to restore the lost functions which may threaten the patient's life (Figure 1). When the damage is relatively small and the tissue is able to rapidly regenerate, such as the skin or veins, it is usual to retrieve tissue from a distal

location in the same patient and graft it in the wounded place. This is called an autograft. However, oftentimes this method is not applicable and tissues from donors are required. When the donor is human the process is called allograft, while if the donor is from a different species it is termed xenograft.

Moving tissue from one position to another may produce biological changes because of their abnormal interaction of the tissue at its new location. For instance, when skin grafts were utilized to reconstruct esophageal tubes, skin tumors were detected after 20-30 years. Similarly, the diverting of urine into the gastrointestinal tract led to fatal colon cancer.[2, 4]

Currently organ and tissue transplantation is the standard of care for survival of many patients.[1, 5] Regretfully, those patients must face a major problem, as an extremely low number of organs is available for transplantation.[6] Currently, only in the U.S. approximately 123,000 patients are waiting for available organs but only 8,500 of them (7%) will have the opportunity to receive an organ (according to statistics for October 2015: http://optn.transplant.hrsa.gov/). This means that 22 lives of patients end daily while being on a waiting list. Furthermore, even those patients who endure an organ transplantation are at a high risk that the recipient's immune system will identify the organ as foreign and attempt to destroy it, causing rejection of the allograft or xenograft.[2, 3]

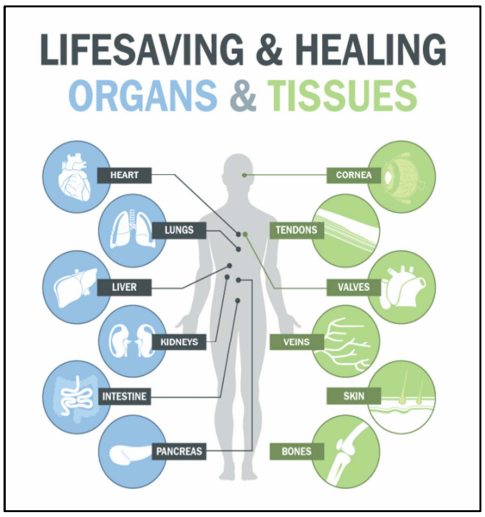

Figure 1. Scheme of organs and tissues that can be repaired or restored by transplantation. Reproduced from: http://www.lifeshareoklahoma.org/about-donation.html

In order to minimize the immune reactions, lifelong immunosuppression therapy is essential. Unfortunately this therapy can cause substantial and serious side effects, such as formation of tumors, risk of acquiring infections and overall impairment of quality of life.[2, 3, 7-9] Lastly, several tissues cannot be transplanted and require to be regenerated or repaired in the wounded place. Thus, finding new avenues to restore the function of organs and tissues is therefore of major societal concern and of urgent need.

Currently, artificial prostheses and mechanical devices (*e.g.* pumps, heart–lung machine, etc.) save and improve the lives of millions of patients but are not ideal since they are subjected to mechanical failure after long-term implantation. Artificial materials rarely integrate with host tissues and can trigger host immune response damaging healthy tissue around the implant. Even in the most favorable cases, inflammation and foreign body response and/or fibrous encapsulation generally follow. Moreover, these strategies usually fail to replace all the functions of the original tissue and can develop malignant tumors, as well as surgical complications.

Tissue engineering has emerged as another possible strategy to meet these challenges.[3] The term "tissue engineering" was coined by Prof. Fung in a National Science Foundation meeting in 1987 and further develop by Profs. Langer and Vacanti. The primary goal of tissue engineering is to provide a biological surrogate to treat tissues/organs loss or failure by integrating multiple aspects of engineering, biology and medicine.[10-12] Conceptually, the introduction of this new field to human health care can be rationalized as a refinement of a previously defined route used in medicine. In traditional medicine, the physician treated certain disease processes by supporting nutrition, minimizing hostile factors and optimizing the environment so that the body can heal itself. Tissue engineering aims at accomplishing the same goal but at the cellular level. The harmful or damaged tissue is removed; the cells necessary for repair are then introduced in a configuration optimizing the survival of the cells in an environment that will permit the body to heal itself. Tissue engineering offers an advantage over cell transplantation in that organized 3D tissue is designed and developed. By the achievement of normal tissue development, this field of science represents a strategy to restore, maintain and improve tissue function and ultimately aiming at complete organ replacement.

2 Tissue Engineering Approaches

2.1 Cell Injection Method

The cell injection method involves delivery of cells through a systemic injection into the blood stream, directly into the affected organ or through direct transplantation into a local tissue. The transplanted cells use the vascular supply for nutrition and the stroma provided by the host tissue as a matrix for attachment and reorganization. This approach has been used to replace metabolic functions as occurring in liver disease, to treat leukemia or other blood related diseases (injection of multipotent stem cells from the bone marrow) and recently to treat myocardial infarction and brain stroke (injection of mesenchymal stem cells).[2, 13, 14] Although this approach has clear advantages, such as being minimally invasive and not having any artificial material added, it is not exempt of challenges. Sufficient cell mass to replace lost function is difficult to achieve. The survival of the delivered cells is typically low due to a lack of nutrients and oxygen supply. Additionally, this method requires the growth of a large supply of cells. Importantly, during culture expansion changes in the phenotype and accumulation of genetic mutations must be minimized.[4]

2.2 Close Loop Method

In this approach extracorporeal or implantable devices house the transplanted cells. The cells are usually encapsulated in a hydrogel matrix and are isolated from the body by a semipermeable membrane.[4, 15] In this way nutrients and secreted cell products easily diffuse while large entities such as antibodies, complement factors and other immunocompetent cells are prevented from marking and destroying the isolated cells (immune response, phagocytosis, *etc.*). The membrane also protects the patient when the cells are potentially pathological (tumorigenic).

The most common implantable devices are based on “vascular-type” design and on microcapsules. In the former, the transplanted cells are housed in a chamber around a vascular vessel separated from the blood stream by a semipermeable membrane. The circulating blood provides oxygen and nutrient and absorbs substances secreted by the implanted cells. In micro- and macrocapsule-based systems, cells are encapsulated in

hydrogel droplets. The encapsulated cells can be cultured *in vitro* and transplanted *in vivo*. An example is the encapsulation of islets of Langerhans to produce insulin.[16]

In extracorporeal systems the cells are separated from the bloodstream. For instance extracorporeal liver assist devices for the support of patients with acute liver failure have been employed. This relies on the use of hollow fibers on which allogeneic or xenogeneic hepatocytes are cultured.[17]

While close-loop methods offer a viable alternative as cells are protected from immune and complement systems, their use is still limited. Some of the major drawbacks include: fouling on the membrane, fibrous tissue overgrowth, restricted and hindered diffusion and foreign body response. Additionally, the preparation of housing materials supporting mild conditions mimicking the natural extracellular matrix (ECM) remains a challenge.[4]

2.3 Tissue Engineering Using Scaffolds

Although isolated cells, such as those discussed in the cell injection method, have the capacity to reform their respective tissue structure, they do so only to a limited extend. The reconstruction of the vast majority of tissues requires a template guiding the organization and restructure of cells. Moreover, tissues cannot be transplanted in large volumes as restrictions to gas exchange and diffusion of waste products and nutrients lead to the death of those cells further than 200 μm from a nourishment source.[3, 18]

In an effort to overcome these problems, scaffolding was introduced to tissue engineering.[19] The rationale of this approach is that if cells can attach to a scaffold which mimics the natural ECM and guides the cell adhesion, larger tissues can be formed (Figure 2).

While the original idea in tissue engineering was to replace tissues and organs, it was soon recognized that in many instances repairing or regeneration could be valuable or even better strategies. This led to the basic paradigm of tissue engineering, in which the three pillars are cells, scaffolds and signals (Figure 3). The cells could be stem cells or even fully differentiated ones. Scaffolds could be made from natural materials, synthetic materials or even a decellularized matrix.[20-22]

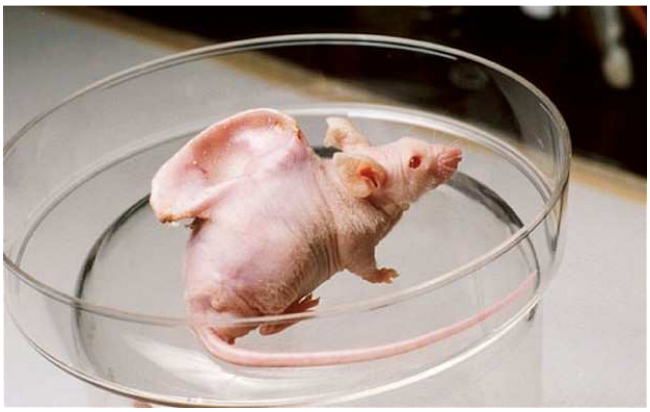

Figure 2. The Vacanti mouse is the mouse that underwent the implantation of the biodegradable human-ear-shaped scaffold with ingrowth cartilage tissue by initial seeding of cow cartilage cells into the scaffold. The cartilage naturally grew to complete the shape of ear by itself after implantation. The picture was reproduced from: https://en.wikipedia.org/wiki/Vacanti_mouse.

It was also rapidly recognized that not only the material played a role but also its 3D organization, its ability to allow the diffusion of nutrients and gases, etc. Thus the engineering of the scaffold is also instrumental in tissue engineering. Initially, the engineering of the scaffold focused in the replication of the physical and mechanical properties of the desired tissue neglecting the negative host response.[3, 11, 23] Later it was recognized that more emphasis should be places on improving the integration of the scaffold with the surrounding tissues.

A perhaps less evident but equally important component or pillar in tissue engineering are the signals for the cells. The advances in cell and molecular biology, chemistry, physics and material science allowed a better understanding of the scaffold-tissue interaction and the critical importance of the cell's microenvironment in determining its function.[11, 24] *In vivo* cell function is controlled by a combination of signals that includes soluble molecules (growth factors), chemotactic factors, cell adhesion molecules, the mechanical environment, *i.e.*, physical forces, to which the cell is exposed.[3, 25, 26] It is noteworthy that the functional characteristics of cells are determined by the cues or signals which define their microenvironment. Thus, when engineering a material for tissue engineering, the signals introduced in the material must aim at replicating the cell microenvironment *in vivo*.

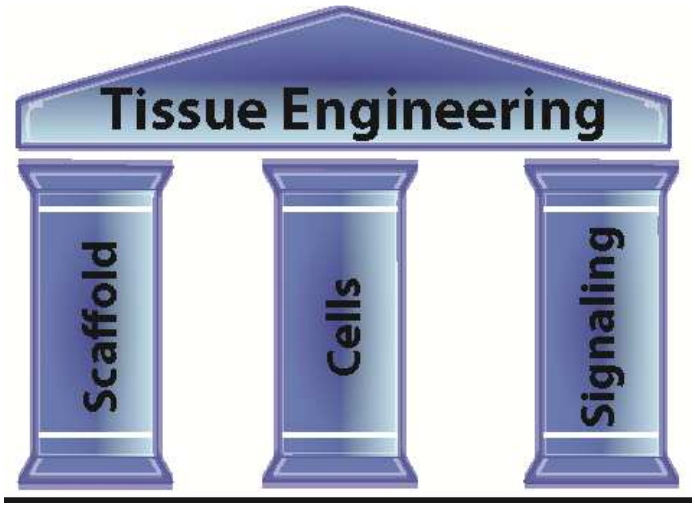

Figure 3. Illustrating the basic paradigm for tissue engineering showing the three "pillars", *i.e.* cells, scaffold and signaling.

While the importance of the signals is widely recognized, the vast majority of the works in the field do not focus on the interplay of various signals but on the effect of a single signal. This reductionist approach overlooks the synergies between the signals. It also overlooks that when engineering a scaffold with specific signals for cells, other non-specific interactions such as protein adsorption will change the interface of the scaffold and the cells and ultimately resulting in a different signaling that the intended.[2, 3, 11]

From a practical point of view two main approaches exist for fabricating the constructs of cells on scaffolds. In the first approach the organ/tissue replacement is fabricated outside of the body. Firstly the scaffold is engineered and then cells are seeded, for instance in a bioreactor. Once the construct is finished, it is implanted into the body (Figure 4A). More recently another approach has been explored in which the scaffold with engineered signals is implanted into the body so that cells are directly recruited from the patient (Figure 4B). The regeneration depends on the success of either recruiting the correct cells or giving the signals for other cells to differentiate in the required types.

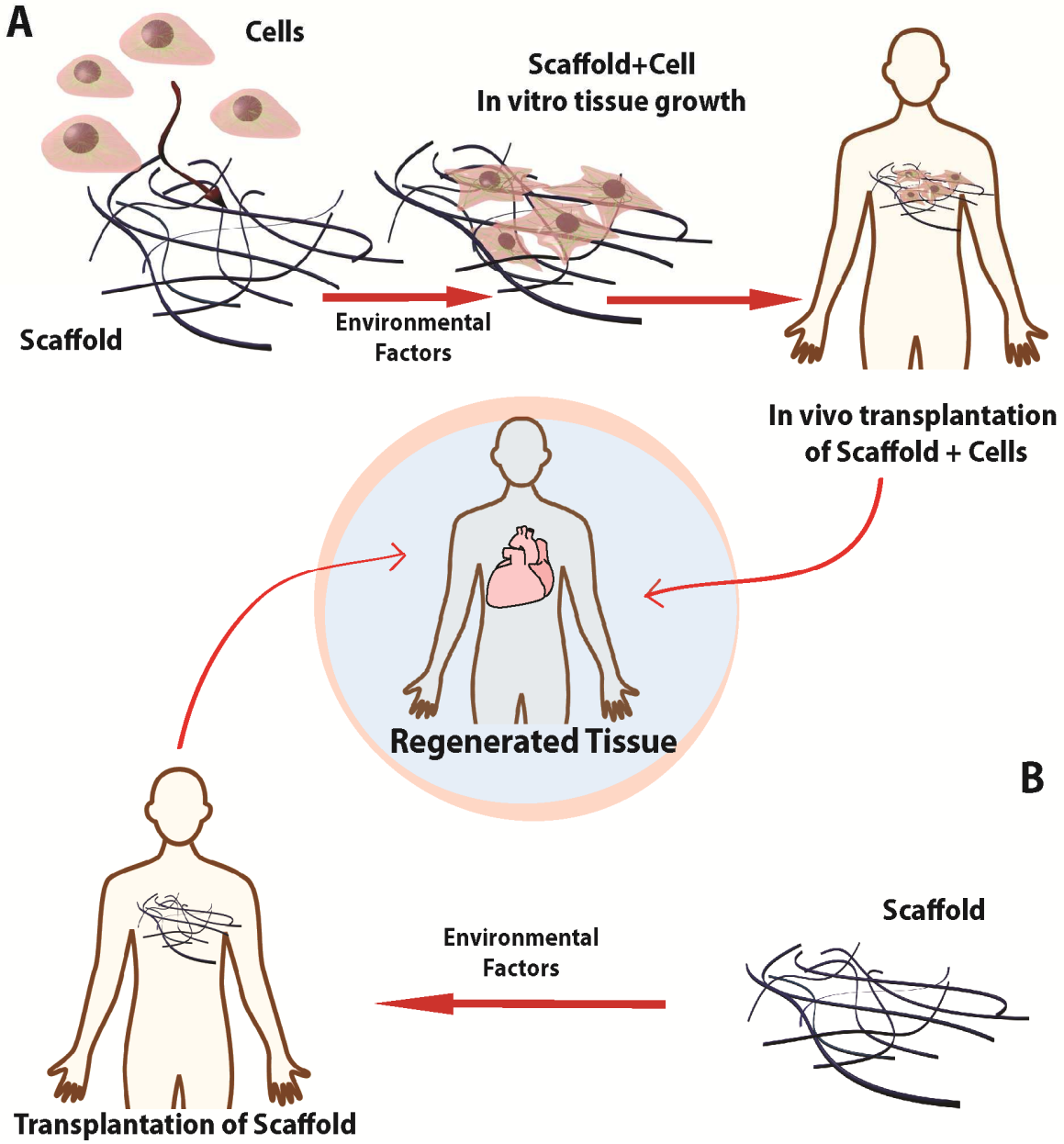

Figure 4. Tissue engineering approaches: A-transplantation of a scaffold with *in vitro* grown tissues; and B-promotion of tissue regeneration *in situ*. In both approaches the scaffold or artificial matrices, often biodegradable polymers, are integrated with microenvironmental factors, such as cytokines, growth factors, mechanical forces, physicochemical factors, spatial and temporal signals, and ECM molecules.

3 Components of Tissue Engineering

Tissue engineering has emerged to meet a global clinical need for the replacement and regeneration of the functions of tissues and organs. Tissue engineering strategies typically involve the combination of three main components, namely: (i) cells, (ii) precisely designed scaffolds, and (iii) specific signals to promote tissue regeneration and integration of the construct onto functional and organized tissue.

3.1 Cells for Tissue Engineering

Cells are the basic building and functional blocks of all tissues and play a crucial role in stimulating healing and regeneration of damaged tissue. Tissue engineering strategies utilize cells either as components of *in vitro* constructs or by recruiting them from the host *in vivo* with the aid of specific signals. Cells utilized for tissue engineering have to be free of pathogens and contaminants. Cell types can be selected from variety of sources which include immune acceptable patients' own cells (autologous cells), cells from another human source (allogeneic cells) and cells from different species (xenogeneic cells). However, allogeneic and xenogeneic cells often cause immune reactions.[3, 4]

Currently, there is considerable interest in the use of stem cells. Stem cells are undifferentiated cells that can differentiate into specialized cells. Stem cells can be divided in (i) embryonic stem cells and (ii) adult stem cells. Embryonic stem cells are very attractive for tissue engineering due to their ability to self-renew without differentiation, can be culture-expanded, and can differentiate into any cell type.

Embryonic stem cells can develop into any of the three germ layers: endoderm (interior stomach lining, gastrointestinal tract, the lungs); mesoderm (muscle, bone, blood, urogenital); or ectoderm (epidermal tissues and nervous system).[4] Human embryonic stem cells can be utilized for treating various diseases, such as Parkinson's disease, spinal cord injury, and diabetes.[27] However, despite all the advantages of embryonic stem cells there are ethical difficulties regarding the use of human embryos. Additionally, their use may induce the immunogenicity issues and rejection upon transplantation.[3, 27] One way to circumvent these issues is to reprogram differentiated cells from the patient into an embryonic-like state. These cells are termed induced pluripotent stem cells and display a

very similar behavior to embryonic stem cells, having the potential to differentiate into any of the three germ layers.[4, 27] The advantage of iPS cells is that they can be created from a patient's own cells avoiding the risks of host immune rejection.[4, 27]

As mentioned above, another source of cells are adult stem cells, which include mesenchymal, hematopoietic, neural, and hepatic stem cells. The use of mesenchymal stem cells is particularly advantageous as no immunosuppressive drugs are required (allogenic transplantation) and they can differentiate into multiple lineages. However, the use of adult stem cells is limited due to the difficulties in their isolation and expansion without changing cell phenotype.[4]

In order to benefit from the use of stem cells it is important to fully understand the process of differentiation of stem cells into tissue-specific cells. This requires knowledge not only about the molecular pathways of differentiation, but more importantly about the identification of a combination of signals that lead stem cells to become a specific type of differentiated tissue cell.[3]

In addition to stem cells, committed or differentiated cell types are also widely used in tissue engineering. For instance, culture expanded chondrocytes have been used for 15 years to treat cartilage defects; endothelial cells and smooth muscle cells can be utilized for blood vessel substitute; and skin substitutes involve allogeneic fibroblasts and keratinocytes.[3, 28] However, the use of differentiated adult cells is often restricted due to their low proliferation capability, loss of phenotype, and dedifferentiation in culture.[4]

Cells are the key component for effective tissue engineering. Cell behavior is guided by a variety of external cues and signals including ions, soluble growth factors, ECM components and the physical properties of the environment. The understanding at molecular level of how cells respond to molecular signals and how they integrate multiple inputs to generate a certain response are of main importance for the specific selection of signaling cues and the ways to expose the cells to them in order to control their behavior. In this way it is expected that differentiation can be promoted, toward the goal of tissue regeneration.

3.2 Scaffolds for Tissue Engineering

Scaffolds in tissue engineering play a crucial role for successful tissue or organ regeneration. The main role of the scaffold is to mimic the ECM of the intended tissue. The ideal scaffolds provide not only physical support, but also a microenvironment to induce cell attachment, proliferation and *de novo* tissue formation. While designing scaffolds for tissue engineering, their special characteristics must be engineered. Some examples of these engineered characteristics include (i) an interconnected highly porous structure to facilitate cell/tissue growth and diffusion of nutrients, metabolic waste, cytokines and paracrine factors; (ii) water content and mechanical properties to match the tissue at the site of implantation; (iii) suitable surface properties, (iv) inclusion of biological cues, such as peptides, or proteins interacting with integrin receptors of the cell for specific cell attachment, proliferation and differentiation; (v) biodegradability of the scaffold with controllable degradation rate to match with tissue growth, and (vi) moldability to form a variety of shapes and sizes. These key scaffold characteristics can be tailored to the application by careful selection of material, additional scaffold components, and the fabrication technique.[3, 4, 20, 29, 30]

3.2.1 Materials for Tissue Engineering

When selecting the material to prepare a scaffold it is of central importance to avoid any unnecessary harm, produced by the contact of the biomaterial with tissues of the body. Thus, the scaffold material should be non-toxic, non-immunogenic, non-carcinogenic and non-irritant.[23] Materials used in tissue engineering can be divided into three major groups: materials derived from native ECM, naturally derived polymeric materials and synthetic polymers.[2, 20]

A) Scaffolds Derived from Native ECM

Soon after the importance of ECM on cell and tissue survival and normal functioning was recognized, new scaffolds based on the use of native ECM from decellularized tissues and organs were introduced. By decellularizing tissues, the composition, geometry and anatomical features of the native ECM can be preserved in the *de novo* engineered scaffold.

The composition of scaffolds based on ECM consists of a complex mixture of molecules that mediate structural and biological properties. Some examples include different types of collagen for structural and mechanical support, glycosaminoglycans for water retention, adhesion molecules such as fibronectin and laminin and various growth factors.[24, 31, 32] In addition, the preserved microscopic and ultrastructural features of the ECM matrix play important role in modulating the behavior of cells that contact the scaffold by controlling the cell's ability to migrate into the scaffold or by influencing tissue-specific cell phenotype.[31] In an analogous way, it can dramatically affect the differentiation pathway of human embryonic stem cell and selected progenitor cell population.[31]

The ECM of many tissues and organs has been obtained (Figure 5), however, porcine small intestinal submucosa and urinary bladder matrix are the biological scaffold materials that have been most extensively characterized and studied.[31, 33, 34]

Although, these scaffolds have the clear advantages of preserving the features of the ECM, the preparation procedures of these scaffolds are very demanding. Mammalian tissues require several processing steps that can markedly affect their structure and type of host response that these scaffolds induce when used for tissue reconstruction. The native tissues from which an ECM scaffold is prepared must be mechanically or physically separated from unwanted tissue structures, decellularized, dehydrated and sterilized. All of these processing steps can influence the integrity, architecture and chemical composition of the matrix.[31] The total removal of antigenic epitopes of cell membranes and intracellular components of tissues is important to minimize any adverse immunogenic response that could be induced by xenogeneic or allogeneic cells of the donor tissue.[3] Commonly used methods of decellularization include a combination of physical and chemical treatments. Sonication, agitation, freezing and thawing and detergents are used to disrupt cell membranes and release cell contents from the ECM. However, these methods are not sufficient to achieve complete decellularization and some deoxyribonucleic acids (DNA) is retained in ECM scaffold. Additionally, the methods may affect the structure and composition of the ECM. Some detergents used to facilitate decellularization have been shown to disrupt collagen of certain tissues, thereby decreasing their mechanical strength, while the same detergent may have no effect on the collagen in another tissue.[35] The

decellularization method requires optimization for each tissue to remove cellular material without compromising the mechanical properties of the tissue.

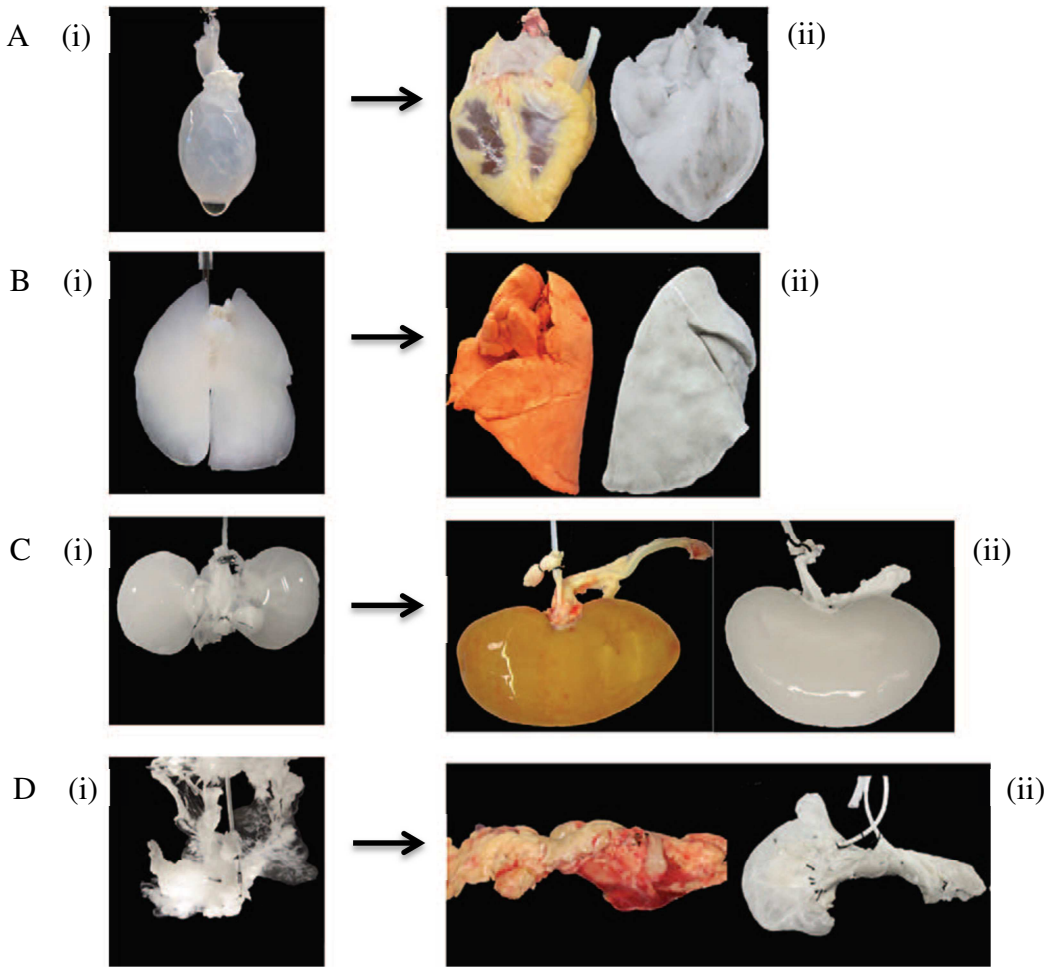

Figure 5. Perfusion-decellularized whole organ scaffolds. The native ECMs of cadaveric organs can be isolated by the perfusion of the native vascular system with detergent solutions. The resulting scaffolds are acellular, but maintain the structure of the native organ. (a) Rat heart scaffold generated from cadaveric heart by perfusion decellularization (i). The ascending aorta was cannulated for perfusion. Cadaveric human heart before and after perfusion decellularization (ii). (b) Rat lung scaffold generated from cadaveric lung by perfusion decellularization (i). Perfusion was performed via the pulmonary artery. Cadaveric sheep lung before and after decellularization (ii). (c) Rat kidney scaffold generated from cadaveric kidney by perfusion decellularization (i). The abdominal aorta was cannulated for perfusion. Porcine kidney before and after perfusion decellularization (ii). (d) Rat pancreas scaffold generated from cadaveric pancreas by perfusion decellularization (i). The abdominal aorta was cannulated for perfusion. Human pancreas before and after perfusion decellularization (ii). Image is reproduced from J. J. Song, H. C. Ott, *Trends in Molecular Medicine,* 17, 424.

Another challenge that ECM-based scaffolds face is conservation before implantation. Two strategies are in use: (i) keep the scaffold hydrated and (ii) lyophilization. The former ensures the preservation of the tissue architecture by preventing morphological changes in structural proteins as well as being beneficial for the integrity of signaling molecules. [36] However, in continuously hydrated materials, a continuous leaching of soluble growth factors has been observed with the concomitant change in properties and efficacy.[31, 36] On the other hand by lyophilizing —the most widely used method— the ECM-based scaffolds no leaching is produced. However, some changes in the fibers of the ECM occurs which not only modify the structural properties but also the water uptake.[36] An alternative method used to dehydrate ECM-based scaffolds is vacuum pressing, which allows for the lamination of multiple sheets of ECM to increase the strength. Although vacuum pressing is an effective method for constructing a variety of 3D shapes of ECM-based scaffold, the lamination of ECM scaffolds significantly reduces their extensibility, and changes the ultrastructural morphology of the resulting construct which affects cell attachment, *in vivo* degradation rate and cellular infiltration.[31, 36]

While ECM-based scaffolds may provide in some cases a feasible approach for tissue engineering, several challenges still remain to be addressed before clinical translation; (i) decellularization of tissue, dehydration and sterilization of scaffolds without compromising the micro and ultrastructure and protein framework, (ii) sufficient cell numbers, (iii) the need for clinical grade bioreactors, and (iv) the clinical logistics of this approach.[24] Moreover, ECM-based scaffolds do not solve the problems connected with the deficiency of organ donors since tissue or organs are needed to build the scaffolds.

B) Naturally Derived Polymeric Materials

To mimic the ECM while avoiding the shortage of ECM-based materials various naturally-derived polymeric materials have been introduced for the development of tissue engineering scaffolds ranging from cartilage to functional pancreatic replacements.[20, 37]

Various protein-based polymers have been used for preparation of scaffolds enabling to direct the migration, growth and organization of cells during tissue regeneration. Among them, collagen is the major protein component of the ECM and provides support to connective tissues such as skin, bones, cartilage, blood vessels and ligaments. Collagen is

characterized by good mechanical strength, biocompatibility, low antigenicity, degradability and water uptake capability. Generally, collagen is isolated from animal tissues thus having the potential for risk of viral and prion contamination. Additionally, collagen is hard to process and its degradation rate difficult to control. Collagen gels are widely used in clinical practice as an artificial skin, anti-microbial wound dressing, treatment of long bone fractures and regeneration of periodontal tissue.[37] Gelatin is derived from collagen by breaking the natural triple-helix into single-strand molecules by hydrolysis.[21] The solution of gelatin easily forms a gel by changing the temperature. Due to its biocompatibility, water content and ease of gelation gelatin has found application in drug delivery, as an absorbable film and disks.[37] Additionally, gelatin microspheres were used for the encapsulation of biomolecules or cells with further incorporation of these microspheres in a second matrix such as hydrogel.[38, 39] However despite all the advantages of gelatin the weakness of gels is a problem for more extensive use.[7] Another the most abundant protein is fibrin. It is produced from the enzymatic polymerization of fibrinogen, which can be isolated from the blood of patients. Thrombin cleaves peptide fragments of fibrinogen, yielding insoluble fibrin peptides that aggregate to form fibrils.[40] Fibrin hydrogels act as an excellent substrate for cell adhesion, spreading, migration and proliferation as they contain specific sites for cell attachment.[37] However, rapid degradation and poor mechanical properties limit their use.[7, 37]

Polysaccharides, such as alginate, chitosan and hyaluronic acid, represent another major class of naturally derived polymers used in scaffolding. Monosaccharide monomers are linked together by *O*-glycosidic bonds forming linear or branched polymers.[21, 37] One of the most widely used polysaccharide is alginate obtained from brown algae. The Alginates, rich in carboxylic groups, in the presence of divalent ions such as Ca^{2+} form physical crosslinks leading to reversible gelation. Their biocompatibility, low toxicity, simple gelation and low cost have led applications such as cell delivery vehicles, wound dressings and mucoadhesive agents.[7, 37, 41] Regretfully, the uncontrolled degradation kinetics lead to a high concentration of divalent ions and alginate chains of varying length that are typically above the renal clearance of the kidney.[7, 37] Chitosan is another polysaccharide used in scaffolding. Chitosan is a cationic polymer obtained by full or partial deacetylation of chitin, a natural polysaccharide found in the shells of crustacean, cuticles of insects and cell wall of fungi. Due to its biodegradability, biocompatibility, non-

antigenic and non-toxic character chitosan has found numerous applications in wound healing, skin and cartilage grafts and drug and gen delivery applications [37, 42, 43]. Additionally, chitosan possesses hydroxyl and amino groups that can be utilized for chemical modification or immobilization of biologically active compounds.[37, 43] The main limitation of chitosan is that it is hardly soluble in media with neutral pH and insoluble at higher pH, therefore, chemical modification is needed.[43] Hyaluronic acid is a naturally occurring non-sulfated glycosaminoglycan and a major macromolecular component of the intercellular matrix of most connective tissues such as cartilage, the vitreous of the human eye, umbilical cord and synovial fluid.[37, 44] Hyaluronic acid is a linear polysaccharide and can be formed into hydrogels by covalent crosslinking with hydrazide derivatives or radical polymerization of glycidyl methacrylate.[7] It has been widely studied for artificial skin, facial intradermal implants, wound healing, drug delivery and soft tissue augmentation applications. [7, 37, 44] The degradation of hyaluronic acid occurs by hyaluronidase which is present in cells and serum.[7]

Natural polymers due to their general biocompatibility and biodegradability are very attractive candidates for the fabrication of scaffolds for tissue engineering. However, a lack of control in the kinetics of enzymatic degradation, poor mechanical properties, difficulties in the reproducibility of chemical and physical properties and potential immunogenic reactions may limit the possibilities for various applications.[3, 21]

C) Synthetic Polymers

Various synthetic polymers have been used for the fabrication of scaffolds for tissue engineering due to the extreme versatility with regard to the control over their physicochemical properties and the ease to process them into scaffolds. Synthesis of these polymers can be tailored to achieve a specific molecular weight, chemical structure, composition and end-group functionality. Synthetic polymers used in tissue engineering can be classified into nonbiodegradable and biodegradable.[7, 21]

Nonbiodegradable polymers find their niche in scaffolding when long-term integrity of the scaffold is required, typically for hard connective tissues.[45-47] The most widely studied synthetic nonbiodegradable polymers are poly(2-hydroxyethyl methacrylate) (poly(HEMA)), poly(vinyl alcohol) (PVA), poly(*N*-isopropylacrylamide) (PNIPAm), and

poly(ethylene glycol) (PEG) (Scheme 1).[7, 21, 48-57] Poly(HEMA) is a non-immunogenic, hydrophilic, chemically stable polymer. It was introduced in 1960 by Prof. Wichterle for the preparation of soft contact lenses.[7, 52, 58] Micro- and macroporous poly(HEMA) gels can be prepared by copolymerization with multifunctional crosslinkers by various types of techniques, such as polymerization of HEMA in aqueous solutions, freeze/thaw, or particulate leaching techniques. [7, 55] Many different types of molecules and cells have also been encapsulated into poly(HEMA) gels, and this approach has been reported to be successful for the delivery of insulin and other proteins into the body.[46, 56, 59] PVA is another widely used and one of the oldest polymers used in biomedical applications with its first use in scaffolding dating to 1924.[59] PVA is linear polymer produced by free radical polymerization of vinyl acetate to poly(vinyl acetate) and subsequent hydrolysis of the acetate groups to alcohol groups.[59] The hydrophilicity and solubility of PVA can be easily controlled by the extent of hydrolysis and molecular weight.[7] PVA hydrogels were widely studied for use in regeneration of artificial articular cartilage, artificial pancreas, and to promote bone-like apatite formation.[7, 45, 59, 60] PVA hydrogels were frequently combined with heparin, a natural sulfated glycosaminoglycan, which displays anticoagulant activity by inactivating blood coagulation factors such as thrombin.[61] PNIPAm is a thermoresponsive polymer which has been introduced in scaffolding. Below the lower critical solution temperature (LCST, ~32°C) [62] the formation of hydrogen bonds between water molecules and the amide groups of PNIPAm plays a dominant role leading to well solvated polymer. However, when the temperature is higher than the LCST, hydrophobic interactions between the isopropyl groups of PNIPAm side chains become dominant resulting in desolvation and collapse of the polymer.[21, 62] This has been utilized to endow PNIPAm hydrogels with thermoresponsiveness. Intact cell sheets, cells cultivated on PNIPAAm hydrogels, can be easily harvested without damage by simply decreasing the temperature which turns the hydrogel less adhesive for cells.[62] This polymer is also being investigated as an injectable delivery vehicle for cartilage and pancreas engineering.[63] PEG is perhaps the most important hydrophilic polymer for biomedical applications which includes surface modification, bioconjugates, drug delivery and tissue engineering. PEG bears unique properties, such as good biocompatibility, non-immunogenicity, and fair resistance to protein adsorption.[7, 21, 64, 65] It is also has been approved by the Food and Drug Administration (FDA) for several medical applications.[7] A contraceptive sponge with the

brand name "Today", based on crosslinked PEG diisocyanates and containing the spermicide nonoxynol-9, was commercialized in the 1980 and is still on the market.[59, 66] Interesting studies are made on the preparation of PEG hydrogels with encapsulated cells. Poly(ethylene glycol dimethacrylate) (PEGDMA) and PEG have been photopolymerized to form hydrogel networks with encapsulated bovine and ovine chondrocytes for cartilage regeneration. After photopolymerization, the cells within the scaffold remained viable and evenly dispersed.[8] This approach can be useful for easier introduction of cells inside of scaffolds.

Even though hydrogels from nonbiodegradable polymers can be utilized in some applications, most scaffolds for tissue engineering require degradation so that they can be replaced by natural ECM secreted by the seeded cells. The lack of biodegradability strongly limits the use of the above-mentioned polymers in engineering vascular constructs and other soft tissues.

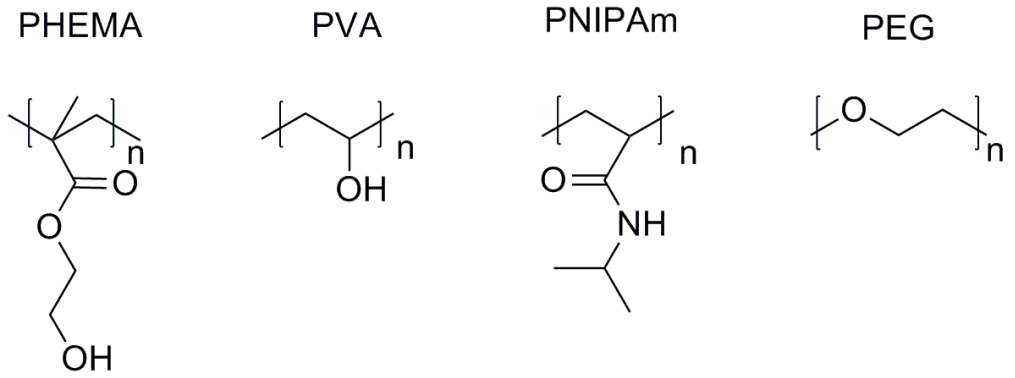

Scheme 1. Chemical structures of nonbiodegradable polymers, such as PHEMA, PVA, PNIPAm and PEG.

Scaffolds based on polymers which degrade to non-toxic products and leave place to the formation of ECM generated from the seeded cells are a feasible avenue to engineer soft tissues. The goal is to implant a scaffold that can persist in a robust state for sufficient time to allow for the formation of new tissue, but will ultimately degrade and be replaced by this tissue.[54] The vast majority of synthetic biodegradable polymers used for tissue engineering belong to polyester family which include poly(lactic acid) (PLA),

poly(glycolic acid) (PGA), poly(ε-caprolactone) (PCL) and their copolymers (Scheme 2).[4, 54, 67] Polyesters degrade by hydrolysis releasing oligomers or monomers that feed into natural metabolic pathways.[54, 68] They have been used for a long time in medicine in the form of degradable sutures and more recently have been studied to promote regeneration of bone, cartilage, bladder, skin and vasculature.[4] The ease of processibility of PLA, PGA and their copolymer poly(lactide-*co*-glycolide) (PLGA) into various shapes is a major advantage and they have been utilized in a vast array of applications including bone, cartilage, liver, tendon, ligaments, neural and intestinal tissue engineering.[4] The degradation of polyesters yields acidic compounds. These acidic compounds usually decrease the pH in the implanted zone causing inflammation. Moreover, the decrease in pH leads to the autoacceleration of the hydrolysis (acidic catalysis).[69] This effect is usually more prominent in the bulk when the scaffold is implanted, leaving a capsule of high molecular weight polymer outside and acidic core which is detrimental to cells and surrounding tissues.[54, 69] Another member of polyester family is PCL, which degrades at slower rate than the above mentioned polyesters. The degradation rate of PCL can be finely tuned by the adjustment of crystallinity and molecular weight of PCL.[70] Scaffolds based on this polymer can be found in bone and vessel tissue engineering.[4]

As mentioned above, the main limitation of polyesters are the acidic degradation products. To circumvent inherent problems of polyesters, other biodegradable polymers have been introduced. For instance, polycarbonates (PC) and polyurethanes (PU) produce less acidic degradation products (Scheme 2). PC are linear polymers that have carbonate groups in the main chain. The carbonate groups are more hydrolytically stable than esters, but still prone to *in vivo* enzymatic degradation.[71] In addition PC can be easily processed into a variety of scaffolds including films, fibers, and gels which found use for bone, vasculature, and muscle tissue engineering.[71] PU are moldable and strong polymers bearing carbamate groups in the main chain. The latter results in even higher hydrolytic stability than PCs.[71] PU can be processed for both hard and soft tissue engineering applications.[54] PU have been used extensively in prostheses such as cardiac assist devices, small vascular shunts, and tracheal tubes.[71, 72]

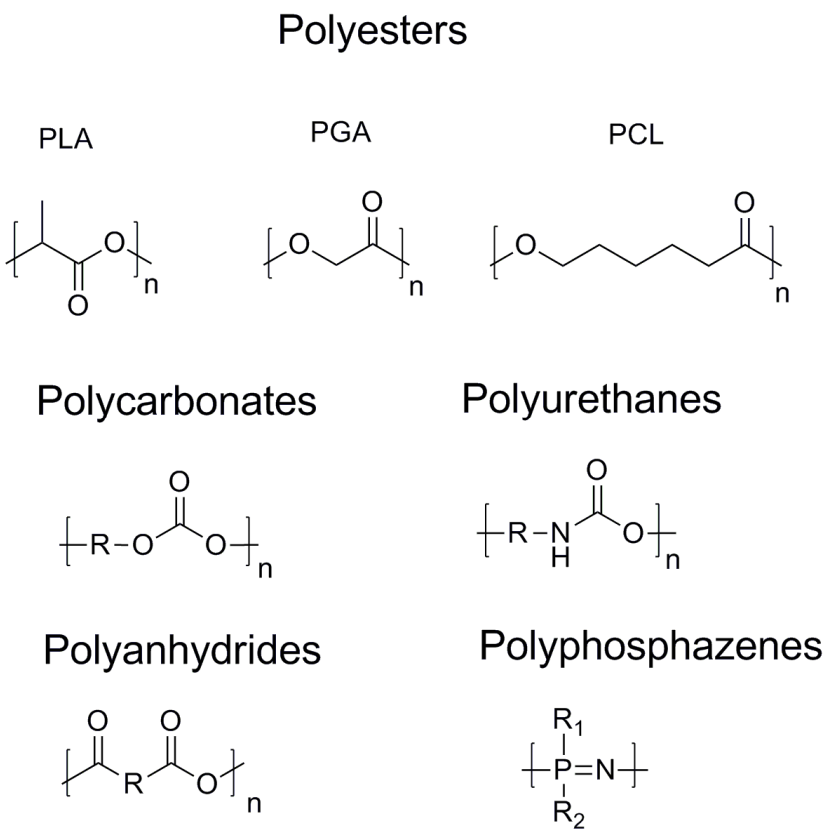

Scheme 2. Chemical structures of biodegradable polymers, such as polyesters, polycarbonates, polyurethanes, polyanhydrides and polyphosphazenes.

Polyanhydrides are a comparatively newer class of biodegradable synthetic polymers developed from the condensation of diacids or a mixture of diacids (Scheme 2). They have a hydrophobic backbone with hydrolytically labile anhydride linkages that can be controlled by manipulation of the polymer composition. Polyanhydrides are of great interest because they show a lower inflammatory reaction and their degraded counterparts are less cytotoxic.[73] Polyanhydrides have been considered to be useful biomaterials for orthopedic applications and as drugs carriers to various organs such as brain, bone, blood vessels, and eyes.[4, 73]

Polyphosphazenes are a unique class of degradable polymers because their backbone is completely inorganic consisting of phosphorous and nitrogen bonded linearly through alternating single and double bonds (Scheme 2).[7, 54, 71] The control over the degradation rate and physical properties of the polymer is also greatly affected by side group substitution. Polyphosphazenes degrade into neutral products that have been found to have

a buffering effect in pH.[71] The large library of side groups and the processibility of polyphosphazenes have spurred their use for the fabrication of particles, micelles, microneedle coatings, and gels. These polymers have shown significant promise in delivery of anti-inflammatory drugs, chemotherapeutics, growth factors, DNA, proteins, and vaccines and tissue engineering applications including cartilage, bone, liver, and neural tissue regeneration.[4, 71]

In order to increase wettability, biocompatibility, and tailor the mechanical properties of biodegradable polymers, blends or copolymers with nonbiodegradable polymers have been introduced.[4] The block-copolymers of PEG and polyesters such as PLA, PLGA and PCL were synthesized for the preparation of the scaffold for soft tissue, tubular tissue and bone tissue engineering and drug delivery.[4, 74, 75]

While many challenges remain to be solved for successful scaffolding with synthetic polymers, these man-made materials show great promise. In particular, recent advancements in polymer and organic chemistry give access to a much broader palette of synthetic routes to prepare polymers with precise chemical composition, size, dispersity, *etc.*, thus ultimately tailoring the bulk and interfacial properties of the material. Moreover, by careful designing of the backbone and lateral groups, properties such as biodegradation, thermo- and pH-responsiveness, hydrophilicity, toxicity, *etc.*, can be tuned. Therefore, synthetic polymers are ideal candidates for the preparation of tissue engineering scaffolds.

3.2.2 Scaffold Types

Typical scaffolds are produced as porous scaffolds, including meshes, sponges and foams, hydrogel scaffolds and fibrous scaffolds. A highly porous structure which allows uniform cell distribution and diffusion of nutrients is always preferred.[4, 29, 76]

A) Porous Scaffolds

Sponge and foam scaffolds are highly porous materials with an interconnected pore structure, which simulates the architecture of the ECM, allowing cells to interact effectively with their environment (Figure 6). Porous scaffold can be manufactured with specific pore size, porosity, surface area, and crystallinity. For the control over porosity

and pore diameter, solvent casting and particulate leaching techniques have been used.[4, 29, 76] Natural and synthetic materials have been utilized for the fabrication of porous scaffolds. They have been useful for the growth of host tissue, bone regrowth, and organ vascularization.[29]

B) Hydrogel Scaffolds

In the last decade, hydrogels have played a significant role in the field of tissue engineering. Due to their structural similarity to the macromolecular-based components in the body and the ability to swell in aqueous media, hydrogels provide an excellent environment for promoting cell migration, angiogenesis, and new tissue formation. [8, 49, 50, 77]

Hydrogels are 3D networks formed from hydrophilic homopolymers, copolymers, or macromers (preformed macromolecular chains), crosslinked to form insoluble polymer matrices. The crosslinked structure of hydrogels is characterized by junctions or tie points, which may be formed from strong chemical linkages (such as covalent and ionic bonds), permanent or temporary physical entanglements, microcrystallite formation, and weak interactions (such as hydrogen bonds).[8] In general, monomer/macromer, crosslinker, initiator and diluent are important components for the hydrogel formulation. The hydrogel properties can be modulated by varying the synthetic conditions, such as conversion, degree of crosslinking, temperature or light exposure (depending on the type of initiator), type of monomer/macromer and crosslinker, ratio of crosslinker to monomer, and type and concentration of initiator. Synthetic hydrogels are generally produced via bulk, solution, and inverse dispersion techniques.[78] Hydrogels are usually defined by their degree of swelling (Figure 6). The swelling capacity of a hydrogel can be determined by the amount of space inside the hydrogel network available to accommodate water and the polymer-water interaction and it depends on the nature of the polymer chains and the crosslinking density.[78] The water accommodated by a hydrogel can be classified into four types: (i) free water, located in the outermost layer and can be easily removed from the hydrogel under mild conditions; (ii) interstitial water, not attached to the hydrogel network, but physically trapped in between the hydrated polymer chains; (iii) bound water, directly attached to the polymer chain through hydration of functional groups or ions and can only be separated at high temperatures; and (iv) semi-bound water, a type of water with intermediate properties

between bound water and free water.[78] The hydrogel scaffolds have received intensive study for their use in the engineering of various tissues and organs regeneration such as liver, skin, bone, cartilage, vascular and other tissues.[77] However, while possessing high water content, the applications of hydrogels are often limited due to structural instability and insufficient mechanical properties for placement within a dynamic environment.[4]

C) Fibrous Scaffolds

The development of nanofibrous scaffolds has introduced a new avenue to finely mimic ECM architectures (Figure 6). The microporous structure of nanofibers provides a dynamic, three-dimensional microenvironment with interconnected porosity and very high surface area, in which cells can maintain, adhere, proliferate, migrate, and differentiate. Currently, there are three techniques available for the synthesis of nanofibers: electrospinning, self-assembly, and phase separation.[79] However, electrospinning is the most widely used technique that can generate continuous micro- or nanoscale diameter fibers in a random or oriented manner.[4, 29] Nanofibers have been fabricated from natural and synthetic polymers, including collagen, gelatin, chitosan, PLA, PU, PCL, *etc*. [4, 29, 79] Nanofibers have been studied for musculoskeletal tissue engineering including bone, cartilage, ligament, and skeletal muscle, skin, vascular, neural tissue engineering and as vehicle for drug, protein and gene delivery.[29]

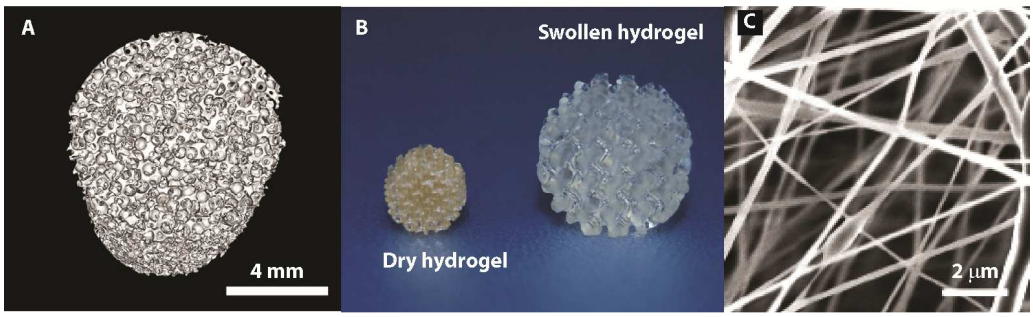

Figure 6. Types of scaffolds for tissue engineering: (A) Microcomputed tomography visualization of a sponge structure scaffold prepared by salt-leaching; (B) hydrogel scaffold prepared by stereolithography; (C) nanofibrous scaffold prepared by electrospinning. The picture is adapted from F. P. Melchels, *et al.*, *Acta Biomaterialia* 2010, 6, 4208 and N. Yu. Kostina, *et al.*, *Macromolecular Bioscience* 2015, DOI:10.1002/mabi.201500252.

3.2.3 Scaffold Fabrication Methods

Various manufacturing methodologies have been developed or evolved to fabricate porous 3D scaffolds for tissue engineering, including leaching processes, freeze-drying, phase separation, gas foaming and supercritical fluid processing, solid freeform fabrication, and electrospinning.[4, 80] In each of these techniques, one or more polymers of desired characteristics are processed uniquely to produce a porous 3D structure of particular shapes, morphologies and mechanical properties.[4]

A) Leaching Processes

Leaching processes consist of the use of solid or semisolid particles (porogen) as pore templates. The porogens are suspended in a polymer or prepolymer matrix. The latter is crosslinked and the porogen is dissolved or extracted by a solvent, leaving behind a pore of similar size to the porogen. By selecting the size, loading and type of surface of the porogen it has been possible to design macroporous hydrogels with tailor-made porosity.

Natural and synthetic polymers have been processed into macroporous scaffolds by leaching techniques for the fabrication of matrices for 3D cell cultivation and tissue engineering attempts.[81]

A variation of the described leaching method is the solvent casting/particulate leaching (SC/PL) technique, widely used for biomembranes. The process involves the introduction of water soluble particles of specific diameter into a polymer solution in organic solvent. Subsequently the mixture is poured into a mold and allowed to solidify by evaporation of the polymer solvent. Finally this polymer matrix is immersed in water, where the particles dissolve producing a porous structure.[80] This method was used for the fabrication of PLA membranes with porosities of up to 93% and pore diameters up to 500 μm.[80] Scaffolds produced by SC/PL technique have been shown to support cell attachment and growth *in vitro* and *in vivo*.[4] While SC/PL technique is simple and inexpensive, some of the disadvantages include that it can only be used to produce thin membranes up to 3 mm thick and that it is usually based on polymers which can be dissolved in organic apolar solvents, thus with very poor equilibrium water content.[80, 81] The latter is particularly detrimental for engineering soft tissues.

Another leaching method for the fabrication of porous scaffolds is compression molding. This technique involves filling a mold with polymer powder and a porogen and heating to above the glass-transition temperature of the polymer under elevated pressure. When the composite is removed from the mold, the porogen can be leached out to produce pores in the scaffold. Compression molding is a non-solvent fabrication method that allows the control of morphology and shape. In another variation, compression molding can be applied together with SC/PL technique to fabricate porous 3D foams.

B) Freeze-Drying

Porous scaffolds can be prepared by the freeze-drying technique. The polymer is dissolved in a solvent and solution is cooled down to a certain temperature at which all materials are frozen and the solvent forms ice crystals. The frozen solution is lyophilized under high vacuum to remove the randomly dispersed solvent crystals. When the solvent is completely sublimated, a dry polymer scaffold with an interconnected porous microstructure remains. The porosity of the scaffolds and pore size distribution depends on the concentration of the polymer in solution, the freezing temperature and rate of cooling (supercooling).[4, 80] Various polymers such as PLA, PLGA, PNIPAm, *etc*. were used for the preparation of porous scaffolds by the freeze-drying method.

A variation of the freeze-drying approach is the emulsion freeze-drying method. For this, the polymer is firstly dissolved in an organic solvent and then water is added to form a water-in-oil emulsion. Subsequently this emulsion is frozen and lyophilized to remove the dispersed water and solvent. In this case, the polymer-solvent system, molecular weight of the polymer, ratio of polymer solution to water, and emulsion viscosity are important parameters for the design of the properties of the scaffold.[4]

C) Phase Separation

In the thermally induced liquid-liquid phase separation technique, the polymer is firstly dissolved in a solvent that has a low melting point and can be easily sublimated (e.g. phenol, naphthalene or dioxane). Lowering the solution temperature below the melting point leads to a liquid-liquid phase separation to form two phases: a polymer-rich phase and a polymer-poor phase. The polymer-rich phase solidifies and the polymer poor phase is removed. The micro- and macro-structures of the resulting scaffolds are controlled by

varying process parameters such as polymer-solvent system, molecular weight of the polymer, polymer concentration, quenching temperature, and quenching rate. Using phase separation techniques, nanoscale fibrous structures can be produced. This technique has been used to prepare foams with porosities greater than 90% and pore size close to 100 μm.[4, 81]

D) Gas Foaming Process

The porous scaffolds can be fabricated at ambient temperature and high pressure by the gas foaming technique. The polymer is firstly saturated with gas, usually CO_2, at high pressure, which is followed by depressurization to ambient level that results in nucleation of the gas, forming pores in the material. The pore structure and porosity of the resulting scaffold depends on of the amount of dissolved gas, the rate and type of gas nucleation, and the rate of gas diffusion to the pore nuclei.[4, 80] The main drawback of this technique is that an important proportion of pores are not interconnected. Additionally the stability of the scaffolds and pores depends on the glass transition temperature.

E) Solid Freeform Fabrication

Solid freeform fabrication (SFF) or rapid prototyping techniques have significantly improved the production of the scaffolds with precise geometry and internal morphology (Figure 7). SFF refers to a set of automated computer-assisted fabrication techniques, which have been utilized to produce 3D scaffolds with intended size and architecture of pores and scaffold shape.[4] SFF techniques applied to tissue engineering scaffold fabrication include stereolithography, 3D printing and selective laser sintering (SLS). The basic principle of SFF is analogous to bottom-to-top approaches where the creation of complex structures is achieved in layer-by-layer manner and can be engineered by computer-aided design (CAD) or can even be derived from scanning data of (clinical) imaging technologies such as magnetic resonance imaging or tomography techniques (Figure 7).[82]

Stereolithography is one of the most developed computer-aided rapid prototyping techniques for the construction of complex three-dimensional scaffolds with respect to the freedom of structure exterior and interior design with the highest accuracy. This technique is based on the spatially controlled solidification of liquid-based resins by

photopolymerization.[53, 82-84] During fabrication by stereolithography, ultraviolet (UV) light is irradiated with a precise pattern on the photosensitive resin surface. Free radicals and other reactive species are formed upon excitation of photoinitiator molecules by UV light, causing polymerization of the resin and formation of a solid phase of the material. The first layer of polymer is adhered to a build platform, which provides support for structures as they are fabricated. Once this layer is polymerized, the platform is moved a defined step height for polymerization of the subsequent layer. The process of moving the support platform and curing each layer individually is repeated until the three-dimensional structure is complete.[53, 82, 85] Various modified polymers, such as PLA, PC, PEG, *etc*. were used for the fabrication of the scaffolds for tissue engineering.[85-88]

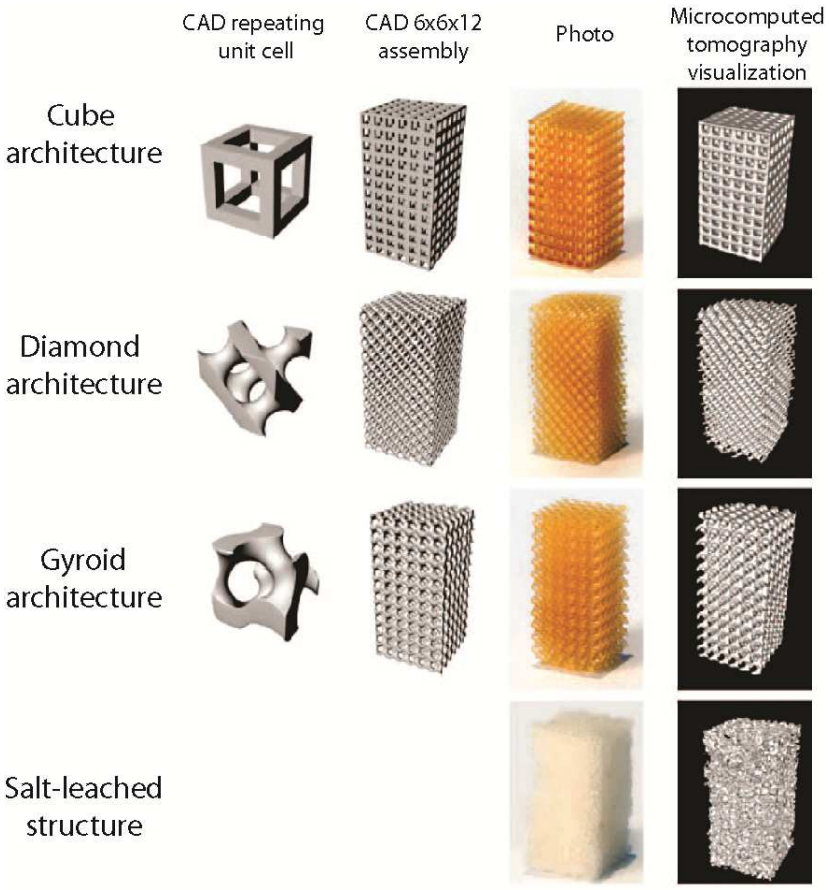

Figure 7. Recent advances in solid freedom fabrication technology allow designing a range of complex internal scaffold architectures with a range of length scales. This figure shows the design file, image of fabricated scaffold, and 3D tomographic reconstruction for three different designed scaffold architectures and a salt-leached structure formed by a random foaming process. Figure is reproduced from B. Derby, *Science*, 2012, 338, 921

The 3D printing technique is an automated inkjet printing-based technology. A layer of polymer powder is first spread over a building platform and by using the print head of an inkjet printer a pattern profile is made by depositing organic solvent over this layer to selectively bind the polymer powder. Alternatively, a polymer melt or a resin can be used and cured using UV irradiation. After preparation of one layer the building platform is lowered and the process is repeated with a fresh layer of powder placed over the last finished layer until the desired structure is obtained. Various direct and modified 3D printing techniques have been utilized to create scaffolds for bone tissue engineering.[4, 22]

The principle of the SLS method for 3D porous scaffold fabrication is identical to 3D printing techniques. However, instead of using solvent for binding the layer of polymer powder SLS involves computerized laser scanning. The pattern profile is created by selectively scanning the polymer powder by an x-y controlled laser beam, which heats the polymer surface to or above glass transition temperature. After cooling down, polymer particles fuse together with surrounding particles. By this method many biodegradable materials such as PLA, PCL and PGLA have been utilized for scaffold fabrication.[4]

Recently, direct laser writing (DLW) has been introduced for the fabrication of microstructures with submicrometer features. In DLW a femtosecond pulsed laser beam is focused into a photoreactive resist. In the confined volume where the laser is focused the curing of the resist occurs via a non-linear absorption mechanism. Resins based on vinyl polymerization (radical polymerization) have been mostly employed; however, resins based on click reactions have been introduced. In the former, the curing process involves a radical photoinitiator and crosslinking via radical addition (radical polymerization), therefore radicals can migrate out of the focusing volume and impair the resolution. In the latter case, the reactive species react only in the focusing volume yielding non-reactive, with a concomitant increase in the resolution.

F) Electrospinning

Electrospinning techniques have been widely exploited for the fabrication of porous scaffolds with fibrous architecture. Highly porous nano- and microfibers with high surface area to volume ratio can be produced by electrospinning of solutions of natural or synthetic polymers. In a typical electrospinning setup (Figure 8A), a solution of polymer passes through a needle at a controlled rate. Using a high voltage source across the needle the polymer solution becomes charged when an electric field applied to a droplet. When the forces of electrostatic repulsion within a solution overcome the surface tension, a thin polymer jet formed. Solvent evaporates while the jet flying from the needle tip to a collector where polymer fibers are formed and deposited on the collector. Depending on the type of collector fibers can be fabricated as a random mesh if the collector is a plate or as annulus-oriented fibers in the case of a rotating cylinder being used as a collector.[4, 79, 80]

An electrospinning technique —Roller Electrospinning— that allows for industrial continuous production of nanofibers recently was developed in Czech Republic.[89] This method is also known as Nanospider.[89] It consists of rotating roller to spin fibers directly from the polymer solution. This roller is a spinning electrode partially immersed in the tank with the polymer solution. A grounded collector electrode is placed at the top of the spinner. A backing material moves along the collector electrode which makes the production of the nanofiber layer a continuous process (Figure 8B).[89]

There are several variables that influence the process of electrospinning and can be varied to obtain the desired fiber and scaffold morphology. The variables include: solution viscosity, polymer charge density, polymer molecular weight, surface tension, electric field strength, tip/roller to collector distance, the composition and the design of collector. In the past decade, significant developments in electrospinning allowed for the creation of scaffolds with different materials, such as PLA, PCL, gelatin, chitosan, PVA, *etc*.[4, 79]

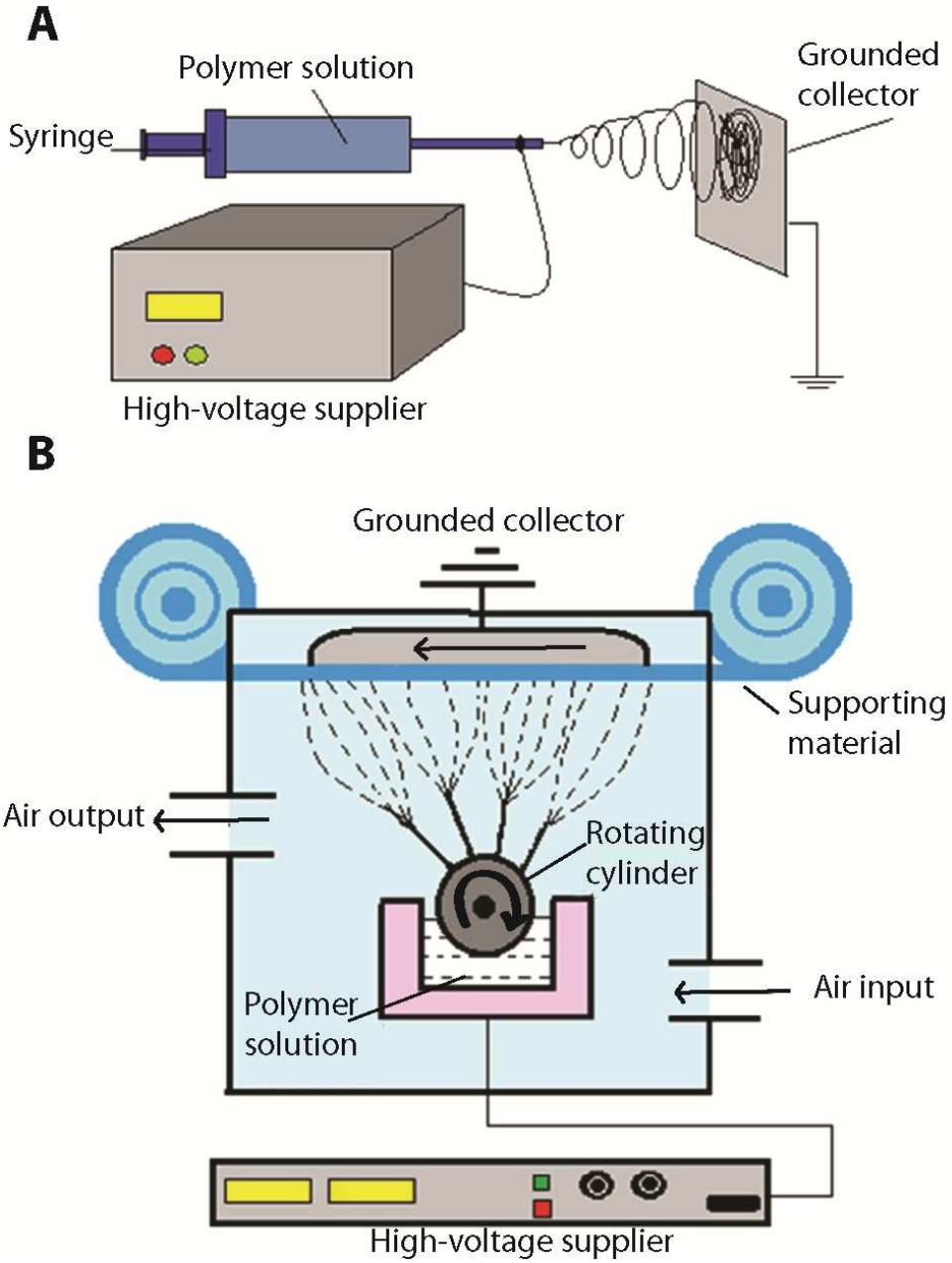

Figure 8. Schemes of needle electrospinning (A) and roller electrospinning (B). Schemes are reproduced from F. Yener, O. Jirsak, *Journal of Nanomaterials* **2012**, *2012*, 1.

3.3 Signaling

A few decades ago the fabrication of materials for tissue engineering was mainly focused on the bioinertness in order to minimize interactions with the host or surrounding tissues. However, later the importance of material that mimic the ECM not only as a structural support, but also to interact with surrounding tissues and cells was recognized.[11] Cells are intrinsically responsive to physical, biochemical and chemical stimuli of the environment.[90] The local cell niche provides multiple signals to the cells guiding their behavior and fate. Depending on the type of signals, cells may undergo either cell-specific attachment to the ECM, proliferation, differentiation, and final tissue regeneration, or cell apoptosis.[54, 90] It is a critical challenge for successful tissue engineering to understand and control those signaling processes to promote cells for tissue regeneration.[91]

A vast variety of signals are chemical and biochemical in nature, they include ions, growth factors, cytokines, ECM elements, *etc.* Growth factors are soluble molecules that control a wide variety of cellular responses through specific binding to cell transmembrane receptors. The induction of biological responses mediated by growth factors depends on the type of growth factor and cells. For instance, angiogenesis —the development of new blood vessels— is regulated by endothelial growth factor, platelet-derived growth factor, fibroblast growth factor, and insulin-like growth factor. The control of inflammation, on the other hand, involves the action of proinflammatory cytokines and peptide growth factors.[91] The composition of ECM varies from tissue to tissue, however, each contains various insoluble proteins such collagen, elastin, laminin, fibronectin, *etc*. The mechanical strength, cell response, and even tissue organization are a consequence of the organization, density, spatial geometry, and chemical composition of the ECM components.[90] These ECM proteins interact with cells surface receptors. These surface receptors are a large family of transmembrane cell surface proteins termed integrins that govern the adhesive interaction between cells and macromolecular components of the ECM.[54, 90] Usually the binding motifs are specific peptide sequences. The binding of the integrin receptors to ECM motifs activates various signaling paths mediating cell attachment, proliferation, organization of the actin cytoskeleton, and formation of focal adhesions. Integrins play a critical role in cell-matrix interactions and proteins or peptides that interact with integrins are considered as targets to control receptor-mediated cell adhesion.[92]

The scaffold has to be engineered to elicit specific cellular responses upon signaling and direct new tissue formation mediated by specific interactions.[92] The signaling molecules have to be incorporated in the scaffold in a certain way to promote the processes of cell–biomolecular recognition. Thus, one approach is to incorporate soluble bioactive molecules into the scaffold for their free or controlled release. These bioactive factors can be entrapped within the scaffold during or upon fabrication and their release to the cell environment will be direct, but not controlled.[4] In order to gain a temporal control over the release of the factors, bioresorbable carriers loaded with the desired biomolecules can be incorporated in the scaffold. Upon degradation these carriers free growth factors or other biomolecules.[4, 93] Alternatively, growth factors can be incorporated directly to the scaffold using a heparin bridge. The growth factors are released upon degradation of the heparin or in some cases by cleavage of protease sites within the growth factor.[54] In contrast to the previous methods in which the growth factors are added to the scaffold, an alternative approach makes use of scaffolds which can produce their own signaling molecules. This is accomplished by seeding genetically modified cells that produce bioactive factors at the site of application.[4, 94]

To facilitate specific cell attachment to the tissue engineering scaffold for further cell proliferation, differentiation and ECM production, the approach of integration of ECM proteins or their motifs into the scaffold via covalent immobilization can be utilized. Early work was focused in the covalent immobilization of long chains of ECM proteins such as fibronectin, vitronectin and laminin to the surface of the scaffold. However, the proteins tend to fold randomly during the coating process to the surface of the scaffold such that the receptor binding domains are not always sterically available. Additionally, there are certain adverse effects, including immune response and risk of infection when adhesive proteins are used.[90, 92] With the advancement in molecular and cell biology it was recognized that only specific domains in the ECM proteins were responsible for the interactions and binding with cell receptors. These domains consist of short sequences of amino acids. These short peptide fragments have been utilized for surface modification in numerous studies instead of the whole protein.[92] Various ECM peptide sequences, which have been determined to influence cell behavior, have been isolated or synthesized and grafted on scaffolds to enhance specific cell attachment.[90] Peptide sequences such as Arg-Gly-Asp (RGD), Tyr-Ile-Gly-Ser-Arg (YIGSR), Arg-Glu-Asp-Val (REDV) and Ile-Lys-Val-Ala-

Val (IKVAV) derived from fibronectin and laminin, have been immobilized on various model substrates.[92, 95-98] Different coupling methods have been exploited for the covalent immobilization of these peptides on the surface of the scaffolds.[99-101] However, most of these methods require the availability of functional groups on the scaffold, such as amino, carboxyl or hydroxyl groups. For materials that lack functional groups, additional steps of surface modification or additional of functional components during the fabrication are required.[92]

Indeed, the structural design and surface decoration with signaling motifs are critical steps in the fabrication of a scaffold that can imitate native ECM. However, generally upon the contact of artificial scaffolds with a physiological milieu, the surface of the scaffold will be rapidly coated with proteins from blood or interstitial fluid. The non-specific protein adsorption —protein fouling— is a complex and dynamic process, which affects the surface of most (bio)materials.[102-104] This ubiquitous problem can mask the bioactive molecules previously immobilized on the material surface, thus promoting non-specific cell adhesion, which will lead to loss of control over the behavior and fate of the cells. Moreover, protein fouling induces a series of adverse effects, such as the inflammatory response and complement and platelet activation, which may lead to thrombus formation and facilitates the attachment of nosocomial pathogens.[105-107] Therefore, the successful use of scaffolds in tissue engineering can only be conceived if firstly their surface is engineered to minimize protein fouling and subsequently the essential biological cues are incorporated without affecting the properties of the scaffold.

4 Challenges of Tissue Engineering

The current progress in the field of tissue engineering has brought considerable improvements in the healthcare field. The advantages in the basic strategy of tissue engineering that include the combination of artificial scaffolds with cells in order to induce new tissue production and regeneration of their functions has already resulted in many applications in clinical practice for the treatment of patients.[4]

Despite all the advantages and breakthroughs achieved there are many challenges yet to solve. The classic paradigm is based on the idea that tissue engineering lays on three main pillars: the scaffold, cells and signals. As discussed above each of these parts has considerable challenges, however, if the mimicking of native tissues is to be achieved an integrated approach is necessary. This integrated approach must consider the challenges of the three pillars together. For instance, it is critical to access reliable cell sources sufficient for the restoration of damaged tissue and to understand how the cells function at molecular level and how they respond to a given signals. Additionally, the viability of the cells upon transplantation is reduced due to limited diffusion of oxygen and nutrients.[4, 108] Hence, another important issue arises: cells need to be in a very close proximity to blood vessels and it may take weeks and months for vascularization to reach the cells, leading to cell and tissue death. Vascularization is another major challenge for the fabrication of functional tissue and organ replacements. This problem is substantial especially for the creation of large scale 3D tissues.[4, 109] The efficient diffusion of oxygen, nutrients and waste products is critical for cell survival and normal metabolism. Currently many studies are focused on the prevascularization of the scaffold before implantation; however, the development of a complex vascular network and its integration with host vasculature remain critical issues.

The current paradigm of tissue engineering assumes that the fate of the engineered tissue is dictated by the design and control of the interactions between (bio)material and cells. Arguably, the control of such interactions is one or perhaps the most difficult challenge to be met. To date the mechanisms behind the interaction between cells and scaffold remain not fully understood. It is essential not only to identify which biological cues are important but also to select the optimal way of presenting them. The latter is usually neglected, even if the enormous importance of surface organization, clustering, and

distances of the biological cues has already been recognized.[110-114] This also comes together with other properties of the surface of the material interfacing the world (cells and biological media) such as the mechanical properties of the surface, surface chemistry, etc. Mechanobiology has recently showed —for a limited number of biological ligands on surfaces— that the elasticity of the surface can even produce changes in the phenotype and functions of cells.[111]

The understanding of these interactions requires the systematic study of scaffolds with encoded biological, chemical and physical cues. However, to be able to embark on such an extremely complex systematic study, it is of utmost importance to prevent any non-specific interaction, usually caused by protein fouling.

The contact between biological media and an artificial material commonly starts with protein adsorption.[115-118] Various amino acid residues on the peptide backbone can mediate adsorption of proteins via hydrogen bonds, ionic and other polar or hydrophobic interactions.[115, 116] The protein adsorption from biological media is a complex and dynamic process in which proteins can change their conformation thus, firstly adsorbed proteins can be subsequently replaced with proteins of higher affinity to the surface.[119] Non-specific protein adsorption or fouling from complex biological fluids irreversibly affects the properties of the scaffolds.

As mentioned before, a successful scaffold for tissue engineering requires to be decorated with biological cues able to promote/guide the formation of a functional tissue so that the functions of the organ are restored. However, protein fouling interferes with the signaling mechanisms by masking the biological elements immobilized at the surface and by creating a film of proteins which supports non-specific adhesion of cells. Besides this, the protein fouling usually leads to the initiation of the coagulation cascade, immune responses and even fibrous capsule formation. Therefore scaffolds able to prevent the fouling and thrombosis are necessary. Although modification of 2D surfaces with coatings resistant to fouling has been achieved, the problem of protein fouling for 3D scaffolds for tissue engineering is generally neglected. Only few attempts were made in the preparation of 3D scaffolds able to resist protein fouling and most of them were based on the utilization of PEG.[120-122] PEG-based materials have been widely studied and have been considered as the gold standard for the prevention of protein fouling. However, it has been

proved that PEG-based surface modifications cannot meet the challenge. Their contact with real biological media led to fouling regardless of the type of polymer architecture.[64, 102, 121, 123, 124] Thus it is imperative to develop new strategies to prepare scaffolds that prevent fouling, a real biotechnological plague.

In view of this, it was clear that in order to fabricate functional scaffolds for tissue engineering, the protein fouling from complex biological media on the surface of the scaffold must be prevented. Consequently, the topic of my PhD work was set.

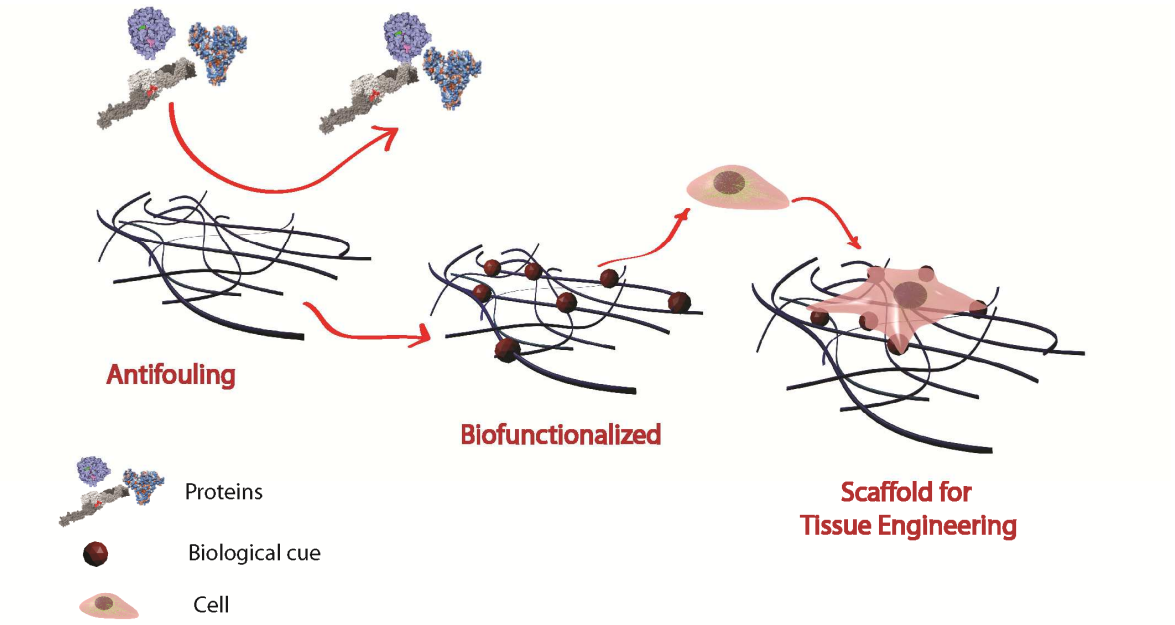

Figure 9. Fabrication of antifouling biofunctionalized scaffolds for tissue engineering

Goals of the Thesis

As explained in the previous chapter, the scaffolds for tissue engineering must provide not only structural support for the cells but also interact with cells providing special biological signals and cues for specific cell attachment, proliferation and new tissue formation. However, upon the contact with bodily fluids, the surface of nearly all exogenous materials is rapidly covered by a layer of proteins. The adsorbed proteins cover the bioactive compounds previously immobilized on the surface, which causes the loss of control over cell behavior. Moreover, fouling may induce severe inflammation, facilitate the attachment of microorganisms, thrombus formation, generation of a fibrous capsule around the implant and ultimately lead to rejection of the material. Therefore, the main objective of my Thesis was to fabricate scaffolds for tissue engineering resistant to non-specific protein adsorption from complex biological media, *i.e.* antifouling. It is envisioned that such an antifouling scaffold will become a starting platform for further functionalization with bioactive compounds for specific interaction of the scaffold within the physiological milieu.

The work has three main foci:

• The selection of monomers suitable for the preparation of antifouling scaffolds utilizing model system based on polymer brushes

• Preparation of antifouling hydrogels with different properties and architecture synthesized by copolymerization with zwitterionic carboxybetaine monomers

• Modification of nanofibers with selected antifouling polymer brushes

Summary of Results

1 Selection of Monomers[†]

The resistance to protein fouling is central for the control of the interaction of the scaffold with the biological world and to avoid the occurrence of adverse effects. From previous studies it is well known that to avoid protein adsorption the surface of the material must not be hydrophobic or charged.[123, 125] However, there are a very large number of monomers which fulfill these requisites. In this chapter the assessment of the resistance to fouling of various polymers is presented. The results obtained in this chapter are the basis for the selection of the polymers to be used for the scaffold design along this thesis.

Accurately measuring the fouling on scaffolds is very challenging. This is even more difficult when it is necessary to determine extremely low values of fouling. Thus, it was necessary to develop a model system to enable the fast screening of various monomers and those which displayed the best resistance to fouling were selected for the following work on scaffold design presented in this thesis.

Surface plasmon resonance (SPR) is one of the most sensitive techniques to measure changes occurring on the surface of materials. [126] When molecules adsorb to the surface of an SPR sensor, the refractive index changes, causing a change in the propagation constant of light and the concomitant change in the resonant wavelength of the plasmons. The change in the resonant wavelength can be directly correlated with the amount of mass

[†] Parts of the chapter were reproduced from Kostina, N. Yu.; Rodriguez-Emmenegger, C.; Houska, M.; Brynda, E.; Michalek, J. *Biomacromolecules*, 2012, 13 (12), 4164-4170; de los Santos Pereira, A.; Kostina, N. Yu.; Bruns, M.; Rodriguez-Emmenegger, C.; Barner-Kowollik, C. *Langmuir*, 2015, 31(21), 5899-5907, and Surman, F.; Riedel, T., Bruns, M.; Kostina, N. Yu.; Sedláková, Z.; Rodriguez-Emmenegger, C. *Macromolecular Bioscience*, 2015, 15(5), 636-646. All the experimental methods for this chapter are described in Appendices 1-3.

deposited on the surface. However, the evanescent nature of the electromagnetic field of SPR results in this technique being only sensitive to changes occurring not further than approximately 100 nm away from the surface of the sensor. Thus, to study the fouling, the polymer layer should not exceed this thickness. In order to have a precise model system polymer brushes were utilized. The monomers to be assessed were grown from self-assembled monolayers of initiators formed on the gold-coated SPR sensors. The brushes were grown by previously optimized surface-initiated atom transfer radical polymerization (SI-ATRP). The controlled nature of the polymerization allowed to prepare brushes with precise thickness in a reproducible manner.

1.1 Synthesis and Characterization of Polymer Brushes

Polymer brushes based on hydrophilic electroneutral monomers, such as 2-hydroxyethyl methacrylate (HEMA), *N*-(2-hydroxypropyl) methacrylamide (HPMA), oligo(ethylene glycol) methyl ether methacrylate (MeOEGMA), and oligo(ethylene glycol) methacrylate (HOEGMA) as well as zwitterionic monomers, such as sulfobetaine methacrylate (SBMA), phosphorylcholine methacrylate (PCMA), carboxybetaine methacrylate (CBAA), and carboxybetaine methacrylamide (CBMAA) were grown from self-assembled monolayers of initiator on gold or silicon surfaces at room temperature (Scheme 3). Surface-initiated atom transfer radical polymerization (SI-ATRP) was selected for the synthesis of polymer brushes due to the ease of implementation and its capability to polymerize a broad range of monomers. The thickness of polymer brushes was kept bellow 30 nm in dry state as determined by spectroscopic ellipsometry (SE) (Table 1). In previous studies from our group, it has been demonstrated that higher thicknesses do not improve the resistance to fouling but only impair the correct detection of fouling via SPR. SPR measures the changes in the refractive index in the close vicinity (*ca.* 100 nm) of the gold surface due to the evanescent nature of its electromagnetic field.

The chemical structure of the brushes was confirmed by XPS (Figure 10 and 11)[*]. The high-resolution XPS spectra of the C 1s region for poly(HEMA), poly(HOEGMA), poly(MeOEGMA), poly(SBMA) and poly(PCMA) show a contribution approximately at 288.9 eV corresponding with the methacrylate ester (Figure 10, left). For poly(CBAA),

[*] XPS measurements was performed by Dr. Pop-Georgievski

poly(CBMAA), and poly(HPMA) the peak observed at 287.9 eV arises from the (meth)acrylamide in the structure (Figure 10, left). Poly(HOEGMA) and poly(MeOEGMA) show a dominant contribution from C–O at 286.7 eV which originates from the oligo(ethylene glycol) side chains (Figure 10, left). In the case of poly(HEMA) this peak is observed with lower intensity due to the single ethylene glycol unit per monomeric unit. Poly(SBMA), poly(PCMA), poly(CBAA), poly(CBMAA) and poly(HPMA) present a peak at 286.3 eV, which is caused by the C–N bonds in the covalent structure (Figure 10, left).

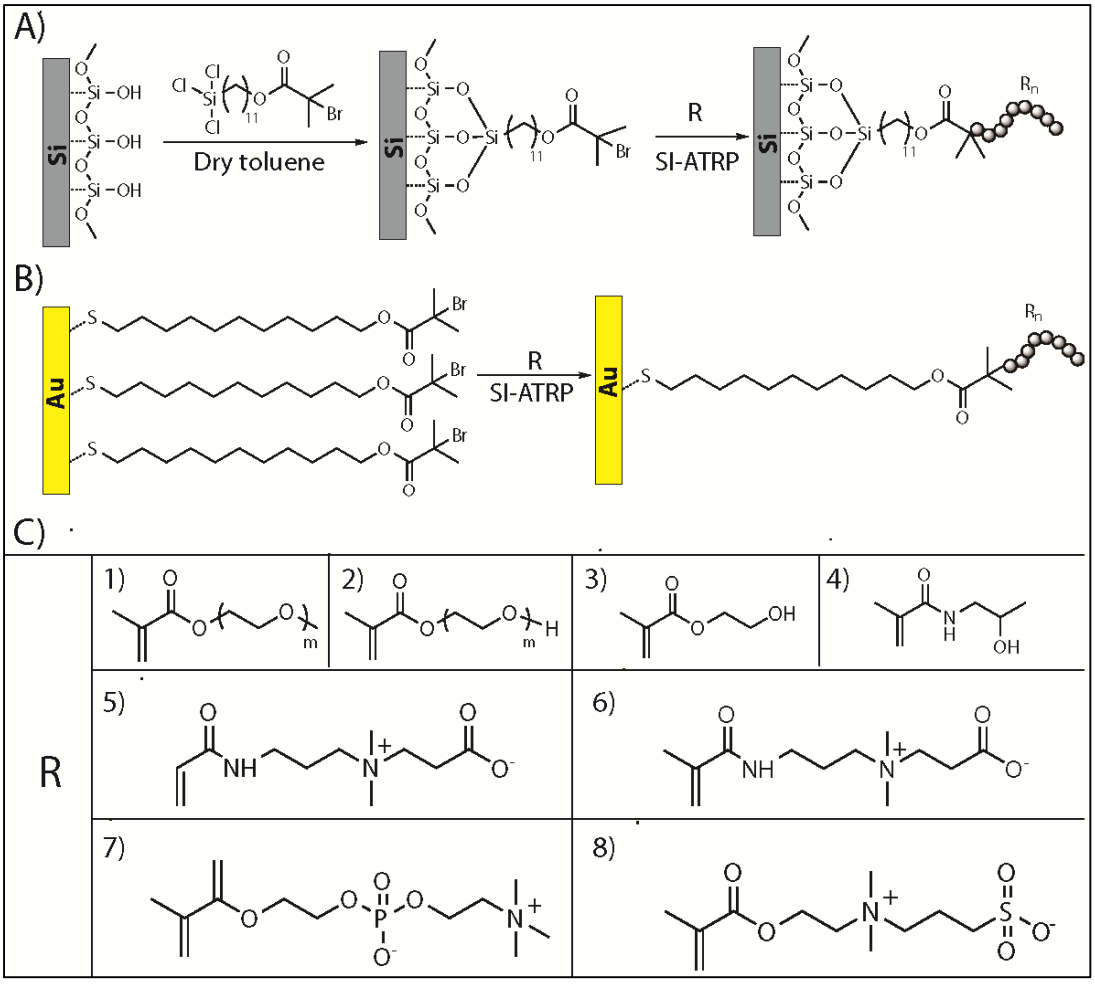

Scheme 3. (A) Immobilization of the ATRP initiator SAM on silicon followed by SI-ATRP; (B) synthesis of polymer brushes by SI-ATRP from self-assembling monolayer of initiator on gold; (C) and chemical structures of monomers utilized for synthesis of the polymer brushes, where (1) MeOEGMA; (2) HOEGMA; (3) HEMA; (4) HPMA; (5) CBAA; (6) CBMAA; (7) PCMA, and (8) SBMA.

Table 1. Thickness of polymer brushes determined by SE.

Polymer	Thickness of the polymer layer [nm]
Poly(MeOEGMA)	30.6
Poly(HOEGMA)	30.2
Poly(HEMA)	28.7
Poly(HPMA)	29.5
Poly(CBAA)	22.2
Poly(CBMAA)	19.5
Poly(SBMA)	25.2
Poly(PCMA)	31.1

As expected, the high resolution N 1s spectra (Figure 10, right) of poly(HEMA), poly(HOEGMA) and poly(MeOEGMA) lacked contributions of nitrogen, whereas two peaks were observed on those brushes containing this element. The contributions in the N 1s spectra of poly(HPMA) and poly(CBAA) at 399.7 and 400.3 eV arise from the acrylamide and (meth)acrylamide groups. The positively charged quaternary ammonium group in poly(SBMA), poly(PCMA), poly(CBAA), poly(CBMAA), and gives rise to the peak at 402.5 eV.

The high resolution S 2p spectrum of poly(SBMA) brushes (Figure 11A) is characterized by a split spin $2p_{1/2}$ – $2p_{3/2}$ doublet having its contributions at 168.6 and 167.4 eV. These contributions prove the presence of sulfur in the negatively charged C-$(SO_3)^-$ species. Similarly the P 2p spectrum of poly(PCMA) (Figure 11B) could be deconvoluted with one $2p_{1/2}$-$2p_{3/2}$ doublet with contributions at 133.0 and 134.0 eV originating from the $(PO_4)^-$ groups of the side chain.

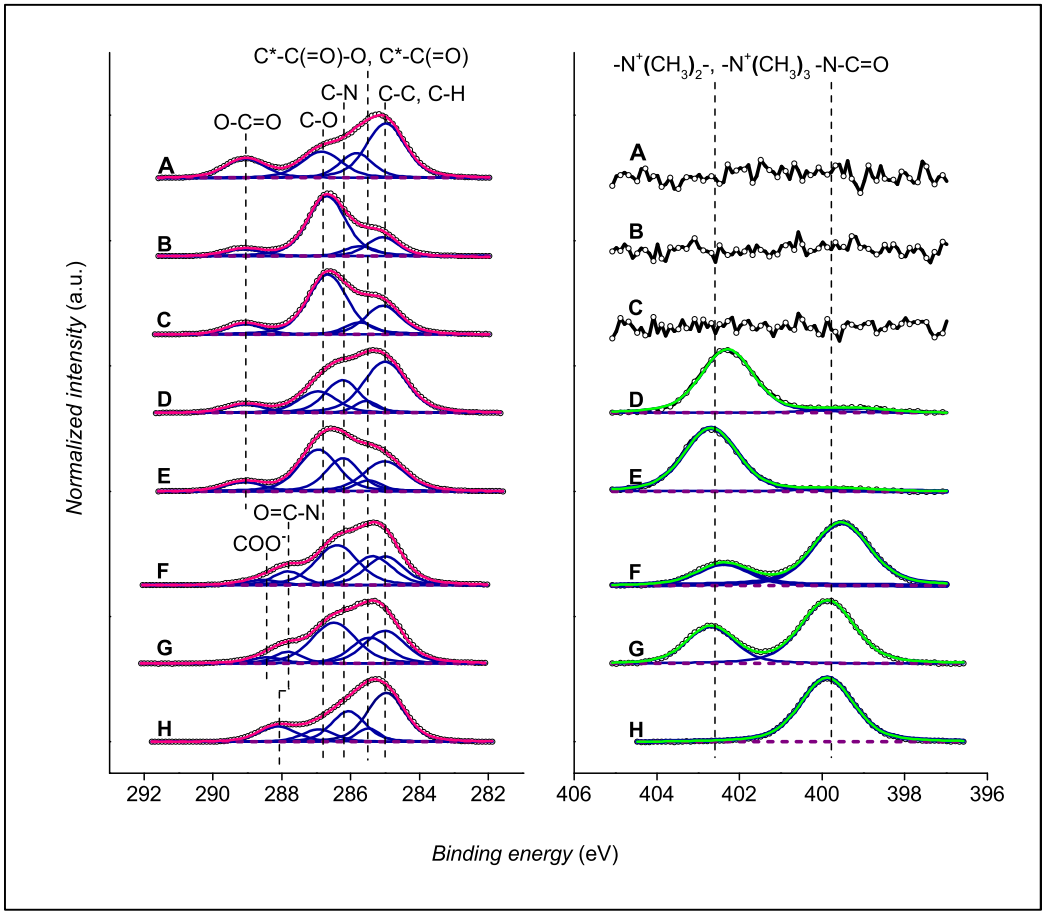

Figure 10. High resolution C 1s (left) and N 1s (right) XPS spectra of (A) poly(HEMA), (B) poly(HOEGMA), (C) poly(MeOEGMA), (D) poly(SBMA), (E) poly(PCMA), (F) poly(CBAA), (G) poly(CBMAA), and (H) poly(HPMA) polymer brushes.

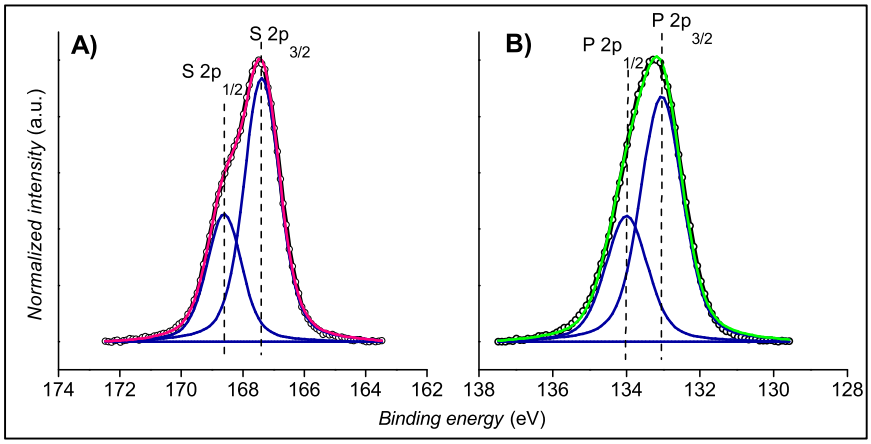

Figure 11. High resolution S 2p (left) and P 2p (right) XPS spectra of poly(SBMA) and poly(PCMA), respectively

The growth of polymer brushes was accompanied by an increase in the surface wettability. This is evidenced by the reduction in the dynamic water contact angles owing to the hydrophilic character of the polymer side chains (Table 2). The more pronounced decrease in the receding contact angles can be explained by the strong interaction with water of the swollen polymer layers. The polymers presenting zwitterionic groups hydrate more strongly, resulting in the lowest water contact angles.

High roughness and presence of pinholes can cause high protein fouling and preferential places for protein or cell adsorption. Thus, the morphology of the polymer brushes was assessed by AFM (Figure 12 and 13). All brushes displayed a homogenous coating of the surface without pinholes. The observed roughness (R_q) on the brushes was below 2.5 nm and no special organization or assemblies could be distinguished on the surfaces suggesting that the brushes were highly homogenous and closely packed.

Table 2. Dynamic contact angle.

Surface	**Water contact angle [°]**	
	Advancing	**Receding**
Gold	75	63
Poly(MeOEGMA)	59	27
Poly(HOEGMA)	55	26
Poly(HEMA)	55	34
Poly(HPMA)	52	9
Poly(PCMA)	18	7
Poly(CBAA)	23	8
Poly(CBMAA)	30	10
Poly(SBMA)	20	5

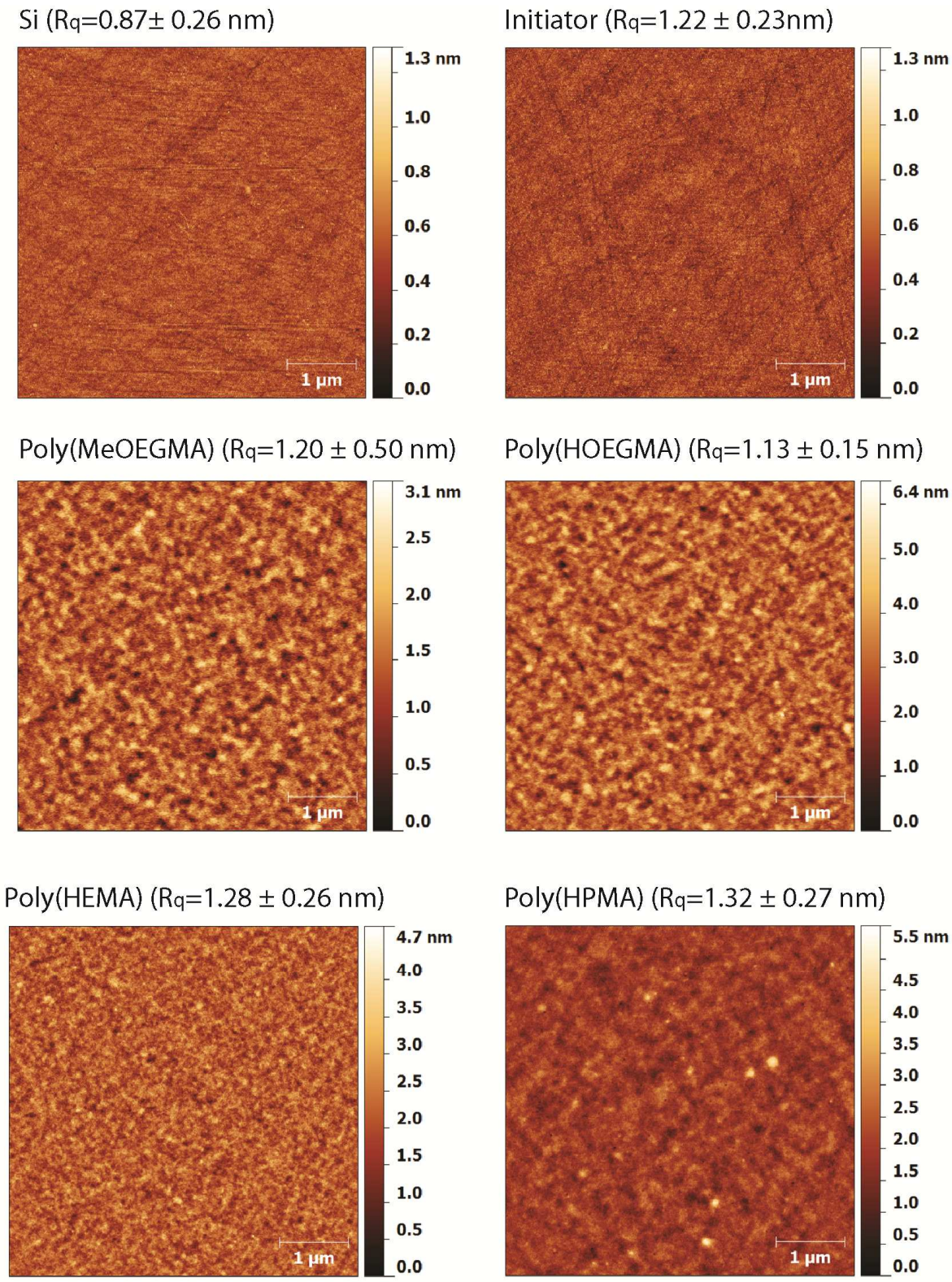

Figure 12. Representative AFM topography images of electroneutral polymer brushes grown from the surface of silicon chips. The root-mean-square roughness (R_q) is reported for each figure. The scale bar is 1 µm

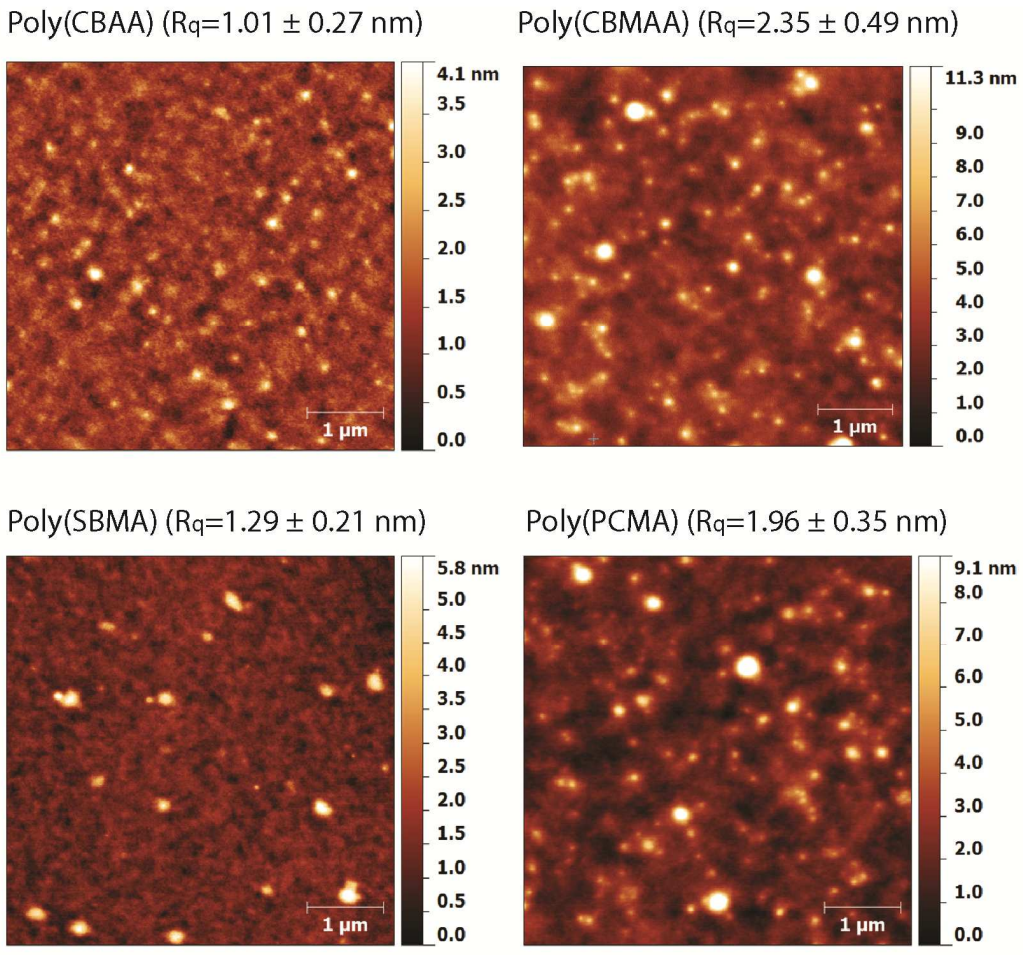

Figure 13. Representative AFM topography images of the zwitterionic polymer brushes grown from the surface of silicon chips. The root-mean-square roughness (R_q) is reported for each figure. The scale bar is 1 µm.

1.2 Protein Fouling Assessment

The resistance to protein fouling was studied with SPR. The custom made SPR has a limit of detection of 0.2 ng·cm^{-2} which represents about 0.01% of a protein monolayer.[127] The polymer brushes were challenged with model buffered solutions of human serum albumin (HSA) (5 mg·mL^{-1}), fibrinogen (Fbg) (1 mg·mL^{-1}), and undiluted human blood plasma (BP). HSA was selected because it is the most abundant protein in blood while Fbg was chosen due to its central role in the coagulation cascade. Undiluted blood plasma was also assessed as it is the most fouling bodily fluid.

The protein solutions were contacted with the surfaces for 15 min while the changes in the resonant wavelength of surface plasmon were recorded. A 1 nm shift in the resonant wavelength in the utilized SPR is equivalent to 150 pg·mm^{-2}. The irreversible fouling is displayed in Figure 14. The fouling on bare gold was measured as a positive control.

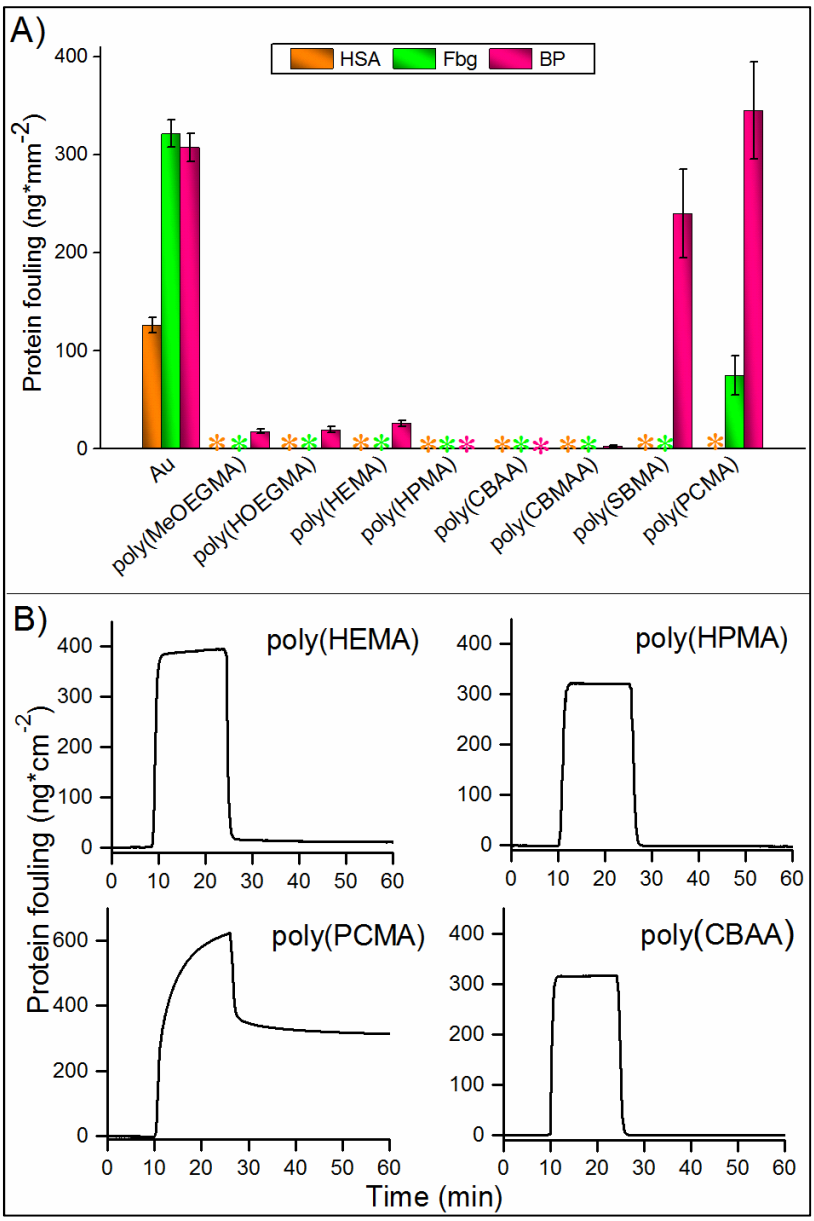

Figure 14. (A)Fouling from undiluted BP (pink), HSA- (orange) and Fbg-buffered solution (green). An asterisk represents a value of protein adsorption below the detection limit of SPR (0.2 ng·cm^{-2}). (B) SPR traces showing the fouling from undiluted BP on poly(HEMA), poly(HPMA), poly(SBMA), poly(CBAA).

All the brushes tested fully resisted the fouling from HSA (Figure 14), the most abundant plasma protein. Analogously, all brushes except for PCMA completely prevented Fbg adsorption. This is in sharp contrast with the generalized claims that Fbg is a "highly sticky" protein. The claimed is rooted in the belief that because fibrinogen has a major role in the coagulation cascade it should be fouling. While most brushes readily resist the adsorption from model solutions of buffered proteins, undiluted blood plasma (BP) posed a much higher challenge. The highly hydrophilic brushes based on poly(PCMA) and poly(SBMA) were not able to resist the fouling from undiluted BP, leading to protein deposits on poly(PCMA) (345 $ng \cdot cm^{-2}$) and poly(SBMA) (240 $ng \cdot cm^{-2}$) that are close to a protein monolayer (Figure 14). Phosphorycholine was introduced as a mimic of phospholipid in cell membranes with the hope of obtaining a biomimetic surface with resistance to fouling. Unfortunately, the results presented here clearly show that brushes based on this monomer are not able to resist fouling from complex biological media. Poly(MeOEGMA), poly(HOEGMA) and poly(HEMA) displayed very low fouling corresponding to a 18 $ng \cdot cm^{-2}$, 20 $ng \cdot cm^{-2}$, and 26 $ng \cdot cm^{-2}$, respectively (Figure 14 and 15). These figures correspond to a decrease in fouling of about 90 – 95% compared to bare gold. Poly(CBMAA) brushes (a methacrylamide) showed remarkable 99% reduction in protein fouling in comparison with bare gold (Figure 14). It is noteworthy, that only two surfaces were able to reach undetectable levels of protein fouling from undiluted BP, brushes based poly(CBAA) and poly(HPMA) brushes (Figure 14).

1.3 Summary

In this chapter, eight monomers were screened by utilizing model systems based on polymer brushes synthesized by SI-ATRP. The resistance to protein fouling from buffered solutions of HSA and Fbg and from undiluted BP was evaluated by one of the most sensitive technique, SPR. Based on the knowledge gained from these studies, the monomers showing the best resistance to non-specific protein adsorption such as MeOEGMA, HOEGMA, HPMA, CBAA and CBMAA were selected for the further preparation and/or modification of the scaffold for tissue engineering presented in this thesis.

2 *Non-fouling Poly(HEMA-co-CB(M)AA) Hydrogels*[†]

Among various classes of materials for tissue engineering scaffolds, hydrogels are of great interest due to their tunable viscoelastic mechanical properties, high water content, and structural similarity to macromolecular-based components of the body, which mimics the interstitial tissue environment ensuring high diffusion.[7, 8, 49, 58, 74] Poly(HEMA) hydrogels are very attractive for biomedical applications due to their chemical stability, good biocompatibility, hydrophilic character, excellent mechanical properties, and low level of immunogenicity.[58, 128, 129] However, despite all these advantages, the use of poly(HEMA) hydrogels is limited by a moderate wettability, which is lower than that of most natural tissues.[8] Additionally, Brynda *et al*. showed that poly(HEMA) hydrogel suffers from important protein fouling, equivalent to 0.23±0.01 μg·cm^{-2} (ca. 50% of a protein monolayer) only from Fbg.[104] Moreover, fouling from blood plasma is considerably higher and can lead to irreversible changes in the surface properties and loss of the control over the functions and fate of the material.[104, 106, 117, 123] Therefore, in order to design new biomaterials with tailor-made properties, prevention of protein fouling, in particular from blood plasma, is essential.

In this chapter an avenue to address the aforementioned drawbacks by combining the excellent mechanical properties of poly(HEMA) hydrogels with the resistance to blood plasma fouling of zwitterionic carboxybetaine polymers, such as poly(CBAA) and poly(CBMAA) is introduced. It was hypothesized that the addition of zwitterionic monomers to the widely used poly(HEMA) hydrogels would result in novel highly wettable and protein-resistant materials (Figure 15).

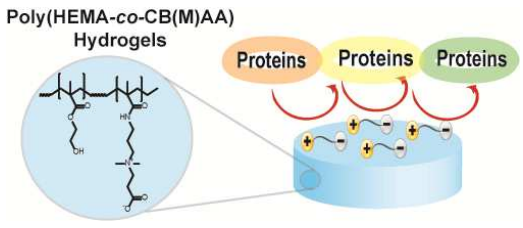

Figure 15. Illustration of the hypothesis that addition of zwitterionic carboxybetaine comononer will lead to highly wettable and protein fouling resistant hydrogels.

[†] Parts of the chapter were reproduced from Kostina, N. Yu.; Rodriguez-Emmenegger, C.; Houska, M.; Brynda, E.; Michalek, J. *Biomacromolecules*, 2012, 13 (12). All the experimental methods for this chapter are described in Appendix 3.

2.1 *Preparation and Characterization of the Hydrogels*

Poly(HEMA), poly(HEMA-*co*-CBAA), and poly(HEMA-*co*-CBMAA) hydrogels were synthesized by photoinitiated radical polymerization with different molar concentrations of zwitterionic comonomer (Table 3). Ethylene glycol dimethacrylate and benzoin ethyl ether were utilized as crosslinker and initiator, respectively (Scheme 4). Monomer conversion for all compositions was about 95%, as determined gravimetrically. All hydrogels were transparent and robust in the swollen state.

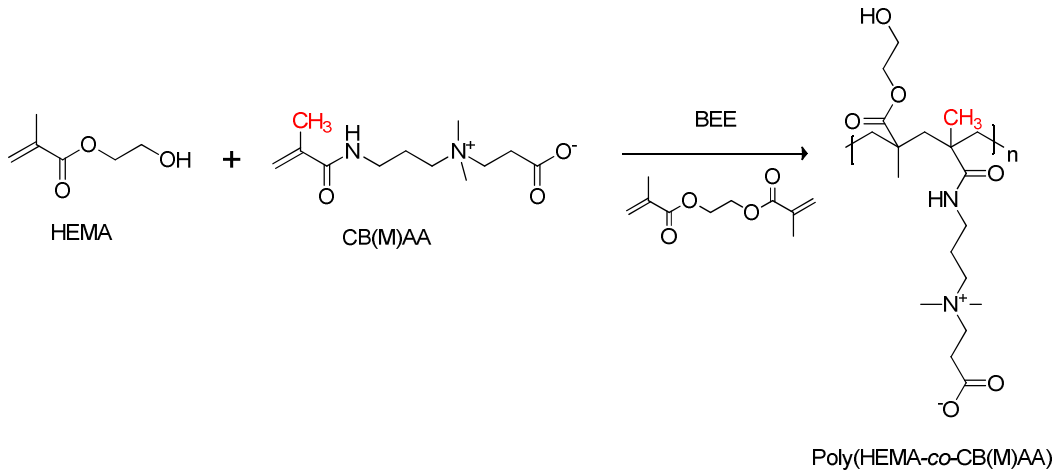

Scheme 4. Synthesis of the poly(HEMA-*co*-CBAA) and poly(HEMA-*co*-CBMAA) hydrogels.

Table 3. Composition of formulations of poly(HEMA), poly(HEMA-*co*-CBAA), and Poly(HEMA-*co*-CBMAA) hydrogels with different molar ratio of comonomers.

Hydrogel name	HEMA/CBAA	Hydrogel name	HEMA/CBMAA
Poly(HEMA)	1/0		
1%CBAA	0.990/0.010	1%CBMAA	0.990/0.010
2.5%CBAA	0.975/0.025	2.5%CBMAA	0.975/0.025
5%CBAA	0.950/0.050	5%CBMAA	0.950/0.050
7.5%CBAA	0.925/0.075	7.5%CBMAA	0.925/0.075
10%CBAA	0.900/0.100	10%CBMAA	0.900/0.100

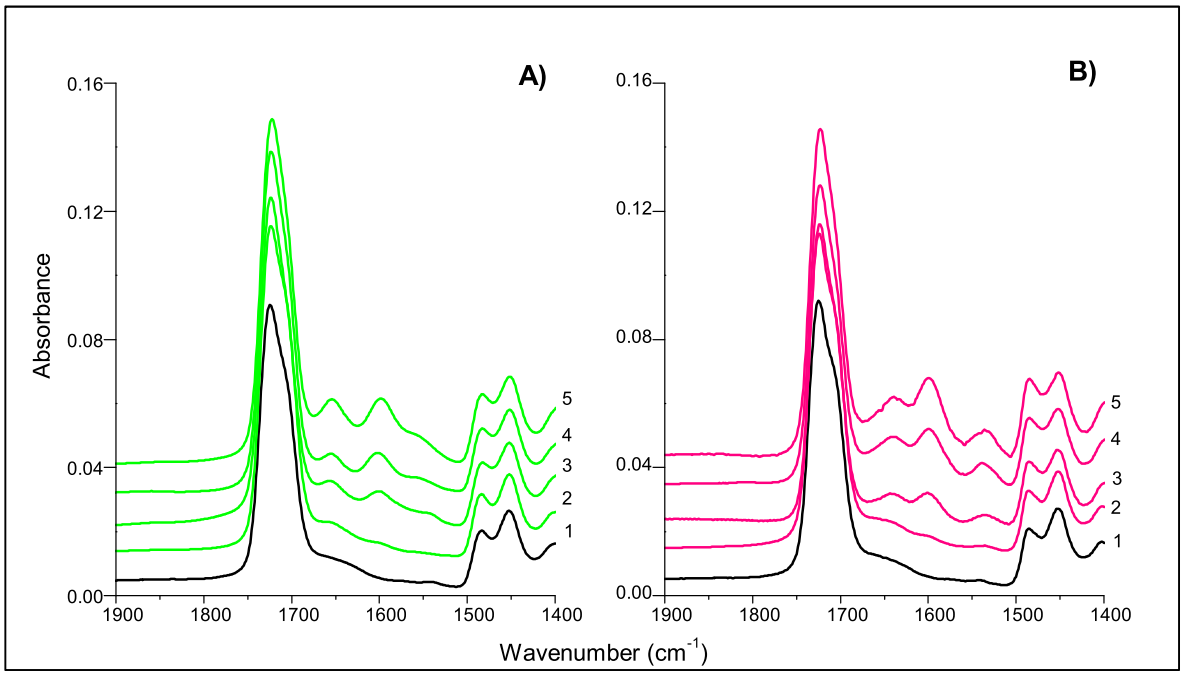

Figure 16. Amidic region of the FTIR-ATR spectra of hydrogels of (A) poly(HEMA-*co*-CBAA) and (B) poly(HEMA-*co*-CBMAA) for different concentration of the zwitterionic monomer: (1) 0%, (2) 1%, (3) 5%, (4) 7.5%, and (5) 10%.

The successful copolymerization was confirmed by FTIR-ATR spectroscopy (Figure 17). The increase in the amount of zwitterionic comonomer was in good agreement with the increase in the intensity of amide bands at 1654 cm^{-1} and 1558 cm^{-1}, and the carboxyl band at 1609 cm^{-1} arising from the betaines added (Figure 16).

The equilibrium water content (EWC) for poly(HEMA), poly(HEMA-*co*-CBAA), and poly(HEMA-*co*-CBMAA) hydrogels was calculated by the difference in mass of fully hydrated (m_s) and dehydrated gels (m_d) (Equation 1, Figure 17). The swelling behavior and water content are very important properties for hydrogels for bioapplications. High water content, close to that of natural tissues, is essential for cell growth and proliferation.[19, 78, 130] While HEMA can only bind water *via* hydrogen bonding with its hydroxyl group, carboxybetaines can bind water more and strongly water *via* electrostatic interactions.[131] The EWC steadily increases with the addition of betaines to the polymerization feed.

$$EWC(\%) = \frac{m_s - m_d}{m_d} * 100\% \qquad \text{(Equation 1)}$$

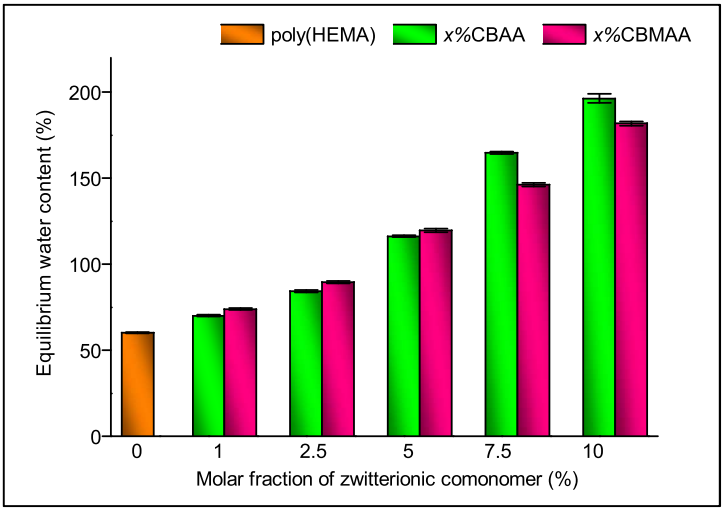

Figure 17 EWC of poly(HEMA) (orange), poly(HEMA-*co*-CBAA) (green), and poly(HEMA-*co*-CBMAA) (pink) with different molar ratios of carboxybetaines.

Remarkably, even a small addition such as 5 mol% led to 2-fold increase in the amount of water in the hydrogel with the EWC reaching a value of 116.0±0.5% for poly(HEMA-*co*-CBAA) and 119.0±0.9% for poly(HEMA-*co*-CBMAA). A further increase to 10 mol% of CBAA or CBMAA in the polymerization feed accounted for an EWC of 196.0±2.0% and 181.0±1.2% respectively, *i.e.* hydrogels binding approximately 4 times more water than pure poly(HEMA). In this way, the EWC of hydrogels can be easily tuned to match the desired application by varying the ratio of monomers.

In order to evaluate the effect of the high water content of the hydrogels on the mechanical properties, the tensile strength, tensile stress at break and Young's modulus were determined on fully hydrated poly(HEMA), poly(HEMA-*co*-CBAA), and poly(HEMA-*co*-CBMAA) hydrogels (Figure 18). All the mechanical tests were carried out in water to prevent drying of the swollen samples. All zwitterionic hydrogels showed very similar elastic behavior comparable to poly(HEMA) hydrogels (Figure 18A). The addition of zwitteroinic comonomer of 1 mol% resulted in materials with mechanical behavior similar to the widely used poly(HEMA) hydrogels with tensile stress at break as high as 600 kPa (Figure 18B) and a Young's modulus of 850 kPa (Figure 18C). A gradual decrease of resistance to break was observed with increasing amount of carboxybetaine, probably due to the higher amount of incorporated water (Figure 18B). Hydrogels with 5%CBAA and 5%CBMAA containing 2 times more water than those based only on

poly(HEMA) (EWC~120%), were able to resist stress as high as 300 kPa. In spite of the big increase of EWC of the zwitterionic hydrogels, the Young's modulus decreased slightly. The hydrogels with 5% of zwitterionic comonomer showed only a 25% decrease in the Young's modulus while having an EWC twice as high as that of pure poly(HEMA) hydrogels (Figure 18C).

Only minor differences in the EWC and mechanical properties of hydrogels based on CBAA and CBMAA were observed. Due to the differences in hydrophilicity between acrylamides and methacrylamides, the hydrogels containing CBMAA bound less water compared to those based on CBAA and therefore their mechanical properties are slightly better.

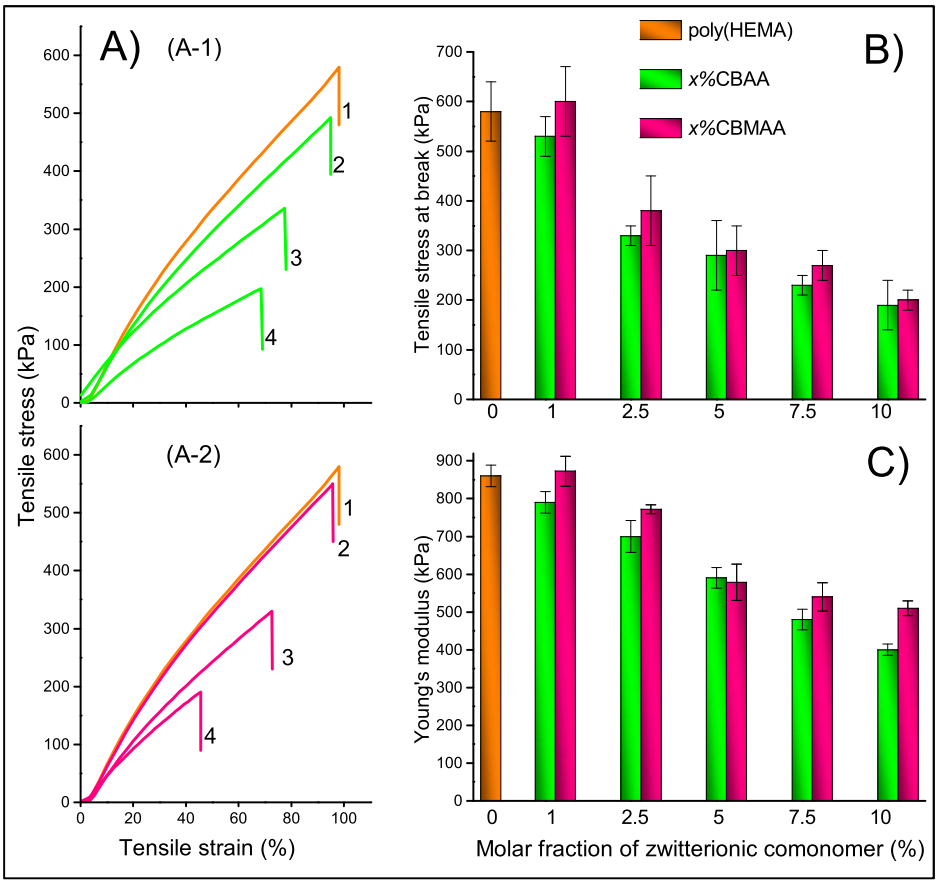

Figure 18. Mechanical properties of hydrogels. (A) Stress–strain curves of (A-1) poly(HEMA-*co*-CBAA) and(A-2) poly(HEMA-*co*-CBMAA) for molar ratios of carboxybetaines of(1) 0%, (2) 1%, (3) 5%, and (4) 10%. (B) Tensile stress at break and (C) Young's modulus of poly(HEMA) (orange), poly(HEMA-*co*-CBAA) (green), and poly(HEMA-*co*-CBMAA) hydrogels (pink).

2.2 *Protein Fouling Test*

Poly(HEMA) hydrogels with different contents of carboxybetaines (0, 1, 5, and 10 mol%) were incubated in undiluted human BP. The protein fouling was evaluated by FTIR-ATR. Spectra of each sample were recorded before and after incubation and washing. Figure 19 shows the amide region before and after contact of hydrogels with BP. Pure poly(HEMA) hydrogels suffered an important protein fouling as evidenced by an increase in the region of 1648 cm^{-1} and 1545 cm^{-1} (Figure 19). Hydrogels containing the zwitterionic comonomers showed an important reduction in plasma fouling. More than 40% and 50% of the fouling could be reduced by addition of 1 mol% of CBAA or CBMAA, respectively. Hydrogels with 5 mol% of CBAA or CBMAA further reduced the fouling by 70% and 65% (Figure 19). Remarkably, no fouling from BP could be detected when the content of CBAA was 10 mol% (Figure 19), while only minor protein fouling (95% reduction) was observed on the 10%CBMAA hydrogel (Figure 19). The high adsorption from BP on pure poly(HEMA) hydrogels and the higher protein resistance of CBAA compared to CBMAA is in close agreement with the results observed on the model based on polymer brushes.[104]

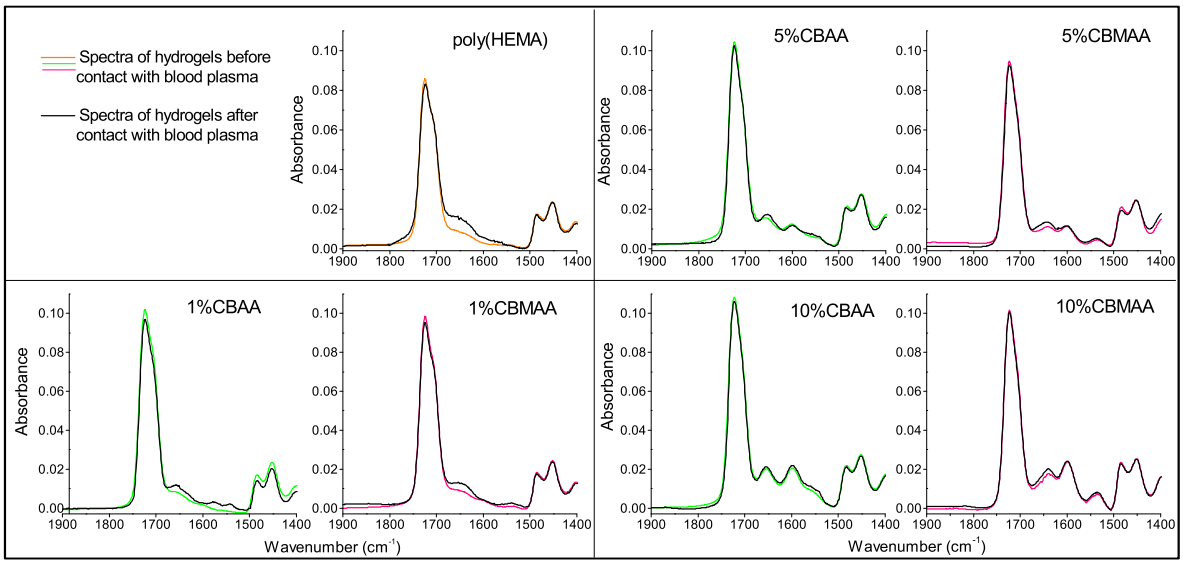

Figure 19. FTIR-ATR spectra (amidic region) of poly(HEMA) (orange line), poly(HEMA-*co*-CBAA) (green line), and poly(HEMA-*co*-CBMAA) (pink line) before and after (black line) 3 h contact with BP.

2.3 Summary

Carboxybetaine monomers were selected as comonomers for the fabrication of hydrogels based on poly(HEMA) due to their resistance to blood plasma fouling and to improve hydration. Even small additions (1 – 5%) of carboxybetaine monomers led to a very high increase in the EWC without impairing the mechanical properties. All zwitterionic hydrogels prepared showed an unprecedented reduction of fouling from blood plasma; in particular, copolymers of HEMA with 10% of CBAA led to hydrogels fully resistant to blood plasma adsorption. Additionally, the copolymerization of HEMA with CBAA or CBMAA results in hydrogels with readily biofunctionalizable carboxyl groups arising from carboxybetain moieties. The carboxyl groups can be utilized for the further immobilization of bioactive molecules to the hydrogel in order to induce specific interactions and signaling to cells.

All these advantages make these hydrogels very promising for biomedical applications. However, due to the fixed and rigid junction points, chemically cross-linked hydrogels are restricted in the degree of freedom for rearrangements of polymer chains in response to high load, and are not able to self-heal, *i.e.* to autonomously and spontaneously repair themselves, which reduce the number of possible applications.

3 Self-healing Poly(HEMA-co-CBMAA) Nanocomposite Hydrogels with Superior Mechanical Properties[†]

Hydrogel possessing the ability to self-heal and to withstand a high degree of deformations are very attractive for tissue engineering. Such materials can mimic the tissues of living organisms which are able to heal and re-shape after external stimuli. Moreover, if mechanical damage to materials could be repaired autonomously, it would be possible to increase the useful lifetime of materials and reduce the total cost of systems in the long term.

Current advances in hydrogel fabrication have resulted in different strategies for the development of self-healing and mechanically robust hydrogels.[51, 132, 133] The most common approach is the preparation of nanocomposite gels consisting of polymer chains physically cross-linked with particles. The physical crosslinking of hydrogels not only endows self-healing properties, but can also improve the mechanical properties of the hydrogels.[134, 135] However, the physical cross-link may lead to leaching of the cross-linking agent.

In this chapter a novel type of self-healing hydrogels was fabricated. The preparation consisted in the free radical copolymerization of CBMAA and HEMA in the presence of Laponite XLG clay nanoparticles (LN). The rationale behind the concept was that negatively charged LN nanoparticles would act as a physical crosslinker for poly(HEMA-*co*-CBMAA). As CBMAA bears charged groups (quaternary ammonium) it is expected to interact strongly with LN as well as to prevent the fouling.

3.1 Preparation and Characterization of the Hydrogels

With the aim of achieving improved mechanical and self-healing properties, nanocomposite poly(HEMA-*co*-CBMAA) hydrogels with different molar concentrations of zwitterionic comonomer and LNs were synthesized by radical polymerization

[†] Parts of the chapter were reproduced from Kostina, N. Yu.; Sharifi, S.; de los Santos Pereira, A.; Michálek, J.; Grijpma, D. W.; Rodriguez-Emmenegger, C. *Journal of Materials Chemistry B*, 2013, 1 (41), 5644-5650. All the experimental methods for this chapter are described in Appendix 4.

photoinitiated with Irgacure (2-hydroxy-1-[4-(2-hydroxyethoxy)phenyl]-2-methyl-1-propanone) and crosslinked by LNs (Table 4).

Table 4. Formulation of the prepared hydrogels as a function of the molar ratio of monomers and the concentration and the concentration of Laponite nanoparticles (LN).

Molar ratio of HEMA/CBMAA	Concentration of LN, wt%		
	1	3	5
100/0	HEMA1LN	HEMA3LN	HEMA5LN
95/5	5CBMAA1LN	5CBMAA3LN	5CBMAA5LN
90/10	10CBMAA1LN	10CBMAA3LN	10CBMAA5LN
80/20	20CBMAA1LN	20CBMAA3LN	20CBMAA5LN

All hydrogels were robust and tough. The hydrogels were characterized by FTIR-ATR, which shows the success of the copolymerization (Figure 20). The increase in the amount of zwitterionic comonomer was evidenced by the concomitant increase in the intensity of amide bands at 1640 cm^{-1} and 1535 cm^{-1} and the carboxyl band at 1600 cm^{-1} arising from the CBMAA added.

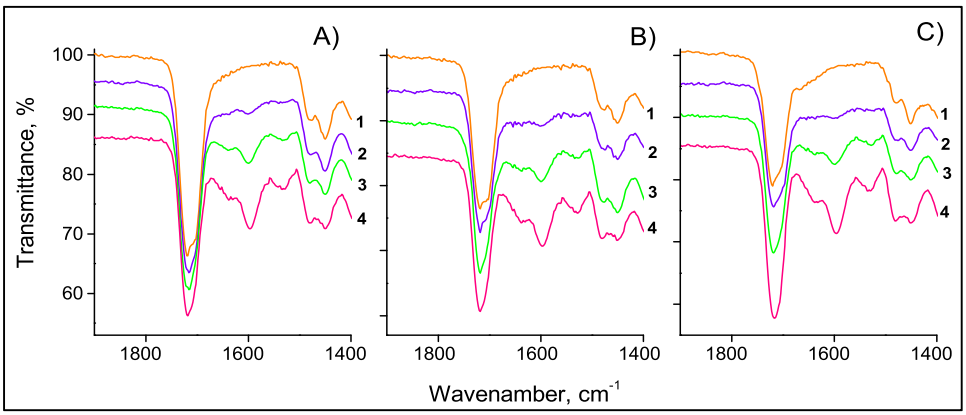

Figure 20. Amidic region of the FTIR-ATR spectra of hydrogels of poly(HEMA) and poly(HEMA-*co*-CBMAA) containing (A) 1 wt% of LN, (B) 3 wt% of LN, and (C) 5 wt% of LN. Curves 1–4 show increasing concentrations of CBMAA comonomers: (1) pure poly(HEMA), (2) 5 mol% CBMAA, (3) 10 mol% CBMAA, and (4) 20 mol% CBMAA.

The long-term stability in aqueous media is a major challenge for physically crosslinked hydrogels and an important criterion for their applicability. The physical nature of the crosslinking could lead to leaching of nanoparticles or polymer chains, thus assessment of their stability is essential. The stability in water of 10CBMAA3LN hydrogels was evaluated by the gel ratio (*GR*) as the ratio of masses of dried hydrogels after washing in water for 1, 2, 3, 4 or 6 days (m_{w+d}) to the masses of freshly prepared hydrogels (m_{fp}) (Figure 21A, Equation 2). The gel ratio of the hydrogel before the stability test was determined to be 0.2. No significant changes were observed even after 6 days of immersion in water, clearly indicating the stability of the material (Figure 21A).

$$GR = \frac{m_{w+d}}{m_{fp}} \qquad \text{(Equation 2)}$$

The EWC of poly(HEMA) and poly(HEMA-*co*-CBMAA) hydrogels was determined gravimetrically. As expected, the EWC dramatically increases with the addition of the zwitterionic comonomer to the polymerization feed (Figure 21B). A 15% increase in the water uptake capability of hydrogels was observed with the addition of only 5 mol% of CBMAA. A further addition of CBMAA led to a significant five-fold increase in the amount of water in the hydrogel, reaching a value of EWC of 27.7±2.0 for 10CBMAA1LN, 24.2±0.2 for 10CBMAA3LN, and 23.0±0.7 for 10CBMAA5LN. The addition of 20 mol% of CBMAA resulted in EWCs of 295.0±10.0 for 20CBMAA1LN, 39.0±2.2 for 20CBMAA3LN and 38.0±7.0 for 20CBMAA5LN, *i.e.* water uptake by the hydrogels is 60, 8 and 7 times more than pure poly(HEMA) respectively.

A minor decrease in water uptake capability was observed with increasing nanoparticle concentration. This behavior can be explained by the clay platelets acting as effective cross-linking agents. The increase in the cross-linking point density results in a denser network structure and shorter interlinked polymer chains, restricting a higher water uptake.

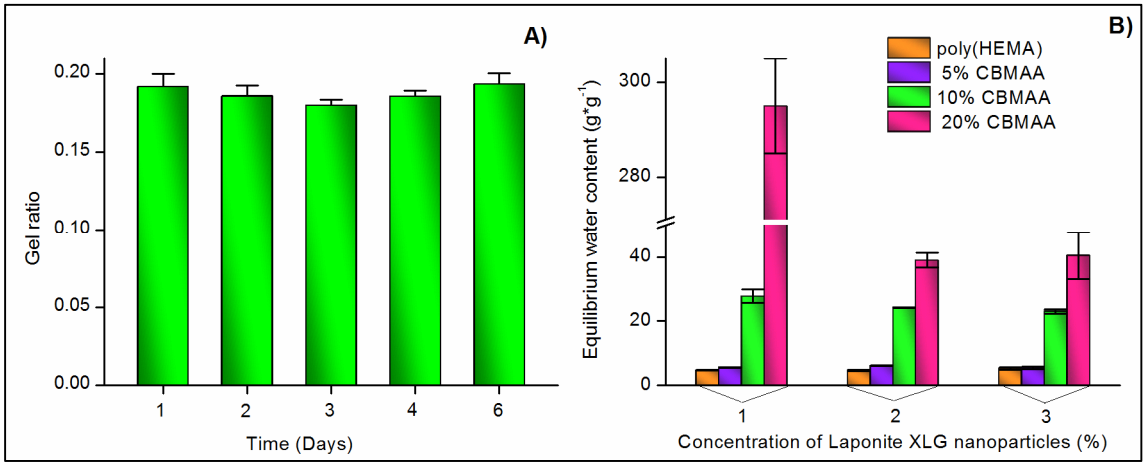

Figure 21. (A) Assessment of the stability of 10CBMAA3LN hydrogels in water, by measuring the gel ratio as the ratio of mass of dried hydrogel to original mass after immersion in water for a specified time. The theoretical ratio corresponding to the polymerization mixture is 0.20. (B) The EWC of hydrogels, defined as the ratio between the mass of absorbed water after reaching the equilibrium and the mass of dried hydrogels.

Mechanically, all hydrogels containing zwitterionic comonomers were robust and tough, withstanding high degrees of various deformations (Figure 22A and 23A). In order to evaluate their mechanical resistance, the elongation at break and Young's modulus of poly(HEMA) and poly(HEMA-*co*-CBMAA) hydrogels were determined (Figure 22B). The addition of 5 mol% of zwitterionic comonomer resulted in materials with similar tensile behavior to poly(HEMA) hydrogels, resulting in elongations at break as high as 390±28% for 5CBMAA1LN, 436±21% for 5CBMAA3LN and 140±25% for 5CBMAA5LN (Figure 22A). However, the Young's moduli increased two-fold compared to poly(HEMA) hydrogels corresponding to 19.9±0.7 kPa, 33.3±2.2 kPa and 76.7±1.5 kPa for 1, 3 and 5 wt% of LNs respectively (Figure 22B). Further increments in the CBMAA concentration in the polymerization feed such as 10 and 20 mol% led to a marked increase of elongation at break of the material. A remarkable strain at break as high as 1800±42% was achieved by the 20CBMAA3LN hydrogel (Figure 22A).

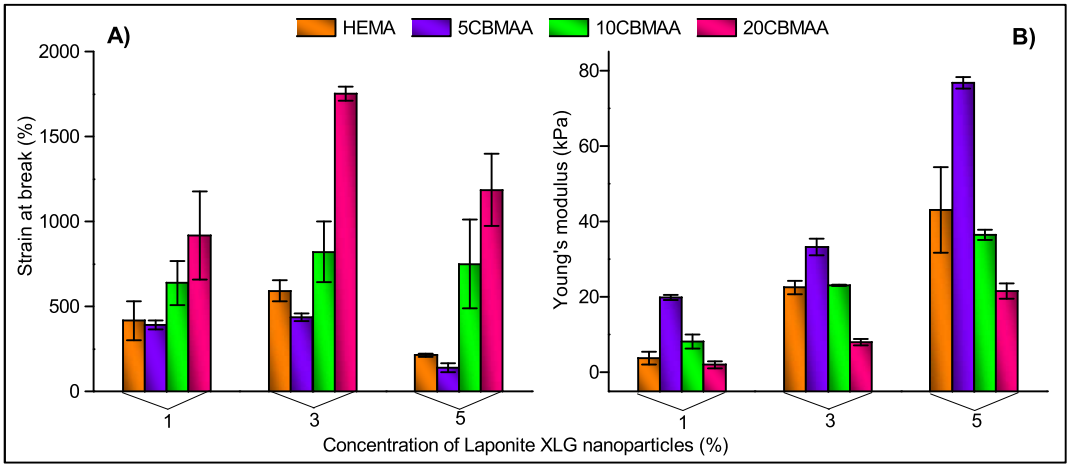

Figure 22. Mechanical properties of hydrogels under tensile testing. (A) Elongation at break and (B) Young's modulus.

An increase in the concentration of nanoparticles leads to higher Young's moduli due to an increase in the number of crosslinking points resulting in tougher hydrogels. However, the dependence of the elongation at break on the concentration of nanoparticles is not linear and achieves its maximum at concentration of 3 wt% of LNs for the entire range of CBMAA comonomer addition. The low elongation at break for hydrogels containing only 1 wt% of LNs can be explained by the interaction between long polymer chains with sparsely scattered nanoparticles not being strong enough to withstand a high applied load. Consequently, a higher concentration of LNs, such as 5 wt%, led to an increase in the number of crosslinking points, enhancing the interaction between polymer chains and nanoparticles. However, the shorter length of the polymer segments between junction points restricts greater elongation.

Additionally, 10CBMAA3LN hydrogel rods colored in yellow and blue were prepared for a visual demonstration of their ability to return to their initial shape after an applied deformation (Figure 23A). The hydrogel rods could resist high levels of deformations such as compression and elongation and quickly recover the initial shape. Furthermore, the presented hydrogels containing zwitterionic comonomers were able to heal after mechanical damage without the use of any healing agent or harsh conditions. Only keeping the cut surfaces in contact at room temperature for 5 min was sufficient for the hydrogels to heal. Figure 23B shows the self-healed ring obtained from two separate hydrogel rods. The ring was mechanically stable and resistant to handling. Another

demonstration of self-healing was performed with hydrogel rods of a larger diameter (d=10, l=15 mm) (Figure 23C). The two differently colored hydrogels were cut into half and brought into contact in alternating order of colors for 5 min at room temperature. The healed rod was placed on two platforms in order to show that the healed joints can withstand the load of the rod's weight without breaking. Shorter healing times were observed with an increasing content of CBMAA. In contrast, no healing was observed in bare poly(HEMA) hydrogels.

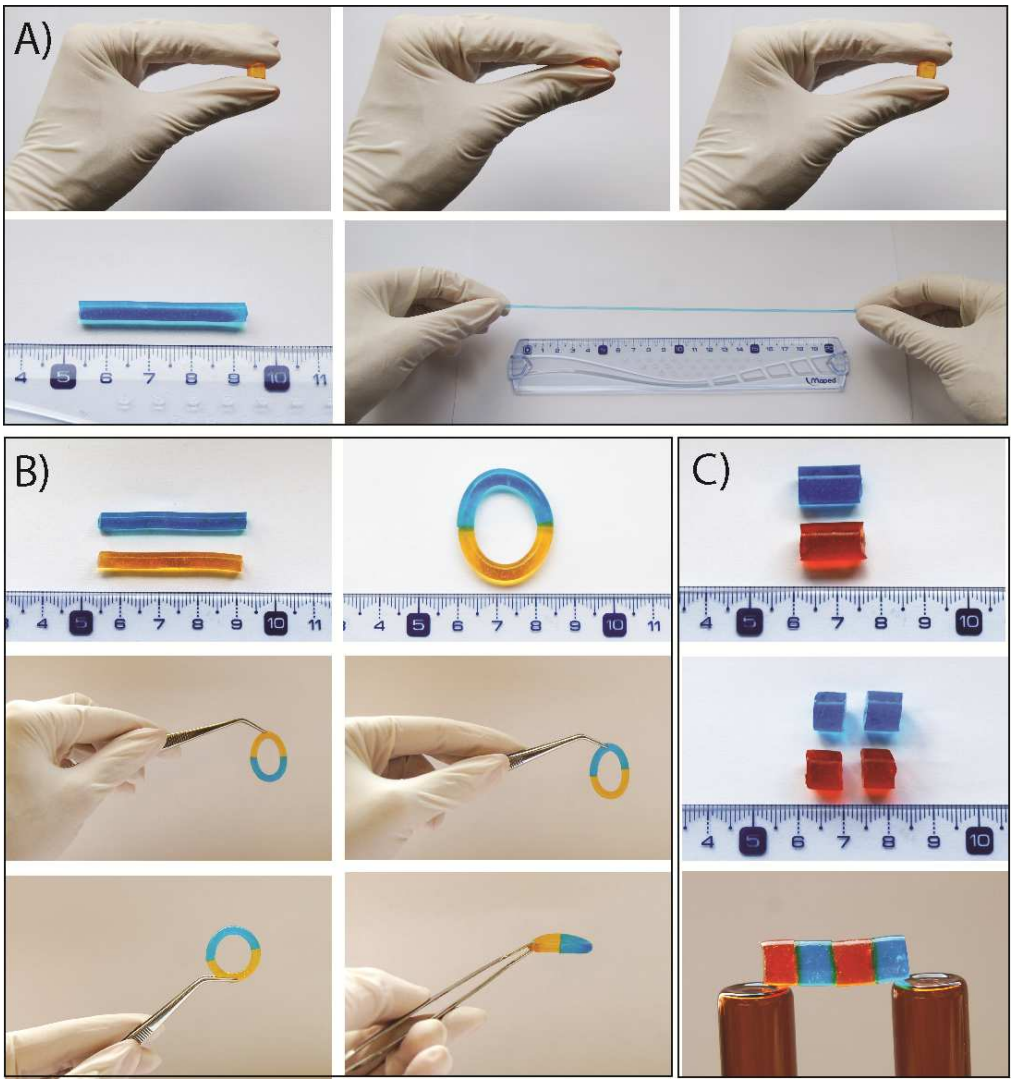

Figure 23. (A) Mechanical resistance of 10CBMAA3LN hydrogels to different type of deformations. Self-healing of 10CBMAA3LN hydrogels: (B) hydrogel ring healed from two separate hydrogel rods and (C) hydrogel rod healed from four pieces.

3.2 Protein Fouling Test

In previous chapter poly(HEMA-*co*-CB(M)AA) hydrogels showed an unprecedented reduction of protein fouling.[136] Since the ability of biomaterials to prevent protein fouling is critical for several possible applications, a test to confirm the antifouling characteristics of the newly poly(HEMA-*co*-CBMAA) physically crosslinked by LNs hydrogels was performed.

The non-specific protein adsorption from a 10% fetal bovine serum (FBS) solution was evaluated by Ultraviolet-visible (UV-Vis) spectroscopy. Protein fouling was estimated from the difference in intensity of the protein absorbance peak at λ=277 nm by subtracting the spectra of the solution contacted with the hydrogels from the blank spectrum (Figure 24A). With the addition of CBMAA a significant decrease in the difference of subtracted spectra was observed (Figure 24A). The protein fouling was expressed as the relative amount of adsorbed protein (%) taking the hydrogel with HEMA1LN as the reference (Figure 24B).

For the determination of the influence of LNs on the fouling of hydrogels, the fouling on a chemically crosslinked poly(HEMA) hydrogel, without LNs, was also measured (HEMA0LN). The fouling for HEMA0LN amounted to about 60% of the fouling observed on the HEMA1LN. Further increases in the amount of LNs, such as 3 and 5 wt%) caused only a minor increase in the fouling (Figure 24B). However, with the addition of only 5 mol% of CBMAA comonomer, a dramatic reduction in the fouling, such as 60 to 70 % was achieved regardless the concentration of Laponite. A subsequent increase in the ratio of CBMAA to 10 mol% reduced the fouling by 85%, 80% and 75% (Figure 24B) for hydrogels with 1, 3 and 5 wt% of LNs, respectively. Remarkably, further increases in the ratio of CBMAA in the polymerization feed helped suppress the fouling even further, resulting in a 95% decrease for 20CBMAA1LN hydrogels, demonstrating the much acclaimed antifouling properties of carboxybetaines.

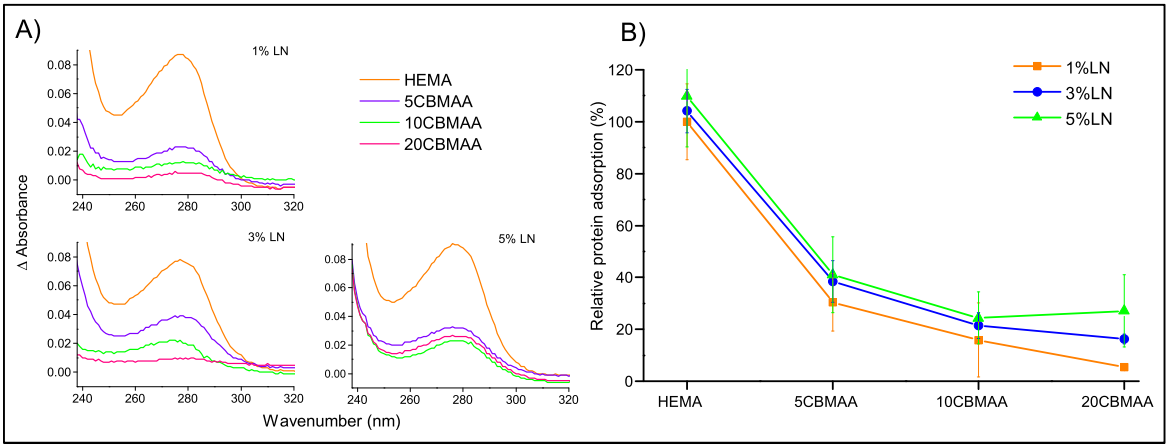

Figure 24 (A) UV-Vis absorbance spectra of FBS (after subtraction of the blank) after incubating hydrogels containing 1%, 3% and 5% LN.(B) Decrease in non-specific protein adsorption from 10% FBS on hydrogels containing CBMAA, related to poly(HEMA) hydrogel.

3.3 Summary

Novel physically crosslinked poly(HEMA-*co*-CBMAA) nanocomposite hydrogels with antifouling characteristics were synthesized. The cross-linking via Laponite nanoparticles endowed the hydrogels with self-healing properties, excellent mechanical resistance and very high elongation at break, and an extremely high water uptake capacity. A wide range of properties, such as a degree of swelling from 5 to 300, elongation at break from 150 to 1800%, and Young's modulus from 4 to 80 kPa, are accessible and can therefore be easily tuned by variation of concentration of CBMAA or LNs.

The antifouling characteristics, ease of functionalization with bioreceptors of carboxybetaine moieties, the exceptional mechanical and self-healing properties make these new materials a highly promising platform for the fabrication of scaffolds for tissue engineering. However, additional control over the geometry and internal morphology of the scaffold is required for successful tissue engineering. Therefore, fabrication techniques, which enable the design of scaffolds with precise shapes corresponding to the desired application and precise microstructure, such as porosity, pore size, shape, and interconnectivity, for unrestricted diffusion of nutrients, cell waste products, soluble signals, and cell motility, are required.

4 *Biodegradable Zwitterionic Scaffolds with Gyroid Pore Architecture* †

All biological tissues and organs possess specific chemical and physical properties, as well as precise geometrical shape and microarchitecture of pores and topographical features. One of the most important and primary aspects of tissue engineering is to fabricate 3D scaffolds of various shapes and structures in order to mimic native tissues. Consequently, the development of porous hydrogel-based tissue engineering scaffolds has attracted great attention in recent years. There are several techniques for the preparation of porous polymeric scaffolds, however, most of them do not provide precise control over the internal architecture and pore interconnectivity.[137, 138] Stereolithography is known as one of the most developed computer-aided rapid prototyping techniques for the construction of complex 3D scaffolds with respect to the breadth of exterior and interior structures which can be designed with the highest accuracy. This technique uses a layer-by-layer approach that is based on spatially controlled solidification of liquid-based resins by photopolymerization.[53, 82-84] The resin for stereolithography plays an important role in the scaffold fabrication. They contain molecules with polymerizable groups, crosslinkers and photoinitiators in a non-volatile solvent and the viscosity of the mixture is carefully optimized. Resins based on low-molecular weight, multi-functional monomers form a highly crosslinked networks which are predominantly glassy, rigid and brittle. In order to prepare elastomeric objects by stereolithography oligo-/polymeric macromers are necessary for the resin formulations.

In this chapter stereolithography was utilized for the preparation of scaffolds with precisely designed gyroid pore architecture. A hydrophilic biodegradable tri-block-copolymer macromer based on PDLLA-PEG-PDLLA was synthesized for the fabrication of hydrogels. Based on the studies described in previous chapters, CBMAA monomer was added to the resin formulation as a comonomer to provide antifouling properties and functional carboxyl groups to the hydrogels, which were utilized for protein immobilization.

† Parts of the chapter were reproduced from Kostina, N. Yu.; Blanquer, S.; Pop-Georgievski, O.; Höcherl, A.; Grijpma, D. W.; Michálek, J.; Rodriguez-Emmenegger, C. *Macromolecular Bioscience*, (under review). All the experimental methods for this chapter are described in Appendix 5.

4.1 Synthesis of the Macromer

The tri-block-copolymer poly(D,L-lactide)-poly(ethylene glycol)-poly(D,L-lactide) (PDLLA-PEG-PDLLA) was synthesized by bulk ring-opening polymerization of D,L-lactide, initiated by the hydroxyl terminal groups of the (α-hydroxy, ω-hydroxy)-PEG, M_n=4000 g·mol^{-1} and catalyzed by stannous octanoate (Scheme 5). The chemical structure of the synthesized oligomer was confirmed by FTIR-ATR and ^{1}H NMR.† The conversion of D,L-lactide was calculated as 93% from ^{1}H NMR spectra of the reaction mixture.† The M_n of PDLLA-PEG-PDLLA oligomer was determined to be 5250 g·mol^{-1}, as estimated by NMR. In order to enable the radical polymerization and crosslinking, the hydroxyl end groups of the synthesized PDLLA-PEG-PDLLA oligomer were reacted with an excess of methacrylic anhydride (MAAH) to obtain MA-PDLLA-PEG-PDLLA-MA macromers (Scheme 5). The quantitative functionalization of hydroxyl groups was confirmed by ^{1}H NMR.†

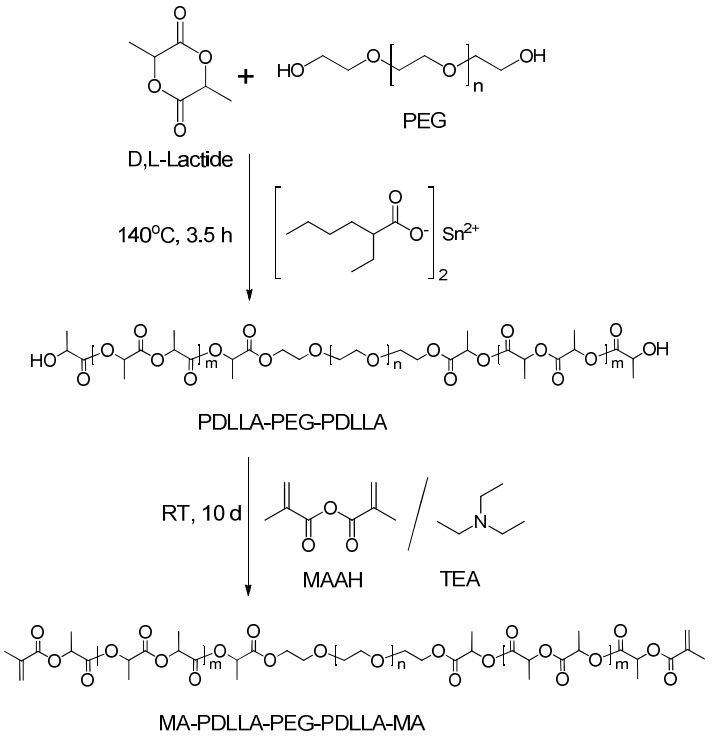

Scheme 5. Synthesis of PDLLA-PEG-PDLLA oligomer and MA-PDLLA-PEG-PDLLA-MA macromer.

† Data is described in Appendix 5.

4.2 Preparation and Characterization of the Hydrogels

Hydrogels based on MA-PDLLA-PEG-PDLLA-MA and CBMAA with precise pore structure were prepared by stereolithography. Three photopolymerizable resins with different weight ratios of CBMAA were prepared (Table 5) and the time of polymerization was optimized. Subsequently, hydrogels with gyorid pores were prepared.

All hydrogel structures were soft and highly flexible, their shape and structure precisely matched their design. The chemical composition of the hydrogels was confirmed by XPS. Figure 25 reports the high resolution core level C 1s and N 1s regions of the spectra of the bulk poly(CBMAA) material and 0%CBMAA, 10%CBMAA, and 20%CBMAA hydrogels. The C 1s spectrum of poly(CBMAA) bulk material is characterized by a C—C contribution at 285.0 eV, which is accompanied by contributions at 285.6±0.1 eV, 286.2±0.2 eV, 287.9±0.1 eV and 288.3±0.1 eV arising from the secondary chemical shift, *i.e.* the effect of the amide group on the tertiary carbon atom in the CH_3—C*—C(=O)—NH structure, the C—N^+ moieties, the amide group C(=O)—NH and the carboxylic (O—C=O) group. The N 1s spectrum is characterized by contributions at 399.5±0.1 eV and 402.5±0.1 eV of amides and charged quaternary ammonium groups, respectively. The 0%CBMAA hydrogel shows the characteristic contributions for the lactide and ethylene oxide monomers as well as the methacrylate groups that did not react during the photo-curing reaction. The contributions centered at 284.5±0.1 eV, 285.0 eV, 286.3±0.2 eV, 287.0±0.2 eV, and 289.0±0.5 eV arise from the C=C, C—C, C—O—C, O—C*—C(=O)O, and ester O—C=O group, respectively. The N 1s spectrum of 0%CBMAA completely lacks nitrogen (amides and charged quaternary ammonium groups) contributions.

Table 5. The composition of formulations of hydrogels with different weight ratio of macromer to monomer

Hydrogels abbreviation	MA-PDLLA-PEG-PDLLA-MA / CBMAA, wt%
0% CBMAA	100 / 0
10% CBMAA	90 / 10
20% CBMAA	80 / 20

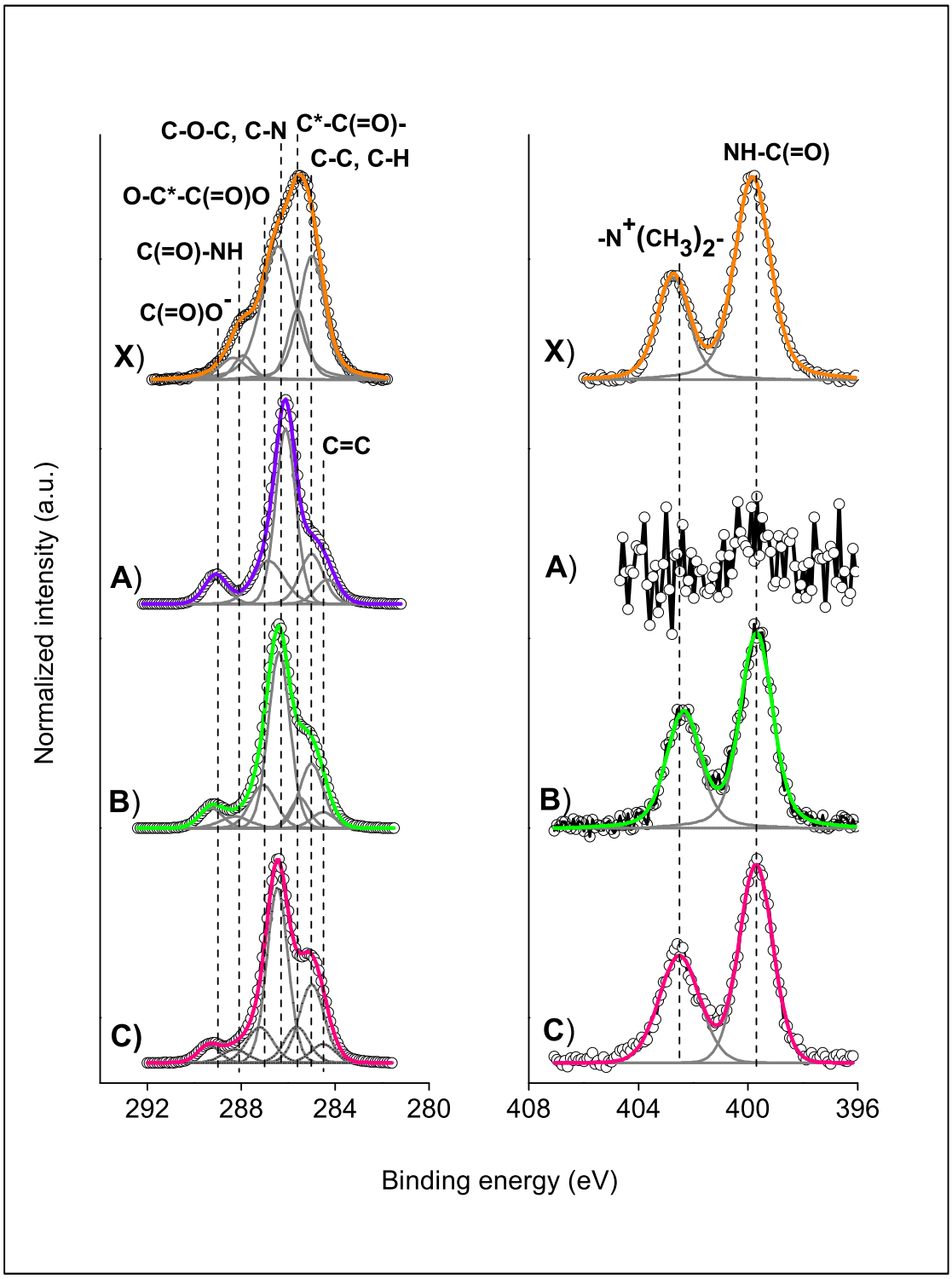

Figure 25. High resolution C 1s (left) and N 1s (right) XPS spectra of (X) poly(CBMAA), (A) 0%CBMAA, (B) 10%CBMAA, and (C) 20%CBMAA dry hydrogels.

The incorporation of CBMAA monomer units into the MA-PDLLA-PEO-PDLLA-MA structure is clearly observed in the high resolution C 1s and N 1s spectra of the 10%CBMAA and 20%CBMAA hydrogels. The presence of CBMAA can be verified by the increase of the contributions of C—C (at 285.0 eV), CH3—C*—C(=O)—NH (at 285.6±0.1 eV), the C—N^+ moieties (which strongly overlap with the O—C*—C(=O)O contributions of PDLLA at 286.3±0.2 eV) and the C(=O)—NH group (at 288.1±0.2 eV) within the C 1s spectra, as well as the occurrence of contributions arising from amide (at 399.7±0.1 eV) and charged quaternary ammonium groups (at 402.5±0.1 eV) in the high resolution N 1s spectra. The increase of CBMAA in the polymerization feed from 10 to 20% lead to increase of the nitrogen content from 1.3 at.% to 2.8 at.%.

The equilibrium water content (EWC) of the hydrogels was evaluated gravimetrically (Figure 26). An increase in amount of CBMAA in the polymerization resin lead to a dramatic increase of EWC. With addition of only 10% of CBMAA hydrogels could bind almost two times more water than hydrogels without addition of CBMAA. A further increment in the CBMAA concentration to 20% led to an unprecedented increase of hydrogel water content, reaching the value of EWC of 700%.

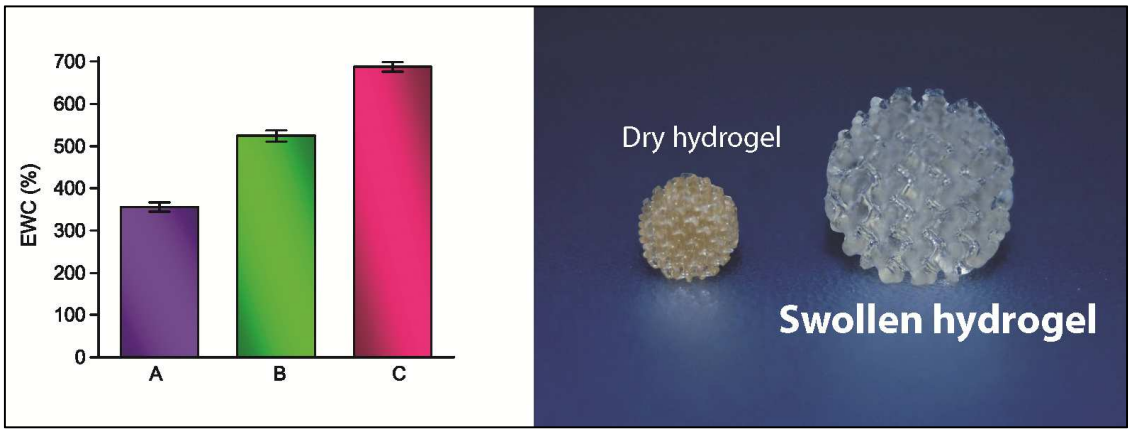

Figure 26. Equilibrium water content (EWC) of hydrogels (A) 0%CBMAA, (B) 10%CBMAA, and (C) 20%CBMAA, defined as the ratio between the mass of absorbed water after reaching the equilibrium and the mass of dried hydrogels (left). The photograph shows dry and swollen hydrogel of 10%CBMAA (right).

4.3 Protein Immobilization

One of the main goals of the scaffolds materials for tissue engineering is to actively promote the tissue formation and regeneration. A widely used approach to induce specific cell adhesion is to immobilize biomolecules, such as peptides or proteins, on the surface of the scaffold to interact with integrin receptors of the cell. To perform the immobilization of bioactive compounds, the material of the scaffold must possess available functional groups while preventing any non-specific interactions that can occur at the interface between the biological medium and the surface of the scaffold. To achieve this, CBMAA was introduced as comonomer. Not only does CBMAA provide resistance to fouling but also its copolymerization will lead to the presence of free carboxylic groups exploitable for the biofunctionalization.

To show the ability to functionalize the interior of the pores of the hydrogels we utilized a fluorescently labelled protein and visualized the immobilization with laser scanning confocal microscopy (LSCM). Bovine serum albumin labeled with fluorescein isothiocyanate (BSA-FITC) was chosen as a model protein for the biofunctionalization of the surface of hydrogels. To prove the absence of non-specific protein adsorption the prepared hydrogels were incubated without functional group activation in a solution of BSA-FITC for 14 h and subsequently analyzed by LSCM (Figure 27A-C). No fluorescence was observed during the scanning of all hydrogels (0%, 10% and 20%CBMAA) with a 488 nm laser for excitation of FITC proving the absence of non-specific albumin adsorption on the hydrogels.

The biofunctionalization of the hydrogels containing CBMAA was performed by amidation with BSA-FITC on the carboxylic groups of CBMAA monomeric units previously activated with *N*-(3-dimethylaminopropyl)-*N*′-ethylcarbodiimide hydrochloride (EDC)/N-hydroxysulfosuccinimide sodium salt (sulfoNHS) (Figure 27D-F). As expected, no BSA immobilization was observed on the hydrogel without any carboxybetaine addition (0%CBMAA) (Figure 27D) due to the lack of functional groups on the MA-PDLLA-PEG-PDLLA-MA chains. Addition of CBMAA resulted in material possessing easily functionalizable carboxylic groups, which were utilized for BSA-FITC immobilization. Figures 27E and F demonstrate the successful immobilization on the hydrogels containing 10% and 20% of CBMAA, respectively, by the strong fluorescent

emission upon laser excitation. Figure 27G represents a three dimensional reconstruction of 20 confocal scans of 10%CBMAA hydrogel, proving the homogeneity of immobilized BSA-FITC within hydrogel pore surface

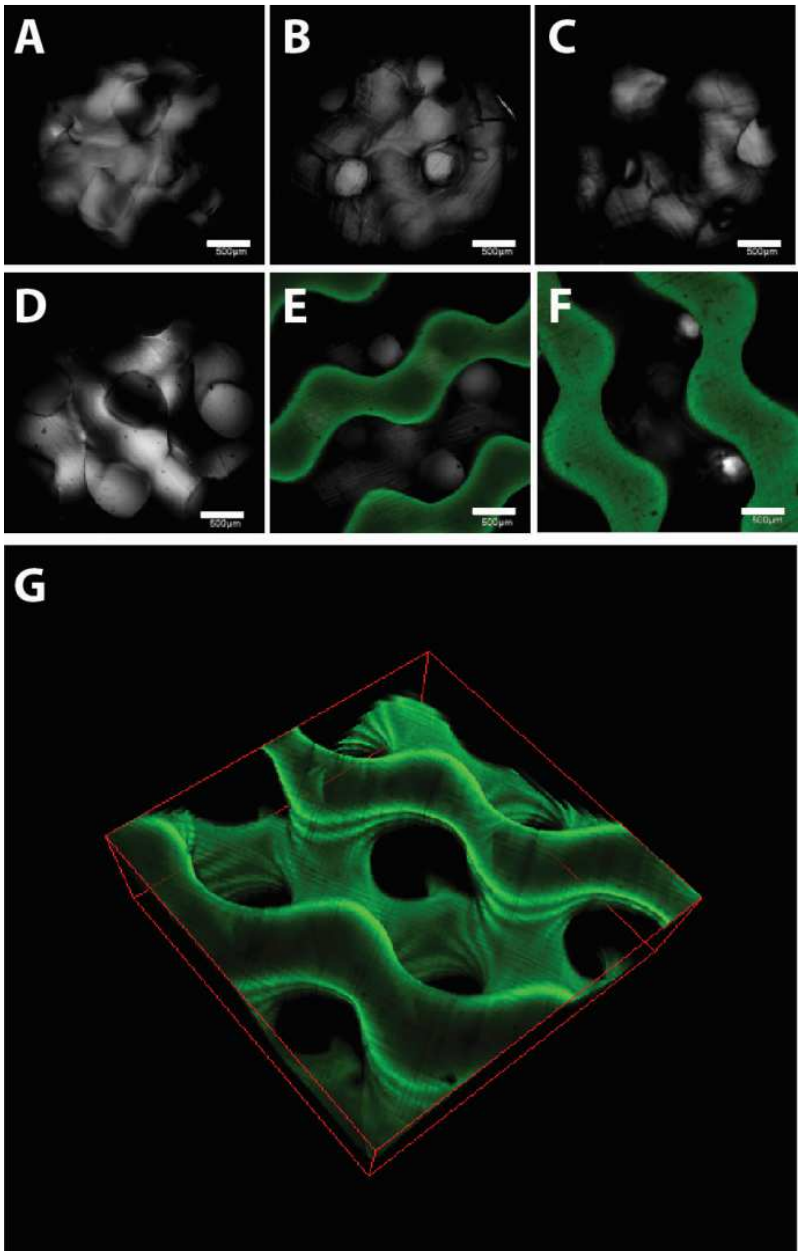

Figure 27. Confocal images D, E and F of the 0%CBMAA, 10%CBMAA and 20%CBMAA hydrogels, respectively, after immobilization of BSA-FITC via EDC/sulfoNHS chemistry. Confocal images A, B and C represent blank experiments for 0%CBMAA, 10%CBMAA and 20%CBMAA hydrogels, respectively, *i.e.* hydrogels were in contact with solution of BSA-FITC without functionalization by EDC/sulfoNHS, (scale bar 500 µm). Image G represent 3D reconstruction of 20 confocal scans of 10%CBMAA hydrogels with immobilized BSA-FITC.

4.4 Summary

Stereolithography was utilized to fabricate hydrogels with precisely designed porosity. The hydrogels were prepared by a mixture of a biodegradable terpolymer MA-PDLLA-PEG-PDLLA-MA and CBMAA. The addition of CBMAA comonomer endowed the hydrogels with a dramatic increase in EWC, reaching an unprecedented level of 700% for 20%CBMAA. All hydrogels showed antifouling character in a contact with BSA-FITC solution. The carboxylic groups of the CBMAA comonomer were exploited for biofunctionalization with BSA-FITC. LSCM demonstrated the successful functionalization of the pores of the hydrogels containing 10% and 20% of CBMAA.

The ability to design the pore architecture, biodegradability, antifouling properties endowed to the prepared hydrogels in combination with the availability of functional groups exploitable for covalent immobilization of cell-binding biomolecules make the presented scaffold a highly promising material for tissue engineering applications.

5 *Modification of Nanofibers with Non-Fouling Polymer Brushes*[†]

As mentioned in previous chapters, a highly interconnected porosity and (bio)degradability are very important characteristics for scaffolds for tissue engineering. Among them, electrospun poly(ε-caprolactone) (PCL) nanofibers have gained wide recognition due to the combination of their intrinsic properties such as high porosity, large surface area, and presence of fibril structures enabling them to mimic the morphology of the native extracellular matrix (ECM).[139] Additionally, the degradation of PCL proceeds by hydrolytic scission without strongly affecting the pH of the surrounding fluids and the rate can be finely tuned by adjustment of molecular weight or crystallinity.[70, 140, 141]

These unique features of PCL nanofibers make them very attractive as scaffolds for tissue engineering, however, their extensive use is limited. Upon contact with biological fluids, the surface of PCL is rapidly coated by proteins, inducing a series of adverse effects.[142] Therefore, the successful use of PCL nanofibers can only be conceived if their surface is engineered to completely prevent any non-specific interactions, such as fouling from multi-component protein solutions, as well as non-specific cell adhesion.

In this chapter a novel route for the modification of PCL nanofibrous scaffold with antifouling polymer brushes is presented. In order to generate functional groups for the effective immobilization of ATRP initiator, a multifunctional biomimetic layer of poly(dopamine) was deposited on the nanofibers surface onto which bromoisobutyryl groups (initiators) were acylated. MeOEGMA, HOEGMA, HPMA, and CBAA monomers were polymerized from the nanofibers decorated with initiator by SI-ATRP.

[†] Parts of the chapter were reproduced from Kostina, N. Yu.; Pop-Georgievski, O.; Bachmann, M.; Neykova, N.; Bruns, M.; Michálek, J.; Bastmeyer, M.; Rodriguez-Emmenegger, C. *Macromolecular Bioscience*, 2015, DOI: 10.1002/mabi.201500252. All the experimental methods for this chapter are described in Appendix 6.

5.1 Modification of the Nanofibers

Although antifouling polymer brushes represent the best alternative to prevent fouling, their growth from inert three-dimensional substrates is not exempt from challenges. Surface-initiated polymerization of polymer brushes is often limited by the absence or availability of functional groups on the material surface onto which initiator molecules can be immobilized. In order to avoid aggressive pre-treatment of the surface for the generation of functional groups, a layer of poly(dopamine) (PDA) was deposited on the surface of PCL nanofibers (Scheme 6). The most striking property of PDA films is its high adhesion to virtually any solid material independently of its surface energy and shape. The formation of the PDA film proceeds by the polymerization of dopamine in slightly alkaline conditions (TRIS buffer). The polymerization forms small colloidal particles which adhere to the surface and converge into a continuous film.[143-145] The film perfectly copies the topography of the modified surface. Moreover, the PDA films have been shown to bind to surfaces via a range of molecular interactions including van der Waals forces to formation of covalent bonds.[143, 146, 147] This is a fundamental prerequisite to withstand the growth of brushes which would otherwise be cleaved from the surface due to the strong osmotic pressure. Further functionalization of PDA was carried out via amine groups present within the PDA layer.

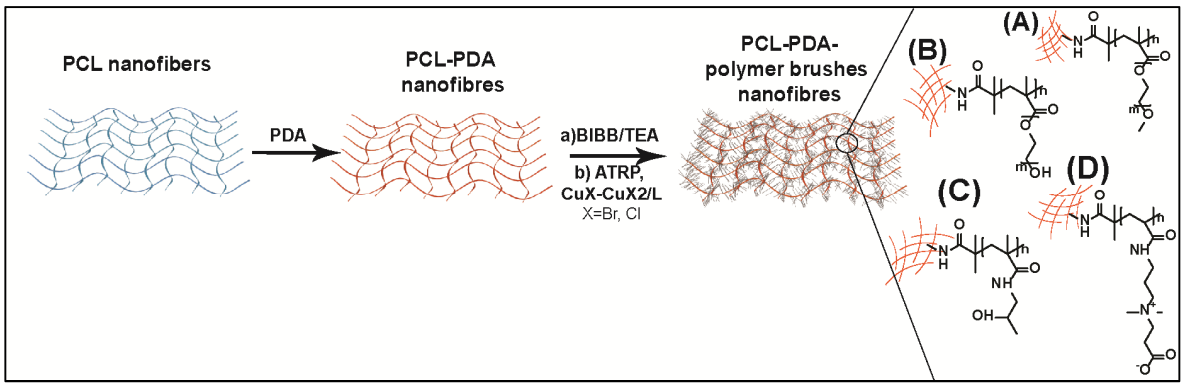

Scheme 6. The sequence of modification of PCL nanofibers.

The successful deposition of PDA layer was confirmed by XPS analysis. An increase of the contribution at 285.0 eV, corresponding to sp^2 and sp^3 carbon species, is clearly observed in the C 1s spectrum (Figure 28). Concomitantly, in the N 1s spectra of PCL-PDA the appearance of a peak at 400.1 eV assigned to the predominant secondary amine groups of indole, non-protonated and protonated primary amine, and imine functionalities of PDA were observed (Figure 28).[106] The scanning electron microscopy (SEM) images clearly show that the morphology of the fibers was preserved after the PDA polymerization. The PDA layer perfectly matched the morphology of the bare fibers (Figure 29) while no PDA aggregates could be observed.

The ATRP initiator was acylated to the residual amine and catechol groups of the PDA layer and subsequently polymer brushes based on MeOEGMA, HOEGMA, HPMA, and CBAA were grown from the initiator molecules by SI-ATRP (Scheme 6). The composition of the polymer brushes on PCL-PDA nanofibers was confirmed by XPS. Analysis of the C 1s spectra of PCL-PDA-poly(MeOEGMA) and PCL-PDA-poly(HOEGMA) brushes shows a strong increase of the contribution at 286.4 eV assigned to C–O bonds of the oligo(ethylene glycol) side chains of the brush and a decrease of the signal at 285.0 eV (Figure 28). The absence of any contributions characteristic of PDA in the high-resolution N 1s spectra confirms the complete coverage of the PLC-PDA-Br surfaces with thick polymer brushes of poly(MeOEGMA) and poly(HOEGMA). The XPS spectra of poly(HPMA) brushes displayed characteristic contributions at 287.8 eV in the C 1s spectrum and the significant narrowing of the peak at 400.0 eV in N 1s spectrum confirming the presence of the O=C—N groups (Figure 28). The C 1s spectrum of PCL-PDA-poly(CBAA) is characterized by a peak at 287.8 eV from the amide functionality (Figure 28). Moreover, the N 1s spectrum of PCL-PDA-poly(CBAA) nanofibers shows a pronounced signal at 402.7 eV characteristic of the quaternary amine $–N^+(CH3)2–$ species of the zwitterionic side chain of the polymer brushes (Figure 28). The absence of XPS spectral features characteristic for the PDA and PCL indicates that the surface of the fibers is modified with a confluent film of more than 10 nm.

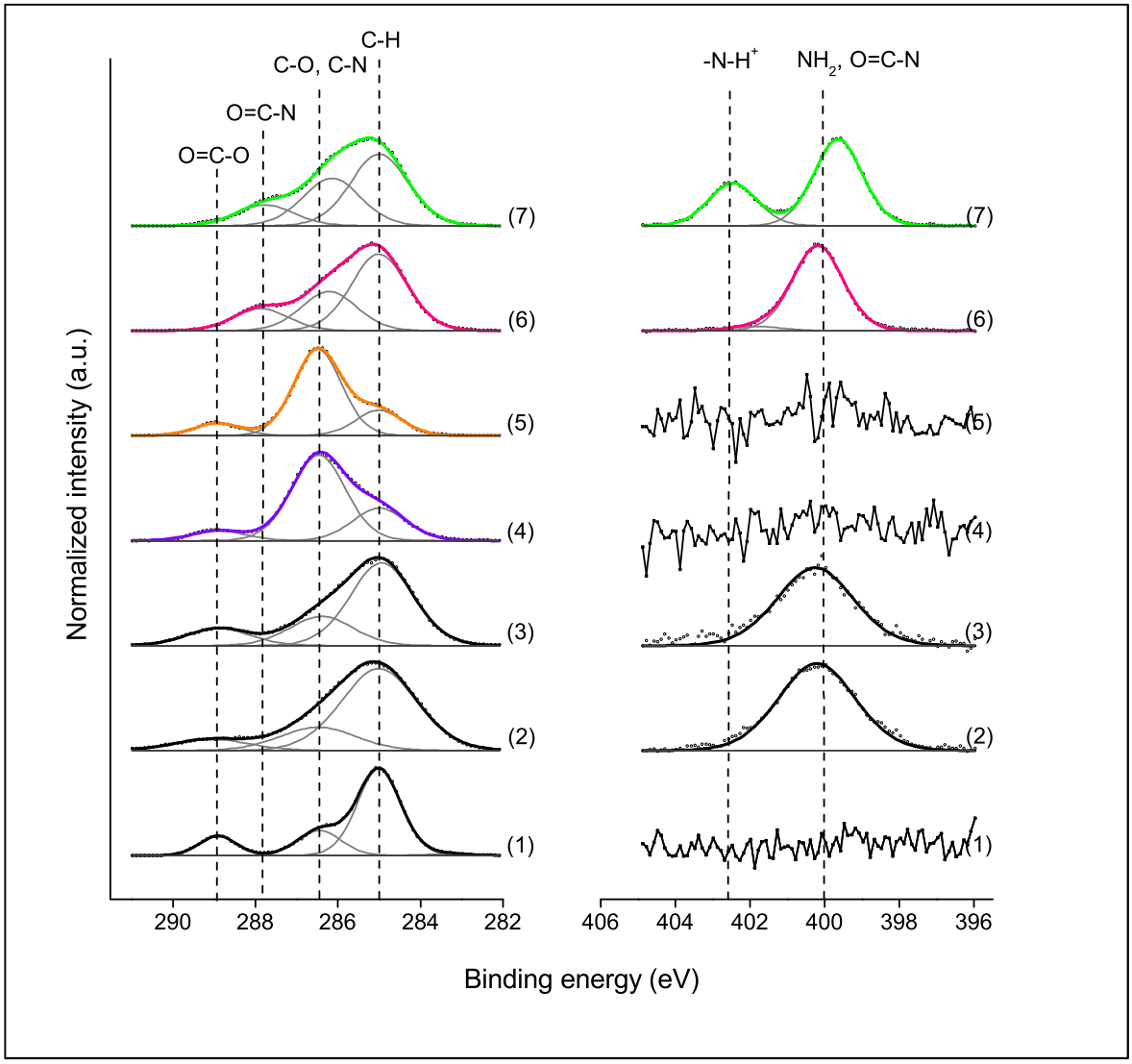

Figure 28. C 1s and N 1s high-resolution XPS spectra of nanofibers; (1) bare PCL, (2) PDA-modified (PCL-PDA), (3) PCL-PDA with immobilized ATRP initiator (PCL-PDA-Br), (4) PCL-PDA-poly(MeOEGMA), (5) PCL-PDA-poly(HOEGMA), (6) PCL-PDA-poly(HPMA), and (7) PCL-PDA-poly(CBAA).

The SEM analysis showed that the polymerization was confined to the surface of the nanofibers, increasing their diameter. However, the morphology of the individual fibers and the highly interpenetrating porous structure of the mesh were preserved (Figure 29).

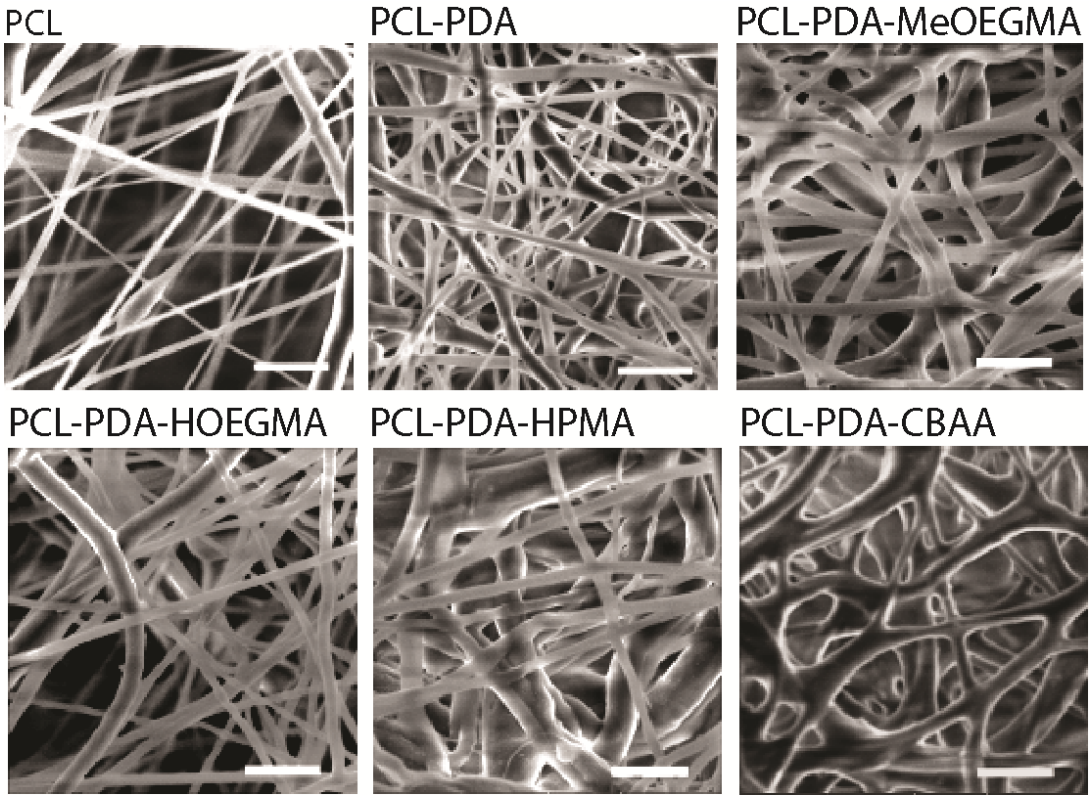

Figure 29. SEM images of nanofibers after each step of modification. Images were acquired at 20.0 kx magnification. Scale bar equals 2 μm.

5.2 Cell Adhesion Experiment

The success of the passivation of the nanofiber by the brushes was assessed by seeding mouse embryonic fibroblasts (MEFs) on PCL, PCL-PDA, and the nanofibers bearing the selected polymer brushes (PCL-PDA-poly(MeOEGMA), PCL-PDA-poly(HOEGMA), PCL-PDA-poly(HPMA), and PCL-PDA-poly(CBAA). The nanofibers were incubated with MEF cells for 7 and 24 h at 37º C, cultivated in cell culturemediumwith10%v/v FBS, to probe the cell adhesion behavior. The cells on the samples were fixed and stained for paxillin (marker of cell–matrix adhesions, CMAs), actin (marker of cytoskeleton) and cell nuclei. Microscopic images revealed that after 7 h the cells adhered in high numbers throughout the PCL and PCL-PDA nanofibrous meshes (Figure 30). Furthermore, 3D high resolution reconstructions of Apo-Tome optical sections (Figure 31) show that they were even able to penetrate the porous PCL nanofibers, adapted their shape to the nanofibers and made preferential cell-matrix adhesion contacts with them. This, together with distinct paxillin-positive clusters, indicates that cells were able to

establish functional, signaling-competent CMAs which truly mimicked cell–matrix interactions. Therefore the MEFs were able to use the non-specifically adsorbed protein deposits on PCL and PCL-PDA as a substitute for extracellular matrix.

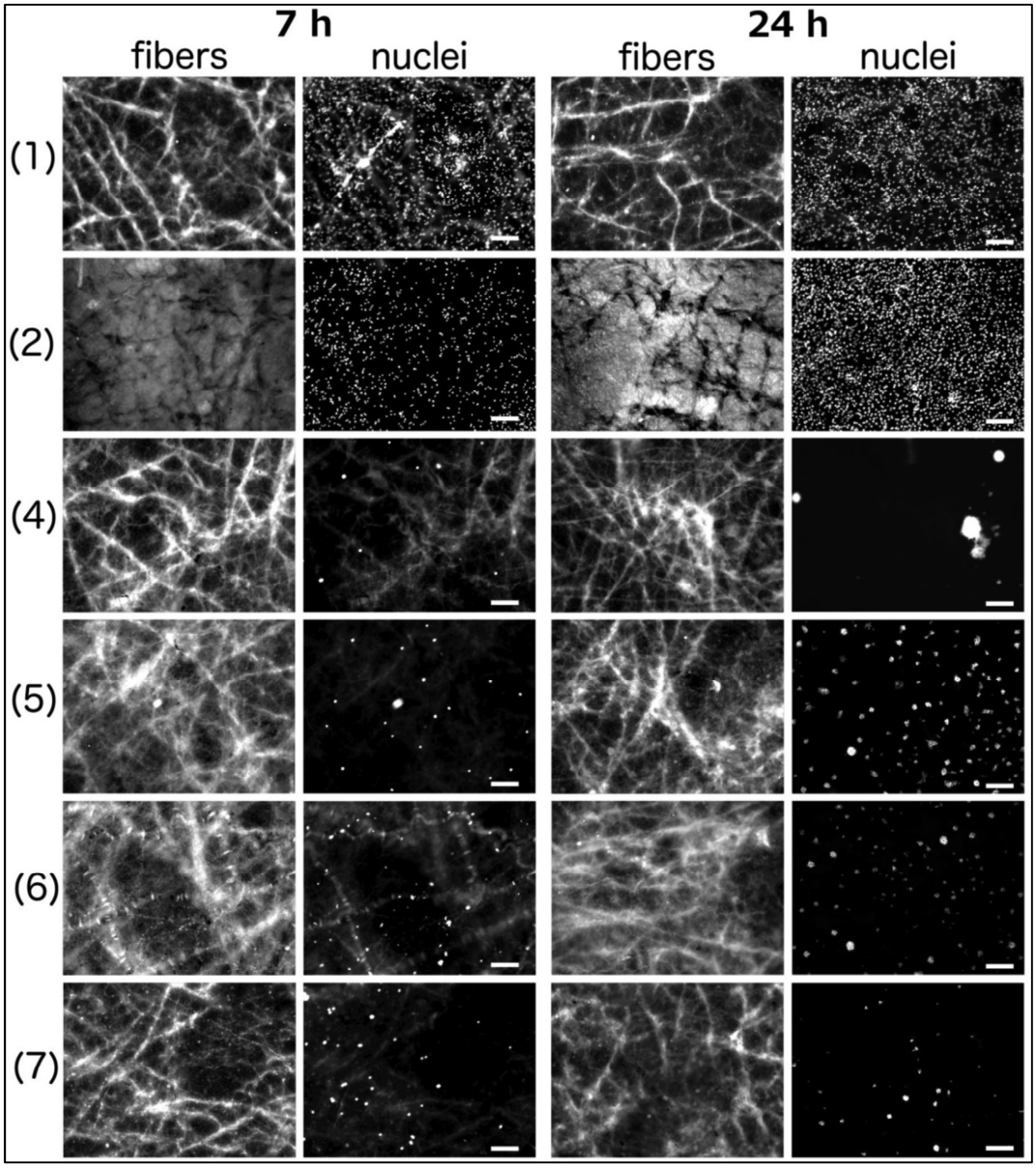

Figure 30. Cell adhesion on (1) PCL, (2) PCL-PDA, (4) PCL-PDA-poly(MeOEGMA), (5) PCL-PDA-poly(HOEGMA), (6) PCL-PDA-poly(HPMA), and (7) PCL-PDA-poly(CBAA) nanofibers after 7 and 24 h (scale bar 200 µm). Fibers are visualized by their autofluorescence after excitation at 488 nm, cell nuclei by staining with DAPI and 405nm excitation. It should be noted that low number of cells on nanofibers with polymer brushes (4–7) required higher excitation energy to visualize them. Therefore, in some cases the autofluorescence of the fibers is visible in the 405 nm channel.

The behavior of MEFs on PCL nanofibers modified with polymer brushes was in sharp contrast to pristine PCL and PDA-PCL. Cells did not show any adhesion to the nanofibers modified with antifouling polymer brushes after 7 h, proving that the polymer brushes minimize the cell–surface interactions. Only after 24 h some fibroblasts were detected among the modified nanofibers (Figure 30). However, closer examination (Figure 31) shows that the fibroblasts did not adhere to the nanofibers but rather stuck to each other. The fibroblasts acquired a roundish shape, organizing themselves in non-spread cell clusters that were only entrapped among the modified nanofibers. Paxillin accumulated in the cytoplasm and no clear colocalization between paxillin and fibers was observed, indicating that cells failed to establish CMAs. It is worth noting that fibroblasts like NIH 3T3 cells used in this work preferably adhere to ECM and avoid forming colonies in physiological situations. Presumably, proteins from the culture media did not adsorb to the surface of nanofibers modified with brushes preventing the formation of cell-matrix adhesions (Figure 30 and 31). Therefore, all polymer brushes tested showed a remarkable passivation against cell adhesion.

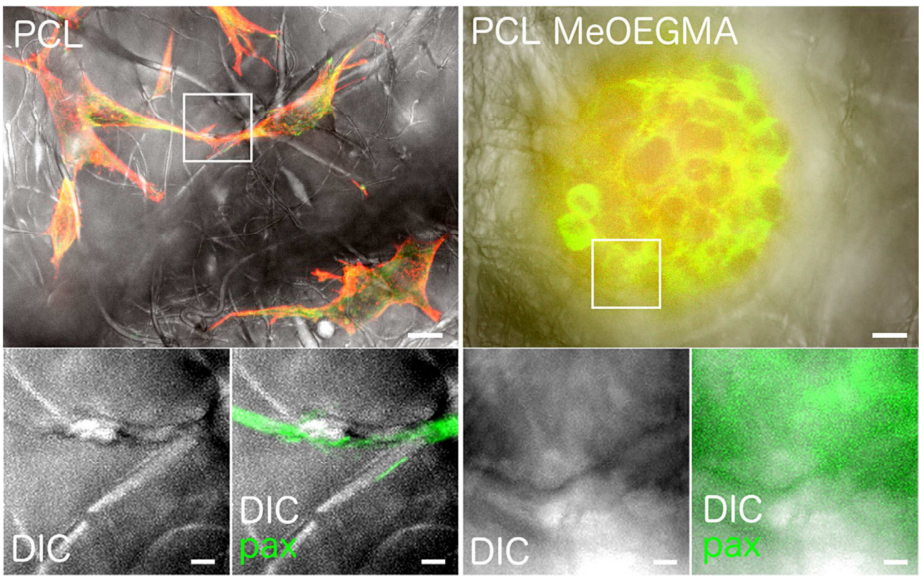

Figure 31. ApoTome optical sections of a 3D image stack at high magnification for cells on PCL and PCL-PDA-poly(MeOEGMA) nanofibers after 24 h. An overview (upper row) shows that the cells adapt their shape to PCL but not to PCL-PDA-MeOGMA nanofibers. Actin (red) indicates cell shape, paxillin (green) cell–matrix adhesions (CMAs) while nanofibers are shown in grayscale. Zoom in of the white boxes (lower row) show clear colocalization for paxillin (green) and PCL (grayscale) but not for paxillin and PCL-PDA-MeOEGMA (garyscale). Scale bars equal 10 μm in first upper row and 2 μm—in lower row.

5.3 Summary

A new route to modify the surface of the scaffolds to prevent non-specific interactions was introduced. Selected antifouling polymer brushes based on MeOEGMA, HOEGMA, HPMA, and CBAA were grown by SI-ATRP from initiators covalently bonded to an ad-layer of PDA. The resistance to non-specific cell adhesion was evaluated by challenging the fibers with fibroblasts. Fibroblasts rapidly adhered to pristine PCL and PDA-coated nanofibers, showing that adhered cells were well spread, elongated along the fibers, and connected to them via cell–matrix interactions. On the other hand, cell adhesion was greatly suppressed on all of the fibers modified with antifouling brushes.

Although demonstrated only on PCL nanofibers, the presented surface modification approach, utilizing a substrate-independent PDA anchor layer and SI-ATRP of antifouling polymer brushes, can be envisioned as a promising route for the modification of other materials being used as vascular grafts or wound dressing, as well as anti-adhesive barriers capable of preventing blood coagulation and tissue adhesion make the presented scaffolds a highly promising material for tissue engineering applications.

Conclusions

The main objective of this Thesis was to develop the methods of fabrication of scaffolds for tissue engineering resistant to protein fouling. Prevention of fouling on the surface of the materials that come into contact with bodily fluids/tissues is of utmost importance in order to gain control over cell functions by eliminating all unwanted, uncontrolled, non-specific interactions of the material surface with the surrounding fluids and providing specific signals to the cells to guide their behavior in the direction of tissue regeneration. To achieve this, the work was developed in three steps, (i) the selection of monomers leading to antifouling properties; (ii) preparation of antifouling hydrogels by copolymerization with zwitterionic carboxybetaine monomers; and (iii) modification of nanofibers with selected polymer brushes resistant to protein fouling.

In order to tackle the first step, a model system based on polymer brushes was utilized. Polymer brushes based on eight different monomers were synthesized, fully characterized, and the fouling from solution of HSA, Fbg, as well as from undiluted blood plasma was assessed by SPR. The monomers MeOEGMA, HOEGMA, HPMA, CBAA and CBMAA showed the best resistance to protein fouling and were selected for the further preparation and/or modification of the scaffold for tissue engineering.

Striving to improve the resistance to protein fouling and hydration of the scaffolds based on poly(HEMA), hydrogels of different compositions were synthesized by copolymerization of HEMA with zwitterionic carboxybetaine (meth)acrylamide (CBAA or CBMAA). These hydrogels showed unprecedented improvement of hydration (up to 30000%), mechanical properties (elongation up to 1800%), abilities to self-heal, and remarkable reduction of protein fouling from complex biological media, such as blood plasma and fetal bovine serum.

To provide control over the precise shape and internal porous architecture of the scaffold, stereolithography was utilized to prepare hydrogels with a finely designed gyroid pore structure based on a biodegradable macromer (MA-PDLLA-PEG-PDLLA-MA) and zwitterionic CBMAA. All hydrogels showed high hydration and antifouling character. The covalent immobilization of protein on the surface of the hydrogels utilizing the carboxylic groups of the CBMAA comonomer was successful and homogeneous across the pores of the hydrogels.

Finally, in order to prevent protein fouling from biological fluids and subsequent cell adhesion, a new approach to modify the surface of PCL nanofibers by growing antifouling polymer brushes by SI-ATRP was introduced. To provide functional groups for the immobilization of SI-ATRP initiator, a biomimetic PDA layer was deposited onto the surface of the PCL nanofibers. Four types of selected antifouling polymer brushes were grown from the surface of nanofibers without impairing the fibrous structure and interconnectivity of the pores. The resistance to non-specific cell adhesion was evaluated by challenging the fibers with fibroblasts. Cells rapidly adhered and spread on pristine PCL and PDA-coated nanofibers forming cell–matrix interactions mediated by a pre-adsorbed layer of proteins from culture media. However, all nanofibers modified with antifouling polymer brushes were able to prevent non-specific protein adsorption and thereby fully suppress cell adhesion.

The materials presented in this Thesis show significant improvements in terms of resistance to protein fouling and non-specific cell adhesion. These scaffolds have high potential to be used as a platform for further functionalization with bioactive compounds for specific cell-matrix communication. The methods applied for the preparation of antifouling scaffolds are universal and can be extended to different types of materials in order to achieve specific properties for the scaffolds.

References

1. M. Al Sebayel, A. M. Alenazi, R. Sabbagh, T. Al Ageel, M. Al Enazi, H. Al Bahili and H. Elsiesy, *Transplant. Proc.*, 2014, **46**, 2030-2035.
2. B. D. Ratner, A. S. Hoffman, F. J. Schoen and J. E. Lemons, *Biomaterials Science: An Introduction to Materials in Medicine, Second Edition* Elsevier Academic Press, 2004.
3. R. Lanza, R. Langer and J. P. Vacanti, *Principles of Tissue Engineering*, Elsevier, Boston, 2007.
4. B. D. Ratner, A. S. Hoffman, F. J. Schoen and J. E. Lemons, *Biomaterials Science: An Introduction to Materials in Medicine, Third Edition*, Elsevier, Oxford, 2013.
5. K. K. Khush, J. G. Zaroff, J. Nguyen, R. Menza and B. A. Goldstein, *Am J Transplant*, 2015, **15**, 642-649.
6. B. Ekser, D. K. Cooper and A. J. Tector, *Int. J. Surg.*, 2015.
7. K. Y. Lee and D. J. Mooney, *Chem. Rev.*, 2001, **101**, 1869-1880.
8. B. V. Slaughter, S. S. Khurshid, O. Z. Fisher, A. Khademhosseini and N. A. Peppas, *Adv. Mater.*, 2009, **21**, 3307-3329.
9. D. M. Bravata and E. B. Keeffe, *Liver Transplant.*, 2001, **7**, s119-s123.
10. R. Langer and J. P. Vacanti, *Science*, 1993, **260**, 920-926.
11. R. Pirraco and R. Reis, *Stem Cell Rev. Rep.*, 2015, **11**, 373-375.
12. R. Langer, *Mol. Ther.*, 2000, **1**, 12-15.
13. M. Grossman, S. E. Raper, K. Kozarsky, E. A. Stein, J. F. Engelhardt, D. Muller, P. J. Lupien and J. M. Wilson, *Nat. Genet.*, 1994, **6**, 335-341.
14. D. Orlic, J. Kajstura, S. Chimenti, I. Jakoniuk, S. M. Anderson, B. Li, J. Pickel, R. McKay, B. Nadal-Ginard, D. M. Bodine, A. Leri and P. Anversa, *Nature*, 2001, **410**, 701-705.
15. A. Murua, A. Portero, G. Orive, R. M. Hernández, M. de Castro and J. L. Pedraz, *J. Controlled Release*, 2008, **132**, 76-83.
16. A. M. A. Rokstad, I. Lacík, P. de Vos and B. L. Strand, *Adv. Drug Delivery Rev.*, 2014, **67–68**, 111-130.
17. F. Wiegand, K. Dietrich and V. Kolb, *Transplantation*, 1993, **56**, 1206-1212.
18. C. A. Vacanti, *J. Cell. Mol. Med.*, 2006, **10**, 569-576.
19. P. X. Ma and J. Elisseeff, *Scaffolding in Tissue Engineering*, CRC Press, Boca Raton, 2006.
20. A. Atala, F. K. Kasper and A. G. Mikos, *Sci. Transl. Med.*, 2012, **4**, 160rv112.
21. J. Zhu and R. E. Marchant, *Expert Rev. Med. Devices*, 2011, **8**, 607-626.
22. B. Derby, *Science*, 2012, **338**, 921-926.
23. D. F. Williams, *Biomaterials*, 2008, **29**, 2941-2953.

24. R. H. Harrison, J. P. St-Pierre and M. M. Stevens, *Tissue Eng Part B Rev*, 2014, **20**, 1-16.
25. V. Vogel and M. Sheetz, *Nat. Rev. Mol. Cell Biol.*, 2006, **7**, 265-275.
26. V. Vogel and M. P. Sheetz, *Curr. Opin. Cell Biol.*, 2009, **21**, 38-46.
27. K. Takahashi and S. Yamanaka, *Cell*, 2006, **126**, 663-676.
28. M. Brittberg, A. Lindahl, A. Nilsson, C. Ohlsson, O. Isaksson and L. Peterson, *N. Engl. J. Med.*, 1994, **331**, 889-895.
29. B. Dhandayuthapani, Y. Yoshida, T. Maekawa and D. S. Kumar, *Int. J. Polym. Sci.*, 2011, **2011**, 1-19.
30. R. Langer and D. A. Tirrell, *Nature*, 2004, **428**, 487-492.
31. S. F. Badylak, D. O. Freytes and T. W. Gilbert, *Acta Biomater.*, 2015, **23, Supplement**, S17-S26.
32. J. J. Lovekamp, D. T. Simionescu, J. J. Mercuri, B. Zubiate, M. S. Sacks and N. R. Vyavahare, *Biomaterials*, 2006, **27**, 1507-1518.
33. H.-K. Lin, S. V. Madihally, B. Palmer, D. Frimberger, K.-M. Fung and B. P. Kropp, *Adv. Drug Delivery Rev.*, 2015, **82–83**, 47-63.
34. J. J. Song and H. C. Ott, *Trends Mol. Med.*, **17**, 424-432.
35. T. Woods and P. F. Gratzer, *Biomaterials*, 2005, **26**, 7339-7349.
36. D. O. Freytes, R. S. Tullius, J. E. Valentin, A. M. Stewart-Akers and S. F. Badylak, *J. Biomed. Mater. Res., Part A*, 2008, **87A**, 862-872.
37. P. B. Malafaya, G. A. Silva and R. L. Reis, *Adv. Drug Delivery Rev.*, 2007, **59**, 207-233.
38. T. A. Holland, Y. Tabata and A. G. Mikos, *J. Controlled Release*, 2003, **91**, 299-313.
39. R. G. Payne, M. J. Yaszemski, A. W. Yasko and A. G. Mikos, *Biomaterials*, 2002, **23**, 4359-4371.
40. S. L. Rowe, S. Lee and J. P. Stegemann, *Acta Biomater.*, 2007, **3**, 59-67.
41. E. Papajová, M. Bujdoš, D. Chorvát, M. Stach and I. Lacík, *Carbohydr. Polym.*, 2012, **90**, 472-482.
42. E. Khor and L. Y. Lim, *Biomaterials*, 2003, **24**, 2339-2349.
43. N. Kostina, M. Gorshkova and V. Izumrudov, *Polym. Sci., Ser. A*, 2011, **53**, 947-954.
44. Y.-H. Liao, S. A. Jones, B. Forbes, G. P. Martin and M. B. Brown, *Drug Delivery*, 2005, **12**, 327-342.
45. M. Kobayashi and M. Oka, *J. Biomater. Sci., Polym. Ed.*, 2004, **15**, 741-751.
46. M. Přádný, L. Martinová, J. Michálek, T. á. Fenclová and E. Krumbholcová, *Cent. Eur. J. Chem.*, 2007, **5**, 779-792.
47. K. Takeda, H. Kitagawa, R. Tsuboi, W. Kiba, J.-I. Sasaki, M. Hayashi and S. Imazato, *Dent. Mater.*, 2015, **31**, 1406-1414.
48. A. La Gatta, C. Schiraldi, A. Esposito, A. D'Agostino and A. De Rosa, *J. Biomed. Mater. Res., Part A*, 2009, **90A**, 292-302.
49. J. Drury, *Biomaterials*, 2003, **24**, 4337-4351.
50. J. Jagur-Grodzinski, *Polym. Adv. Technol.*, 2009, 27-47.
51. K. Haraguchi and T. Takehisa, *Adv. Mater.*, 2002, **14**, 1120-1124.
52. C.-C. Lin and K. Anseth, *Pharm. Res.*, 2009, **26**, 631-643.
53. S. A. Skoog, P. L. Goering and R. J. Narayan, *J. Mater. Sci.: Mater. Med.*, 2014, **25**, 845-856.

54. E. S. Place, J. H. George, C. K. Williams and M. M. Stevens, *Chem. Soc. Rev.*, 2009, **38**, 1139-1151.
55. A. Hejčl, P. Lesný, M. Přádný, J. Šedý, J. Zámečník, P. Jendelová, J. Michálek and E. Syková, *J. Mater. Sci.: Mater. Med.*, 2009, **20**, 1571-1577.
56. P. Lesný, J. De Croos, M. Prádný, J. Vacík, J. Michálek, S. Woerly and E. Syková, *J. Chem. Neuroanat.*, 2002, **23**, 243-247.
57. J. Vacík, B. Dvořánková, J. Michálek, M. Přádný, E. Krumbholcová, T. Fenclová and K. Smetana, *J. Mater. Sci.: Mater. Med.*, 2007, **19**, 883-888.
58. O. Wichterle and D. Lim, *Nature*, 1960, **185**, 117-118.
59. S. J. Buwalda, K. W. M. Boere, P. J. Dijkstra, J. Feijen, T. Vermonden and W. E. Hennink, *J. Controlled Release*, 2014, **190**, 254-273.
60. T.-H. Young, W.-Y. Chuang, M.-Y. Hsieh, L.-W. Chen and J.-P. Hsu, *Biomaterials*, 2002, **23**, 3495-3501.
61. M. F. A. Goosen, M. V. Sefton and M. W. C. Hatton, *Thromb. Res.*, **20**, 543-554.
62. Z. Tang, Y. Akiyama and T. Okano, *J. Polym. Sci., Part B: Polym. Phys.*, 2014, **52**, 917-926.
63. R. A. Stile, W. R. Burghardt and K. E. Healy, *Macromolecules*, 1999, **32**, 7370-7379.
64. T. Riedel, Z. Riedelová-Reicheltová, P. Májek, C. Rodriguez-Emmenegger, M. Houska, J. E. Dyr and E. Brynda, *Langmuir*, 2013, **29**, 3388-3397.
65. J. Zhu, *Biomaterials*, 2010, **31**, 4639-4656.
66. D. A. Edelman, S. L. McIntyre and J. Harper, *Am. J. Obstet. Gynecol.*, 1984, **150**, 869-876.
67. X. Liu, J. M. Holzwarth and P. X. Ma, *Macromol. Biosci.*, 2012, **12**, 911-919.
68. N. Y. Yu, A. Schindeler, D. G. Little and A. J. Ruys, *J. Biomed. Mater. Res., Part B*, 2010, **93**, 285-295.
69. K. Rezwan, Q. Z. Chen, J. J. Blaker and A. R. Boccaccini, *Biomaterials*, 2006, **27**, 3413-3431.
70. Y. Dong, S. Liao, M. Ngiam, C. K. Chan and S. Ramakrishna, *Tissue Eng., Part B*, 2009, **15**, 333-351.
71. B. D. Ulery, L. S. Nair and C. T. Laurencin, *J. Polym. Sci., Part B: Polym. Phys.*, 2011, **49**, 832-864.
72. J. Guan, K. L. Fujimoto, M. S. Sacks and W. R. Wagner, *Biomaterials*, 2005, **26**, 3961-3971.
73. N. Kumar, R. S. Langer and A. J. Domb, *Adv. Drug Delivery Rev.*, 2002, **54**, 889-910.
74. A. S. Hoffman, *Adv. Drug Delivery Rev.*, 2002, **54**, 3-12.
75. D. Cohn and A. Hotovely-Salomon, *Polymer*, 2005, **46**, 2068-2075.
76. D. Wu, F. Xu, B. Sun, R. Fu, H. He and K. Matyjaszewski, *Chem. Rev.*, 2012, **112**, 3959-4015.
77. N. A. Peppas, J. Z. Hilt, A. Khademhosseini and R. Langer, *Adv. Mater.*, 2006, **18**, 1345-1360.
78. R. M. Ottenbrite, K. Park and T. Okano, *Biomedical Applications of Hydrogels Handbook*, Springer, New York, 2010.
79. C. P. Barnes, S. A. Sell, E. D. Boland, D. G. Simpson and G. L. Bowlin, *Adv. Drug Delivery Rev.*, 2007, **59**, 1413-1433.
80. N. Zhu and X. Chen, *Biofabrication of Tissue Scaffolds*, 2013.

81. B. Mattiasson, A. Kumar and I. Y. Galaev, *Macroporous Polymers: Production Propertie and Biotechnological / Biomedical Applications*, CRC Press, Boca Raton, 2010.
82. F. P. Melchels, J. Feijen and D. W. Grijpma, *Biomaterials*, 2010, **31**, 6121-6130.
83. F. P. Melchels, A. M. Barradas, C. A. van Blitterswijk, J. de Boer, J. Feijen and D. W. Grijpma, *Acta Biomater.*, 2010, **6**, 4208-4217.
84. S. B. G. Blanquer, S. P. Haimi, A. A. Poot and D. W. Grijpma, *Macromol. Symp.*, 2013, **334**, 75-81.
85. F. P. W. Melchels, J. Feijen and D. W. Grijpma, *Biomaterials*, 2009, **30**, 3801-3809.
86. A. Ronca, L. Ambrosio and D. W. Grijpma, *Acta Biomater.*, 2013, **9**, 5989-5996.
87. S. Schuller-Ravoo, J. Feijen and D. W. Grijpma, *Macromol. Biosci.*, 2011, **11**, 1662-1671.
88. T. M. Seck, F. P. Melchels, J. Feijen and D. W. Grijpma, *J. Controlled Release*, 2010, **148**, 34-41.
89. F. Yener and O. Jirsak, *J. Nanomater.*, 2012, **2012**, 1-6.
90. A. de Mel, G. Jell, M. M. Stevens and A. M. Seifalian, *Biomacromolecules*, 2008, **9**, 2969-2979.
91. T. N. Vo, F. K. Kasper and A. G. Mikos, *Adv. Drug Delivery Rev.*, 2012, **64**, 1292-1309.
92. H. Shin, S. Jo and A. G. Mikos, *Biomaterials*, 2003, **24**, 4353-4364.
93. M. R. Johnson, H.-J. Lee, R. V. Bellamkonda and R. E. Guldberg, *Acta Biomater.*, 2009, **5**, 23-28.
94. K. K. Macdonald, C. Y. Cheung and K. S. Anseth, *J. Tissue Eng. Regener. Med.*, 2007, **1**, 314-317.
95. A. E. Rodda, F. Ercole, V. Glattauer, J. Gardiner, D. R. Nisbet, K. E. Healy, J. S. Forsythe and L. Meagher, *Biomacromolecules*, 2015.
96. S. Garty, N. Kimelman-Bleich, Z. Hayouka, D. Cohn, A. Friedler, G. Pelled and D. Gazit, *Biomacromolecules*, 2010, **11**, 1516-1526.
97. U. Hersel, *Biomaterials*, 2003, **24**, 4385-4415.
98. S. Noel, A. Hachem, Y. Merhi and G. De Crescenzo, *Biomacromolecules*, 2015, **16**, 1682-1694.
99. P. Vermette, T. Gengenbach, U. Divisekera, P. A. Kambouris, H. J. Griesser and L. Meagher, *J. Colloid Interface Sci.*, 2003, **259**, 13-26.
100. R. E. Ducker, M. T. Montague and G. J. Leggett, *Biointerphases*, 2008, **3**, 59.
101. H. S. Yoo, T. G. Kim and T. G. Park, *Adv. Drug Delivery Rev.*, 2009, **61**, 1033-1042.
102. C. Rodriguez-Emmenegger, E. Brynda, T. Riedel, M. Houska, V. Subr, A. B. Alles, E. Hasan, J. E. Gautrot and W. T. Huck, *Macromol. Rapid Commun.*, 2011, **32**, 952-957.
103. T. Tischer, C. Rodriguez-Emmenegger, V. Trouillet, A. Welle, V. Schueler, J. O. Mueller, A. S. Goldmann, E. Brynda and C. Barner-Kowollik, *Adv. Mater.*, 2014, **26**, 4087-4092.
104. E. Brynda, N. A. Cepalova and M. Štol, *J. Biomed. Mater. Res.*, 1984, **18**, 685-693.
105. C. Rodriguez-Emmenegger, S. Janel, A. de los Santos Pereira, M. Bruns and F. Lafont, *Polym. Chem.*, 2015, **6**, 5740-5751.
106. F. Surman, T. Riedel, M. Bruns, N. Y. Kostina, Z. Sedláková and C. Rodriguez-Emmenegger, *Macromol. Biosci.*, 2015, **15**, 636-646.

107. C. Blaszykowski, S. Sheikh and M. Thompson, *Trends Biotechnol.*, 2014, **32**, 61-62.
108. G. F. Muschler, C. Nakamoto and L. G. Griffith, *J. Bone Jt. Surg.*, 2004, **86**, 1541-1558.
109. S. Soker, M. Machado and A. Atala, *World J. Urol.*, 2000, **18**, 10-18.
110. M. Arnold, E. A. Cavalcanti-Adam, R. Glass, J. Blümmel, W. Eck, M. Kantlehner, H. Kessler and J. P. Spatz, *ChemPhysChem*, 2004, **5**, 383-388.
111. E. A. Cavalcanti-Adam, T. Volberg, A. Micoulet, H. Kessler, B. Geiger and J. P. Spatz, *Biophys. J.*, 2007, **92**, 2964-2974.
112. J. Huang, S. V. Gräter, F. Corbellini, S. Rinck, E. Bock, R. Kemkemer, H. Kessler, J. Ding and J. P. Spatz, *Nano Lett.*, 2009, **9**, 1111-1116.
113. B. Trappmann, J. E. Gautrot, J. T. Connelly, D. G. T. Strange, Y. Li, M. L. Oyen, M. A. Cohen Stuart, H. Boehm, B. Li, V. Vogel, J. P. Spatz, F. M. Watt and W. T. S. Huck, *Nat. Mater.*, 2012, **11**, 642-649.
114. M. J. Dalby, M. O. Riehle, D. S. Sutherland, H. Agheli and A. S. G. Curtis, *Biomaterials*, 2004, **25**, 5415-5422.
115. D. F. Williams, *Biomaterials*, 2009, **30**, 5897-5909.
116. I. Banerjee, R. C. Pangule and R. S. Kane, *Adv. Mater.*, 2011, **23**, 690-718.
117. E. Brynda, J. Drobník, J. Vacík and J. Kálal, *J. Biomed. Mater. Res.*, 1978, **12**, 55-65.
118. V. Erwin A, *Biomaterials*, 2012, **33**, 1201-1237.
119. L. Vroman, *Colloids Surf., B*, 2008, **62**, 1-4.
120. T. Riedel, C. Rodriguez-Emmenegger, A. de los Santos Pereira, A. Bědajánková, P. Jinoch, P. M. Boltovets and E. Brynda, *Biosens. Bioelectron.*, 2014, **55**, 278-284.
121. C. Rodriguez-Emmenegger, M. Houska, A. B. Alles and E. Brynda, *Macromol. Biosci.*, 2012, **12**, 1413-1422.
122. C. Rodriguez-Emmenegger, O. A. Avramenko, E. Brynda, J. Skvor and A. B. Alles, *Biosens. Bioelectron.*, 2011, **26**, 4545-4551.
123. C. Rodriguez Emmenegger, E. Brynda, T. Riedel, Z. Sedlakova, M. Houska and A. B. Alles, *Langmuir*, 2009, **25**, 6328-6333.
124. C. Rodriguez-Emmenegger, O. Kylián, M. Houska, E. Brynda, A. Artemenko, J. Kousal, A. B. Alles and H. Biederman, *Biomacromolecules*, 2011, **12**, 1058-1066.
125. R. G. Chapman, E. Ostuni, S. Takayama, R. E. Holmlin, L. Yan and G. M. Whitesides, *J. Am. Chem. Soc.*, 2000, **122**, 8303-8304.
126. J. Homola, *Chem. Rev.*, 2008, **108**, 462-493.
127. H. Vaisocherová, W. Yang, Z. Zhang, Z. Cao, G. Cheng, M. Piliarik, J. Homola and S. Jiang, *Anal. Chem.*, 2008, **80**, 7894-7901.
128. P. Lesný, M. Přádný, P. Jendelová, J. Michálek, J. Vacík and E. Syková, *J. Mater. Sci.: Mater. Med.*, 2006, **17**, 829-833.
129. B. Rolando, *Hydrogels. Biological Properties And Applications*, Springer, 2009.
130. J. L. Drury and D. J. Mooney, *Biomaterials*, 2003, **24**, 4337-4351.
131. R. G. Laughlin, *Langmuir*, 1991, **7**, 842-847.
132. C.-W. Chang, A. van Spreeuwel, C. Zhang and S. Varghese, *Soft Matter*, 2010, **6**, 5157-5164.
133. Y. Tanaka, J. P. Gong and Y. Osada, *Prog. Polym. Sci.*, 2005, **30**, 1-9.
134. K. Haraguchi, K. Uyama and H. Tanimoto, *Macromol. Rapid Commun.*, 2011, **32**, 1253-1258.

135. Q. Wang, J. L. Mynar, M. Yoshida, E. Lee, M. Lee, K. Okuro, K. Kinbara and T. Aida, *Nature*, 2010, **463**, 339-343.
136. N. Y. Kostina, C. Rodriguez-Emmenegger, M. Houska, E. Brynda and J. Michálek, *Biomacromolecules*, 2012, **13**, 4164-4170.
137. J. C. Ashworth, S. M. Best and R. E. Cameron, *Mater. Technol.*, 2014, **29**, 281-295.
138. G. Antonio, R. Teresa, D. S. Roberto and A. Luigi, *J. Appl. Biomater. Biomech.*, 2009, **7**, 141-152.
139. A. Arinstein and E. Zussman, *J. Polym. Sci., Part B: Polym. Phys.*, 2011, **49**, 691-707.
140. D. Kai, S. S. Liow and X. J. Loh, *Materials Science & Engineering, C: Materials for Biological Applications*, 2014, **45**, 659-670.
141. H.-J. Sung, C. Meredith, C. Johnson and Z. S. Galis, *Biomaterials*, 2004, **25**, 5735-5742.
142. C. Rodriguez-Emmenegger, A. Jäger, E. Jäger, P. Stepanek, A. B. Alles, S. S. Guterres, A. R. Pohlmann and E. Brynda, *Colloids Surf., B*, 2011, **83**, 376-381.
143. O. Pop-Georgievski, C. Rodriguez-Emmenegger, A. d. l. S. Pereira, V. Proks, E. Brynda and F. Rypacek, *J. Mater. Chem. B*, 2013, **1**, 2859.
144. O. Pop-Georgievski, D. Verreault, M.-O. Diesner, V. Proks, S. Heissler, F. Rypacek and P. Koelsch, *Langmuir*, 2012, **28**, 14273-14283.
145. O. Pop-Georgievski, S. Popelka, M. Houska, D. Chvostovaa, V. Proks and F. Rypacek, *Biomacromolecules*, 2011, **12**, 3232-3242.
146. C. Rodriguez-Emmenegger, C. M. Preuss, B. Yameen, O. Pop-Georgievski, M. Bachmann, J. O. Mueller, M. Bruns, A. S. Goldmann, M. Bastmeyer and C. Barner-Kowollik, *Adv. Mater.*, 2013, **25**, 6123-6127.
147. H. Lee, S. M. Dellatore, W. M. Miller and P. B. Messersmith, *Science*, 2007, **318**, 426-430.

List of Abbreviations

3D	Three-dimensional
BP	Blood plasma
BSA-FITC	Fluorescein isothiocyanate bovine serum albumin
CAD	Computer-aided design
CBAA	Carboxybetaine acrylamide
CBMAA	Carboxybetaine methacrylamide
DNA	Deoxyribonucleic acid
ECM	Extracellular matrix
EDC	*N*-(3-dimethylaminopropyl)-*N*′-ethylcarbodiimide hydrochloride
EWC	Equilibrium water content
Fbg	Fibrinogen
FBS	Fetal bovine serum
FDA	Food and Drug Administration
FTIR-ATR	Fourier transform infrared spectroscopy with Attenuated total reflection
HEMA	2-Hydroxyethyl methacrylate
HOEGMA	Oligo(ethylene glycol) methacrylate
HPMA	*N*-(2-hydroxypropyl) methacrylamide
HSA	Human serum albumin
LCST	Lower critical solution temperature
LN	Laponite nanoparticle
LSCM	Laser scanning confocal microscopy

MAAH	Methacrylic anhydride
MEFs	Mouse embryonic fibroblasts
MeOEGMA	Oligo(ethylene glycol) methyl ether methacrylate
MRI	Magnetic resonance imaging
NMR	Nuclear magnetic resonance
PC	Polycarbonate
PCL	Poly(ε-caprolactone)
PCMA	Phosphorylcholine methacrylate
PDA	Poly(dopamine)
PEG	Poly(ethylene glycol)
PEGDMA	Poly(ethylene glycol dimethacrylate)
PGA	Poly(glycolic acid)
PGLA	Poly(lactide-*co*-glycolide)
Poly(HEMA)	Poly(2-hydroxyethyl methacrylate)
PLA	Poly(lactic acid)
Poly(NIPAm)	Poly(*N*-isopropylacrylamide)
PU	Polyurethane
PVA	Poly(vinyl alcohol)
SBMA	Sulfobetaine methacrylate
SC/PL	Solvent casting/particulate leaching
SE	Spectroscopic ellipsometry
SEM	Scanning electron microscopy
SFF	Solid freeform fabrication
SI-ATRP	Surface-initiated atom transfer radical polymerization
SLS	Selective laser sintering
SPR	Surface plasmon resonance
sulfoNHS	*N*-Hydroxysulfosuccinimide sodium salt
UV	Ultraviolet

Appendix 1

Polymer brushes interfacing blood as a route toward high performance blood contacting devices

Macromolecular Bioscience, 2015, 15(5), 636-646

Polymer Brushes Interfacing Blood as a Route Toward High Performance Blood Contacting Devices

František Surman, Tomáš Riedel, Michael Bruns, Nina Yu. Kostina, Zdeňka Sedláková, Cesar Rodriguez-Emmenegger*

In the current study, well-defined polymer brushes are shown as an effective surface modification to resist the adhesion of whole blood and its components. Poly[oligo(ethylene glycol)methylether methacrylate] (poly(MeOEGMA)), poly(hydroxyethyl methacrylate) (poly(HEMA)), poly[N-(2-hydroxypropyl) methacrylamide] (poly(HPMA)), and poly(carboxybetaine acrylamide) (poly(CBAA)) brushes were grown by surface initiated atom transfer radical polymerization (SI-ATRP) and subsequently characterized by Fourier-transform infrared (FTIR) spectroscopy, X-ray photoelectron spectroscopy (XPS), dynamic contact angle measurements, atomic force microscopy (AFM), and surface plasmon resonance (SPR) spectroscopy. All brushes decreased the fouling from blood plasma over 95% and prevented the adhesion of platelets, erythrocytes, and leukocytes as evidenced by SPR and SEM measurements.

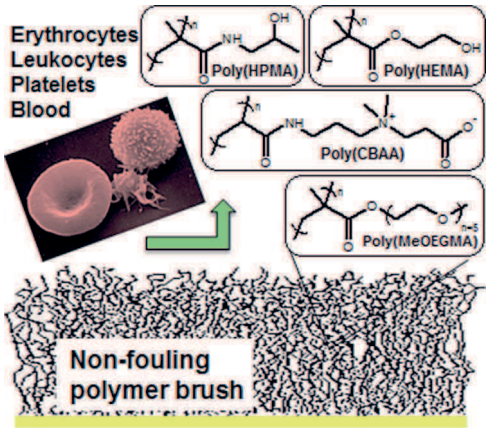

1. Introduction

The interaction of blood with non-endothelial artificial surfaces contributes to severe pathological events encountered in cardiovascular clinical practice.[1] About the 6 million cardiovascular procedures utilizing more than 50 million blood contacting devices have been performed annually only in the United States.[2,3] Synthetic medical devices operating in human bloodstream include catheters for surgical procedures, stents to reinforce blood vessels, vascular grafts for replacement of diseased arteries, artificial kidneys, prosthetic heart valves, or ventricular circulatory supports to replace the function of a failing heart.[4] The interaction of an implanted foreign biomaterial with blood is very complex and its intimate understanding requires integrating the several branches of research. Generally, when any artificial material comes into contact with biological fluid that contains soluble proteins, in particular blood plasma (BP), proteins rapidly adsorb and form the monolayer on the surface.[5–7] The adsorbed proteins as well as platelet adhesion lead to the complement activation and attract leukocytes, thus enabling the immune system to identify the foreign-body surfaces with concomitant detrimental effects. In addition,

F. Surman, T. Riedel, N. Kostina, Z. Sedláková, C. Rodriguez-Emmenegger
Institute of Macromolecular Chemistry, Academy of Sciences of the Czech Republic, v.v.i., Prague 162 06, Czech Republic
E-mail: rodriguez@imc.cas.cz
M. Bruns
Institute for Applied Materials (IAM), Karlsruhe Nano Micro Facility (KNMF), Karlsruhe Institute of Technology (KIT), Hermann-von-Helmholtz-Platz 1, 76344 , Eggenstein-Leopoldshafen, Germany

[a]**Supporting Information** is available online from the Wiley Online Libraryor from the author.

DOI: 10.1002/mabi.201400470

the protein adsorption may initiate the coagulation cascade. As a result, blood–material interactions progressively impair the function of a device and contribute to thromboembolic complications, which can cause lethal complications.[8] Therefore, the prevention of fouling from plasma proteins seems to be essential for medical blood contacting devices.

Extensive research has been done on surfaces resistant to fouling.[9,10] Traditionally, the adsorption from human serum albumin (HSA) and fibrinogen has been used to characterize the resistance to fouling.[9,10] However, we have demonstrated that the resistant to these abundant proteins is not a proof of the resistance to BP.[7,11,12] Thus, the process of plasma fouling is of very complex nature.

Polymer brushes grown from the surface of the substrate have become the powerful alternative to ultra-thin polymer coatings. With the advent of surface initiated reversible deactivation radical polymerization, such as (photoinduced)[13,14] atom transfer radical polymerization (ATRP),[15] reversible addition fragmentation transfer (RAFT)[16,17] polymerization, and single electron transfer radical polymerization (SET-LRP), [18] it has been possible to prepare ultra-thin coatings with an unique level of control over composition, structure, and properties. However, only few types of these brushes;[9,19] based on 2-hydroxyethethyl methacrylate, oligo(ethylenglycol) methylether methacrylate (MeOEGMA), hydroxyethyl acrylamide,[20] oxazolines,[21] carboxybetaines (CB), and *N*-(2-hydroxypropyl) methacrylamide have shown a real reduction or even complete suppression of BP fouling.[7,11,12,18,22] These brushes have displayed an excellent resistance to fouling from BP as well as different cells lines and bacteria.[7,11,12,18,22,23]

However, the complexity of blood poses more serious challenges than BP. Various leukocytes trigger the processes during inflammation or infection responses. Leukocytes adhesion can be mediated by preadhesion of platelets or their clusters, which rapidly adhere to surfaces by modifying their cytoskeleton and by producing actin fibers. Additionally, the platelet activation can initiated thrombosis. Erythrocytes usually do not participate in processes of thrombosis, therefore the process of direct attachment has been considered to be of minor importance. However, they mechanically influence the diffusion and convection transport of other blood elements.[24] Therefore, the design of materials able to interface blood requires that whole blood is tested instead of single protein solutions.[25,26]

In this study, we evaluate the resistance to deposition from full blood and its main components – platelet rich plasma (PRP), erythrocytes, leukocytes, and full blood on four ultra-low fouling polymer brushes, poly[oligo-(ethylene glycol) methylether methacrylate] (poly-(MeOEGMA)), poly(2-hydroxyethyl methacrylate) (poly-(HEMA)), poly[*N*-(2-hydroxypropyl) methacrylamide] (poly-(HPMA)), and poly(carboxybetaine acrylamide) (poly-(CBAA)). The surfaces were fully characterized and their resistance to BP proteins assessed. Their resistance to protein fouling is compared with the reduction of surface coverage after contact with whole blood showing not a direct relation. While most studies have focused in the fouling from proteins and other biological fluids,[7,9,25] a comparative study of the fouling from whole blood on antifouling brushes has not been assessed. The results herein presented suggest general trends on the design of surfaces to interface blood causing minimal effects.

2. Experimental Section

2.1. Materials

All chemical reagents were purchased from Sigma–Aldrich, Acros or Serva at the highest available quality and used without further purification unless otherwise stated. Ligands 2,2′-bipyridyl (BiPy, 99%), 1,4,8,11-tetramethyl-1,4,8,11-tetraazacyclotetradecane (Me_4Cyclam, 98%), catalysts CuCl (≥99.995%), CuBr (99.999%), $CuBr_2$ (99.999%), and biochemical reagents fibrinogen from human BP (Fbg, 90%), albumin from human serum (HSA, ≥97%), and BP were purchased from Sigma–Aldrich and used as received. Initiator ω-mercaptoundecylbromoisobutyrate was synthesized by reaction of α-bromoisobutyryl bromide (Sigma–Aldrich, 98%) with 11-mercapto-1-undecanol (Sigma–Aldrich, 99%) according to a literature procedure.[27] *N*-[3-(Dimethylamino) propyl] acrylamide (DMAPA, 98%) and β-propiolactone (90%) were purchased from TCI Europe and Serva Electrophoresis GmbH, respectively. Water was purified by a Millipore (Milli-Q). THF, dichloromethane, ether, ethanol were purchased from LachNer, Czech Republic. The monomers 3-acryloylaminopropyl-2-carboxyethyl-dimethylammonium (carboxybetaine acrylamide, CBAA) and *N*-(2-hydroxypropyl) methacrylamide (HPMA) were synthesized according to literature procedures.[28–31] 2-Hydroxyethyl methacrylate (HEMA) and oligo(ethylene glycol) methylether methacrylate $\overline{M}_n$ 300 (MeOEGMA) were purchased from Sigma–Aldrich and disinhibited passing through a basic alumina column prior to the polymerization. Blood and BP was kindly provided by the Institute of Hematology and Blood Transfusion, Prague, Czech Republic.[32] Gold coated surfaces were prepared by evaporation of a titanium adhesion layer (3 nm) and subsequent evaporation of gold; 50 nm for chips for surface plasmon resonance (SPR) and blood compatibility experiments, as well as 200 nm for the Si wafers for ellipsometry experiments.

2.2. Self-assembled Monolayer of Initiator

Gold-coated glass slides (SPR chips) and gold-coated Si-wafer chips (for ellipsometry) were rinsed twice with ethanol and deionized Mili-Q water, blow-dried with nitrogen, and cleaned in a UV/Ozone cleaner (Jelight) for 20 min. Immediately after cleaning, the chips were immersed in a 1 mm solution of ω-mercaptoundecyl

bromoisobutyrate in ethanol and kept overnight in the dark at room temperature to allow the formation of a SAM.

2.3. Preparation of Polymer Brushes via Surface-initiated Atom Transfer Radical Polymerization (SI-ATRP)

2.3.1. Poly(MeOEGMA) Brushes

$CuBr_2$ (10.1 mg, 45 μmol) and 2,2′-bipyridyl (92.9 mg, 595 μmol) were added to a one-neck Schlenk tube equipped with a magnetic stirring bar, rubber septum, and filled with argon. Subsequently CuBr (32.3 mg, 225 μmol) was added under argon positive pressure. Then, the flask was quickly evacuated and backfilled with argon followed by the addition of 3 mL previously degassed (via six freeze–pump–thaw cycles) methanol by gastight syringe. In the second flask, a solution of MeOEGMA (3.4 g, 11.4 mmol) in 3 mL of water was degassed using argon bubbling for 40 min at 0 °C. After the catalyst was fully dissolved, the monomer solution was transferred to the catalyst solution by gastight syringe. Subsequently, the homogenized polymerization mixture was transferred using cannula to the reactor containing gold-coated substrates with the initiator SAM. The polymerization was carried out at 30 °C for 45 min. The samples were taken out of the reactor, washed successively with ethanol and water, and stored in water.

2.3.2. Poly(HEMA) Brushes

Poly(HEMA) brushes were prepared in an analogous fashion as poly(MeOEGMA) using ethanol/water 1/1 vol.-% (8 mL) as a solvent. The polymerization mixture consisted of $CuBr_2$ (4.9 mg, 22 μmol), 2,2′-bipyridyl (87.8 mg, 562 μmol), CuCl (22.5 mg, 228 μmol), and HEMA (3.5 g, 22.6 mmol). The polymerization was carried out at 30 °C for 20 min. The samples were taken out of the reactor, washed successively with ethanol and water, and stored in water.

2.3.3. Poly(HPMA) Brushes

4 mL of methanol was degassed via six freeze–pump–thaw cycles and subsequently transferred under argon atmosphere to a Schlenk tube containing CuCl (12 mg, 121 μmol), $CuCl_2$ (3.6 mg, 27 μmol), and Me_4Cyclam (41.5 mg, 162 μmol). In a second Schlenk tube HPMA (958 mg, 6.7 mmol) was dissolved in 4 mL of water previously degassed via six freeze–pump–thaw cycles. The monomer solution was transferred to the blue catalyst solution using a gastight syringe. Subsequently, the homogenized polymerization mixture was transferred using a cannula to the reactor containing the substrates with initiator SAM. The polymerization was carried out at 30 °C for 2 h. The samples were taken out of the reactor, washed successively with water, and stored in water.

2.3.4. Poly(CBAA) Brushes

These brushes were grown using a similar procedure as for poly(HPMA) using phosphate buffered saline (PBS, 8 mL) as a solvent. The polymerization mixture consists of $CuCl_2$ (29.2 mg, 217 μmol), Me_4Cyclam (82 mg, 320 μmol), CuCl (10.6 mg, 107 μmol), and CBAA (1.2 g, 5.3 mmol). The polymerization was carried out at 30 °C for 2 h. The samples were taken out of the reactor, washed successively with water, and stored in water.

2.4. Physicochemical Characterization of Polymer Brushes

2.4.1. Spectroscopic Ellipsometry

The dry thickness of the polymer brushes was determined by ellipsometry using Variable Angle Spectroscopic Imaging Auto-Nulling Ellipsometer EP^3-SE (Nanofilm Technologies GmbH, Germany) in the wavelength range of $\lambda = 399$–811 nm (source Xe-arc lamp, wavelength step ca. 10 nm) at an angle of incidence (AOI) = 70° in air, at room temperature. The thickness and refractive index of polymer layers were obtained from simultaneous fitting of the obtained ellipsometric data using Cauchy relationship model.

2.4.2. Contact Angle

The wettability of surfaces was examined by dynamic sessile water drop method using a DataPhysics OCA 20 contact angle system. A 5 μL drop was placed on the surface, and advancing and receding contact angles were determined while the volume of the drop was increased up to 15 μL and decreased at flow rate of 0.5 $\mu L \cdot min^{-1}$. Data were processed by circular fitting algorithm. Reported values are averages of at least three measurements recorded at different positions on each substrate.

2.4.3. Fourier Transform Infrared Grazing Angle Specular Reflectance Spectroscopy (FTIR GASR)

Spectra of dry polymer brushes were measured directly using FTIR Bruker IFS 55 spectrometer equipped with Pike Technologies 80Spec GASR attachment and polarizer (grazing angle 80°, p-polarization, MCT detector, resolution 2 cm^{-1}, 128 scans). The spectrometer was purged continuously with dry air.

2.4.4. X-Ray Photoelectron Spectroscopy (XPS)

XPS measurements were performed using a K-Alpha XPS spectrometer (Thermo Fisher Scientific, East Grinstead, UK). All the samples were analyzed using a microfocused, monochromated Al Kα X-ray source (400 μm spot size). The kinetic energy of the electrons was measured by a 180° hemispherical energy analyzer operated in the constant analyzer energy mode (CAE) at 50 eV pass energy for elemental spectra. Data acquisition and processing using the Thermo Advantage software is described elsewhere.[33] The spectra were fitted with one or more Voigt profiles (binding energy uncertainty: ± 0.2 eV). The analyzer transmission function, Scofield sensitivity factors,[34] and effective attenuation lengths (EALs) for photoelectrons were applied for quantification. EALs were calculated using the standard TPP-2M formalism.[35] All spectra were referenced to the C1s peak of hydrocarbons at 285.0 eV binding energy controlled by means of the well-known photoelectron peaks of metallic Cu, Ag, and Au.

2.4.5. Atomic Force Microscopy (AFM)

All images were acquired with a Multimode Atomic Force Microscope NanoScope IIIa (Digital Instruments) as topological scans in tapping mode in air, using silicon probes OTESPA (Veeco Instruments) with a nominal spring constant of 42 $N \cdot m^{-1}$ and a tip radius of 7–10 nm. Areas of $5 \times 5\ \mu m^2$ (512×512 pixels) were scanned at a rate of 1 Hz. The scans were analyzed using Gwyddion software.

2.5. Protein Fouling

The irreversible fouling from biological media on chips coated with the antifouling films was measured by SPR using an instrument based on the Kretschmann geometry and spectral interrogation developed at the Institute of Photonics and Electronic of the Academy of Sciences of the Czech Republic.[31,36] The shift in the resonant wavelength is proportional to the refractive index change at the interface of the sensor and the tested medium. The acquired spectra were analyzed in-real time with software package SPR-UP which allowed the determination of the resonant wavelength for each sensing channel. The refractive index resolution was 3×10^{-7} RIU. The tested solutions were driven for 15 min at $25\ \mu L \cdot min^{-1}$ by a peristaltic pump through four independent channels of a flow cell in which SPR responses were measured simultaneously. Typically, PBS was flowed until a stable baseline was achieved (approximately 15 min). Subsequently, it was replaced by the samples to be tested for 15 min and then replaced once again with PBS. The sensor response ($\Delta\lambda_{Res}$) was obtained as the difference between the baselines in PBS before and after the injection of the tested samples. The sensor response was calibrated to the mass proteins deposited on the surface. For this SPR working in the vicinity of $\lambda_{Res} = 750$ nm a 1 nm SPR wavelength shift represents a surface coverage of 15 $ng \cdot cm^{-2}$.[31,37,38] The limit of detection (LOD) was estimated as the sensor response equivalent to 3 standard deviations of the baseline noise. For this set-up the LOD correspond to a SPR wavelength shift of 0.02 nm, which represents 0.3 $ng \cdot cm^{-2}$ of proteins at the surface. The interaction of the surfaces with undiluted human BP as well as with model solutions of plasma proteins; HSA ($5\ mg \cdot mL^{-1}$) and fibrinogen (Fbg, $1\ mg \cdot mL^{-1}$) in PBS (pH 7.4) were assessed. All the fouling studies were carried out in triplicate. A fouling below the SPR detection limit ($0.3\ ng \cdot cm^{-2}$ for our device) was equated to zero.

2.6. Blood Components Preparation

Human blood was freshly collected from healthy volunteers by venipuncture into 3.8% trisodium citrate. All individuals tested agreed to this study at the time of blood collection. All samples were obtained in accordance with the Ethical Committee regulations of the Institute of Hematology and Blood Transfusion, Prague and with release of informed consent.

Platelet rich plasma (PRP) was obtained by the centrifugation of blood at $250 \times g$ at 37 °C for 15 min and the supernatant containing platelets was collected. Erythrocytes were isolated from citrated blood by centrifugation at $250 \times g$ for 15 min at RT. The bottom fraction of erythrocytes was collected and washed with PBS pH 7.4, and centrifuged at $1\ 000 \times g$ for 10 min at RT. The process was repeated twice. Leukocytes were isolated from citrated blood by centrifugation after specific lysis of erythrocytes. Erythrocytes were lysed after addition of ice-cold lysis buffer in 4:1 ratio (155 mm ammonium chloride, 10 mm sodium bicarbonate, 1 mm EDTA) for 5 min. The mixture was then centrifuged at $1\ 500 \times g$ for 5 min at 4 °C. Supernatant was discarded and the pellet was resuspended in ice-cold lysis buffer and centrifuged again at $1\ 500 \times g$ for 5 min at 4 °C. The leukocyte pellet was than reconstituted in 0.9% saline and centrifuged at $200 \times g$ for 5 min at 4 °C. Finally, the leukocyte pellet was resuspended in 0.9% saline and used immediately.

2.7. Hemocompatibility Test

Four different surfaces based on polymer brushes of poly(MeOEGMA), poly(HEMA), poly(HPMA), poly(CBAA), and control bare gold surface were incubated with PRP, leukocytes, erythrocytes, and whole blood (citrated). A 400 μL drop of blood or blood component was deposited on $1 \times 1\ cm^2$ coupons decorated with the brushes and incubated for 2 h at 37 °C. In this way any contact with container surfaces is prevented avoiding the possible interfering complement activation by the container. Subsequently, the surfaces were washed thoroughly with 0.9% saline and prepared for scanning electron microscopy (SEM). The deposits were fixed by glutaraldehyde (0.5%) for 1 h and subsequently washed with water, ethanol dried, coated with 4 nm thick platinum by sputtering and observed using SEM. Images were evaluated using ImageJ data analysis software. The number of adherent platelets, erythrocytes, and leukocytes was determined by calculating the surface coverage of individual components. Three independent spots were analyzed for each sample. The studies were carried out in triplicate.

3. Results and Discussion

The current study reports the adhesion of individual blood components – erythrocytes, leukocytes, PRP, and citrated full blood on highly protein resistant polymer brushes, poly(MeOEGMA), poly(HEMA), poly(HPMA), and poly(CBAA). Polymer brushes were grown from gold, fully characterized and subsequently challenged with BP. The surfaces were then contacted with blood cells and with whole blood to estimate the resistance of the surface to fouling from blood.

3.1. Polymer Brushes

Initially, poly(MeOEGMA) (30.6 nm), poly(HEMA) (28.7 nm), poly(HPMA) (29.5 nm), and poly(CBAA) (38.1 nm) were successfully grown from a densely packed SAM of ω-mercaptoundecyl bromoisobutyrate on Au via SI-ATRP (Scheme 1 and Table 1). Poly(MeOEGMA) stands as one of the most versatile polymer brush for antifouling properties and its surface initiated polymerization via SI-ATRP has been shown to be well controlled in water, buffers and even

Table 1. Water advancing (θ_{adv}) and receding (θ_{rec}) contact angles.

	Contact angle [°]		Thickness [nm]
	θ_{adv}	θ_{rec}	
Gold	75.4 ± 0.6	63.2 ± 0.9	–
Poly(HEMA)	56.1 ± 0.7	16.0 ± 1.0	28.7 ± 0.7
Poly(MeOEGMA)	55.3 ± 1.3	22.4 ± 1.2	30.6 ± 0.3
Poly(HPMA)	40.0 ± 0.9	21.1 ± 0.7	29.5 ± 0.8
Poly(CBAA)	23.2 ± 1.4	8.0 ± 1.5	38.1 ± 0.8

Thickness of dry polymer brushes was determined by spectroscopic ellipsometry.

biological fluid as evidenced by the linear evolution thickness with time (see SI).[39–44] In this work, poly(MeOEGMA) was synthesized according a reported polymerization protocol employing the catalytic system based on CuBr/$CuBr_2$/2,2′-bipyridyl complexes.[39] Similarly, well-controlled polymerization of HEMA was achieved using the CuBr/$CuCl_2$/2,2′-bipyridyl complexes (Figure S1, SI). The SI-ATRP of HPMA and CBAA are not well controlled, a typical featured for the ATRP of (meth)acrylamide monomers, however the use of earlier optimized conditions[38,40] leads to poly(HPMA) and poly(CBAA) brushes of reproducible thickness.

The chemical composition of the prepared polymer brushes was proved XPS analysis and FTIR GASR. Importantly the XPS survey spectra of all the surfaces clearly show that no residual Cu remaining after the polymerization (Figure S2, SI). Comparison of C1s XPS spectra (Figure 1) of the SAM initiator and of poly(MeOEGMA) shows a strong increase of the peaks assigned to [C-O] bonds at 286.8 eV, stemming from oligo(ethylene glycol) side chains and [C-C_3] and [O–C = O] of the backbone at 285.9 and 289.1 eV, respectively, while it decreases the signal corresponding to [C–H, C–C] at 285.0 eV, proving the successful polymerization.[45,46] FTIR GASR spectrum of poly(MeOEGMA) (Figure 2) exhibits a strong peak of ester carbonyl vibration (1 730 cm^{-1}) and a prominent band of C–O–C stretching (1 145 cm^{-1}). In the region below 1 500 cm^{-1}, the spectrum is characterized by bands having their origin in CH_2 scissoring (≈1 465 cm^{-1}), wagging (≈1 350 cm^{-1}), twisting (≈1 250 cm^{-1}), and rocking (≈950 cm^{-1}) modes. In addition, poly(MeOEGMA) displays the characteristic methoxy-terminal group (OCH_3) at 2 818 cm^{-1} and small vibration band of ethylene glycol units at 2 720 cm^{-1}. Similarly, poly(HEMA) brushes show signals of [C-C_3], [C-O], and [O–C = O] at 285.8, 286.8, and 289.1 eV, respectively, in the C1s spectrum. In addition, the FTIR GASR shows similar bands characteristic bands for methacrylates: ester carbonyl vibration (1 730 cm^{-1}), CH_2 scissoring (≈1 465 cm^{-1}), wagging (≈1 350 cm^{-1}), twisting (≈1 250 cm^{-1}), and rocking (≈950 cm^{-1}) modes as well as a broad band at 3 250 cm^{-1} arising from H-bonded hydroxyl.

The C1s spectrum of poly(HPMA) brushes depicts clear bands of [C–H, C–C], [C-C_3], [C-O], and [N–C = O] at 285.0, 285.7, 286.7, and 288.1 eV while the N1s spectrum clearly evidenced a [C-NH] band at 400.1 eV. Additionally, the FTIR GASR spectrum exhibits two amide bands at ≈1 554 and 1 664 cm^{-1} and a broad band at 3 250 cm^{-1} stemming from H-bonded hydroxyls. The zwitterionic poly(CBAA) shows also a distinct C1s spectrum with bands stemming from [C–H, C–C], [C-O], and [N–C = O] at 285.0, 286.2, and 287.8 eV, respectively, while the N1s spectrum display two bands at 399.9 and 402.4 eV originating from [C-NH] and [N^+].[17,18] In addition, to the amide bands, FTIR GASR of poly(CBAA) exhibits a dominant COO^- symmetric (1 363 cm^{-1}) and asymmetric (1 610 cm^{-1}) stretching modes.

All prepared polymer brushes increased the wettability of the surfaces as evidenced by a decrease in the water contact angles (Table 1). Wettability has been linked previously with the resistance to fouling.[47,48] However, we have shown that while a surface may not be hydrophobic (high water contact angles) a high wettability not necessarily leads to full prevention of protein fouling from complex biological samples.[12]

High roughness and presence of pinholes can cause high protein fouling and preferential places for protein or cell adsorption. Thus, the morphology of the surfaces was assessed by AFM. Figure 3 confirms that all surfaces were homogeneous without pinholes enabling direct contact with the substrate. A smooth topography is usually associated with better control in polymerization as well as a higher resistance to protein fouling.[49]

3.2. Protein Fouling

Protein fouling is an adverse event occurring at nearly any surface coming to contact with biological media. The compatibility of a surface with blood can be impaired by the

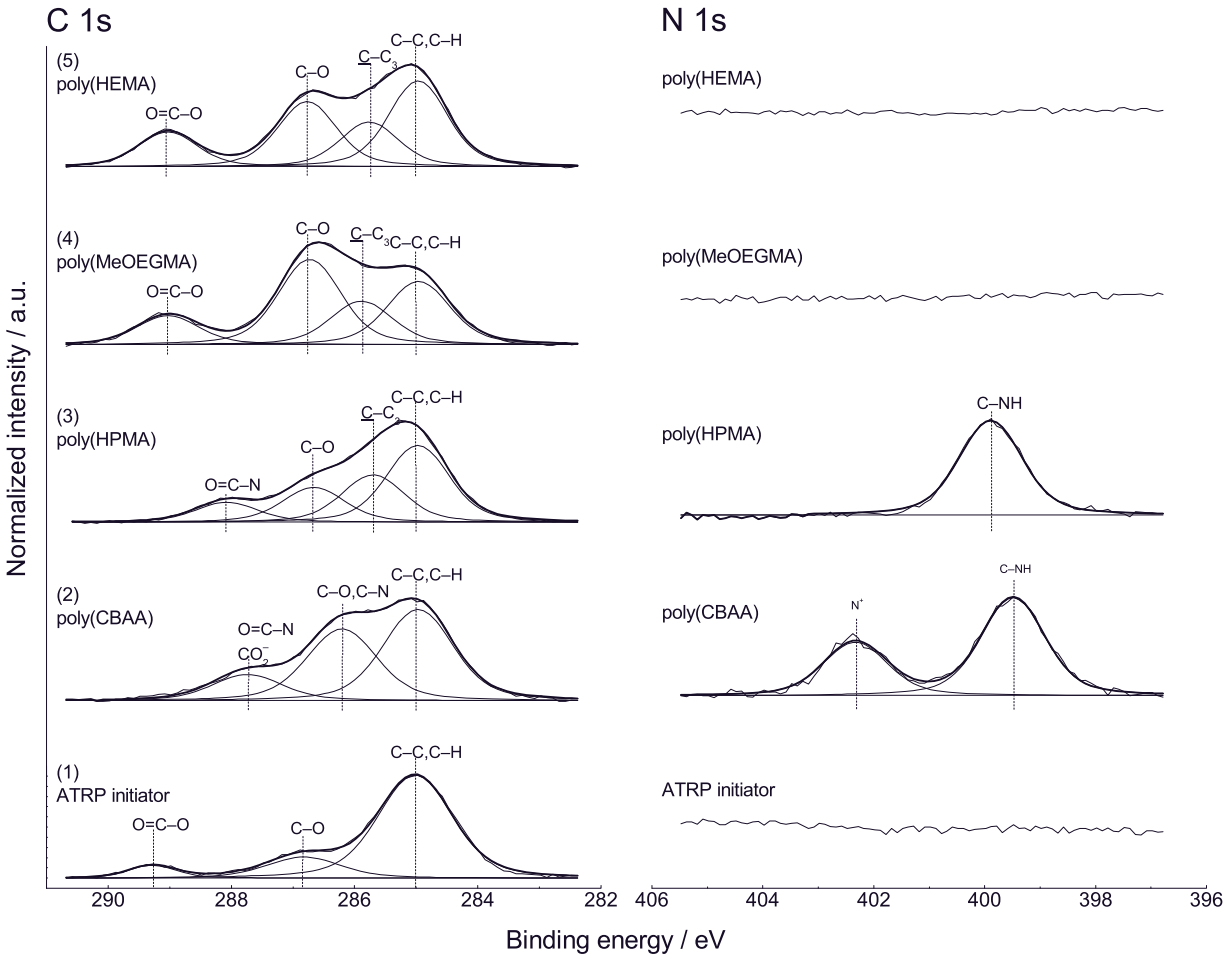

Figure 1. XPS C1s and N1s core level spectra of the studied surfaces: (1) SAM, (2) poly(CBAA), (3) poly(HPMA), (4) poly(MeOEGMA), (5) poly(HEMA) brushes.

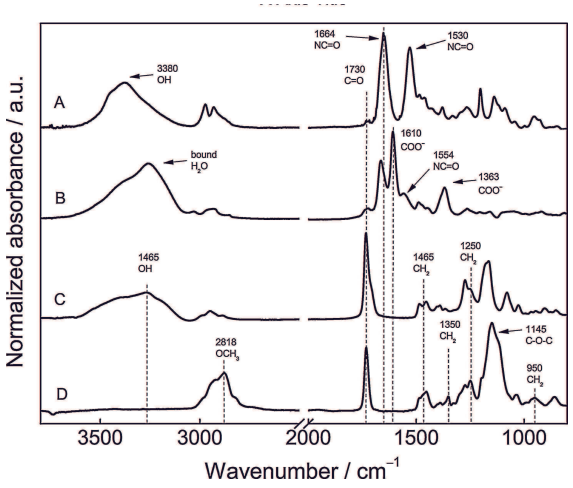

Figure 2. FTIR GASR spectra of polymer brushes prepared on gold surface of SPR chips. (A) poly(HPMA), (B) poly(CBAA), (C) poly(HEMA), (D) poly(MeOEGMA).

fast adsorption of proteins, which can lead to subsequent detrimental problems such as complement activation, initiation of coagulation cascade, and/or immune response. Thus, prevention of the protein fouling is a corner-stone for the design of blood-compatible surfaces. To assess the resistance of the brushes we challenged all the surfaces with model solutions of HSA (5 mg · mL^{-1}, the main plasma protein), fibrinogen (Fbg, 1 mg · mL^{-1}), and undiluted human BP. The irreversible non-specific adsorption was determined by SPR spectroscopy. All the brushes fully prevent the fouling from model solutions in agreement with our previous reports. Poly(HEMA) and poly(MeOEGMA) displayed a remarkable low fouling corresponding to a 92 (26 ng · cm^{-2}) and 94% (18 ng · cm^{-2}) reduction of BP fouling, respectively. Poly(CBAA) and poly(HPMA), however, stand so far as the only two surfaces able to reach undetectable levels of undiluted BP fouling (Figure 4 and Table S1 the SI). Various studies have tried to link the protein fouling with wettability and the ability to structure water.[48,50,51] The slightly lower resistance of

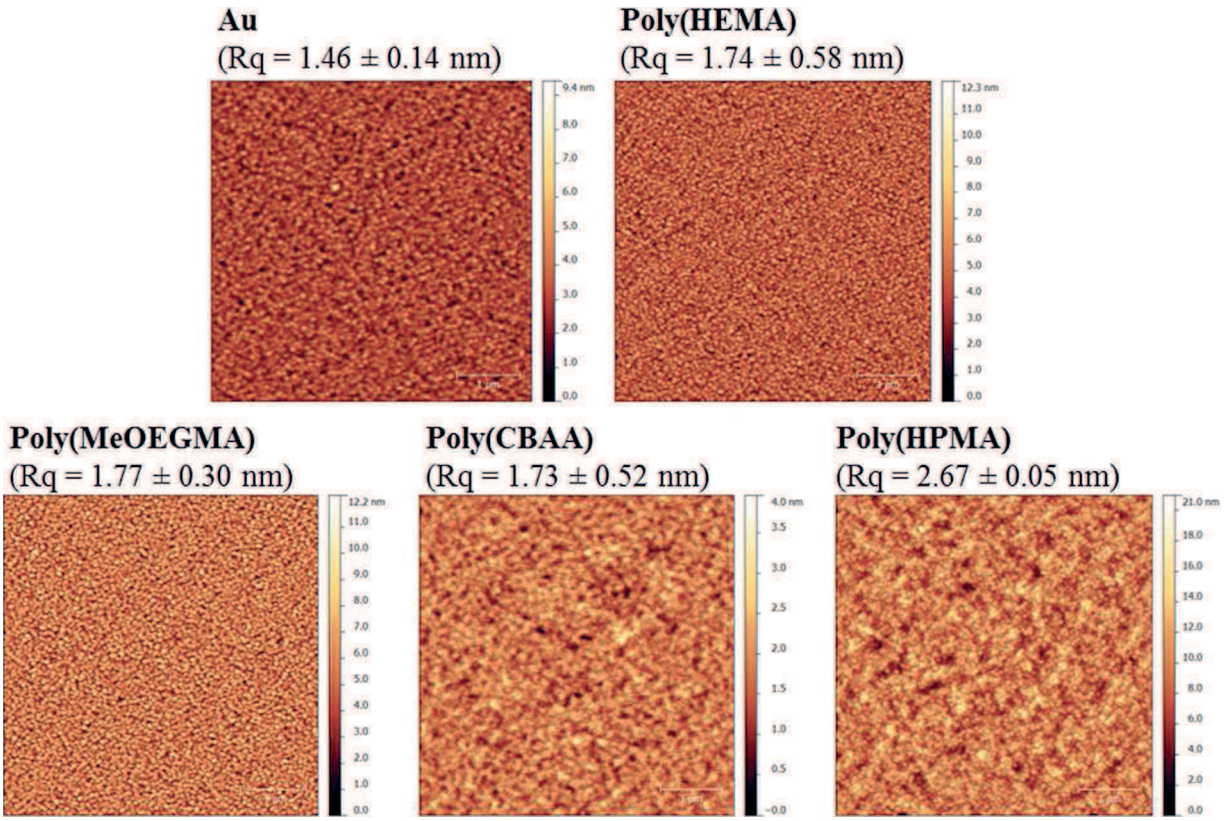

Figure 3. Representative AFM topography images of the different types of polymer brushes grown from the surface of silicon chips. The root-mean-square roughness (R_q) is reported for each figure. The scale bar is 1 μm.

poly(HEMA) compared to poly(MeOEGMA) can be associated with its content of hydrogen bonds donors and lower wettability. The remarkable resistance of the presented poly(CBAA) brushes was previously linked with their electrostatically induced hydration, comparatively stronger than dipole–dipole or hydrogen bonding interactions with water as observed by sum frequency generation spectroscopy[52] as well as with the ability of carboxybetaine groups to structure water around proteins—kosmotropes—stabilizing them.[53] Zwitterionic and polyampholyte polymers bearing ionic groups have typically shown excellent resistance to single protein solution, cells, and bacteria.[23,48,54,55] However, our previous studies have shown that poly(HPMA) brushes bearing hydrogen bond donors and displaying a medium wettability can also reached levels of resistance to fouling as low as the best betaine polymers.[7] This seems to be in line with the recent findings from Thompson and coworkers shown that even poorly wettable ultra-thin organosilane monolayers can resist the fouling by creation of an interphase of water with distinct physical property compared to bulk water as evidenced by neutron reflectivity.[56]

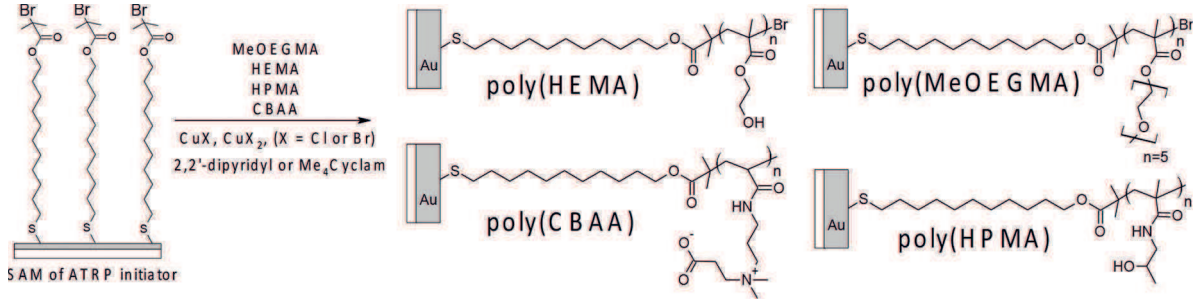

Scheme 1. Synthesis of polymer brushes via SI-ATRP. Chemical structures of SAM of initiator, poly(HEMA), poly(MeOEGMA), poly(CBAA), and poly(HPMA).

As described above the fouling from BP is believed to be linked to detrimental reactions for the biomaterial thus its prevention is a pre-requisite for hemocompatibility. The radical reduction of fouling from two main BP proteins HSA and Fbg and remarkable reduction of fouling from HBP place these polymer brushes as the superior candidates for hemocompatible surfaces for real applications.

3.3. Hemocompatibility Study

To assess the hemocompatibility of the surface modification, the antifouling polymer brushes were challenged with blood components, i.e., erythrocytes, leukocytes, PRP; as well as with whole citrated human blood in vitro. The surfaces were incubated for 2 h at 37 °C in static conditions and the fouling was quantified using SEM.

Erythrocytes displayed no adhesion on polymer brushes nor on bare gold surface (control surface) (Figure 5, A1–E1). To prove that this is not due to artifacts on the imaging of samples we deposited erythrocytes on gold and did not rinse but directly dried the sample and imaged it by SEM (Figure 5, insert in A1). The lack of erythrocyte adsorption/adhesion to surfaces is not surprising as their biological function is to carry oxygen not to interact or attach to surfaces.

Leukocytes respond to inflammation by releasing inflammatory mediators, thus the reduction of leukocytes adhesion can reduce the foreign body response to implanted biomaterial. In contrast to erythrocytes, an important adhesion of leukocytes was observed on gold accounting for 9.6% of surface coverage (Figure 5, A3 and Figure 6). Interestingly, this value is similar to the fouling observed by other groups on the widely acclaimed antifouling SAMs.[57] On those works the leukocyte adhesion on SAM bearing various terminal groups (–OH, $–CH_3$, –COOH) ranged from 6 to 10%, thus as high as the one we observed on our blank of bare gold.[57] Conversely, no leukocyte adhesion was observed on the polymer brushes (Figure 5, B3–E3) presented in this work. Small particles can be observed on poly(HEMA) and poly(CBAA) (Figure 5, B3 and E3) after contact with the leukocyte suspension. It must be noted that this particles are not leukocytes but platelets aggregates remaining from the preparation of the

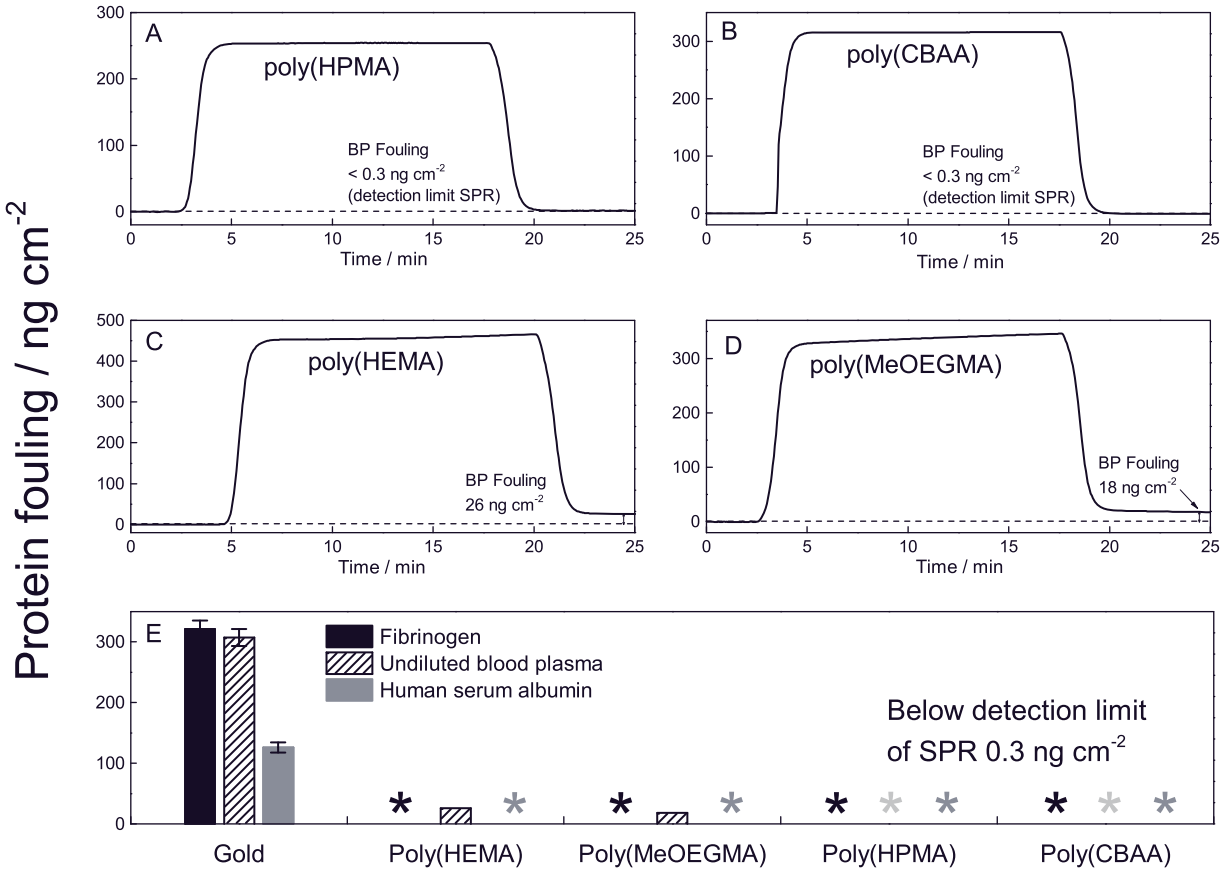

Figure 4. SPR traces showing the fouling from undiluted BP on poly(HPMA) (A), poly(CBAA) (B), poly(HEMA) (C), poly(MeOEGMA) (D). Fouling from human fibrinogen (1 mg · mL^{-1}), HSA (5 mg · mL^{-1}), and undiluted human BP (E). An asterisk represents a value of protein adsorption below the detection limit of SPR (0.3 ng · cm^{-2}).

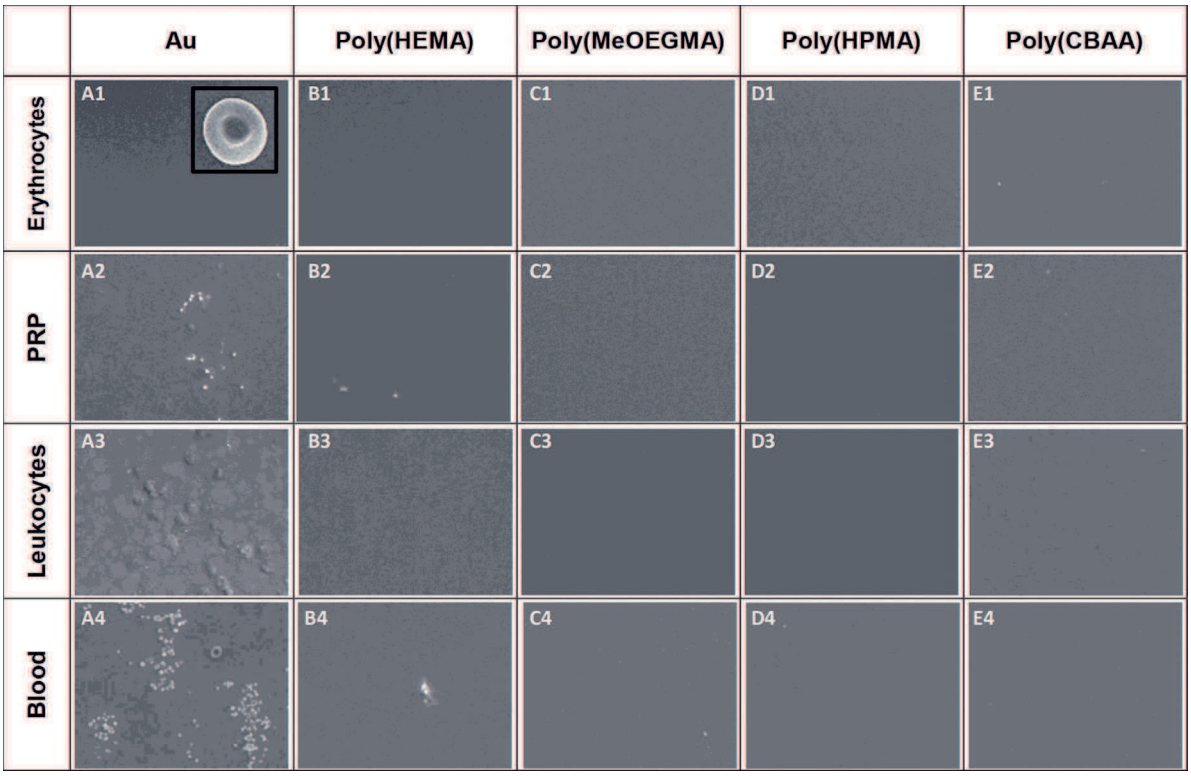

Figure 5. A scanning electron micrograph of polymer coatings based of poly(HEMA), poly(MeOEGMA), poly(HPMA), and poly(CBAA) exposed to citrated human blood and blood components – erythrocytes, PRP, and leukocytes. Gold surface was utilized as a reference hydrophobic substrate. 120 × 100 μm^2.

leukocyte suspension. It is worth noting that previous studies have shown a strong link between fibrinogen adsorption on SAMs and leukocyte adhesion[58] thus the prevention of protein fouling might be the central parameter explaining the prevention of leukocyte adhesion on the presented brushes.

Platelet poses a more serious challenged as they are design to adhere to surfaces and upon activation they form clusters or aggregates. This can be evidenced on Au substrates (Figure 5, A2 and Figure 6). The morphology and shape of adhered platelets on Au is modified due to changes in cytoskeleton. Additionally, the aggregates show the characteristic formation of actin filaments enabling spreading over the surface.[59] After 2 h contact with PRP the platelets covered 12% of the Au surface, while very few aggregates could be observed on poly(HEMA) and poly(CBAA) both reducing the surface coverage by 99% (compared to gold). SEM images of poly(MeOEGMA) and poly(HPMA) surfaces (Figure 5, C2–D2) evidence that no platelets nor platelets aggregates adhered. The presence of small platelets aggregates on fully protein resistant poly(CBAA) suggests that the mechanisms driving the platelets to this surface was not exclusively mediated by preadsorbed proteins.

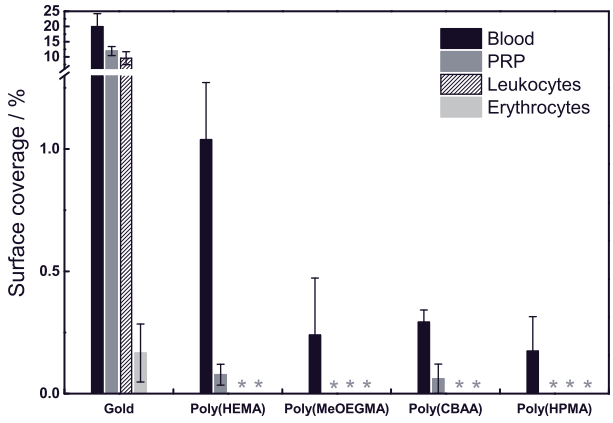

Figure 6. Fouling from blood components; PRP, leukocytes, and erythrocytes as well as blood on gold and polymer brushes.

The fouling from whole blood is a more complex event that the fouling from its components. A very high fouling was observed on gold as evidenced in Figure 5, picture A4. Platelets aggregates dominate the surface coverage (20%), however, erythrocytes, which did not adhere from their suspension, could be found on gold after contact with blood. The adhesion of erythrocytes might be mediated by the preadsorption of platelets. All polymer brushes reduced the adsorption of cellular components from blood to a very

large extend. Only poly(HEMA) and poly(CBAA) displayed a very mild adhesion of platelets, however, their total surface coverages were 1.0 and 0.3%, which correspond with a reduction on fouling higher than 94%. In summary the test suggests an increasing hemocompatibility in the order: poly(HEMA) < poly(MeOEGMA) ≈ poly(CBAA) < poly-(HPMA). While the good hemocompatibility of poly(CBAA) can be linked to a strong hydration, there is no direct link between the excellent properties of poly(HPMA) bursches and it surface wettability and presence of hydrogen bond donors. The complete lack of cell components on poly-(HPMA) as well as its undetectable fouling render this surface as an excellent candidate for blood contacting devices and sensors with an enhanced hemocompatibility.

4. Conclusion

Polymer brushes of HEMA, MeOEGMA, CBAA, and HPMA were prepared via SI-ATRP and characterized by XPS, FTIR, AFM, and dynamic water contact angles. After contact with leukocytes and erythrocytes extremely low surfaces coverages were observed on all brushes while some platelets aggregates were observed on HEMA and on CBAA which was shown to be fully resistant to BP adsorption. The latter suggests that platelet adsorption is not exclusively mediated by protein fouling.

The fouling from whole blood led to very high surface coverage on gold surfaces, however all brushes reduced it by at least 94%. Remarkably, no cellular components were observed on poly(HPMA) rendering these brushes as an excellent candidate to modify surfaces of blood contacting devices.

ACKNOWLEDGEMENTS: This research was supported by the Grant Agency of the Czech Republic (GACR) under contract no. P106/12/1451 and by the Ministry of Education Youth and Sport of the Czech Republic under contract no. LH13178 and EE2.3.30.0029. CR-E acknowledges support by the project "BIOCEV – Biotechnology and Biomedicine Centre of the Academy of Sciences and Charles University" (CZ.1.05/1.1.00/02.0109), from the European Regional Development Fund, and by the Karlsruhe Nano Micro-Facility (KNMF), a Helmholtz Research Infrastructure at KIT.

Received: October 25, 2014; Revised: November 28, 2014; Published online: January 21, 2015; DOI: 10.1002/mabi.201400470

Keywords: blood compatibility; blood plasma; non-fouling; surfaces; proteins

[1] R. G. Mason, R. W. Shermer, N. F. Rodman, *Am. J. Pathol.* **1972**, *69*, 271.
[2] M. J. Hall, C. J. DeFrances, S. N. Williams, A. Golosinskiy, A. Schwartzman, National Hospital Discharge Survey: 2007 Summary, In *National Health Statistics Reports*, **2010**, 29, 1–21.
[3] B. D. Ratner, *J. Biomater. Sci. Polym. Ed.* **2000**, *11*, 1107.
[4] B. D. Ratner, A. S. Hoffman, F. J. Schoen, J. E. Lemons, *"Biomaterials Science: An Introduction to Materials in Medicine"*, Elsevier Science, Oxford **2012**.
[5] A. Hucknall, S. Rangarajan, A. Chilkoti, *Adv. Mater.* **2009**, *21*, 2441.
[6] O. Pop-Georgievski, C. Rodriguez-Emmenegger, A. de los, P. Santos, E. Proks, F. Brynda, Rypacek, *J. Mater. Chem. B* **2013**, *1*, 2859.
[7] C. Rodriguez-Emmenegger, E. Brynda, T. Riedel, M. Houska, V. Šubr, A. Bologna, E. Alles, J. E. Hasan, W. T. S. Gautrot, Huck, *Macromol. Rapid Commun.* **2011**, *32*, 952.
[8] D. F. Mosher, *Cardiovasc. Pathol.* **1993**, *2*, 149.
[9] C. Blaszykowski, S. Sheikh, M. Thompson, *Chem. Soc. Rev.* **2012**, *41*, 5599.
[10] Q. Wei, T. Becherer, S. Angioletti-Uberti, J. Dzubiella, C. Wischke, A. T. Neffe, A. Lendlein, M. Ballauff, R. Haag, *Angew. Chem. Int. Ed. Engl.* **2014**, *53*, 8004.
[11] T. Riedel, Z. Riedelova-Reicheltova, P. Majek, C. Rodriguez-Emmenegger, M. Houska, J. E. Dyr, E. Brynda, *Langmuir* **2013**, *29*, 3388.
[12] C. Rodriguez-Emmenegger, E. Brynda, T. Riedel, Z. Sedlakova, M. Houska, A. B. Alles, *Langmuir* **2009**, *25*, 6328.
[13] S. Gam-Derouich, M. Gosecka, S. Lepinay, M. Turmine, B. Carbonnier, T. Basinska, S. Slomkowski, M. C. Millot, A. Othmane, D. Ben, M. M. Hassen-Chehimi, Chehimi, *Langmuir* **2011**, *27*, 9285.
[14] S. Gam-Derouich, A. Lamouri, C. Redeuilh, P. Decorse, F. Maurel, B. Carbonnier, S. Beyazít, G. Yilmaz, Y. Yagci, M. M. Chehimi, *Langmuir* **2012**, *28*, 8035.
[15] R. Barbey, L. Lavanant, D. Paripovic, N. Schuwer, C. Sugnaux, S. Tugulu, H. A. Klok, *Chem. Rev.* **2009**, *109*, 5437.
[16] M. Zamfir, C. Rodriguez-Emmenegger, S. Bauer, L. Barner, A. Rosenhahn, C. Barner-Kowollik, *J. Mater. Chem. B* **2013**, *1*, 6027.
[17] B. Yameen, C. Rodriguez-Emmenegger, I. Ahmed, C. M. Preuss, C. J. Durr, N. Zydziak, V. Trouillet, L. Fruk, C. Barner-Kowollik, *Chem. Commun. (Camb)* **2013**, *49*, 6734.
[18] T. Tischer, C. Rodriguez-Emmenegger, V. Trouillet, A. Welle, V. Schueler, J. O. Mueller, A. S. Goldmann, E. Brynda, C. Barner-Kowollik, *Adv. Mater.* **2014**, *26*, 4087.
[19] Q. Yu, Y. Zhang, H. Wang, J. Brash, H. Chen, *Acta Biomater.* **2011**, *7*, 1550.
[20] C. Zhao, J. Zheng, *Biomacromolecules* **2011**, *12*, 4071.
[21] L. Tauhardt, D. Pretzel, K. Kempe, M. Gottschaldt, D. Pohlers, U. S. Schubert, *Polym. Chem.-Uk.* **2014**, *5*, 5751.
[22] C. Rodriguez-Emmenegger, C. M. Preuss, B. Yameen, O. Pop-Georgievski, M. Bachmann, J. O. Mueller, M. Bruns, A. S. Goldmann, M. Bastmeyer, C. Barner-Kowollik, *Adv. Mater.* **2013**, *25*, 6123.
[23] C. Rodriguez-Emmenegger, A. Decker, F. Surman, C. M. Preuss, Z. Sedlakova, N. Zydziak, C. Barner-Kowollik, T. Schwartz, L. Barner, *RSC Adv.* **2014**, *4*, 64781.
[24] S. M. Slack, Y. W. Cui, V. T. Turitto, *Thromb. Haemostasis* **1993**, *70*, 129.
[25] C. Blaszykowski, S. Sheikh, M. Thompson, *Trends Biotechnol.* **2014**, *32*, 61.
[26] K. Fedorov, C. Blaszykowski, S. Sheikh, A. Reheman, A. Romaschin, H. Ni, M. Thompson, *Langmuir* **2014**, *30*, 3217.
[27] D. M. Jones, A. A. Brown, W. T. S. Huck, *Langmuir* **2002**, *18*, 1265.
[28] C. Rodriguez-Emmenegger, B. V. Schmidt, Z. Sedlakova, V. Subr, A. B. Alles, E. Brynda, C. Barner-Kowollik, *Macromol. Rapid Commun.* **2011**, *32*, 958.

[29] C. Rodriguez-Emmenegger, M. Houska, A. B. Alles, E. Brynda, *Macromol. Biosci.* **2012**, *12*, 1413.
[30] K. Ulbrich, V. Šubr, J. Strohalm, D. Plocová, M. Jelínková, B. Říhová, *J. Controlled Release* **2000**, *64*, 63.
[31] H. Vaisocherova, W. Yang, Z. Zhang, Z. Cao, G. Cheng, M. Piliarik, J. Homola, S. Jiang, *Anal. Chem.* **2008**, *80*, 7894.
[32] P. Májek, Z. Reicheltová, J. Suttnar, M. Malý, M. Oravec, K. Pečánková, J. E. Dyr, *J. Transl. Med.* **2011**, *9*, 84.
[33] K. L. Parry, A. G. Shard, R. D. Short, R. G. White, J. D. Whittle, A. Wright, *Surf. Interface Anal.* **2006**, *38*, 1497.
[34] J. H. Scofield, *J. Electron. Spectrosc. Relat. Phenom.* **1976**, *8*, 129.
[35] S. Tanuma, C. J. Powell, D. R. Penn, *Surf. Interface Anal.* **1994**, *21*, 165.
[36] J. Homola, H. B. Lu, G. G. Nenninger, J. Dostálek, S. S. Yee, *Sens. Actuators, B: Chem.* **2001**, *76*, 403.
[37] C. Rodriguez, E. Emmenegger, T. Brynda, Z. Riedel, M. Sedlakova, A. B. Houska, Alles, *Langmuir* **2009**, *25*, 6328.
[38] C. Rodriguez-Emmenegger, E. Brynda, T. Riedel, M. Houska, V. Subr, A. B. Alles, E. Hasan, J. E. Gautrot, W. T. Huck, *Macromol. Rapid Commun.* **2011**, *32*, 952.
[39] A. de los Santos Pereira, T. Riedel, E. Brynda, C. Rodriguez-Emmenegger, *Sens. Actuators, B: Chem* **2014**, *202*, 1313.
[40] C. Rodriguez-Emmenegger, E. Hasan, O. Pop-Georgievski, M. Houska, E. Brynda, A. B. Alles, *Macromol. Biosci.* **2012**, *12*, 525.
[41] C. Rodriguez-Emmenegger, C. M. Preuss, B. Yameen, O. Pop-Georgievski, M. Bachmann, J. O. Mueller, M. Bruns, A. S. Goldmann, M. Bastmeyer, C. Barner-Kowollik, *Adv. Mater.* **2013**, *25*, 6123.
[42] H. Ma, J. Hyun, P. Stiller, A. Chilkoti, *Adv. Mater.* **2004**, *16*, 338.
[43] H. Ma, M. Wells, T. P. Beebe, A. Chilkoti, *Adv. Funct. Mater.* **2006**, *16*, 640.
[44] A. A. Brown, N. S. Khan, L. Steinbock, W. T. S. Huck, *Eur. Polym. J.* **2005**, *41*, 1757.
[45] A. R. Kuzmyn, A. de los, P. Santos, M. Pop-Georgievski, E. Bruns, C. Brynda, Rodriguez-Emmenegger, *Polym. Chem.* **2014**, *5*, 4124.
[46] N. Zydziak, C. Hubner, M. Bruns, C. Barner-Kowollik, *Macromolecules* **2011**, *44*, 3374.
[47] C. Zhao, L. Li, Q. Wang, Q. Yu, J. Zheng, *Langmuir* **2011**, *27*, 4906.
[48] S. Chen, L. Li, C. Zhao, J. Zheng, *Polymer* **2010**, *51*, 5283.
[49] X. Shi, Y. Wang, D. Li, L. Yuan, F. Zhou, Y. Wang, B. Song, Z. Wu, H. Chen, J. L. Brash, *Langmuir* **2012**, *28*, 17011.
[50] S. Herrwerth, W. Eck, S. Reinhardt, M. Grunze, *J. Am. Chem. Soc.* **2003**, *125*, 9359.
[51] M. Zolk, F. Eisert, J. Pipper, S. Herrwerth, W. Eck, M. Buck, M. Grunze, *Langmuir* **2000**, *16*, 5849.
[52] C. Leng, X. Han, Q. Shao, Y. Zhu, Y. Li, S. Jiang, Z. Chen, *J. Phys. Chem. C* **2014**, *118*, 15840.
[53] R. S. Kane, P. Deschatelets, G. M. Whitesides, *Langmuir* **2003**, *19*, 2388.
[54] Z. Zhang, J. A. Finlay, L. Wang, Y. Gao, J. A. Callow, M. E. Callow, S. Jiang, *Langmuir* **2009**, *25*, 13516.
[55] H. Vaisocherova, Z. Zhang, W. Yang, Z. Q. Cao, G. Cheng, A. D. Taylor, M. Piliarik, J. Homola, S. Y. Jiang, *Biosens. Bioelectron.* **2009**, *24*.
[56] N. M. Pawlowska, H. Fritzsche, C. Blaszykowski, S. Sheikh, M. Vezvaie, M. Thompson, *Langmuir* **2014**, *30*, 1199.
[57] C. Sperling, R. B. Schweiss, U. Streller, C. Werner, *Biomaterials* **2005**, *26*, 6547.
[58] J. N. Barbosa, M. C. L. Martins, S. C. Freitas, I. C. Goncalves, A. P. Aguas, M. A. Barbosa, *J. Biomed. Mater. Res. A* **2010**, *93A*, 12.
[59] M. B. Gorbet, M. V. Sefton, *Biomaterials* **2004**, *25*, 5681.

Supporting Information

for *Macromol. Biosci.*, DOI: 10.1002/mabi.201400470

Polymer brushes interfacing blood as a route toward high performance blood contacting devices [a]

František Surman, Tomáš Riedel, Michael Bruns, Nina Kostina, Zdeňka Sedláková and Cesar Rodriguez-Emmenegger*

M.Sc. František Surman, Dr. Tomáš Riedel, M.Sc. Nina Kostina, Dr. Zdeňka Sedláková, Dr. Cesar Rodriguez-Emmenegger
Institute of Macromolecular Chemistry, Academy of Sciences of the Czech Republic, v.v.i., Prague, 162 06, Czech Republic
Dr. Michael Bruns
Institute for Applied Materials (IAM), Karlsruhe Nano Micro Facility (KNMF), Karlsruhe Institute of Technology (KIT), Hermann-von-Helmholtz-Platz 1, 76344
Eggenstein-Leopoldshafen, Germany
E-mail: rodriguez@imc.cas.cz

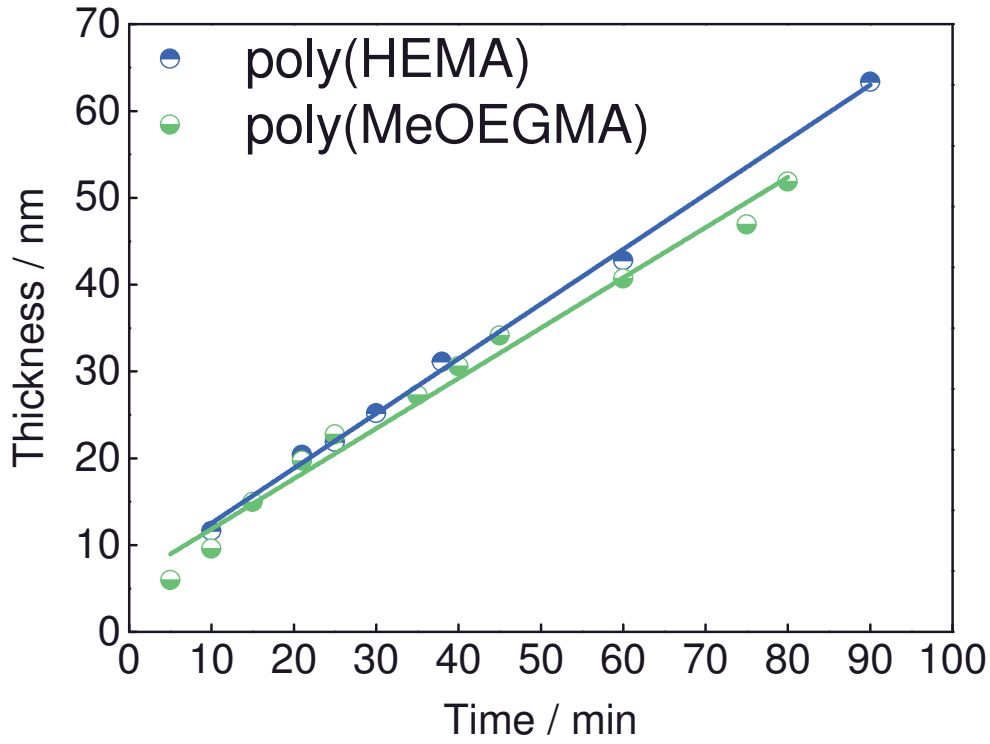

Figure S1. Evolution of poly(HEMA) and poly(MeOEGMA) brush dry thickness with polymerization time, measured by spectroscopic ellipsometry.

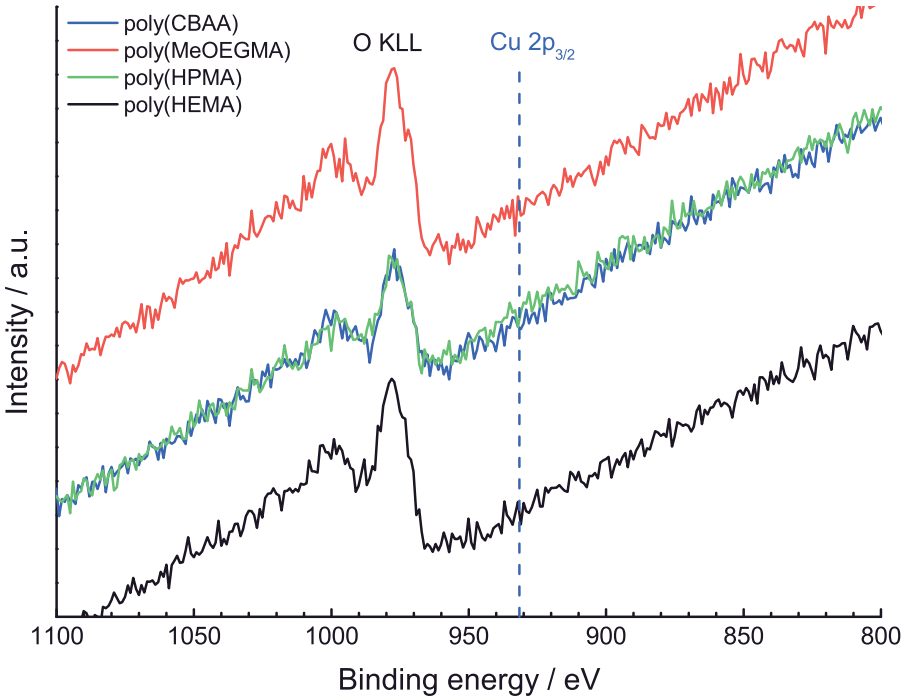

Figure S2. XP-Survey spectra of polymer brushes showing no Cu contamination

Table S1. Nonspecific protein adsorption measured by SPR.

	Protein fouling [ng cm^{-2}]		
	Undiluted Blood Plasma	**Fibrinogen**	**Human Serum Albumin**
Gold	307 ± 14	321 ± 14	126 ± 8
Poly(HEMA)	26 ± 3	0	0
Poly(MeOEGMA)	18 ± 2	0	0
Poly(HPMA)	0	0	0
Poly(CBAA)	0	0	0

Table S2. Fouling from blood components and whole blood

	Surface coverage [%]			
	Blood	**PRP**	**Leukocytes**	**Erythrocytes**
Gold	20.00 ± 4.20	12 ± 0.02	9.6 ± 2.1	0.17 ± 0.12
Poly(HEMA)	1.04 ± 0.23	0.08 ± 0.04	0	0
Poly(MeOEGMA)	0.24 ± 0.25	0	0	0
Poly(HPMA)	0.17 ± 0.14	0	0	0
Poly(CBAA)	0.29 ± 0.05	0.06 ± 0.01	0	0

Appendix 2

Photo-triggered functionalization of hierarchically structured brushes

Langmuir, 2015, 31(21), 5899-5907

Langmuir

Article

pubs.acs.org/Langmuir

Phototriggered Functionalization of Hierarchically Structured Polymer Brushes

Andres de los Santos Pereira,[†] Nina Yu. Kostina,[†] Michael Bruns,[‡] Cesar Rodriguez-Emmenegger,*[,†] and Christopher Barner-Kowollik*[,∥,§]

[†]Institute of Macromolecular Chemistry, Academy of Sciences of the Czech Republic, v.v.i., Heyrovsky sq. 2, 162 06 Prague, Czech Republic

[‡]Institut für Angewandte Materialien (IAM), Karlsruhe Nano Micro Facility (KNMF), Karlsruhe Institute of Technology (KIT), Hermann-von-Helmholtz-Platz 1, 76344 Eggenstein-Leopoldshafen, Germany

[∥]Preparative Macromolecular Chemistry, Institut für Technische Chemie und Polymerchemie, Karlsruhe Institute of Technology (KIT), Engesserstr. 18, 76131 Karlsruhe, Germany

[§]Institut für Biologische Grenzflächen, Karlsruhe Institute of Technology (KIT), Hermann-von-Helmholtz-Platz 1, 76344 Eggenstein-Leopoldshafen, Germany

Supporting Information

ABSTRACT: The precise design of bioactive surfaces, essential for the advancement of many biomedical applications, depends on achieving control of the surface architecture as well as on the ability to attach bioreceptors to antifouling surfaces. Herein, we report a facile avenue toward hierarchically structured antifouling polymer brushes of oligo(ethylene glycol) methacrylates via surface-initiated atom transfer radical polymerization (SI-ATRP) presenting photoactive tetrazole moieties, which permitted their functionalization via nitrile imine-mediated tetrazole-ene cycloclooaddition (NITEC). A maleimide-functional ATRP initiator was photoclicked to the side chains of a brush enabling a subsequent polymerization of carboxybetaine acrylamide to generate a micropatterned *graft-on-graft* polymer architecture as evidenced by X-ray photoelectron spectroscopy (XPS) and time-of-flight secondary ion mass spectrometry (ToF-SIMS). Furthermore, the spatially resolved biofunctionalization of the tetrazole-presenting brushes was accessed by the photoligation of biotin-maleimide and subsequent binding of streptavidin. The functionalized brushes bearing streptavidin were able to resist the fouling from blood plasma (90% reduction with respect to bare gold). Moreover, they were employed to demonstrate a model biosensor by immobilization of a biotinylated antibody and subsequent capture of an antigen as monitored in real time by surface plasmon resonance.

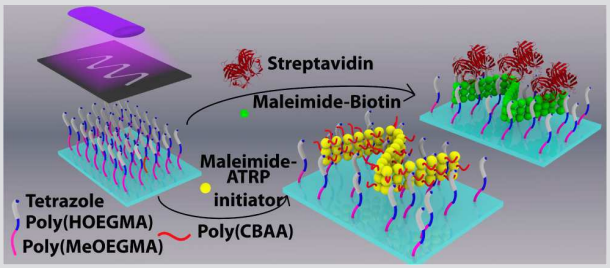

INTRODUCTION

The control of the interactions of biological molecules at the interface between artificial surfaces and biological systems is critical for the success of devices that operate in direct contact with biological fluids and environments.[1,2] These include biosensors, tissue engineering scaffolds, and bioimplants.[3] For this purpose, precisely engineered bioactive surfaces can be achieved by the controlled grafting of well-defined polymer layers.[4] In particular, polymer brushes show great promise and have begun to be applied in research.[5−10] Arguably, a carefully designed macromolecular architecture plays a fundamental role in these systems, determining the performance of the surfaces under study and expanding the synthetic tool box available for the polymer chemist.[4,9,11] The architecture of the polymer brushes has been shown to critically determine the properties, including the resistance to fouling, immobilization capacity of bioreceptors, and stimuli-responsive behavior.[11−13] Of the myriad of synthetic techniques that have been developed in recent years, controlled radical polymerization and modular ligations (often adhering to the click chemistry criteria) are among the most valuable tools available for this purpose.[14] Surface-initiated atom transfer radical polymerization (SI-ATRP) provides a versatile route to build polymer layers on a surface via a "grafting from" approach with a vast array of available monomers to provide the desired properties and functionalities.[4,9,10]

Moreover, the postpolymerization modification of the polymer architectures obtained via "grafting-from" processes further expands the accessible functionalities and allows for the binding of bioreceptors onto the surface.[15−18] The tailoring of the surface properties and its interactions with biological media requires the immobilization of bioactive motifs on the surface,

Received: March 28, 2015
Revised: May 9, 2015
Published: May 11, 2015

DOI: 10.1021/acs.langmuir.5b01114
Langmuir 2015, 31, 5899−5907

such as biorecognition elements in the case of biosensors[19] or cell attachment cues for scaffolds for tissue engineering.[20,21] In this context, the ability to achieve spatial control of the reaction is a requirement for several applications. In the design of high-throughput biosensors and DNA/protein arrays, the location on the surface of the biomolecules must be precisely controlled.

Previously, we reported the use of a catalyst-free ligation reaction to achieve the rapid biofunctionalization of polymer brushes under mild conditions without the need for a catalyst, taking advantage of the polymer end groups.[22] Nevertheless, the ability to address only selected sites or areas for the functionalization can be accessed by employing phototriggered ligation reactions.[23] Photoactivated reactions including thiol−ene coupling,[24,25] strain-promoted alkyne−azide cycloaddition,[26] those employing a photocaged diene in a Diels−Alder ligation,[23,27] or nitrile imine-mediated tetrazole-ene cycloadditions[5,28] (NITEC) as well as the reaction of photogenerated thioaldehydes with nucleophiles or dienes[29] have been used on surfaces to achieve their functionalization in a spatially selective manner. NITEC—the reaction between a nitrile imine dipole and a dipolarophile such as an alkene or alkyne—in particular presents several advantages, such as high selectivity, bioorthogonality, and sensitivity to relatively long wavelengths of UV light.[3,5,30] The irradiation of a diaryl tetrazole with UV-light generates the highly reactive nitrile imine coupled with the release of N_2, while the absorption peak of the transition can be conveniently tuned by the selection of the substituents.[31] The application of NITEC for the functionalization of a poly(dopamine)-coated surface allowed to spatially confine the growth of antifouling polymer brushes, capable of preventing cell adhesion, effectively achieving the high fidelity patterning of cells.[5]

Herein, we present the application of the phototriggered NITEC reaction for the spatially resolved (bio)-functionalization of hierarchically structured polymer brushes, demonstrated by the immobilization of biotin and the subsequent capture of streptavidin, which is subsequently exploited to demonstrate a model label-free biosensing platform. Moreover, the patterning of an ATRP-initiator moiety on the side chains of the brushes is carried out. Thus, the control of the macromolecular architecture is simultaneously achieved, taking advantage of the successive SI-ATRP of different monomers to generate graft-on-graft structures. Thus, the chemical route reported provides access to antifouling polymer brushes of controlled macromolecular architecture that can be biofunctionalized in a spatially resolved manner.

EXPERIMENTAL SECTION

Materials. Oligo(ethylene glycol) methyl ether methacrylate (M_n = 300 g·mol^{-1}, MeOEGMA), oligo(ethylene glycol) methacrylate (M_n = 500 g·mol^{-1}, HOEGMA), $CuBr_2$ (99%), CuBr (99.99%), 2,2′-bipyridyl (99%), 1,4,8,11-tetramethyl-1,4,8,11-tetraazacyclotetradecane (Me_4Cyclam, 98%), triethylamine (TEA, 99%) NaN_3 (99%), maleimide-biotin (*N*-biotinoyl-*N*′-(6-maleimidohexanoyl) hydrazide, ≥95%), and human serum were purchased from Sigma−Aldrich, Czech Republic. Streptavidin, biotin-conjugated rabbit IgG, biotin-conjugated goat IgG anti(mouse IgG), and mouse IgG were purchased from Thermo Fisher Scientific, Czech Republic. Human blood plasma (mix from 5 donors) was provided by the Institute of Hematology and Blood Transfusion, Czech Republic. ω-Mercaptoundecyl bromoisobutyrate and (3-acryloylaminopropyl)-(2-carboxyethyl)-dimethylammonium (CBAA) were synthesized according to procedures published earlier.[32,33] The tetrazole acid chloride (4-(2-(4-methoxyphenyl)-2H-tetrazol-5-yl)benzoic acid chloride) and the maleimide-conjugated ATRP initiator (2-bromo-2-methyl propionic acid 2-(3,5-dioxo-10-oxa-4-aza-tricyclo[5.2.1.0^{2,6}]dec-8-en-4-yl) ethyl ester) were synthesized according to our previously published methods.[5]

Self-Assembled Monolayer (SAM) of the ATRP Initiator. The substrates used for all experiments except surface plasmon resonance (SPR) were silicon wafer chips (1 cm × 1 cm) coated with an intermediate titanium layer for adhesion (2 nm) and a thin layer of gold on the surface (about 150 nm). For surface plasmon resonance, the substrates used were microscope glass slides coated with a titanium adhesion layer and 50 nm of gold. The chips were rinsed with ethanol followed by deionized water twice, blow dried with nitrogen, and air plasma cleaned for 20 min. Subsequently, the wafers were immediately placed in a 1 mM solution of ω-mercaptoundecyl bromoisobutyrate in absolute ethanol and kept overnight at room temperature to form the initiator SAM. After rinsing with ethanol and water, the samples were blow dried with nitrogen.

ATRP of the Bottom Block of the Polymer Brush. Three round-bottom flasks containing: (1) methanol, (2) a solution of MeOEGMA (M_n = 300 g·mol^{-1}, 5.7 g, 19 mmol) in 5 mL of water, and (3) 2,2′-bipyridyl (155 mg, 991 μmol), $CuBr_2$ (16.8 mg, 75 μmol), and $CuBr_2$ (53.8 mg, 375 μmol) were deoxygenated separately by bubbling with Ar for 1 h. Methanol (5 mL) was transferred under Ar-protection from flask 1 to flask 3, which was stirred until dissolution. Subsequently, the monomer solution was transferred under Ar-protection from flask 2 to flask 3 and thoroughly mixed. The polymerization mixture was transferred to Ar-filled reactors containing the substrates coated with initiator SAM. The reaction was allowed to proceed at 30 °C for 15 min and then stopped by removing the chips from the solution and rinsing them with ethanol and water, and blow drying with nitrogen.

Diblock Architecture via ATRP. The top block of poyl-(HOEGMA) was grown according to the same procedure employed for the bottom poly(MeOEGMA) block. The monomer employed was HOEGMA (M_n = 500 g·mol^{-1}, 9.5 g, 19 mmol) for the same quantities of all other reagents. The substrates employed were already coated with the poly(MeOEGMA) brushes which served as macro-initiators. The reaction proceeded for 30 min at 30 °C.

Deactivation of the Br End Groups by Nucleophilic Substitution. NaN_3 (51 mg, 785 μmol) was dissolved in 15 mL of anhydrous dimethylformamide (DMF). The solution was deoxygenated by bubbling of Ar and transferred to Ar-filled reactors containing the poly(MeOEGMA-*b*-HOEGMA)-coated substrates. The reaction proceeded at 50 °C for 3 h. Finally, the wafers were rinsed with DMF, ethanol, and deionized water, and blow dried with nitrogen.

Decoration of the Surface with Tetrazole Acid Chloride. The tetrazole acid chloride was reacted with the hydroxy groups in the side chains of the poly(HOEGMA) block of the brushes.[5,34] The substrates were placed in 30 mL of a 0.12 M solution of TEA (364 mg, 502 μL) in tetrahydrofuran (THF) at ambient temperature. Fifteen milliliters of a 0.12 M solution of tetrazole chloride (565 mg) in THF were added dropwise and the reaction was allowed to proceed under gentle shaking for 1 h. After rinsing with THF, dichloromethane (DCM), ethanol, and deionized water, the samples were blow dried with nitrogen and kept in the dark.

Phototriggered Click Reactions. The phototriggered immobilizations of both maleimide-biotin (for subsequent biofunctionalization) and maleimide-ATRP-initiator (for formation of graft-on-graft structures) were carried out employing the same procedure. The tetrazole-functionalized polymer brushes samples were placed vertically in individual headspace vials. In the case of the samples on which patterning was conducted for ToF-SIMS imaging, the sample was placed in a sample holder with a shadow mask on top of the surface.[28] The vials were filled with sufficient volume to cover the sample of a solution of either maleimide-biotin (1 mg·mL^{-1} in dry DMF) or maleimide-ATRP-initiator (1 mg·mL^{-1} in dry DCM), crimped airtight, and purged with nitrogen for 5 min in the dark to remove atmospheric oxygen and avoid undesired photooxidation reactions. The samples to be irradiated were placed in a custom-made

DOI: 10.1021/acs.langmuir.5b01114
Langmuir 2015, 31, 5899−5907

Scheme 1. Chemical Route Employed for the Generation of the Tetrazole-Functional Hierarchically Structured Polymer Brushes and Their Subsequent Functionalization

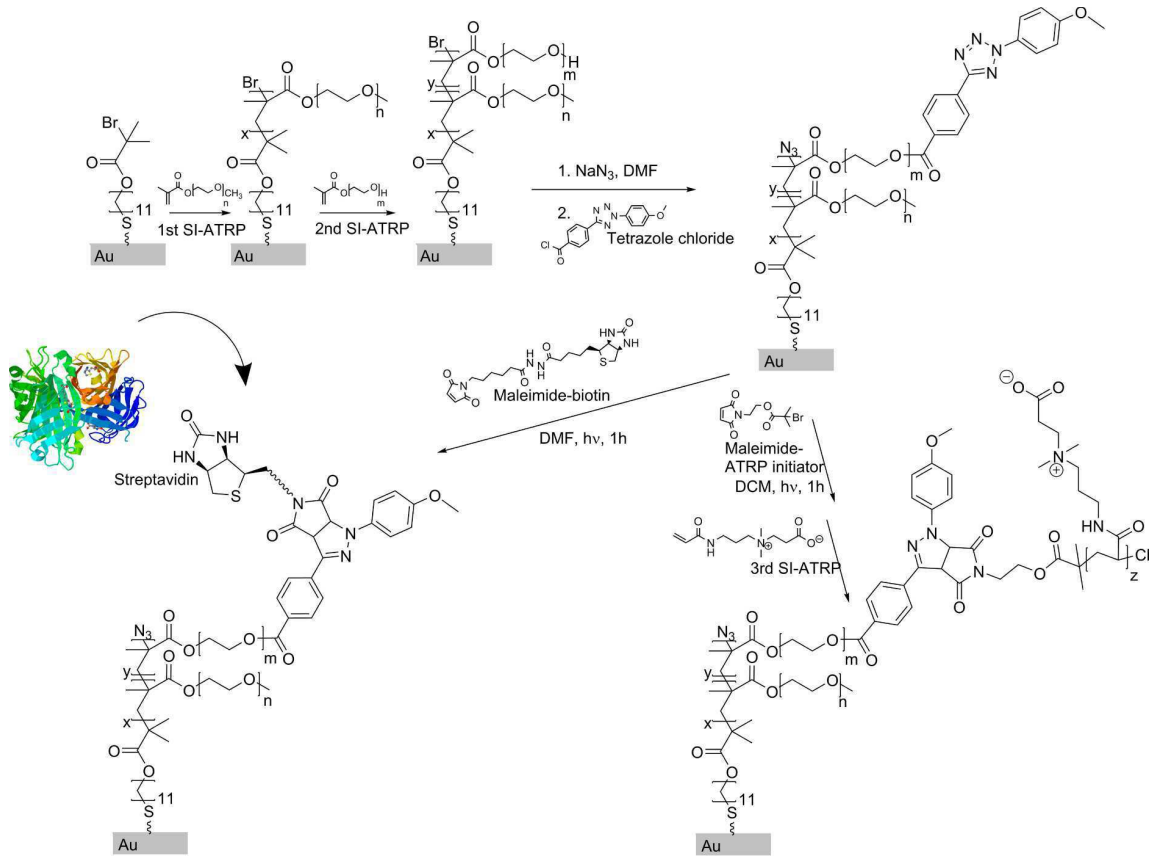

photoreactor suspended from a metallic disk (diameter 4−5 cm) slowly revolving around a compact low-pressure lamp (Arimed B6, Cosmedico GmbH, Germany) emitting at λ = 320 nm (±30 nm, 36 W, the emission spectrum of the UV-lamp employed is shown elsewhere[5]). After 1 h of irradiation, the vials were opened, and the samples removed and rinsed copiously with the solvent used for the corresponding reaction (either DMF or DCM), followed by ethanol and water, and dried by blow drying with nitrogen.

Biofunctionalization with Streptavidin. The substrates coated with maleimide-biotin-functionalized polymer brushes were placed in individual vials and covered with a 0.5 mg·mL^{-1} solution of streptavidin in phosphate buffered saline (PBS, pH 7.4). After 3 h of contact the samples were rinsed with abundant PBS, followed by water, and dried by gentle blowing of nitrogen.

Preparation of a Model Biosensing Platform. SPR chips coated with biotin-presenting polymer brushes were biofunctionalized in situ in the SPR setup. After establishing a baseline in PBS, a solution of streptavidin (100 μg·mL^{-1} in PBS) was injected over the surface and replaced with PBS after 30 min. Subsequently, on two independent channels solutions of biotinylated nonspecific rabbit IgG or biotinylated goat polyclonal antibody against mouse IgG (50 μg·mL^{-1} in PBS) were flowed for 10 min and replaced with PBS. The capture capacity and specificity of the sensing surfaces obtained were then tested by simultaneously injecting in both channels for 10 min a 50 μg·mL^{-1} solution of mouse IgG in PBS.

Poly(carboxybetaine acrylamide) Graft-on-Graft. The polymerization of CBAA was carried out according to our previously published procedure.[33] PBS (10 mL) was degassed by three cycles of freeze−pump−thaw and transferred under inert atmosphere to a degassed Schlenk flask containing CuBr (19.1 mg, 133 μmol), $CuBr_2$ (5.9 mg, 26.5 μmol), and Me_4Cyclam (40.9 mg, 160 μmol). After dissolution, the catalyst mixture was transferred to a Schlenk flask containing CBAA (1.5 g, 6.7 mmol) and stirred. The polymerization solution was transferred to Ar-filled reactors containing the substrates coated with the polymer brushes functionalized with maleimide-ATRP-initiator and left to react for 2 h at 30 °C. The reactors were subsequently opened and the substrates removed, rinsed with water, ethanol, and finally water, and blow dried with nitrogen

Ellipsometry. The dry thickness of the layers after each relevant modification step was measured by ellipsometry using a Variable Angle Spectroscopic Imaging Auto-Nulling Ellipsometer EP3-SE (Nanofilm Technologies GmbH, Germany) with a laser at a wavelength λ = 532 nm at angles of incidence AOI = 60, 65, and 70° in air at room temperature. The data were fitted using multilayer models with the EP4Model analysis software.

X-ray Photoelectron Spectroscopy (XPS). XPS measurements were carried out with a K-Alpha XPS spectrometer (Thermo Fisher Scientific, East Grinstead, UK). The samples were analyzed using a microfocused, monochromated Al Kα X-ray source (400 μm spot size). The kinetic energy of the electrons was measured using a 180° hemispherical energy analyzer operated in the constant analyzer energy mode (CAE) at 50 eV pass energy for elemental spectra. Data acquisition and processing using the Thermo Avantage software is described elsewhere.[35]

The spectra were fitted with one or more Voigt profiles (binding energy uncertainty: ± 0.2 eV). The analyzer transmission function, Scofield sensitivity factors,[36] and effective attenuation lengths (EALs) for photoelectrons were applied for quantification. EALs were calculated using the standard TPP-2M formalism.[37] All spectra were referenced to the C 1s peak of hydrocarbons at 285.0 eV binding energy controlled by means of the well-known photoelectron peaks of metallic Cu, Ag, and Au.

Time-of-Flight Secondary Ion Mass Spectrometry (ToF-SIMS). Imaging by ToF-SIMS was performed on a TOF.SIMS-V

DOI: 10.1021/acs.langmuir.5b01114
Langmuir 2015, 31, 5899−5907

instrument (ION-TOF GmbH, Münster, Germany) equipped with a Bi cluster liquid metal primary ion source and a nonlinear time-of-flight analyzer. The Bi source was operated in the "bunched" mode, providing 0.7 ns Bi^+ ion pulses at 25 keV energy and a lateral resolution of ~4 μm. The short pulse length allowed for high mass resolution to analyze the complex mass spectra of the immobilized organic layers. Images larger than the maximum deflection range of the primary ion gun of 500 × 500 μm^2 were obtained using the manipulator stage scan mode. Negative polarity spectra were calibrated on the C^-, C_2^-, C_3^-, and Br^- peaks. Primary ion doses were kept below 10^{11} ions·cm^{-2} (static SIMS limit).

Surface Plasmon Resonance (SPR). The immobilization of streptavidin and biotin-conjugated antibodies on biotin-functionalized polymer brushes was followed by SPR using an instrument based on the Kretschmann configuration and spectral interrogation, monitoring the resonance wavelength λ_{res}. The temperature was set at 25 °C, and all solutions were flowed through the flow cell at 25 μL·min^{-1}. After a stable baseline was achieved in PBS (pH 7.4), the solutions were injected in the flow cell for a specified time and subsequently replaced by PBS. The fouling was measured from undiluted human blood plasma after 15 min of contact. The sensor response is recorded as the difference in resonance wavelength $\Delta\lambda_{res}$ before and after contact with the solutions and is proportional to the mass deposited on the surface.[16]

RESULTS AND DISCUSSION

Preparation of Polymer Brushes Bearing Photofunctonalizable Side Groups. Antifouling polymer brushes consisting of two blocks were grown as depicted in Scheme 1.[16,33] A SAM of ATRP initiator was prepared on the surface of gold-coated silicon wafer substrates. Polymer brushes of oligo(ethylene glycol) methyl ether methacrylate were grafted from the surface, and subsequently a second block of hydroxy-functional oligo(ethylene glycol) methacrylate was grown. The use of gold as a model surface was chosen due to the importance of this material in biosensor transducers[38] and the simplicity with which polymer brushes can be grafted from and characterized on a SAM of thiol-containing initiator molecules.[16] Nevertheless, the approach does not restrict the general applicability of the procedure, since such functional polymer brushes can be grown on virtually any substrate through the use of an appropriate linker specific for the material of interest or a substrate-independent adlayer such as poly(dopamine).[34,39−41]

The success of each step in the modification of the surfaces to achieve the desired structures was confirmed by monitoring the dry layer thickness by ellipsometry and the chemical composition by XPS. The formation of the initiator SAM can be observed in the XPS spectrum of the C 1s region (Figure 1A) showing the predominance of C−C and C−H bonds of the alkane backbone at 285.0 eV as well as the O−C═O peak of the initiator ester moiety. The presence of Br forming C−Br bonds, entailed in the initiator group, is also detected on the surface (Figure 1B). The contributions arising from Br^- ions are caused by decomposition due to the irradiation with X-rays during analysis. The C 1s spectra for both types of polymer brushes, poly(MeOEGMA) and poly(MeOEGMA-*b*-HOEGMA), share a predominance of carbon in the C−O bonds seen at 286.4 eV (Figure 1A). The methacrylate ester group appears close to 289.9 eV. It is interesting to note how the ratio of the C−O to O−C═O peak increases when going from pure poly(MeOEGMA) to the diblock polymer brush. This can be explained by the higher number of ethylene glycol units in the longer oligo(ethylene glycol) side chains of HOEGMA. A thickness of 15 nm was obtained for the first polymer block,

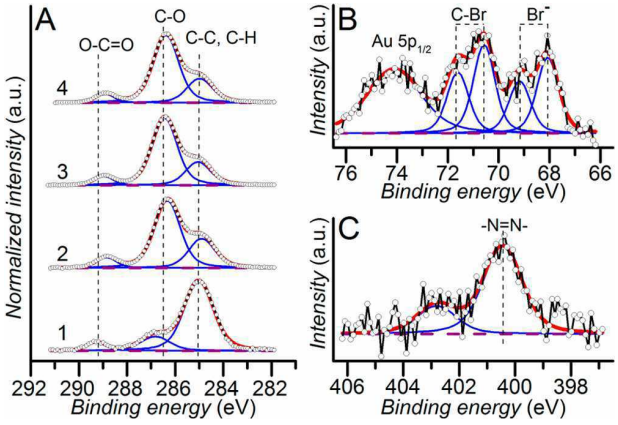

Figure 1. (A) High-resolution XPS spectrum of the C 1s region of the surface modification steps: (1) initiator SAM, (2) poly(MeOEGMA), (3) poly(MeOEGMA-*b*-HOEGMA), and (4) tetrazole-functionalized polymer brush. (B) High-resolution XPS spectrum of the Br 3d region of the initiator SAM. (C) High-resolution XPS spectrum of the N 1s region of the tetrazole-functional polymer brush.

while the growth of a second block caused an increase in thickness of 21 nm to reach a total of 35 nm (Table 1).

Table 1. Dry Layer Thickness of the Polymer Brushes

surface	thickness/nm
initiator SAM	1
poly(MeOEGMA)	15
poly(MeOEGMA-*b*-HOEGMA)	36

The well-controlled nature of the SI-ATRP process of the methacrylate monomers[16] makes it possible to reinitiate the polymerization centers and obtain a diblock bottle brush architecture in which the side groups of the polymer chains present hydroxy functionalities only along a desired top region of the polymer chain. These functional groups are subsequently addressed during the arylation with the photoactive tetrazole. In comparison with the chain end approach for the modification of polymer brushes, this route has the advantage of enabling the tuning of the extent of the functional group desired modification by adjusting the length of the two blocks, which can be achieved simply by varying the polymerization times of each step.[40] The thicknesses selected for the two blocks of the polymer brushes are consistent with what has been observed in our previous work to yield good results for resistance to protein fouling and functionalization capacity.[40,42] In order to prevent the growth from the polymer end groups in subsequent ATRP steps, the Br end groups were removed by a nucleophilic substitution with NaN_3.

To address the requirements for more complex macromolecular architectures and spatially resolved biofunctionalization of the polymer brushes, we introduced tetrazole groups onto their side chains after polymerization. These groups can be subsequently addressed by the photoactivated NITEC reaction to ligate the desired molecules to the surface. Immobilization of the tetrazole moiety on the top block of the polymer layer was achieved by the arylation of the hydroxy groups of the polymer side chains with the acyl chloride form of the tetrazole in dry THF for 1 h. The thickness of the layer did not appreciably increase after the reaction. However, the high-resolution XPS spectrum of the N 1s region clearly shows the

DOI: 10.1021/acs.langmuir.5b01114
Langmuir 2015, 31, 5899−5907

appearance of a signal at 400.5 and 402.8 eV, which corresponds to the expected tetrazole species (−N═N−) and probably positively charged nitrogen, respectively (Figure 1C).[28] The contributions observed in the XPS spectrum of the C 1s region of the tetrazole-functionalized polymer brushes indicate a predominance of the features corresponding to the polymer (Figure 1A).

Encoding Biofunctionality by Photopatterning of Biotion and Capture of Streptavidin. The tetrazole-functional polymer brushes were employed to biofunctionalize the surface with streptavidin. This protein is an ideal choice to assess the biofunctionalization of these surfaces, as it can bind to a wide range of bioreceptors conjugated with biotin. Thus, a generic platform allowing for the further encoding of variable biofunctionalities can be achieved. Initially, the phototriggered and spatially resolved immobilization of a maleimide-functional biotin was carried out. The biotin−streptavidin couple displays one of the highest affinities of noncovalent interactions known, characterized by an extremely low dissociation constant, $K_D \approx 10^{-14}$ M, which was further exploited to decorate the surfaces with streptavidin biomolecules. To achieve the immobilization of biotin on the tetrazole-containing polymer side chains, the samples were contacted with a 1 mg·mL^{-1} maleimide−biotin solution in DMF in a crimped headspace vial, purged with nitrogen to remove atmospheric oxygen and irradiated for 1 h with a UV lamp, λ_{max} = 320 nm. The use of a tetrazole with a methoxy substituent in the *para* position of the N2 in the ring enables the photoactivation to occur under UV irradiation of relatively long wavelengths, resulting in milder ligation conditions.[5] This fact, together with the removal of oxygen from the vials, helps to minimize undesired photooxidation reactions which could degrade the thiol SAM on gold,[43] with a concomitant damage to the polymer brush. The change in the XPS spectrum's N 1s region upon irradiation with UV light in the presence of biotin is consistent with the activation of the tetrazole moiety through the loss of N_2 (Table S1 in the Supporting Information). Upon contact with a 0.5 mg·mL^{-1} streptavidin solution in phosphate buffered saline (PBS, pH 7.4) for 3 h, a large increase in the signal at 400.1 eV in the XPS spectrum of the N 1s region is observed (Figure 2B and Table S1, Supporting Information), corresponding to the N atoms in the peptide bond expected in the streptavidin. Furthermore, the relative contribution of the C−O bonds, corresponding to the ethylene glycol units of the underlying polymer brush, decreases in comparison to the C−C, C−H, and O−C═O more prevalent in the protein (Figure 2).

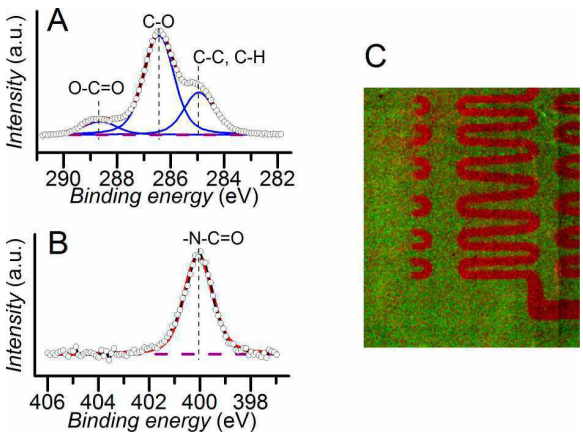

Figure 2. Functionalization with streptavidin. High-resolution XPS spectra of the C 1s (A) and N 1s (B) regions. (C) ToF-SIMS image showing an overlay of CN^- (red) stemming from protein fragments and $C_7H_4N^-$ (green) arising from the unreacted tetrazole.

To demonstrate the spatial control of the functionalization achievable by directing and restricting the irradiation with UV light, a shadow mask was employed, followed by contact with a streptavidin solution under the same conditions as described above. ToF-SIMS was subsequently employed to map the surface according to the presence of specific fragments that can be correlated to the expected chemical structures (refer to Figure 2C). The image obtained for the nitrogen-containing residue CN^- stemming from protein residues[28] clearly follows the wave-like pattern, with a sharp increase in the irradiated area, in which biotin was expected to be immobilized, indicating the presence of streptavidin with its protein structure. Furthermore, the overlay image shows the presence of the unreacted tetrazole (102.0 u, $C_7H_4N^-$) exclusively in the nonirradiated areas. It is expected that the presence of this moiety could be employed for the further functionalization of the nonirradiated areas of the surface with a different molecule. The ToF-SIMS image for the tetrazole fragment evidences the absence of unreacted groups in the area inside of the pattern after 1 h of irradiation, which might interfere in a subsequent photoligation with a different molecule (Figure S2 in the Supporting Information).

To further confirm the specificity of immobilization of streptavidin on the surface, we contacted a tetrazole-functional polymer brush with biotin in the absence of irradiation by UV-light (refer to the Supporting Information). After rinsing, the sample was contacted with a streptavidin solution and the XPS spectrum was recorded. The signal in the N 1s region corresponds to the original tetrazole, while no changes originating from a potential nonspecific adsorption of streptavidin could be detected (refer to Figure S1 in the Supporting Information), in agreement with the excellent protein resistance of the block copolymer brushes.[16,33] Importantly, the control experiment evidences that maleimide-functional biotin could only be immobilized under irradiation with UV-light. Thus, the ability to obtain a pattern of immobilized streptavidin arises both from the resistance to protein fouling provided by the polymer brushes and the requirement of a light stimulus for the functionalization reaction to proceed.

The attachment of streptavidin on the biotin-functionalized polymer brushes was also monitored by SPR. This technique is able to follow the increase in deposited mass on the surface via the changes it causes in the propagation coefficient of the surface plasmons at the interface between a metal and the solution of interest. The obtained sensogram reflects the attachment of the streptavidin (from a 100 μg·mL^{-1} solution in PBS) as a function of time on the surface presenting biotin (Figure 3A). A small decrease at the beginning of the attachment and final increase at the end of the contact period are caused by the difference in refractive indices between the PBS and the streptavidin solution in PBS. After a baseline was re-established in PBS, an immobilized amount of streptavidin of 21 ng·cm^{-2} was observed. Since no unreacted tetrazole groups were detected by ToF-SIMS in the irradiated area after 1 h of UV irradiation, longer reaction times are not expected to increase the attainable immobilized amount of biotin and streptavidin. A possible way to achieve an increase in the load

DOI: 10.1021/acs.langmuir.5b01114
Langmuir 2015, 31, 5899−5907

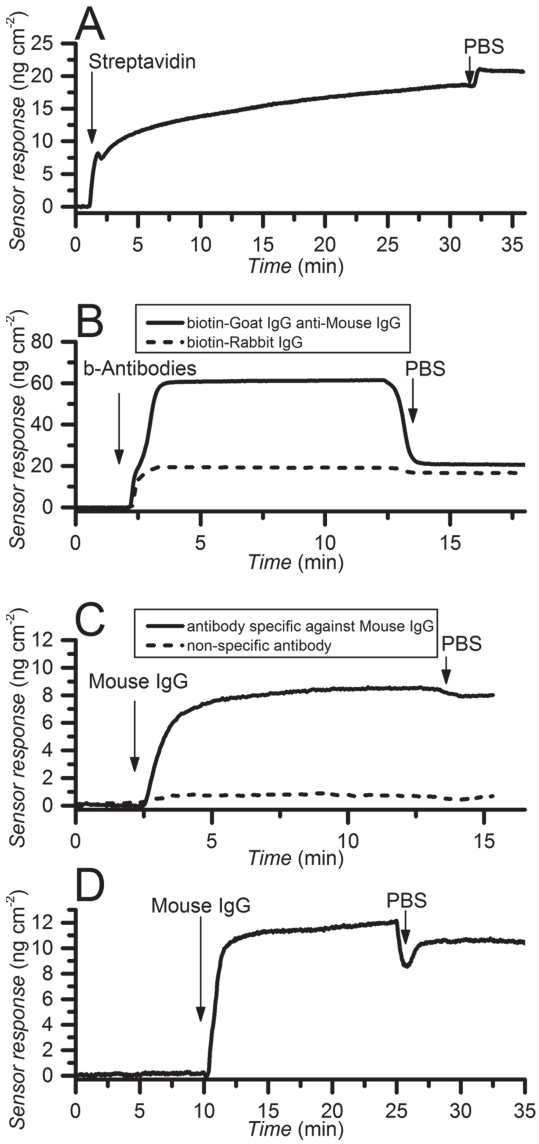

Figure 3. (A) Immobilization of streptavidin followed by SPR. (B) Capture of two different biotinylated antibodies on a streptavidin-functionalized polymer brush. (C) Specific detection of a model immunoglobulin on a channel functionalized with an antibody able to capture it. The second channel was functionalized with a nonspecific antibody and shows no binding. (D) Reference-compensated detection response to mouse IgG in human serum (10%) in PBS, on a polymer brush surface functionalized with an antibody against mouse IgG.

of bioreceptor would be to tune the relative thicknesses of the polymer blocks to obtain a higher ratio of the blocks of poly(HOEGMA) to poly(MeOEGMA). However, in our previous work concerning the functionalization of hierarchically structured antifouling polymer brushes, a trade-off between the immobilized amount of bioreceptors and the antifouling performance was observed.[16]

The fouling from undiluted blood plasma and serum, two of the most challenging biological matrices encountered in biosensing, was also quantified by SPR and was found to be (35.8 ± 1.3) ng·cm^{-2} and (35.5 ± 3.6) ng·cm^{-2}, respectively (example sensograms are shown in Figure S3 in the Supporting Information). This represents a reduction of close to 90% in comparison to bare gold and is on a comparable level with other available state-of-the-art functionalized antifouling surfaces.[16,44,45]

In Situ Fabrication of a Model Biosensing Platform. In order to illustrate an example application of our precision biofunctionalization for the fabrication of a truly functional and bioactive surface, the capability of the streptavidin-functional polymer brushes to immobilize model biotin-conjugated antibodies was examined by SPR. Antibodies are commonly employed as biorecognition elements in the fabrication of biosensors as well as for the capture of other target molecules or cells. Furthermore, biotin conjugates of antibodies are widely available commercially as they are often used in immunoassays and the technology for their production is well developed. The rapid immobilization of a biotinylated rabbit antibody and a biotinylated polyclonal goat antibody against mouse IgG was observed when the surface was contacted with 50 μg·mL^{-1} antibody solutions in PBS for 10 min in two independent flow cell channels in the SPR setup (Figure 3B), reaching immobilization densities of 17 and 21 ng·cm^{-2}, respectively. To evidence the activity and specificity of the antibody-functionalized surfaces, a solution of mouse IgG (50 μg·mL^{-1} in PBS) was subsequently injected on both channels for 10 min. The sensogram obtained shows how the specific antibody against the model analyte is able to capture and immobilize it from the solution, while the surface presenting a nonspecific antibody shows no interaction. Thus, the specificity of the capture is confirmed, while the nonspecific adsorption or capture of the mouse IgG can be excluded. The ability to achieve the spatially resolved immobilization of biorecognition elements on antifouling polymer brushes, accessible through the phototriggered ligation employed, is of particular interest for biosensing applications such as SPR imaging and protein arrays.[46−48] Furthermore, the ability to capture mouse IgG from diluted human serum (10% in PBS) was examined by spiking the solution with the model analyte. Figure 3D shows the reference-compensated response as the difference between the signals in the detection channel and a reference channel (nonspiked 10% human serum) measured simultaneously. The analyte is rapidly detected in diluted serum giving a signal of similar magnitude as in PBS, confirming the potential of the surface for biosensing applications.

Spatially Resolved Grafting of Poly(carboxybetaine acrylamide). Given the importance of the precise control not only of the chemistry, but also of the macromolecular architecture of antifouling polymer brushes, we exploited this functionalization strategy to design a more complex structure. The polymer brushes presenting tetrazole-functional side chains were employed to create a hierarchical macromolecular architecture of the type graft-on-graft. A maleimide incorporating a tertiary alkyl bromide group (1 mg·mL^{-1} in DCM)[5] was immobilized by the attachment to the tetrazole-moieties in the top block of the polymer brushes under UV light irradiation. Thus, the side chains of this polymer region were effectively rendered into initiators for a successive step of SI-ATRP.

Before the photoligation of the maleimide-ATRP-initiator, the Br chain ends were replaced with azide via a nucleophilic substitution with NaN_3 (3.4 mg·mL^{-1} in DMF at 50 °C for 3 h).[49] Thus, we prevent further chain extension from the polymer end groups during the graft-on-graft polymerization, thereby confining the growth to irradiated areas. The third polymer block consisted of poly(carboxybetaine acrylamide)

DOI: 10.1021/acs.langmuir.5b01114
Langmuir 2015, 31, 5899−5907

(poly(CBAA)), a zwitterionic polymer which has been shown to have ultralow fouling properties.[33] The total layer thickness for the triblock structure reached 42 nm, yielding a thickness increment of 7 nm after the poly(CBAA) block. XPS further confirmed the success of the grafting of poly(CBAA) by evidencing the presence of the expected features for the polymer, namely, two signals in the N 1s region corresponding to the amide (399.8 eV) and the quaternary ammonium (402.5 eV) (Figure 4B).[28] Moreover, the C 1s region's spectrum reveals a relative increase in the content of carbon stemming from C−C or C−H bonds.

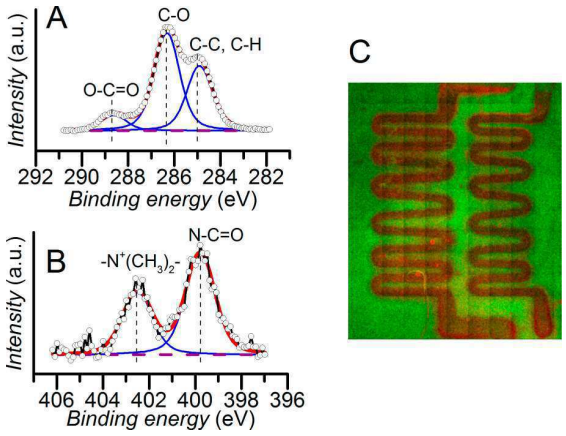

Figure 4. Grafting of poly(CBAA). High-resolution XPS spectra of the C 1s (A) and N 1s (B) regions. (C) ToF-SIMS image showing an overlay of CN^- (red, arising from the poly(CBAA) block) and the ethylene glycol fragments $C_2H_3O^-$ and $C_4H_5O_2^-$ (green).

In order to unambiguously evidence that the poly(CBAA) block was grown from the initiator moiety clicked onto the tetrazole, the same procedure was applied using a shadow mask to restrict the irradiation with UV light to the wave-shaped opening and the resulting surfaces were analyzed by ToF-SIMS (Figure 4C). An increase in the counts for CN^- as well as a decrease for the fragments arising for the ethylene glycol side chains of the underlying polymer blocks are observed for the patterned area, confirming the localization of the newly grown poly(CBAA).

CONCLUSIONS

In summary, we have demonstrated the introduction of photoactive tetrazole units to hierarchically structured polymer brushes. These were employed for the localized immobilization of streptavidin through the phototriggered ligation of a maleimide-containing biotin. An example application of the streptavidin-functionalized polymer brushes was demonstrated with a model biosensor showing the specific capture of a model analyte in PBS and serum by an immobilized antibody. Furthermore, an ATRP initiator was also selectively attached to the side chains of the top block of the polymer brush. This enabled the growth of a further polymer block in a graft-on-graft architecture. The strategy introduced through these two examples permits functionalization of antifouling polymer brushes under mild conditions via the immobilization of maleimide-containing molecules, while simultaneously adding the possibility of patterning via a UV lithographic process. Thus, a substantial increase in the accessible complexity for the bottom-up design of surface architectures has been achieved, adding a valuable tool to attain precisely engineered bioactive surfaces.

ASSOCIATED CONTENT

Supporting Information

Chemical characterization of the polymer brushes after the phototriggered functionalization reactions, confirmation of the specificity of the immobilization of streptavidin, imaging the conversion of the tetrazole groups by ToF-SIMS, and example SPR sensograms of the measurement of fouling from blood plasma and serum. The Supporting Information is available free of charge on the ACS Publications website at DOI: 10.1021/acs.langmuir.5b01114.

AUTHOR INFORMATION

Corresponding Authors

*E-mail: rodriguez@imc.cas.cz; Fax: +420 296 809 410; Tel: +420 296 809 333 (C.R.-E.).

*E-mail: christopher.barner-kowollik@kit.edu. Web: http://www.macroarc.de (C.B.-K.).

Notes

The authors declare no competing financial interest.

ACKNOWLEDGMENTS

The work was supported by the Program of Project Based Personal Exchange ASCR-DAAD (no. 14/08), the Grant Agency of the Czech Republic (GACR) under contract no. 15-09368Y, and the European Regional Development Funds under the project "BIOCEV − Biotechnology and Biomedicine Centre of the Academy of Sciences and Charles University" (CZ.1.05/1.1.00/02.0109) and OPPK CZ.2.16/3.1.00/21545. C.B.-K. thanks the German Academic Exchange Service (DAAD) for funding a research stay of A.S.P. and N.K. at the Karlsruhe Institute of Technology (KIT). C.B.-K. additionally acknowledges support for the project from the BioInterfaces program of the Helmholtz association at the KIT.

REFERENCES

(1) Blaszykowski, C.; Sheikh, S.; Thompson, M. Surface chemistry to minimize fouling from blood-based fluids. *Chem. Soc. Rev.* **2012**, *41* (17), 5599−5612.

(2) Blaszykowski, C.; Sheikh, S.; Thompson, M. Biocompatibility and antifouling: Is there really a link? *Trends Biotechnol.* **2014**, *32* (2), 61−62.

(3) Yu, Q.; Zhang, Y.; Wang, H.; Brash, J.; Chen, H. Anti-fouling bioactive surfaces. *Acta Biomater.* **2011**, *7* (4), 1550−1557.

(4) Xu, F. J.; Neoh, K. G.; Kang, E. T. Bioactive surfaces and biomaterials via atom transfer radical polymerization. *Prog. Polym. Sci.* **2009**, *34* (8), 719−761.

(5) Rodriguez-Emmenegger, C.; Preuss, C. M.; Yameen, B.; Pop-Georgievski, O.; Bachmann, M.; Mueller, J. O.; Bruns, M.; Goldmann, A. S.; Bastmeyer, M.; Barner-Kowollik, C. Controlled cell adhesion on poly(dopamine) interfaces photopatterned with non-fouling brushes. *Adv. Mater.* **2013**, *25* (42), 6123−6127.

(6) Ma, H.; Hyun, J.; Stiller, P.; Chilkoti, A. "Non-fouling" oligo(ethylene glycol)—Functionalized polymer brushes synthesized by surface-initiated atom transfer radical polymerization. *Adv. Mater.* **2004**, *16* (4), 338−341.

(7) Hucknall, A.; Kim, D. H.; Rangarajan, S.; Hill, R. T.; Reichert, W. M.; Chilkoti, A. Simple Fabrication of Antibody Microarrays on Nonfouling Polymer Brushes with Femtomolar Sensitivity for Protein Analytes in Serum and Blood. *Adv. Mater.* **2009**, *21* (19), 1968−1971.

(8) Gautrot, J. E.; Huck, W. T.; Welch, M.; Ramstedt, M. Protein-resistant NTA-functionalized polymer brushes for selective and stable

DOI: 10.1021/acs.langmuir.5b01114
Langmuir 2015, 31, 5899−5907

immobilization of histidine-tagged proteins. *ACS Appl. Mater. Interfaces* **2010**, *2* (1), 193−202.
(9) Barbey, R.; Lavanant, L.; Paripovic, D.; Schuwer, N.; Sugnaux, C.; Tugulu, S.; Klok, H. A. Polymer brushes via surface-initiated controlled radical polymerization: Synthesis, characterization, properties, and applications. *Chem. Rev.* **2009**, *109* (11), 5437−527.
(10) Krishnamoorthy, M.; Hakobyan, S.; Ramstedt, M.; Gautrot, J. E. Surface-initiated polymer brushes in the biomedical field: Applications in membrane science, biosensing, cell culture, regenerative medicine and antibacterial coatings. *Chem. Rev.* **2014**, *114* (21), 10976−1026.
(11) Gunkel, G.; Weinhart, M.; Becherer, T.; Haag, R.; Huck, W. T. Effect of polymer brush architecture on antibiofouling properties. *Biomacromolecules* **2011**, *12* (11), 4169−4172.
(12) Huang, C. J.; Li, Y.; Jiang, S. Zwitterionic polymer-based platform with two-layer architecture for ultra low fouling and high protein loading. *Anal. Chem.* **2012**, *84* (7), 3440−3445.
(13) Peng, S. J.; Bhushan, B. Smart polymer brushes and their emerging applications. *RSC Adv.* **2012**, *2* (23), 8557−8578.
(14) Chen, Y. X.; Triola, G.; Waldmann, H. Bioorthogonal chemistry for site-specific labeling and surface immobilization of proteins. *Acc. Chem. Res.* **2011**, *44* (9), 762−73.
(15) Tugulu, S.; Arnold, A.; Sielaff, I.; Johnsson, K.; Klok, H. A. Protein-functionalized polymer brushes. *Biomacromolecules* **2005**, *6* (3), 1602−1607.
(16) de los Santos Pereira, A.; Riedel, T.; Brynda, E.; Rodriguez-Emmenegger, C. Hierarchical antifouling brushes for biosensing applications. *Sens. Actuators, B* **2014**, *202*, 1313−1321.
(17) Trmcic-Cvitas, J.; Hasan, E.; Ramstedt, M.; Li, X.; Cooper, M. A.; Abell, C.; Huck, W. T.; Gautrot, J. E. Biofunctionalized protein resistant oligo(ethylene glycol)-derived polymer brushes as selective immobilization and sensing platforms. *Biomacromolecules* **2009**, *10* (10), 2885−2894.
(18) Orski, S.; Sheppard, G.; Arnold, R.; Grubbs, J.; Locklin, J. Post-polymerization modification of polymer brushes. In *Functional Polymers by Post-Polymerization Modification: Concepts, Guidelines, and Applications*; Theato, P., Klok, H. A., Eds.; Wiley-VCH Verlag GmbH & Co. KGaA: Weinheim, Germany, 2012.
(19) Sheikh, S.; Sheng, J. C. C.; Blaszykowski, C.; Thompson, M. New oligoethylene glycol linkers for the surface modification of an ultra-high frequency acoustic wave biosensor. *Chem. Sci.* **2010**, *1* (2), 271−275.
(20) Ayres, N. Polymer brushes: Applications in biomaterials and nanotechnology. *Polym. Chem.* **2010**, *1* (6), 769−777.
(21) Ebara, M.; Yamato, M.; Aoyagi, T.; Kikuchi, A.; Sakai, K.; Okano, T. A novel approach to observing synergy effects of PHSRN on integrin−RGD binding using intelligent surfaces. *Adv. Mater.* **2008**, *20* (16), 3034−3038.
(22) Kuzmyn, A. R.; de los Santos Pereira, A.; Pop-Georgievski, O.; Bruns, M.; Brynda, E.; Rodriguez-Emmenegger, C. Exploiting end group functionalization for the design of antifouling bioactive brushes. *Polym. Chem.* **2014**, *5* (13), 4124−4131.
(23) Tischer, T.; Claus, T. K.; Bruns, M.; Trouillet, V.; Linkert, K.; Rodriguez-Emmenegger, C.; Goldmann, A. S.; Perrier, S.; Börner, H. G.; Barner-Kowollik, C. Spatially controlled photochemical peptide and polymer conjugation on biosurfaces. *Biomacromolecules* **2013**, *14* (12), 4340−4350.
(24) Jonkheijm, P.; Weinrich, D.; Kohn, M.; Engelkamp, H.; Christianen, P. C.; Kuhlmann, J.; Maan, J. C.; Nusse, D.; Schroeder, H.; Wacker, R.; Breinbauer, R.; Niemeyer, C. M.; Waldmann, H. Photochemical surface patterning by the thiol-ene reaction. *Angew. Chem., Int. Ed. Engl.* **2008**, *47* (23), 4421−4424.
(25) Lin, P. C.; Weinrich, D.; Waldmann, H. Protein Biochips: Oriented Surface Immobilization of Proteins. *Macromol. Chem. Phys.* **2010**, *211* (2), 136−144.
(26) Orski, S. V.; Poloukhtine, A. A.; Arumugam, S.; Mao, L.; Popik, V. V.; Locklin, J. High density orthogonal surface immobilization via photoactivated copper-free click chemistry. *J. Am. Chem. Soc.* **2010**, *132* (32), 11024−11026.
(27) Preuss, C. M.; Tischer, T.; Rodriguez-Emmenegger, C.; Zieger, M. M.; Bruns, M.; Goldmann, A. S.; Barner-Kowollik, C. A bioinspired light induced avenue for the design of patterned functional interfaces. *J. Mater. Chem. B* **2014**, *2* (1), 36−40.
(28) Tischer, T.; Rodriguez-Emmenegger, C.; Trouillet, V.; Welle, A.; Schueler, V.; Mueller, J. O.; Goldmann, A. S.; Brynda, E.; Barner-Kowollik, C. Photo-patterning of non-fouling polymers and biomolecules on paper. *Adv. Mater.* **2014**, *26* (24), 4087−4092.
(29) Glassner, M.; Oehlenschlaeger, K. K.; Welle, A.; Bruns, M.; Barner-Kowollik, C. Polymer surface patterning via Diels−Alder trapping of photo-generated thioaldehydes. *Chem. Commun. (Cambridge, U. K.)* **2013**, *49* (6), 633−5.
(30) Wang, Y.; Hu, W. J.; Song, W.; Lim, R. K.; Lin, Q. Discovery of long-wavelength photoactivatable diaryltetrazoles for bioorthogonal 1,3-dipolar cycloaddition reactions. *Org. Lett.* **2008**, *10* (17), 3725−3728.
(31) Yu, Z.; Ho, L. Y.; Wang, Z.; Lin, Q. Discovery of new photoactivatable diaryltetrazoles for photoclick chemistry via 'scaffold hopping'. *Bioorg. Med. Chem. Lett.* **2011**, *21* (17), 5033−5036.
(32) Jones, D. M.; Brown, A. A.; Huck, W. T. S. Surface-initiated polymerizations in aqueous media: Effect of initiator density. *Langmuir* **2002**, *18* (4), 1265−1269.
(33) Rodriguez-Emmenegger, C.; Hasan, E.; Pop-Georgievski, O.; Houska, M.; Brynda, E.; Alles, A. B. Controlled/living surface-initiated ATRP of antifouling polymer brushes from gold in PBS and blood sera as a model study for polymer modifications in complex biological media. *Macromol. Biosci.* **2012**, *12* (4), 525−532.
(34) Rodriguez-Emmenegger, C.; Kylian, O.; Houska, M.; Brynda, E.; Artemenko, A.; Kousal, J.; Alles, A. B.; Biederman, H. Substrate-independent approach for the generation of functional protein resistant surfaces. *Biomacromolecules* **2011**, *12* (4), 1058−1066.
(35) Parry, K. L.; Shard, A. G.; Short, R. D.; White, R. G.; Whittle, J. D.; Wright, A. ARXPS characterisation of plasma polymerised surface chemical gradients. *Surf. Interface Anal.* **2006**, *38* (11), 1497−1504.
(36) Scofield, J. H. Hartree−Slater subshell photoionization cross-sections at 1254 and 1487 eV. *J. Electron Spectrosc. Relat. Phenom.* **1976**, *8* (2), 129−137.
(37) Tanuma, S.; Powell, C. J.; Penn, D. R. Calculations of electron inelastic mean free paths. V. Data for 14 organic compounds over the 50−2000 eV range. *Surf. Interface Anal.* **1994**, *21* (3), 165−176.
(38) Homola, J. Surface plasmon resonance sensors for detection of chemical and biological species. *Chem. Rev.* **2008**, *108* (2), 462−93.
(39) Ma, H.; Li, D.; Sheng, X.; Zhao, B.; Chilkoti, A. Protein-resistant polymer coatings on silicon oxide by surface-initiated atom transfer radical polymerization. *Langmuir* **2006**, *22* (8), 3751−3756.
(40) Pop-Georgievski, O.; Rodriguez-Emmenegger, C.; de los Santos Pereira, A.; Proks, V.; Brynda, E.; Rypáček, F. Biomimetic non-fouling surfaces: Extending the concepts. *J. Mater. Chem. B* **2013**, *1*, 2859−2867.
(41) Fan, X.; Lin, L.; Dalsin, J. L.; Messersmith, P. B. Biomimetic anchor for surface-initiated polymerization from metal substrates. *J. Am. Chem. Soc.* **2005**, *127* (45), 15843−15847.
(42) Riedel, T.; Rodriguez-Emmenegger, C.; de los Santos Pereira, A.; Bedajankova, A.; Jinoch, P.; Boltovets, P. M.; Brynda, E. Diagnosis of Epstein−Barr virus infection in clinical serum samples by an SPR biosensor assay. *Biosens. Bioelectron.* **2014**, *55*, 278−84.
(43) Love, J. C.; Estroff, L. A.; Kriebel, J. K.; Nuzzo, R. G.; Whitesides, G. M. Self-assembled monolayers of thiolates on metals as a form of nanotechnology. *Chem. Rev.* **2005**, *105* (4), 1103−1169.
(44) Vaisocherova, H.; Zhang, Z.; Yang, W.; Cao, Z.; Cheng, G.; Taylor, A. D.; Piliarik, M.; Homola, J.; Jiang, S. Functionalizable surface platform with reduced nonspecific protein adsorption from full blood plasma—Material selection and protein immobilization optimization. *Biosens. Bioelectron.* **2009**, *24* (7), 1924−1930.
(45) Vaisocherova, H.; Sevcu, V.; Adam, P.; Spackova, B.; Hegnerova, K.; de los Santos Pereira, A.; Rodriguez-Emmenegger, C.; Riedel, T.; Houska, M.; Brynda, E.; Homola, J. Functionalized ultra-low fouling carboxy- and hydroxy-functional surface platforms: Functionalization

DOI: 10.1021/acs.langmuir.5b01114
Langmuir 2015, 31, 5899−5907

capacity, biorecognition capability and resistance to fouling from undiluted biological media. *Biosens. Bioelectron.* **2014**, *51*, 150−157.
(46) Scarano, S.; Mascini, M.; Turner, A. P.; Minunni, M. Surface plasmon resonance imaging for affinity-based biosensors. *Biosens. Bioelectron.* **2010**, *25* (5), 957−966.
(47) Shumaker-Parry, J. S.; Zareie, M. H.; Aebersold, R.; Campbell, C. T. Microspotting streptavidin and double-stranded DNA arrays on gold for high-throughput studies of protein−DNA interactions by surface plasmon resonance microscopy. *Anal. Chem.* **2004**, *76* (4), 918−929.
(48) Rusmini, F.; Zhong, Z.; Feijen, J. Protein immobilization strategies for protein biochips. *Biomacromolecules* **2007**, *8* (6), 1775−1789.
(49) Brault, N. D.; Sundaram, H. S.; Huang, C. J.; Li, Y.; Yu, Q.; Jiang, S. Two-layer architecture using atom transfer radical polymerization for enhanced sensing and detection in complex media. *Biomacromolecules* **2012**, *13* (12), 4049−56.

DOI: 10.1021/acs.langmuir.5b01114
Langmuir 2015, 31, 5899−5907

SUPPORTING INFORMATION

Photo-Triggered Functionalization of Hierarchically Structured Polymer Brushes

Andres de los Santos Pereira,[†] *Nina Yu. Kostina,*[†] *Michael Bruns,*[‡] *Cesar Rodriguez-Emmenegger,*[*,†] *and Christopher Barner-Kowollik*[*,‖,§]

[†]Institute of Macromolecular Chemistry, Academy of Sciences of the Czech Republic, v.v.i., Heyrovsky sq. 2, 162 06 Prague, Czech Republic. E-mail: rodriguez@imc.cas.cz.

[‡]Institut für Angewandte Materialien (IAM), Karlsruhe Nano Micro Facility (KNMF), Karlsruhe Institute of Technology (KIT), Hermann-von-Helmholtz-Platz 1, 76344 Eggenstein-Leopoldshafen, Germany

[‖]Preparative Macromolecular Chemistry, Institut für Technische Chemie und Polymerchemie, Karlsruhe Institute of Technology (KIT), Engesserstr. 18, 76131 Karlsruhe, Germany. Web: http://www.macroarc.de, E-mail: christopher.barner-kowollik@kit.edu.

[§]Institut für Biologische Grenzflächen, Karlsruhe Institute of Technology (KIT), Hermann-von-Helmholtz-Platz 1, 76344 Eggenstein-Leopoldshafen, Germany.

Chemical characterization of the polymer brushes after the photo-triggered functionalization

Table S1 presents the C1s and N1s regions of the XPS spectra of the polymer brushes after functionalization by NITEC. After the immobilization of either maleimide-ATRP-initiator or maleimide-biotin, the C1s region still retains a predominance of the features of the underlying polymer brush. On the other hand, the N1s region shows the disappearance of the signal at 402.8 eV together with a slight increase in the signal around 400.3 eV, consistent with the activation of the tetrazole and binding of nitrogen-containing compounds. The increase in the signal is more pronounced in the case of the immobilization of maleimide-biotin, which is explained by the higher content of nitrogen in the biotin itself (urea in the structure) and the linker, composed of a hydrazide.

After the immobilization of streptavidin on the biotin presenting surface, the marked increase in the signal of the N1s region proves the presence of the protein on the surface.[1] This is explained by the abundance of N atoms in peptide bonds. Moreover, the ratio of the intensity of the component corresponding to C-O bonds from the ethylene glycol units to C-C, C-H, and O-C=O shows a decrease, as the latter groups more prevalent in the protein.

The growth of poly(CBAA) as a graft-on-graft is accompanied by the appearance of two distinct signals at 399.8 and 402.5 eV in the N1s spectrum. These correspond to the acrylamide groups and the positively charged quaternary ammonium groups respectively. The C1s region of the spectrum reveals a relative increase in the content of in the C-C, C-H signal.

Scheme S1. Chemical structures of the functionalized surfaces prepared and characterized by XPS.

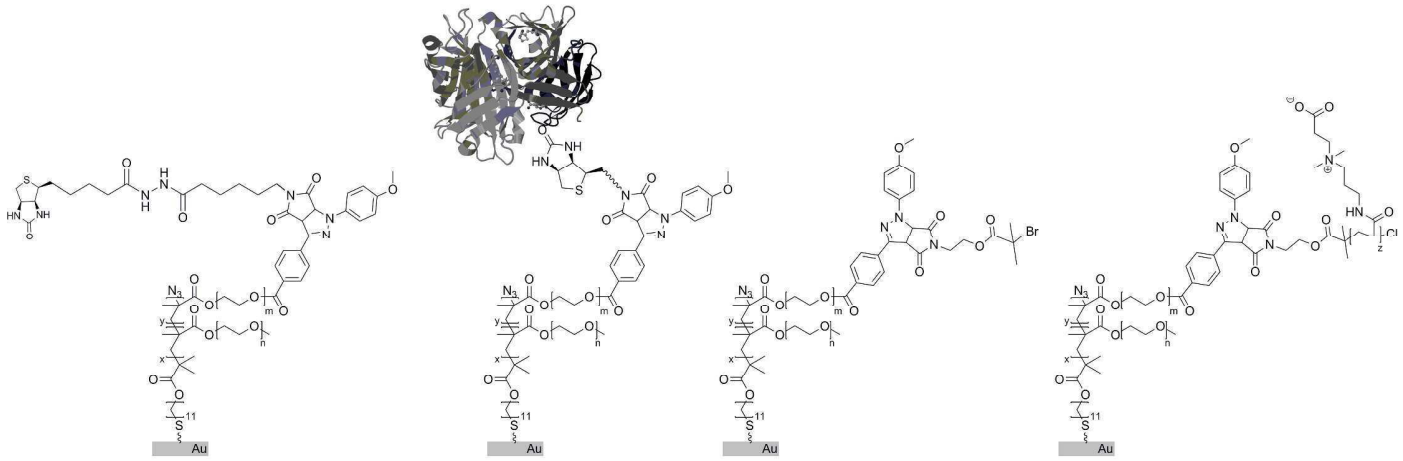

(1) Clicked maleimide-biotin

(2) Streptavidin on biotin-functionalised poly(MeOEGMA-*b*-HOEGMA)

(3) Clicked maleimide-ATRP-Initiator

(4) Poly(CBAA) grafted from poly(MeOEGMA-*b*-HOEGMA)

Table S1. Chemical characterization of the functionalized polymer brushes by XPS (numbered according to Scheme S1)

Surface	XPS spectra of the **C1s** region	XPS spectra of the **N1s** region
(1) Clicked maleimide-biotin	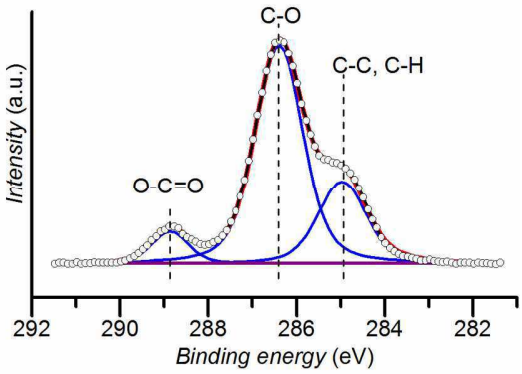	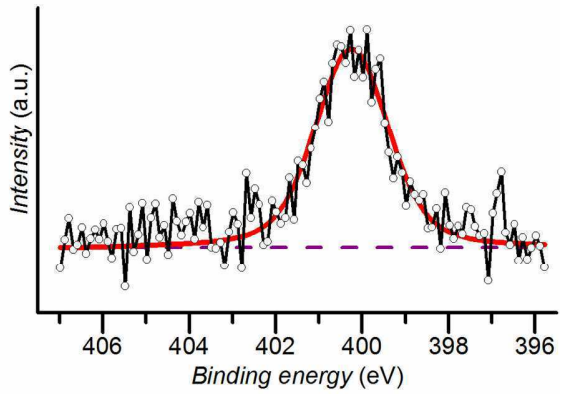
(2) Streptavidin on biotin-functionalized poly(MeOEGMA-*b*-HOEGMA)	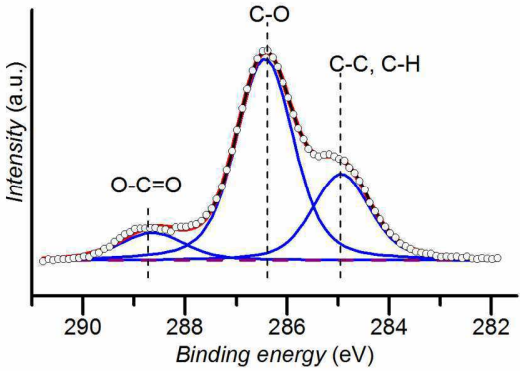	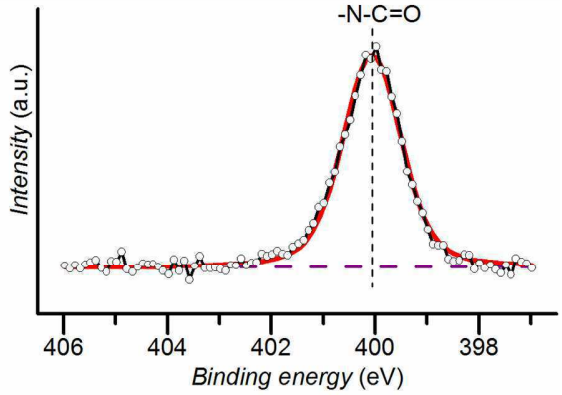
(3) Clicked maleimide-ATRP-Initiator	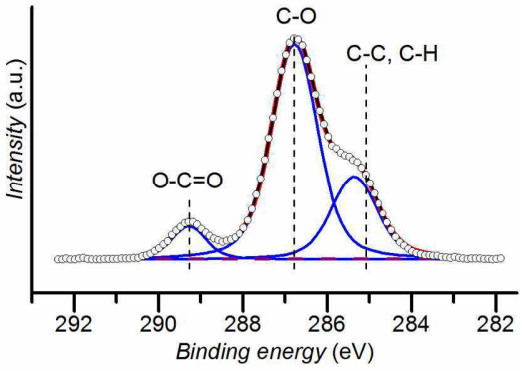	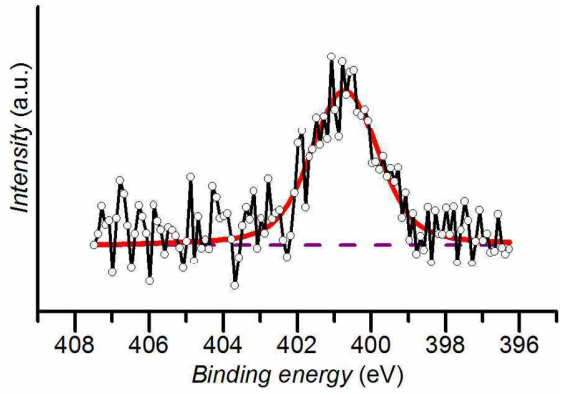
(4) Poly(CBAA) grafted from poly(MeOEGMA-*b*-HOEGMA)	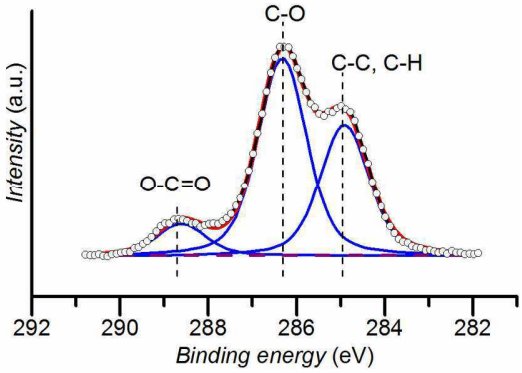	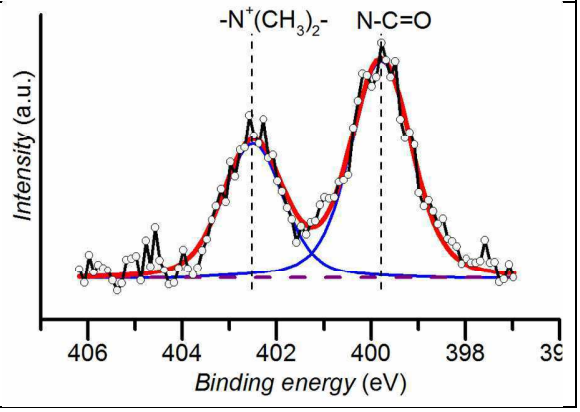

Confirmation of the specificity of the immobilization of streptavidin by XPS

In order to provide further confirmation that the streptavidin immobilized on the surfaces was only specifically attached to maleimide-biotin, *i.e.* photo-clicked to the tetrazole groups, a control sample was prepared in exactly the same way as the streptavidin-functionalized polymer brushes, with the sole exception that it was not irradiated by UV-light. The substrate coated with the tetrazole-functionalized polymer brush was placed vertically in a headspace vial and covered with a 1 $mg \cdot mL^{-1}$ solution of maleimide-biotin in DMF. The vial was crimped air-tight and purged for 5 min with nitrogen in the dark and kept in the dark. After 1 h, the sample was removed and rinsed intensively with DMF, ethanol, water, and blow dried with nitrogen. Subsequently, the sample was contacted for 3 h with a 0.5 $mg \cdot mL^{-1}$ solution of streptavidin in PBS (pH 7.4), rinsed with PBS and water, and blow dried with nitrogen. Figure S1 shows the obtained XPS spectra. It is evident that the features of the spectra are identical with those of the tetrazole-functionalized polymer brushes, indicating that no streptavidin was immobilized on the blank, consistent with the patterning observed by ToF-SIMS on the sample irradiated using a shadow mask. This is due to the excellent antifouling properties of the polymer brushes, which are able to resist the non-specific protein adsorption even under the most demanding conditions.[2] Therefore, the streptavidin attachment observed on the surfaces can only be a result of its specific affinity interaction with the biotin, immobilized by photo-triggered NITEC to the tetrazole present on the brushes.

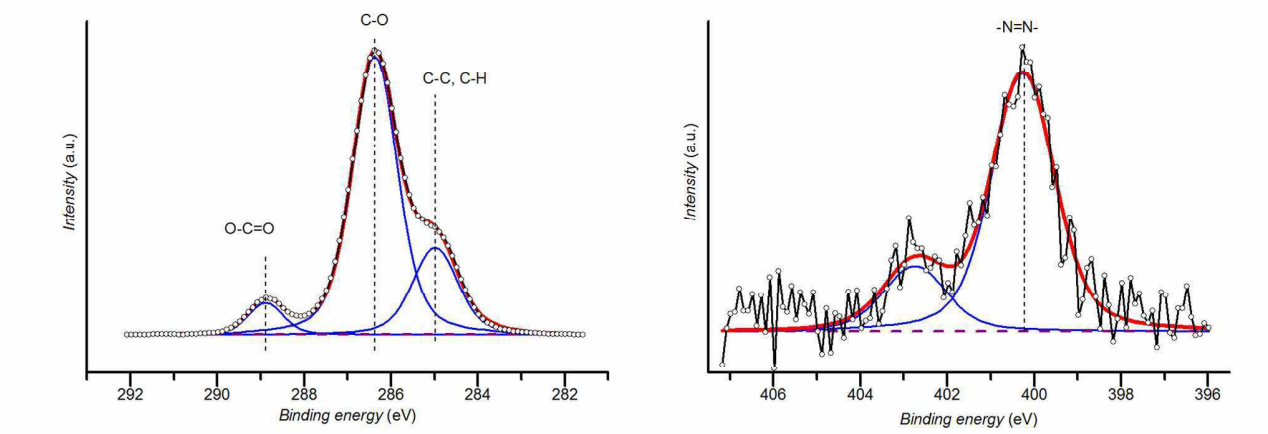

Figure S1. C1s (left) and N1s (right) regions of the XPS spectrum of the blank prepared without irradiation for the streptavidin-functionalized polymer brushes. The features are identical as for the tetrazole-functionalized polymer brushes, indicating that no streptavidin adsorbed non-specifically on the blank.

Conversion of the Tetrazole group by ToF-SIMS

The individual ToF-SIMS image of the tetrazole fragment on the polymer brush surface after phototriggered ligation of maleimide-biotin shows no counts in the irradiated area. This indicates that the conversion of the tetrazole groups (present on the surface of the brush) was complete. Therefore, in a subsequent photo-ligation step with a different dipolarophile-containing molecule to orthogonally functionalize the remaining area, no contamination of the already functionalized regions is expected due to the unavailability of tetrazole groups. It should be noted that the ToF-SIMS technique is only sensitive to fragments arising from the outer-most layer of the surface.

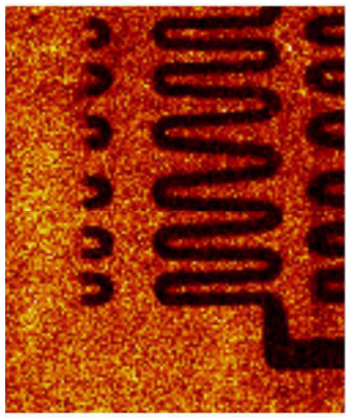

Figure S2 Individual ToF-SIMS of tetrazole fragment $C_7H_4N^-$ (102.0 u).

Fouling experiments

Figure S3 shows examples sensograms of the measurement of fouling from undiluted human blood plasma and serum on the antibody-functionalized polymer brushes. It can be seen that the polymer brush modification reduces the fouling by approximately 90% in both cases.

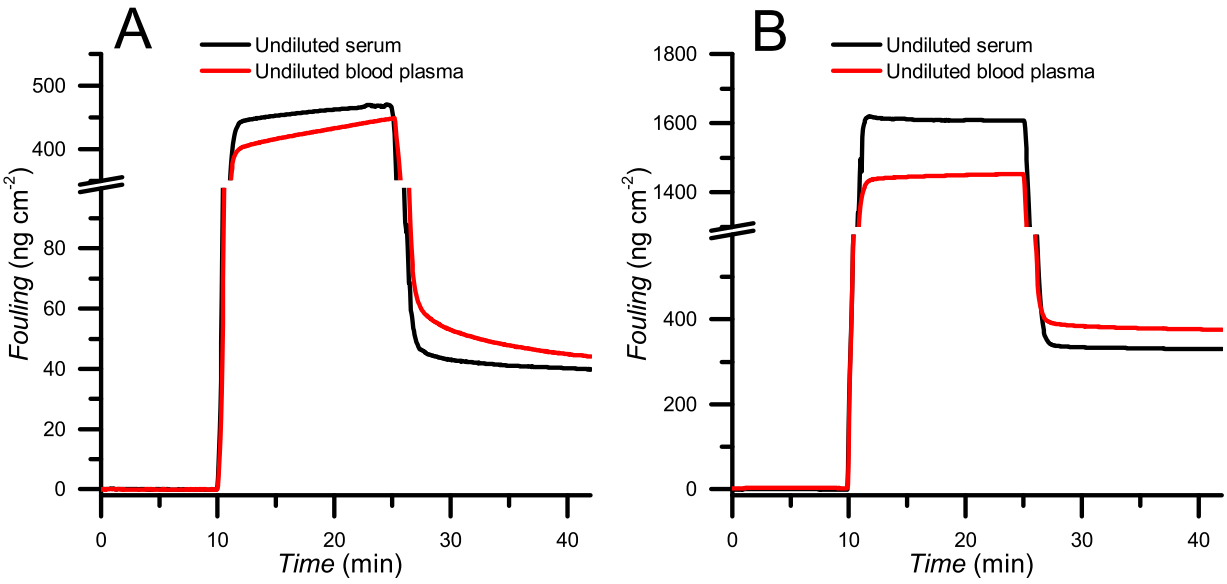

Figure S3 Fouling from undiluted human blood plasma and serum on (A) antibody-functionalized polymer brushes and (B) bare gold measured by SPR.

REFERENCES

1. Zhang, F.; Kang, E. T.; Neoh, K. G.; Wang, P.; Tan, K. L. Surface modification of stainless steel by grafting of poly(ethylene glycol) for reduction in protein adsorption. *Biomaterials* **2001,** *22* (12), 1541-1548.

2. Rodriguez-Emmenegger, C.; Houska, M.; Bologna Alles, A.; Brynda, E. Surfaces resistant to fouling from biological fluids: towards bioactive surfaces for real applications. *Macromolecular Bioscience* **2012,** *12*, 1413-1422.

Appendix 3

Non-fouling hydrogels of 2-hydroxyethyl methacrylate and zwitterionic carboxybetaine (meth)acrylamides

Biomacromolecules, 2012, 13 (12), 4164-4170

Article

pubs.acs.org/Biomac

Non-fouling Hydrogels of 2-Hydroxyethyl Methacrylate and Zwitterionic Carboxybetaine (Meth)acrylamides

Nina Yu. Kostina, Cesar Rodriguez-Emmenegger,* Milan Houska, Eduard Brynda, and Jiří Michálek

Institute of Macromolecular Chemistry, Academy of Sciences of the Czech Republic, v.v.i., Prague, 16206, Czech Republic

Supporting Information

ABSTRACT: Five poly(betaine) brushes were prepared, and their resistance to blood plasma fouling was studied. Two carboxybetaines monomers were copolymerized with 2-hydroxyethyl methacrylate (HEMA) to prepare novel hydrogels. By increasing the content of the zwitterionic comonomer, a 4-fold increase in the water content could be achieved while retaining mechanical properties close to the widely used poly(HEMA) hydrogels. All hydrogels showed an unprecedentedly low fouling from blood plasma. Remarkably, by copolymerization with 10 mol % of carboxybetaine acrylamide, hydrogels fully resistant to blood plasma were prepared.

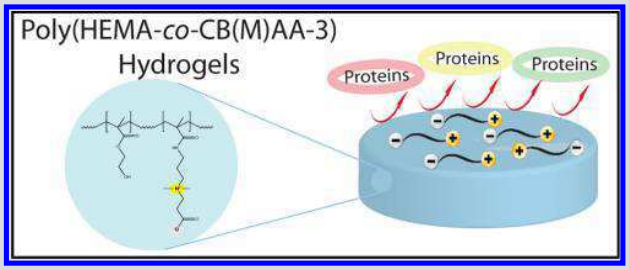

INTRODUCTION

Currently, there is an increasing concern in healthcare and life quality resulting in the current medical technologies encompassing a novel range of biomaterials, tissue engineering, and cell therapy methodologies. In particular, research focused on tissue and organ regeneration or replacement is at the forefront of contemporary research. The precise design of scaffolds employed in tissue engineering plays a crucial role in the successful implantation, providing physical and biological properties such as sufficient mechanical strength, a suitable microenvironment for cells facilitating their proliferation, signaling, and stimulating matrix production by cells. A common strategy for accomplishing these goals is to prepare scaffolds with similar water content and structural mechanical properties to living tissues. A subsequent postmodification to add bioactive molecules to induce cell adhesion and proliferation is crucial to develop tailor-made materials.[1]

Among various classes of materials for scaffolds, hydrogels are of great interest for tissue engineering due to their viscoelastic mechanical properties, high water content, and structural similarity to macromolecular-based components of the body, which mimics the interstitial tissue environment ensuring high diffusion.[2−5] A very attractive type of hydrogels are those based on poly(2-hydroxyethyl methacrylate) (poly(HEMA)). Since the introduction of these hydrogels in 1960 by Wichterle,[5] they have found numerous applications in the biomedical field due to their chemical stability, good biocompatibility, hydrophilic character, excellent mechanical properties, and low level of immunogenicity.[6−8] However, despite all these advantages, the use of poly(HEMA) hydrogels is limited. These materials display only a moderate wettability, lower than that of natural tissues.[2] In addition, the contact with biological fluids, in particular blood plasma, after implantation leads to nonspecific protein adsorption, i.e., fouling, resulting in irreversible changes in the surface properties of the material.[9] This adverse effect causes inflammatory responses, facilitates the attachment of microorganisms on contact lenses[10] and synthetic grafts,[11] and disables cardiovascular devices by thrombus formation.[11] In addition, the protein fouling masks any bioactive molecule immobilized in the material in order to support specific interactions with cells. Thus, the control over the functions and fate of the biomaterial is no longer possible.

Materials with higher wettability and reduced fouling properties are the crucial step in the design of scaffolds. Various types of hydrogels containing poly(ethylene glycol) (PEG) have been prepared.[12] PEG-based materials have been widely studied; however,[13−16] its contact with real biological media led to fouling regardless of the type of architecture.[17−22] It has been hypothesized that the electrostatically induced hydration would aid in the development of highly protein resistant surfaces,[23,24] leading to the preparation of materials with ionic groups. First attempts to increase the wettability of poly(HEMA)-based materials are based on the copolymerization of HEMA with ionic comonomers.[25] This straightforward strategy, however, proved to lead to very poor mechanical properties and high fouling via ionic interactions.[25] With electroneutrality being a precondition for resistance to fouling, it seems natural that zwitterionic monomers are excellent candidates to meet the challenge of minimizing the fouling while increasing wettability.[26,27] Zwitterions are dipolar species, in which the cation and anion are separately bound to the same monomer unit and can be completely dissociated, thus maintaining the overall electroneutrality.[28] Typically, polybetaines are poly(zwitterion)s in which the cation is

Received: September 13, 2012
Revised: November 6, 2012
Published: November 8, 2012

permanently charged, such as in the case of quaternarized ammonium.[28] After Zwaal et al. demonstrated the non-thrombogenic nature of the phosphorylcholine (PC) moiety, an important component of cell membranes,[29] various attempts to prepare low-fouling surfaces were carried out. The use of PC to improve biocompatibility was soon recognized by Nakabayashi[30] and Chapman[31,32] who prepared various nonthrombogenic materials.[33−35] Later some (meth)-acrylamido zwitterionic polymers such as methacryloyloxyethyl phosphorylcholine (phosphorycholine methacrylate, PCMA) and *N*-(3-sulfopropyl)-*N*-(methacryloxyethyl)-*N*,*N*-dimethylammonium (sulfobetaine methacrylate, SBMA) and various carboxybetaines were grafted on surfaces, and their resistance to protein fouling was assessed.[17,20,36] However, only few attempts of preparation of zwitterionic hydrogels have been reported.[37−41] Most of the hydrogels described in the literature are based typically on sulfobetaine monomers due to their commercial availability and simple synthetic accessibility.[37,39−41] These hydrogels, however, showed only poor mechanical properties and limited resistance to proteins.[42,43] Even if later attempts tried to address the poor mechanical properties,[38] sulfobetaine-based polymers suffer from a high fouling from blood plasma.[17] A recent report from Carr et al. tried to address the problem of fouling preparing hydrogel based solely on carboxybetaine methacrylate and a betaine cross-linker.[44] Cross-linker contents as high as 90−100% were necessary to achieve compressive Young modulus as high as 8.2 MPa and good resistance to cell adhesion.[44] Neither tensile test, relevant to many hydrogel applications, nor blood plasma fouling studies were presented.[44]

Herein we introduce an avenue to address the aforementioned drawbacks by combining the excellent mechanical properties of poly(HEMA) hydrogels with blood plasma fouling resistance of zwitterionic polymers. The selection of the zwitterionic comonomers for hydrogels preparation was based on their resistance to blood plasma fouling studied in model systems based on polymer brushes and evaluated by surface plasmon resonance (SPR) spectroscopy. Two carboxybetaine monomers, having the best resistance to fouling, were copolymerized with HEMA to prepare hydrogels with excellent mechanical properties and wettability close to human tissues. The resistance of the newly synthesized hydrogels to blood plasma fouling was assessed by Fourier transform infrared (FTIR) multiple reflection attenuated total reflectance (ATR). The novel hydrogels were able to withstand the fouling from undiluted blood plasma.

EXPERIMENTAL SECTION

Materials. All chemicals and solvents were purchased from Sigma−Aldrich, TCI-Europe, Merck, Vertelius specialties, Acros, or Serva at the highest available purity and were used as received (refer to Supporting Information).

Monomer Synthesis. *(3-Acryloylamino-propyl)-(2-carboxy-ethyl)-dimethyl-ammonium (Carboxybetaine acrylamide, CBAA-3).* The title compound was synthesized by a modification of the procedure reported earlier.[17,45] Dimethyl aminopropyl acrylamide (7.8 g, 55 mmol) was dissolved in 100 mL of anhydrous tetrahydrofuran (THF) and cooled to −20 °C. A pinch of diphenylpicryl hydrazyl (DPPH) was added as inhibitor. Subsequently, β-propiolactone (5.0 g, 69 mmol) was dissolved in 40 mL of THF and added dropwise under nitrogen atmosphere. The reaction was allowed to proceed for 24 h at 4 °C. The white precipitate was washed with dry THF and ether and dried under vacuum. Prior to polymerization, DPPH was removed by reprecipitation from methanol solution by addition of THF to yield 19.4 g (yield: 80%)

(3-Methacryloylamino-propyl)-(2-carboxy-ethyl)-dimethyl-ammonium (Carboxybetaine methacrylamide, CBMAA-3). CBMAA-3 was prepared by an analogous procedure, but utilizing dimethyl aminopropyl methacrylamide (100 mmol). Yield: 80% of CBMAA-3 as a white solid.

(2-Methacryloyl-ethyl)-(2-carboxy-ethyl)-dimethyl-ammonium (Carboxybetaine Methacrylate, CBMA-2). CBMA-2 was prepared by an procedure analogous to that of CBAA-2, but utilizing dimethyl aminoethyl methacrylate (100 mmol) as reported previously. Yield: 90% of CBMA-2 as a white solid.

Polymer Brushes as Model Surfaces. The gold-coated substrates were rinsed with ethanol and water, blow dried with nitrogen, and cleaned with UV-ozone cleaner (Jelight) for 15 min. The substrates were immediately immersed in a 1 mM solution of ω-mercaptoundecyl bromoisobutyrate at room temperature for at least 24 h to allow the formation of a self-assembled monolayer (SAM) of initiator.

Polymer brushes of poly(carboxybetaine acrylamide) (poly(CBAA-3)), poly(carboxybetaine methacrylamide) (poly(CBMAA-3)), poly(carboxybetaine methacrylate) (poly(CBMA-2)), poly(sulfobetaine methacrylate) (poly(SBMA)) and poly(phosphorylcholine methacrylate) were grafted from the SAM of initiator via surface initiated atom transfer radical polymemrization (ATRP).

Polymerization of CBAA-3 and CBMAA-3. The polymerization was carried out according to our optimized procedures.[17,20,46] Ethanol (10 mL) was degassed by three cycles of freeze−pump−thaw and transferred to a Schlenk tube containing CuBr (19.1 mg, 133 μmol), $CuBr_2$ (5.9 mg, 26.5 μmol), and Me_4Cyclam (40.9 mg, 160 μmol). The blue solution of the catalyst was syringed to a Schlenk tube containing the monomer CBMAA-3 (1600 mg, 6.7 mmol) or CBAA-3 (1500 mg, 6.7 mmol). Finally, the polymerization solution was transferred to the reactors containing the substrate coated with a SAM of ω-mercaptoundecyl bromoisobutyrate, and the reaction was allowed to proceed for 2 h at 30 °C to obtain 19.5-nm-thick polymer brushes.

Polymerization of CBMA-2 and SBMA. A solution of 2,2′-dipyridyl (125 mg, 806 μmol) and CBMA-2 (544 mg, 2375 μmol) in 10 mL of water:methanol = 1:1 was degassed by Ar bubbling for 40 min. CuBr (58 mg, 404 μmol) was added and further degassed for 30 min. The polymerization mixture was transferred under Ar protection to the reactor containing the initiator-coated substrate. Polymerization proceeded at 30 °C. The reaction was stopped after 2 h to obtain 20-nm-thick polymer brushes.

The polymerization of SBMA was carried out in an analogous way, but utilizing SBMA (833 mg, 2845 μmol) and only water as solvent. The polymerization was allowed to proceed for 1 h at 30 °C to yield 20-nm-thick brushes.

Polymerization of Phosphorylcholine Methacrylate (PCMA). To a degassed solution of $CuBr_2$ (7.5 mg, 33.6 μmol), 2,2′-dipyridyl (208 mg, 1335 μmol) and (PCMA) (1 g, 3.58 mmol) in 10 mL of water CuBr (96 mg, 671 μmol) was added. The polymerization mixture was transferred to the reactor containing the initiator-coated substrate. The polymerization was carried out at 30 °C for 2 h to obtain 20-nm thick polymer brushes.

Characterization of Polymer Brushes. The thickness of the polymer brushes was determined by spectroscopic ellipsometry using a Variable Angle Spectroscopic Imaging Auto-Nulling Ellipsometer EP3-SE in air at room temperature.

FTIR grazing-angle specular reflectance (FTIR-GASR) spectra of the dried coatings on the gold surface of SPR chips were recorded using a Bruker IFS 55 FTIR spectrometer equipped with a Pike Technologies 80Spec GASR attachment and polarizer (grazing angle 80, p-polarization). The spectrometer was purged continuously with dried air.

The wettability of the samples was examined by a dynamic sessile water drop method using a DataPhysics OCA 20 contact angle system. A 5 μL drop was placed on the surface, and advancing and receding contact angles were determined dynamically while the volume of the drop was increased up to 15 μL and decreased at a flow rate of 0.5 μL·min^{-1}. Data were evaluated using a circular fitting algorithm.

Protein fouling from the solutions of main blood plasma proteins and undiluted blood plasma was quantified by SPR spectroscopy using a custom built instrument described elsewhere.[17] Undiluted human blood plasma and solutions of human serum albumin (HSA), fibrinogen (Fbg), and immunoglobulin G (IgG) were driven for 30 min at 25 μL·min^{-1} by a peristaltic pump through the channels of a flow cell in which SPR responses were measured. The sensor response ($\Delta\lambda_{Res}$) was obtained by the difference between the baselines in phosphate buffered saline (PBS) before and after the injection of the tested samples. The sensor response was calibrated to the mass deposited at the surface of bound molecules. According to a calibration made by FTIR-GASR, a shift $\Delta\lambda_{Res}$ = 1 nm corresponded to a change in the deposited protein mass of 150 pg·mm^{-2}.[17]

Preparation of Poly(HEMA), Poly(HEMA-*co*-CBAA-3), and Poly(HEMA-*co*-CBMAA-3) Hydrogels. The two monomers showing the best resistance to fouling (CBAA-3 and CBMAA-3) were selected as comonomers for the preparation of hydrogels with HEMA. The zwitterionic CBAA-3 or CBMAA-3 was dissolved in HEMA in concentrations of 1, 2.5, 5, 7.5, and 10 mol % (Table1) in a water bath (4 °C). The cross-linker (ethylene glycol dimethacrylate, 0.5 wt %) and photoinitiator (benzoin ethyl ether, 0.5 wt %) were subsequently added to the monomer mixture and stirred in the dark until complete dissolution. The polymerization mixture was transferred into a cast composed of two plates (one glass and one poly(propylene)) separated with a 0.5 mm or 1 mm thick silicon spacer. The photopolymerization reaction was carried out at ambient temperature for 30 min under UV irradiation. After polymerization, poly(HEMA-*co*-CBAA-3) and poly(HEMA-*co*-CBMAA-3) hydrogels were immersed in deionized water. Water was changed every 12 h for 8 days to remove unreacted monomers. Pure poly(HEMA) hydrogels were synthesized utilizing the same procedure but without addition of zwitterionic comonomer.

Table 1. The Composition of Formulations of Poly(HEMA), Poly(HEMA-*co*-CBAA-3), and Poly(HEMA-*co*-CBMAA-3) Hydrogels with Different Molar Ratio of Comonomers

sample name	HEMA/CBAA-3	sample name	HEMA/CBMAA-3
Poly(HEMA)	1/0		
1%CBAA-3	0.990/0.010	1%CBMAA-3	0.990/0.010
2.5%CBAA-3	0.975/0.025	2.5%CBMAA-3	0.975/0.025
5%CBAA-3	0.950/0.050	5%CBMAA-3	0.950/0.050
7.5%CBAA-3	0.925/0.075	7.5%CBMAA-3	0.925/0.075
10%CBAA-3	0.900/0.100	10%CBMAA-3	0.900/0.100

Characterization of Hydrogels. *Chemical Composition of Hydrogels.* Poly(HEMA), poly(HEMA-*co*-CBAA-3), and poly(HEMA-*co*-CBMAA-3) hydrogels were characterized by FTIR single reflection attenuated total reflectance (FTIR-ATR). All samples were washed with water for 8 days after polymerization and dried under a vacuum at room temperature to constant weight. The spectra of the dried hydrogels were recorded using an FTIR Thermo Nicolet Nexus 670 spectrometer equipped with a Specac Golden Gate attachment and diamond reflection prism.

Swelling Properties of Hydrogels. The equilibrium water content (EWC) of hydrogels was determined gravimetrically. Five samples of each composition of hydrogels were immersed in deionized water for swelling to equilibrium for five days, and the mass of the swollen samples was determined (m_s). Subsequently, the samples were dried in vacuum at ambient temperature to constant weight and the mass of dry hydrogels (m_d) was determined. The equilibrium water content was calculated as EWC (%) = $(m_s - m_d)/m_d \cdot 100$.

Mechanical Properties of Hydrogels. For the mechanical characterization 1 mm-thick hydrogel slabs were used. At least seven dog-bone-shaped specimens (35 mm long and 2 mm wide at the narrowest center) for extension tests were cut from the slabs of each sample. All hydrogels were swollen in water for 10 days before tensile tests. Tensile tests of hydrogels were carried out in deionized water at room temperature using an Instron 5800 apparatus at a crosshead speed of 1 mm·min^{-1}. The stress-at-break, elongation at break, and Young's modulus were evaluated.

Blood Plasma Fouling of Hydrogels. The protein fouling of hydrogels from undiluted blood plasma was evaluated by FTIR-ATR technique. Poly(HEMA), poly(HEMA-*co*-CBAA-3), and poly(HEMA-*co*-CBMAA-3) hydrogel films of the size 2.5 cm^{-2} × 2 cm^{-2} and 0.5 mm thick were immersed in PBS solution (pH = 7.4) for 24 h. PBS solution was then replaced with undiluted blood plasma avoiding any air interface, which would induce protein adsorption. Samples were gently shaken in blood plasma for 3 h at room temperature, and then plasma was gradually replaced by PBS solution. Samples were left in water for 12 h and then dried. In order to obtain flat surfaces (necessary for good contact with the FTIR-ATR prism), the samples were initially dried in a chamber saturated with acetone vapors and subsequently dried in vacuum at room temperature for 3 days. FTIR-ATR spectra of hydrogels before and after contact with blood plasma were recorded using a Bruker IFS 55 spectrometer equipped with a Wilks Sci Model 9 reflection attachment and Ge 60° crystal. Protein fouling was estimated from the intensity of amide I and II bands (1655 cm^{-1} and 1547 cm^{-1}, respectively) by subtracting normalized spectra after and before contact with blood plasma. The protein fouling was expressed as a percentage related to the amount of fouling observed on poly(HEMA). The detection limit of the method was 20 ng protein/cm^2.

RESULTS AND DISCUSSION

Selection of Zwitterionic Monomers for the Preparation of Hydrogels. It was hypothesized that the addition of zwitterionic monomers to the widely used poly(HEMA) hydrogels would result in novel highly wettable and protein resistance materials. In order to select the most suitable monomers, a model system based on polymer brushes was utilized. This allowed the study of resistance to protein fouling by SPR spectroscopy. 20-nm-thick polymer brushes of SBMA, PCMA, CBAA-3, CBMAA-3, and CBMA-2 were grafted from gold-coated SPR biosensors via surface-initiated ATRP (Scheme 1). The successful grafting was confirmed via FTIR-GASR (Figure S.I.1 in the Supporting Information). All the surfaces were markedly more hydrophilic than the substrate, as determined by water contact angles (Table S.I.-1 in the Supporting Information). The interaction of these poly(zwitterionic) brushes with the main plasma proteins; HSA (5 mg·mL^{-1}), Fbg (1 mg·mL^{-1}) and IgG (8 mg·mL^{-1}) in PBS and with undiluted human blood plasma was monitored in situ by SPR (Figure 1). Sulfobetaine and carboxybetaine brushes showed high resistance to the adsorption from solutions of proteins, while PCMA brushes suffer high fouling even if these brushes were the most hydrophilic (Table S.I.-1 in the Supporting Information).

Scheme 1. Chemical Structure of the Zwitterionic Betaine Monomers Screened

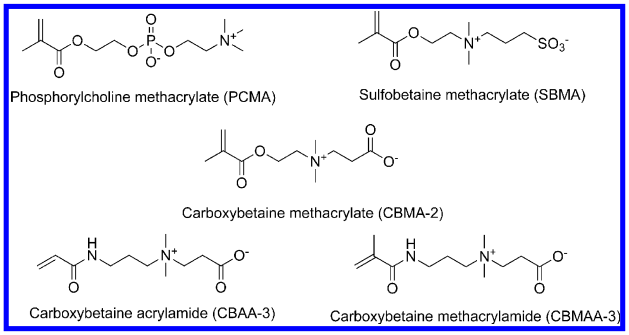

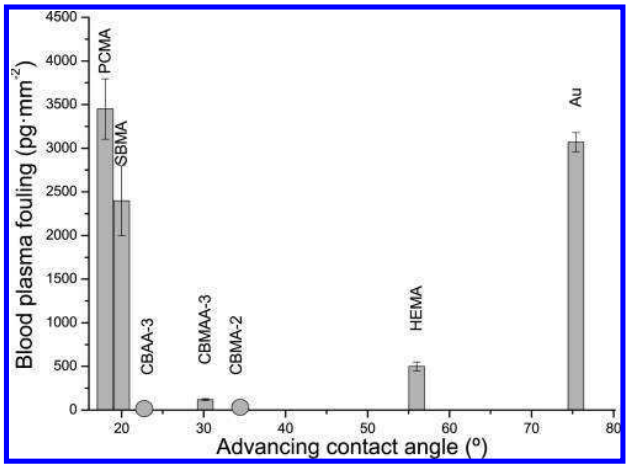

Figure 1. Blood plasma fouling on poly(betaine) brushes determined by SPR (limit of detection 0.3 pg·mm^{-2}).

Blood plasma fouling was a much more challenging fluid. Even if poly(PCMA) and poly(SBMA) brushes were the most hydrophilic among all synthesized zwitterionic polymer brushes, they were not able to resist the fouling from undiluted human blood plasma (Figure 1). The blood plasma deposits on poly(PCMA) (345 ng·cm^{-2}) and poly(SBMA) (240 ng·cm^{-2}) were close to a protein monolayer, ruling out their use for the preparation of fouling resistance hydrogels. On the other hand, the brushes based on the poly(carboxybetaine)s resulted in a remarkably low fouling (25 ng·cm^{-2}) on CBMAA-3 or even undetectable fouling on CBMA-2 and CBAA-3. Inspection of Figure 1 showed no correlation between the wettability of the brushes and their ability to resist fouling from blood plasma evidencing the complex nature of the blood plasma adsorption. From the carboxybetaines tested, CBMAA-3 and CBAA-3 were selected for copolymerization with HEMA due to the higher hydrolytical stability of amides over esters.

Preparation and Characterization of Poly(HEMA-*co*-CBAA-3) and Poly(HEMA-*co*-CBMAA-3) Hydrogels. Poly(HEMA), poly(HEMA-*co*-CBAA-3), and poly(HEMA-*co*-CBMAA-3) hydrogels were prepared with different molar concentrations of zwitterionic comonomer (Table 1). Conversion for all compositions was about 95%, as determined gravimetrically. All hydrogels were transparent and robust in the swollen state. The successful copolymerization was confirmed by FTIR-ATR spectroscopy (Figure 2). The increase in the amount of zwitterionic comonomer was in good agreement with the increase in the intensity of amide bands at 1654 cm^{-1} and 1558 cm^{-1}, and the carboxyl band at 1609 cm^{-1} arising from the betaines added (Figure 2a: poly(HEMA-*co*-CBAA-3) and Figure 2b: poly(HEMA-*co*-CBMAA-3)).

EWC versus Mechanical Properties of Poly(HEMA), Poly(HEMA-*co*-CBAA-3) and Poly(HEMA-*co*-CBMAA-3) Hydrogels. The swelling behavior and water content are very important properties for hydrogels for bioapplications. A high water content, close to natural tissues, is essential for cell growth and proliferation.[47−49] On the other hand, high water content, in general, leads to poor mechanical properties of the material. In this work this was circumvented by copolymerizing HEMA (excellent mechanical properties but poorly hydrated) with carboxybetaines.

The EWC for poly(HEMA), poly(HEMA-*co*-CBAA-3), and poly(HEMA-*co*-CBMAA-3) hydrogels was calculated by the

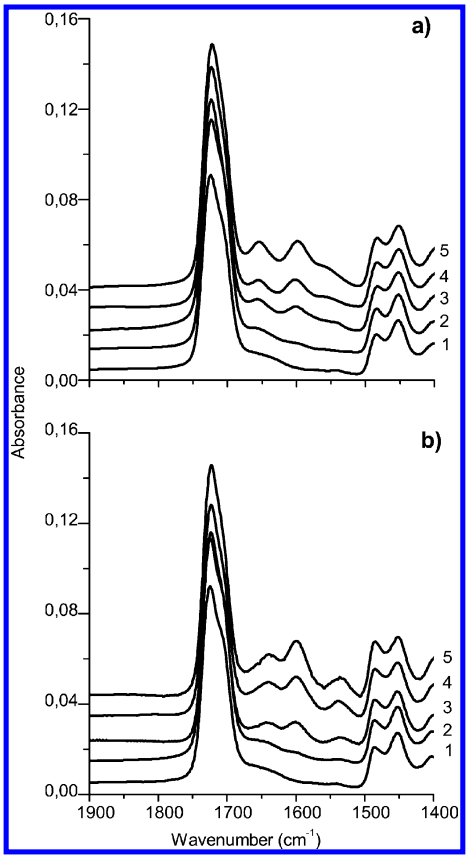

Figure 2. Amidic region of the FTIR-ATR spectra of hydrogels of (a) poly(HEMA-*co*-CBAA-3) and (b) poly(HEMA-*co*-CBMAA-3) for different concentration of the zwitterionic monomer: (1) 0%, (2) 1%, (3) 5%, (4) 7.5%, and (5) 10%.

difference in mass of fully hydrated and dehydrated gels (Figure 3). As expected, the EWC increased dramatically with addition

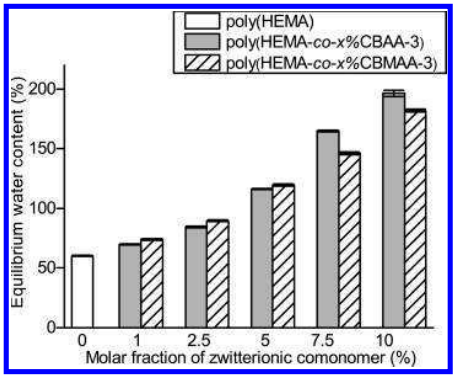

Figure 3. EWC of poly(HEMA), poly(HEMA-*co*-CBAA-3), and poly(HEMA-*co*-CBMAA-3) with different molar ratios of carboxybetaines.

of zwitterionic comonomer. While HEMA can only bind water via hydrogen bonding with its hydroxyl, carboxybetaines can bind more and strongly water via electrostatic interactions.[50] The EWC steadily increases with the addition of betaines to the polymerization feed. Remarkably, even a small addition such as 5 mol % led to 2-fold increase in the amount of water in the hydrogel with the EWC reaching a value of 116.0 ± 0.5% for

dx.doi.org/10.1021/bm301441x | *Biomacromolecules* 2012, 13, 4164−4170

poly(HEMA-*co*-CBAA-3) and 119.0 ± 0.9% for poly(HEMA-*co*-CBMAA-3). A further increase to 10 mol % of CBAA-3 or CBMAA-3 in the polymerization feed accounted for an EWC of 196.0 ± 2.0% and 181.0 ± 1.2% respectively, i.e., hydrogels binding 4 times more water than pure poly(HEMA). In this way, the EWC can be easily tuned to match the desired application by simply selecting the ratio of zwitterionic comonomer.

In order to evaluate the effect of the high water content of the newly synthesized hydrogels on the mechanical properties, the tensile strength (Figure 4), tensile stress at break (Figure 5)

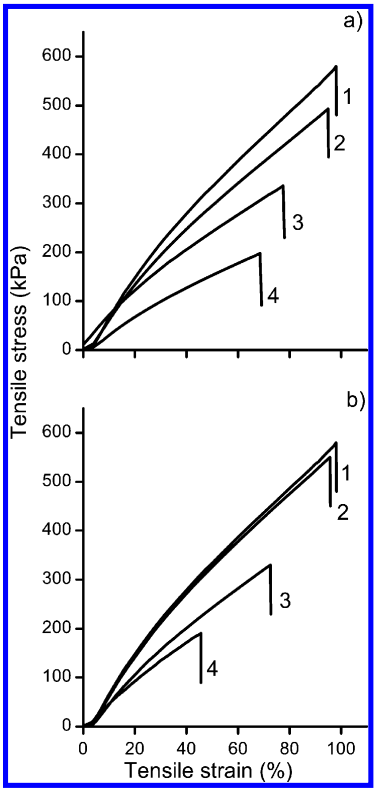

Figure 4. Stress–strain curves of (a) poly(HEMA-*co*-CBAA-3) and (b) poly(HEMA-*co*-CBMAA-3) for molar ratios of carboxybetaines of (1) 0%, (2) 1%, (3) 5%, and (4) 10%.

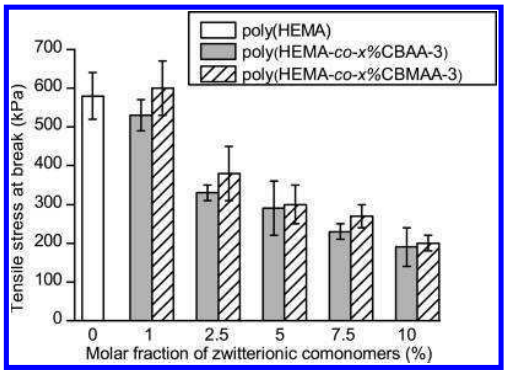

Figure 5. Tensile stress at break of poly(HEMA), poly(HEMA-*co*-CBAA-3), and poly(HEMA-*co*-CBMAA-3) hydrogels.

and Young's modulus (Figure 6) were determined on fully hydrated poly(HEMA), poly(HEMA-*co*-CBAA-3), and poly-

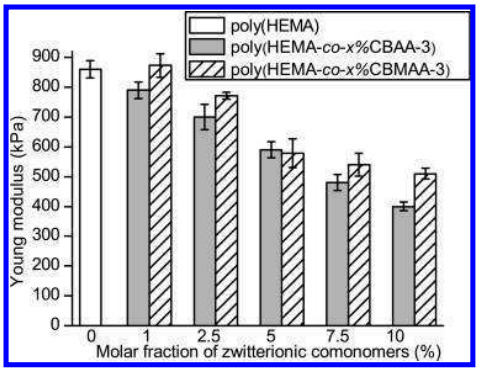

Figure 6. Young's modulus of poly(HEMA), poly(HEMA-*co*-CBAA-3), and poly(HEMA-*co*-CBMAA-3) hydrogels. Tensile tests of swollen hydrogels were carried out in deionized water at room temperature.

(HEMA-*co*-CBMAA-3) hydrogels. All the mechanical tests were carried out in water to prevent drying of the swollen samples. Representative stress–strain curves of poly(HEMA) hydrogels and hydrogels containing 1, 5, and 10 mol % of CBAA-3 or CBMAA-3 are presented in Figure 4. All zwitterionic hydrogels showed very similar elastic behavior comparable to poly(HEMA) hydrogels. The addition of zwitteroinic comonomer of 1 mol % resulted in materials with mechanical behavior similar to the widely used poly-(HEMA) hydrogels (Figures 4, 5, 6) with tensile stress at break as high as 600 kPa (Figure 5) and a Young's modulus of 850 kPa.

A gradual decrease of resistance to break was observed with increasing amount of carboxybetaine, probably due to the higher amount of incorporated water (Figure 5). However, hydrogels containing 2 times more water than poly(HEMA) (EWC ~ 120%), i.e. 5%CBAA-3 and 5%CBMAA-3, were able to resist a stress as high as 300 kPa. In spite of the big increase of EWC of zwitterionic hydrogels, the Young's modulus decrease slightly. The hydrogels with 5% of zwitterionic comonomer showed only 25% decrease of Young's modulus while having an EWC twice as high as that of pure poly(HEMA) hydrogels (Figure 6).

The advantageous high increase in EWC of hydrogels containing zwitterionic comonomer without compromising their resistance to break is of central importance when aiming at real applications.

Only minor differences in the EWC and mechanical properties of hydrogels based on CBAA-3 and CBMAA-3 were observed. Hydrogels containing CBAA-3 bound more water compared to those based on CBMAA-3. This was expected from the differences in hydrophilicity between acrylamides and methacrylamides.

Protein Fouling Test. Practically any surface in contact with blood plasma or other body fluids is rapidly coated with proteins, which impairs its properties and determines the fate of the biomaterial.[51,52] Brynda et al. showed that poly(HEMA) hydrogel suffers from important protein fouling.[53] For example, a fouling from Fbg equivalent to 0.23 ± 0.01 $\mu g \cdot cm^{-2}$ (ca. 50% of a protein monolayer) was found on poly(HEMA).[53] Moreover, the fouling from blood plasma is considerably higher than from single protein solutions.[17] Therefore, in order to design new biomaterials with tailor-made properties, prevention of protein fouling, in particular from blood plasma, is essential. Our group has shown that polymer brushes based on zwitterionic carboxybetaines and poly[*N*-(2-hydroxypropyl)

methacrylamide] are the only polymers able to resist fouling from blood plasma.[17,18,20,22,54] However, the poor mechanical properties of pure, not heavily cross-linked poly(carboxybetaine) hydrogels restrict their application, and therefore copolymerization of poly(CBAA-3) and poly(CBMAA-3) with poly(HEMA) was explored.[44]

Poly(HEMA) hydrogels with different contents of carboxybetaines (0, 1, 5, and 10 mol %) were prepared and incubated in undiluted blood plasma. The fouling was studied by FTIR-ATR. Spectra of each sample were recorded before and after incubation and washing. Figure 7 shows the amide region

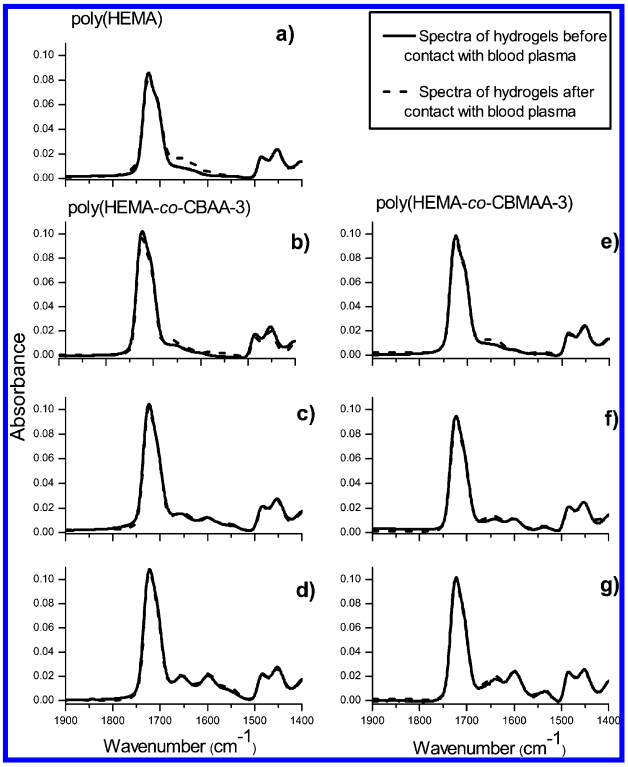

Figure 7. FTIR-ATR spectra (amidic region) of poly(HEMA) (a), poly(HEMA-*co*-CBAA-3), and poly(HEMA-*co*-CBAA-3) before (continuous line) and after (dashed line) 3 h contact with blood plasma. (b) 1%CBAA-3, (c) 5%CBAA-3, (d) 10%CBAA-3, (e) 1%CBMAA-3, (f) 5%CBMAA-3, and (g) 10%CBMAA-3.

before (continuous line) and after (dash line) contact of the hydrogels with blood plasma. Pure poly(HEMA) hydrogels suffered an important protein fouling as evidenced by an increase in the region of 1648 cm^{-1} and 1545 cm^{-1} (Figure 7a). The high adsorption from blood plasma on pure poly(HEMA) hydrogels is in good agreement with previous works.[53] Addition of the zwitterionic comonomer to the polymerization feed resulted in material that reduced plasma fouling. More than 40% or 50% of the fouling could be reduced by addition of 1 mol % of CBAA-3 or CBMAA-3, respectively. Subsequent addition of 5 mol % of CBAA-3 or CBMAA-3 further reduced the fouling by 70% and 65% (Figure 7c,f). Remarkably, no fouling from blood plasma could be detected when the content of CBAA-3 was 10 mol % (Figure 7d), while only minor protein fouling (95% reduction) was observed on the 10% CBMAA-3 hydrogel (Figure 7g). The higher protein resistance of CBAA-3 compared to CBMAA-3 is in close agreement with the results observed on the model based on polymer brushes.

CONCLUSION

Five zwitterionic monomers were screened for improving the EWC and protein resistance of poly(HEMA) hydrogels. Model systems based on betaine brushes were prepared by ATRP, and their resistance to fouling was evaluated. Only the carboxybetaine brushes were able to effectively resist the fouling from blood plasma, thus they were selected as comonomers for the preparation of hydrogels based on poly(HEMA).

Small addition of carboxybetaine monomers led to a very high increase in the EWC without impairing the mechanical properties. Hydrogels with excellent mechanical properties, close to pure poly(HEMA) hydrogels but containing 4 times more water, could be prepared with the addition of 10 mol % of carboxybetaine.

All the hydrogels prepared showed an unprecedented reduction of fouling from blood plasma. Copolymers of HEMA with 10% CBAA-3 led to hydrogels fully resistant to blood plasma adsorption and containing 4 times more water while having mechanical properties close to poly(HEMA).

ASSOCIATED CONTENT

Supporting Information

Materials, FTIR-GASR spectra of polymer brushes, and protein fouling on polymer brushes studied by SPR. This material is available free of charge via the Internet at http://pubs.acs.org.

AUTHOR INFORMATION

Corresponding Author

*E-mail: rodriguez@imc.cas.cz.

Notes

The authors declare no competing financial interest.

ACKNOWLEDGMENTS

This research was supported by the Czech Science Foundation (GACR) under Contract Nos. KAN 200520804, P205/12/1702, P106/12/1451, and P205/12/1451.

REFERENCES

(1) Williams, D. F. *Biomaterials* **2011**, *32*, 4195−4197.
(2) Slaughter, B. V.; Khurshid, S. S.; Fisher, O. Z.; Khademhosseini, A.; Peppas, N. A. *Adv. Mater.* **2009**, *21*, 3307−3329.
(3) Lee, K. Y.; Mooney, D. J. *Chem. Rev.* **2001**, *101*, 1869−1880.
(4) Hoffman, A. S. *Adv. Drug Delivery Rev.* **2002**, *54*, 3−12.
(5) Wichterle, O.; Lim, D. *Nature* **1960**, *185*, 117−118.
(6) Studenovská, H.; Šlouf, M.; Rypáček, F. *J. Mater. Sci.: Mater. Med.* **2007**, *19*, 615−621.
(7) Williams, D. F. *Biomaterials* **2008**, *29*, 2941−2953.
(8) Kubinová, Š.; Horák, D.; Kozubenko, N.; Vaněček, V.; Proks, V.; Price, J.; Cocks, G.; Syková, E. *Biomaterials* **2010**, *31*, 5966−5975.
(9) Brynda, E.; Drobnik, J.; Vacik, J.; Kalal, J. *J. Biomed. Mater. Res.* **1978**, *12*, 55−65.
(10) Thissen, H.; Gengenbach, T.; du Toit, R.; Sweeney, D. F.; Kingshott, P.; Griesser, H. J.; Meagher, L. *Biomaterials* **2010**, *31*, 5510−5519.
(11) Ratner, B. D. *Biomaterials* **2007**, *28*, 5144−5147.
(12) Zhu, J. *Biomaterials* **2010**, *31*, 4639−4656.
(13) Lee, J. H.; Lee, H. B.; Andrade, J. D. *Prog. Polym. Sci.* **1995**, *20*, 1043−1079.
(14) Jeon, S. I.; Lee, J. H.; Andrade, J. D.; De Gennes, P. G. *J. Colloid Interface Sci.* **1991**, *142*, 149−158.
(15) Jeon, S. I.; Andrade, J. D. *J. Colloid Interface Sci.* **1991**, *142*, 159−166.
(16) Unsworth, L. D.; Sheardown, H.; Brash, J. L. *Langmuir* **2008**, *24*, 1924−1929.

(17) Rodriguez-Emmenegger, C.; Brynda, E.; Riedel, T.; Sedlakova, Z.; Houska, M.; Alles, A. B. *Langmuir* **2009**, *25*, 6328−6333.
(18) Rodriguez-Emmenegger, C.; Houska, M.; Alles, A. B.; Brynda, E. *Macromol. Biosci.* **2012**, *12*, 1413−22.
(19) Lynch, I.; Dawson, K. A. *Nano Today* **2008**, *3*, 40−47.
(20) Rodriguez-Emmenegger, C.; Brynda, E.; Riedel, T.; Houska, M.; Šubr, V.; Bologna Alles, A.; Hasan, E.; Gautrot, J. E.; Huck, W. T. S. *Macromol. Rapid Commun.* **2011**, *32*, 952−957.
(21) Rodriguez-Emmenegger, C.; Jäger, A.; Jäger, E.; Stepanek, P.; Alles, A. B.; Guterres, S. S.; Pohlmann, A. R.; Brynda, E. *Colloids Surf., B* **2011**, *83*, 376−381.
(22) Rodriguez-Emmenegger, C.; Kylian, O.; Houska, M.; Brynda, E.; Artemenko, A.; Kousal, J.; Bologna Alles, A.; Biederman, H. *Biomacromolecules* **2011**, *12*, 1058−1066.
(23) Shao, Q.; He, Y.; White, A. D.; Jiang, S. *J. Phys. Chem. B* **2010**, *114*, 16625−16631.
(24) Hower, J. C.; Bernards, M. T.; Chen, S.; Tsao, H.-K.; Sheng, Y.-J.; Jiang, S. *J. Phys. Chem. B* **2008**, *113*, 197−201.
(25) Lord, M. S.; Stenzel, M. H.; Simmons, A.; Milthorpe, B. K. *Biomaterials* **2006**, *27*, 567−575.
(26) Sigal, G. B.; Mrksich, M.; Whitesides, G. M. *J. Am. Chem. Soc.* **1998**, *120*, 3464−3473.
(27) Ostuni, E.; Chapman, R. G.; Holmlin, R. E.; Takayama, S.; Whitesides, G. M. *Langmuir* **2001**, *17*, 5605−5620.
(28) Kudaibergenov, S.; Jaeger, W.; Laschewsky, A. Polymeric Betaines: Synthesis, Characterization, and Application. In *Supramolecular Polymers Polymeric Betains Oligomers*; Harada, A., Hashidzume, A., Takashima, Y., Eds.; Springer-Verlag: Berlin, 2006; Vol. *201*, pp 157−224.
(29) Zwaal, R. F. A.; Comfurius, P.; Vandeenen, L. L. M. *Nature* **1977**, *268*, 358−360.
(30) Kadoma, Y.; Nakabayashi, N.; E., M.; Yamauchi, J. *Kobunshi Ronbushu* **1978**, *35*, 423−427.
(31) Hall, B.; le E. Bird, R.; Kojima, M.; Chapman, D. *Biomaterials* **1989**, *10*, 219−224.
(32) Hayward, J. A.; Chapman, D. *Biomaterials* **1984**, *5*, 135−142.
(33) Ishihara, K.; Tsuji, T.; Kurosaki, T.; Nakabayashi, N. *J. Biomed. Mater. Res.* **1994**, *28*, 225−232.
(34) Ishihara, K.; Oshida, H.; Endo, Y.; Watanabe, A.; Ueda, T.; Nakabayashi, N. *J. Biomed. Mater. Res.* **1993**, *27*, 1309−1314.
(35) Lewis, A. L.; Furze, J. D.; Small, S.; Robertson, J. D.; Higgins, B. J.; Taylor, S.; Ricci, D. R. *J. Biomed. Mater. Res.* **2002**, *63*, 699−705.
(36) Abraham, S.; So, A.; Unsworth, L. D. *Biomacromolecules* **2011**, *12*, 3567−80.
(37) Kasák, P.; Kroneková, Z.; Krupa, I.; Lacík, I. *Polymer* **2011**, *52*, 3011−3020.
(38) Carr, L.; Cheng, G.; Xue, H.; Jiang, S. *Langmuir* **2010**, *26*, 14793−14798.
(39) Zhang, Z.; Chao, T.; Liu, L.; Cheng, G.; Ratner, B. D.; Jiang, S. *J. Biomater. Sci., Polym. Ed.* **2009**, *20*, 1845−1859.
(40) Chang, Y.; Yandi, W.; Chen, W.-Y.; Shih, Y.-J.; Yang, C.-C.; Chang, Y.; Ling, Q.-D.; Higuchi, A. *Biomacromolecules* **2010**, *11*, 1101−1110.
(41) Kabiri, K.; Faraji-Dana, S.; Zohuriaan-Mehr, M. J. *Polym. Adv. Technol.* **2005**, *16*, 659−666.
(42) Zhang, Z.; Chao, T.; Jiang, S. *J. Phys. Chem. B* **2008**, *112*, 5327−5332.
(43) Huglin, M. B.; Rego, J. M. *Polymer* **1991**, *32*, 3354−3358.
(44) Carr, L. R.; Xue, H.; Jiang, S. *Biomaterials* **2011**, *32*, 961−968.
(45) Rodriguez-Emmenegger, C.; Schmidt, B. V. K. J.; Sedlakova, Z.; Šubr, V.; Bologna Alles, A.; Brynda, E.; Barner-Kowollik, C. *Macromol. Rapid Commun.* **2011**, *32*, 958−965.
(46) Rodriguez-Emmenegger, C.; Hasan, E.; Pop-Georgievski, O.; Houska, M.; Brynda, E.; Bologna Alles, A. *Macromol. Biosci.* **2011**, *12*, 525−532.
(47) Bryant, S. J.; Anseth, K. S. In *Scaffolding In Tissue Engineering*, Ma, P. X., Elisseeff, J., Eds.; CRC Press Taylor & Francis Group: Boca Raton, FL: 2006; pp 71−90.
(48) Murphy, B. M.; Mikos, A. G. In *Principles of Tissue Engineering*, 3rd ed.; Lanza, R., Langer, R., Vacanti, J., Eds.; Elsevier Academic Press: San Diego, CA, 2007.
(49) Drury, J. L.; Mooney, D. J. *Biomaterials* **2003**, *24*, 4337−4351.
(50) Laughlin, R. G. *Langmuir* **1991**, *7*, 842−847.
(51) Williams, D. F. *Biomaterials* **2009**, *30*, 5897−5909.
(52) Ratner, B. D. *J. Biomed. Mater. Res.* **1993**, *27*, 283−287.
(53) Brynda, E.; Cepalova, N. A.; Štol, M. *J. Biomed. Mater. Res.* **1984**, *18*, 685−693.
(54) Edlund, U.; Rodriguez-Emmenegger, C.; Brynda, E.; Albersson, A. C. *Polym. Chem.* **2012**, *3*, 2920−2927.

Supplementary Information on

Non-fouling hydrogels of 2-hydroxyethyl methacrylate and zwitterionic carboxybetaine (meth)acrylamides

Nina Yu. Kostina, Cesar Rodriguez-Emmenegger, Milan Houska, Eduard Brynda, Jiří Michálek*

Institute of Macromolecular Chemistry, Academy of Sciences of the Czech Republic, v.v.i., Prague, 16206, Czech Republic

E-mails: rodriguez@imc.cas.cz,

Materials

CuCl (99.99 %), CuBr (99.99 %), $CuBr_2$ (99 %), 2,2'-dipyridyl (BiPy, 99 %), 1,4,8,11-tetramethyl-1,4,8,11-tetraazacyclotetradecane (Me_4Cyclam, 98%), 11-mercapto-1-undecanol (99 %), 2-hydroxyethyl methacrylate (HEMA), ethylene glycol dimethacrylate (EDMA), benzoin ethyl ether (BEE), *N*-[3-(Dimethylamino)propyl]methacrylamide (99%), 2-(*N*,*N*'-dimethyamino)ethyl methacrylate (98%) were purchased from Sigma Aldrich. β-propiolactone and *N*-[3-(dimethylamino)propyl]acrylamide (98%) were purchased from Serva electrophoresis GmbH and TCI Europe. 2-[(methacryloyloxy)ethyl]dimethyl-3-sulfopropyl ammonium hydroxide (SBMA, 97%), 2-(Methacryloyloxy)ethyl 2-(trimethylammonio) phosphate(PCMA) were from Merck and Vertellius Speciallities respectively. Methanol (99.5%), tetrahydrofuran (THF, 99.5%), and ethanol (96%) were purchased from Lachner. *N*,*N*-dimethylformamide (99.5%) and phosphate-buffered saline (PBS, pH 7.4) were from Sigma-Aldrich.

Citrated human plasma from single healthy donor was purchased from the Institute of Hematology and Blood Transfusion, Prague, Czech Republic.

Dry solvents were prepared according to standard procedures. [1]

Initiator ω-mercaptoundecylbromoisubutyrate was synthesized by reacting α-bromoisobutyl bromide with 11-mercapto-1-undecanol according to the method published earlier [2].

Polymer brushes

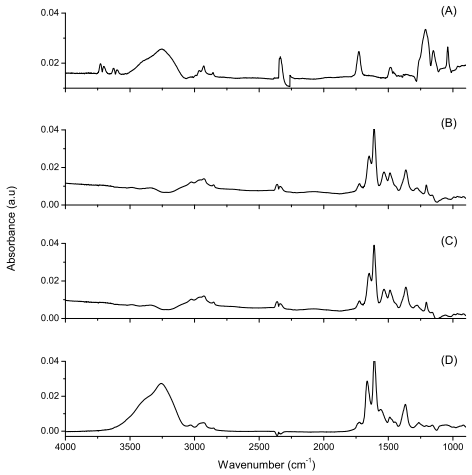

Figure S.I. 1. FTIR-GASR spectra of polymer brushes prepared (A) poly(SBMA), (B) poly(CBMA-2), (C) poly(CBMAA-3), and (D) poly(CBAA-3).

Figure S.I. 1. depicts the FTIR-GASR spectra of the zwitterionic polymer brushes. Spectra (A) poly(SBMA) and (B) poly(CBMA-2) show peaks of ester carbonyl at 1725 cm^{-1} and (A) shows sulphur group peaks at 1213 and 1038 cm^{-1}. Spectrum (B) also shows a prominent band of ionised carboxyl at 1609 cm^{-1} (COO^- asymmetric stretching) and its sym. stretching at 1365 cm^{-1}. The spectra of poly(CBAA-3) (C) and poly(CBMAA-3) (D) show amide bands at 1664 cm^{-1} and 1558 cm^{-1}, the dominant band of ionised carboxyl at 1609 cm^{-1} and its symmetric stretching at 1370 cm^{-1}.

Protein fouling on polymer brushes studied by SPR

Table S.I.-1. Fouling from single protein solutions of zwitterionic polymer brushes

	Water contact angle (º)		Fouling ($pg \cdot mm^{-2}$)		
Surface	Advancing	Receding	IgG	Fbg	HSA
Au	75.4 ± 0.6	63.2 ± 0.9	3123±100	3210±140	1265±82
PCMA	18 ± 0.4	7.0 ± 0.4	135±50	75±20	0
SBMA	20.0 ± 2.0	5.2 ± 1.2	154±60	0	0
CBMA-2	34.1 ± 2.4	11.2 ± 4.1	0	0	0
CBMAA-3	30.2 ± 1.2	10.2 ± 2.1	0	0	0
CBAA-3	23.2 ± 0.8	8.1 ± 1.3	0	0	0

A value of zero is assigned to values below the limit of detection 0.3 $pg \cdot cm^{-2}$.

Table S.I.-1 presents the fouling from single protein solutions on the poly(betaine)s prepared. All the brushes fully prevented the fouling from human serum albumin (HSA, 5 $mg \cdot mL^{-1}$) and importantly reduced the fouling from fibrinogen (Fbg, 1 $mg \cdot mL^{-1}$) and immunoglobulin G (IgG, 8 $mg \cdot mL^{-1}$). The brushes based on carboxybetaines totally prevented the fouling from all the solutions.

References

1. Armarego, W. L. F.; Chai, C. L. L., *Purification of laboratory chemicals*. 5th edition ed.; Butterworth-Heinemann: Oxford, 2009.
2. Jones, D. M.; Brown, A. A.; Huck, W. T. S.; *Langmuir* **2002,** 18, 1265-1269.

Appendix 4

Novel antifouling self-healing poly(carboxybetaine methacrylamide-*co*-HEMA) nanocomposite hydrogels with superior mechanical properties

Journal of Materials Chemistry B, 2013, 1 (41), 5644-5650

Journal of Materials Chemistry B

RSC Publishing

PAPER

Novel antifouling self-healing poly(carboxybetaine methacrylamide-*co*-HEMA) nanocomposite hydrogels with superior mechanical properties†

Cite this: *J. Mater. Chem. B*, 2013, **1**, 5644

Nina Yu. Kostina,[a] Shahriar Sharifi,[b] Andres de los Santos Pereira,[a] Jiří Michálek,[a] Dirk W. Grijpma[bc] and Cesar Rodriguez-Emmenegger*[ad]

Novel antifouling highly wettable hydrogels with superior mechanical and self-healing properties are presented. Hydrogels were prepared by UV-initiated copolymerisation of non-fouling zwitterionic carboxybetaine methacrylamide (CBMAA-3) and 2-hydroxyethyl methacrylate (HEMA) in the presence of uniformly dispersed clay nanoparticles (Laponite XLG) in water. The nanoparticles acted as physical cross-linkers resulting in excellent mechanical resistance. The effects of composition such as the amount of nanoclay and the HEMA/CBMAA-3 molar ratio on the physical properties of the nanocomposite hydrogels were investigated. These gels showed outstanding composition-dependent mechanical properties, exhibiting remarkably large elongations at break (≥1800%) and high strengths and moduli even at higher molar contents of CBMAA-3 and higher degrees of swelling (DS). Furthermore, these hydrogels were able to repair mechanical damage without the use of any healing agent by spontaneous reconstruction of cross-links across a damaged interface.

Received 19th May 2013
Accepted 14th August 2013

DOI: 10.1039/c3tb20704h

www.rsc.org/MaterialsB

Introduction

Hydrogels are very attractive candidates for use as tissue engineering scaffolds due to their viscoelastic mechanical properties, high water content and structural similarity to macromolecular-based components of the body.[1–3] Current research focuses on various types of hydrogels based on natural and synthetic materials.[4] One of the most attractive types among them are the ones based on poly(2-hydroxyethyl methacrylate) (poly(HEMA)).[5] Many advantages of this material such as chemical stability, good biocompatibility, hydrophilic character, excellent mechanical properties and a low level of immunogenicity benefit numerous applications in the biomedical field.[6–12] However, despite all of these advantages the use of poly(HEMA) hydrogels is limited. The moderate swelling of this material in physiological media results in a water content lower than that of natural tissues. Furthermore, the contact with biological fluids, in particular blood plasma, leads to non-specific protein adsorption and fouling, resulting in irreversible changes in the material and biological medium.[13] This adverse effect at the interface of biomaterial and tissue causes inflammatory responses, facilitates the attachment of microorganisms or leads to thrombus formation.[14–16] In addition, protein fouling masks any bioactive molecules previously immobilised on the material, which are critical to support specific interactions with cells as well as their differentiation and proliferation.[17,18] Thus, control over the functions and fate of the biomaterial becomes no longer possible.

It has been hypothesised that electrostatically induced hydration would aid in the development of highly protein resistant surfaces, leading to preparation of a material with ionic groups.[19,20] However, the electroneutrality precondition for resistance to fouling is imposed.[21,22] Widely studied zwitterionic monomers are excellent candidates to minimise the fouling and increase the wettability.[23–27] Zwitterions are dipolar species, in which the cation and the anion are separately bound to the same monomer unit and can be completely dissociated, thus maintaining the overall electroneutrality. Typically polybetaines are a type of poly(zwitterion) in which the cation is permanently charged, such as in the case of quaternarised ammonium.[28] Many different types of betaines, such as phosphorylcholine methacrylate, sulfobetaine methacrylate, and various carboxybetaines, were grafted onto surfaces and their resistance to protein fouling was assessed.[23,29,30] However, much

[a]*Institute of Macromolecular Chemistry, Academy of Science of the Czech Republic, v.v.i., Heyrovsky Sq. 2, Prague, 162 06, Czech Republic. E-mail: rodriguez@imc.cas.cz; Fax: +420 296 809 410; Tel: +420 296 809 111*

[b]*MIRA Institute for Biomedical Technology and Technical Medicine, Department of Biomaterials Science and Technology, Faculty of Science and Technology, University of Twente, P.O. Box 217, 7500 AE Enschede, The Netherlands*

[c]*W.J. Kolff Institute, Department of Biomedical Engineering, University Medical Center Groningen, University of Groningen, Antonius Deusinglaan 1, 9713 AV Groningen, The Netherlands*

[d]*College of Engineering, Universidad de la Republica, Julio Herrera y Reissig 565, 113 00, Montevideo, Uruguay. Fax: +598 2711 5446; Tel: +598 2711 0698*

† Electronic supplementary information (ESI) available: Description of synthesis and characterisation of the (3-methacryloylamino-propyl)-(2-carboxy-ethyl)-dimethylammonium(carboxybetaine methacrylamide) (CBMAA-3) monomer. See DOI: 10.1039/c3tb20704h

fewer attempts at the preparation of non-fouling zwitterionic hydrogels have been reported.[31,32] Due to the commercial availability and simple synthetic accessibility the majority of the hydrogels described in the literature are based typically on sulfobetaine monomers.[33] On the other hand, these hydrogels showed poor mechanical properties restricting their use in real applications.[34,35] Moreover, when in contact with real biological media, such as blood plasma, the sulfobetaine-based polymers suffer from a high protein fouling.[36] Nevertheless, a new family of poly(carboxybetaine)s displayed the non-fouling character even when in contact with blood plasma.[23,26,29–31] Currently, only a few attempts at the preparation of hydrogels based on carboxybetaines are reported.[31,37] However, most of them resulted in poor mechanical resistance and no blood plasma fouling was tested. In particular, the hydrogels introduced by Jiang *et al.* require concentrations of cross-linker as high as 90–100% to achieve a compressive modulus of 8.2 MPa while no tensile test, relevant to many hydrogel applications, was carried out.[37] Such a high concentration of cross-linker could lead to brittle materials.

In our previous work we reported the copolymerisation of poly(HEMA) with poly(carboxybetaine acrylamide) and poly(carboxybetaine methacrylamide).[31] These hydrogels showed excellent mechanical properties, close to those of pure poly(HEMA) hydrogels while containing 4 times more water. It was the first time that the protein fouling from undiluted blood plasma was assessed on hydrogels containing zwitterionic comonomers. All the hydrogels showed an unprecedented reduction of fouling from blood plasma. Copolymers of HEMA with 10 mol% carboxybetaine acrylamide led to hydrogels fully resistant to blood plasma adsorption. All these advantages, wettability close to natural tissues, good mechanical properties and antifouling properties, make this material very promising for biomedical applications. However, the major drawback of chemically cross-linked hydrogels is their lack of ability to self-heal, *i.e.* to autonomously and spontaneously repair themselves. This important characteristic mimics tissues of living organisms which are able to heal and re-shape after external stimuli. If mechanical damage to materials could be repaired autonomously, it would be possible to increase the useful lifetime of materials and reduce the total cost of systems in the long term.

Current advances in hydrogel fabrication have resulted in different strategies for development of self-healing and mechanically robust hydrogels.[38–40] One such approach is the preparation of nanocomposite gels consisting of polymer chains physically cross-linked with nanoparticles such as inorganic clay Laponite XLG. Laponite clays are hydrophilic disk-shaped platelets that can be uniformly dispersed in aqueous media and act as physical cross-linkers.[41] The physical cross-linking of hydrogels not only endows self-healing properties, but can also improve mechanical properties of hydrogels similar to or even better than chemical cross-linkers.[42,43] The types of monomers used provided thermoresponsiveness, but on the other hand they also induced non-specific protein adsorption which is known to be the precursor for non-specific cell adhesion.[44,45] For the development of biomaterials, it is critical to control the interactions between cells and attached biomolecules, which give cues for proliferation and differentiation. The high fouling presented before precludes this kind of control.

Taking advantage of the unique properties of nanocomposite hydrogels and hydrophilic non-fouling zwitterionic poly(carboxybetaine)s herein we introduce a novel type of self-healing hydrogel based on non-fouling poly(carboxybetaine methacrylamide) (CBMAA-3) and 2-hydroxyethyl methacrylate (HEMA) with high wettability without compromising the mechanical properties. Selection of the zwitterionic comonomers for hydrogel preparation was based on their resistance to blood plasma fouling.[23,31] CBMAA-3 was copolymerised with HEMA in the presence of highly dispersed Laponite XLG nanoparticles (LNs) to prepare hydrogels with excellent mechanical properties and wettability similar to human tissues. These hydrogels were able not only to withstand remarkably large elongations (as high as 1800%) but also possessed self-healing properties. This is the first example of self-healing hydrogels with superior mechanical properties based on non-fouling zwitterionic comonomers.

Experimental section

Materials

All chemicals and solvents purchased were of the highest available purity and were used as received. 2-Hydroxyethyl methacrylate (HEMA) (97%, Sigma-Aldrich) was purified prior to use by vacuum distillation at 5 mmHg (boiling point 85 °C) in the presence of 2,2-diphenyl-1-picrylhydrazyl and stored at −18 °C under an Ar atmosphere. Irgacure 2959, *N*-[3-(dimethylamino)propyl]methacrylamide (98%) (DMAPM), methyl red and toluidine blue were purchased from Sigma Aldrich. β-Propiolactone was purchased from Serva electrophoresis GmbH. Tetrahydrofuran (THF), dimethylsulfoxide (DMSO) and diethylether were purchased from Lachner. Laponite XLG nanoparticles (LNs) $[Mg_{5.34}Li_{0.66}Si_8O_{20}(OH)_4]Na_{0.66}$ (diameter = 30 nm and thickness = 1 nm) were purchased from Rockwood Ltd, UK.

Synthesis of (3-methacryloylamino-propyl)-(2-carboxy-ethyl)-dimethylammonium(carboxybetaine methacrylamide) (CBMAA-3) monomer

The carboxybetaine methacrylamide (CBMAA-3) monomer was synthesised as reported earlier[24] (Scheme 1). (Synthesis and ^{1}H- and ^{13}C-NMR are described in the ESI.†)

Synthesis of hydrogels

Poly(HEMA-*co*-CBMAA-3) hydrogels were synthesised by copolymerisation of HEMA and CBMAA-3 in water with dispersed LNs acting as physical cross-linkers (Scheme 1). First, the LNs were dispersed in water in concentrations of 1, 3 and 5 wt% and the zwitterionic CBMAA-3 was dissolved in HEMA in concentrations of 5, 10 and 20 mol%. Then the HEMA/CBMAA-3 solution was added to the dispersed LNs in water at a concentration of 20 wt%. It is noteworthy that as LNs are mildly alkaline silicates, no changes in pH of the polymerisation were

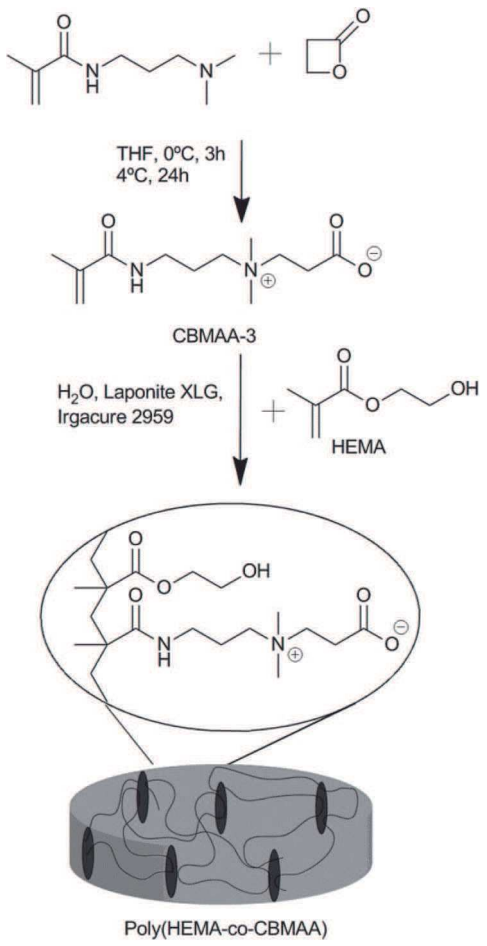

Scheme 1 Synthesis of the CBMAA-3 monomer and hydrogel fabrication based on HEMA/CBMAA-3 monomers cross-linked *via* Laponite XLG nanoparticles.

observed with the addition of the particles under the working conditions. Subsequently, the photoinitiator (Irgacure 2959, 0.5 mol%) was added to the mixture and stirred in the dark until complete dissolution. The polymerisation mixture was transferred into cylindrical moulds with an inner diameter of 4 mm and a length of 70 mm. The photo-polymerisation reaction was carried out at ambient temperature for 60 min under UV-irradiation ($\lambda = 369$ nm, intensity of 3–5 mW cm^{-2}) and a nitrogen atmosphere in an Ultralum cross-linking cabinet. After polymerisation, hydrogels were removed from the moulds and washed in deionised water. Water was changed every 12 h for 6 days to remove unreacted monomers. Pure poly(HEMA) hydrogels were synthesised utilising the same procedure but without the addition of a zwitterionic comonomer, however, 2 wt% of DMSO was added to the polymerisation mixture to avoid possible precipitation of the polymer during polymerisation (Table 1).

Characterisation of hydrogels

Chemical composition of hydrogels. Poly(HEMA) and poly(HEMA-*co*-CBMAA-3) hydrogels were characterised by attenuated total reflectance FTIR spectroscopy (FTIR-ATR). All samples were washed with water for 6 days after polymerisation and dried *in vacuo* at room temperature to constant weight. Spectra of dried hydrogels were recorded using a Thermo Nicolet Nexus 670 FTIR spectrometer with a diamond ATR attachment.

Table 1 Formulations of the prepared hydrogels as a function of the molar ratio of monomers and the concentration of Laponite nanoparticles

Molar ratio of HEMA/CBMAA-3	Concentration of LN, wt%		
	1	3	5
100/0	HEMA1LN	HEMA3LN	HEMA5LN
95/5	5CBMAA1LN	5CBMAA3LN	5CBMAA5LN
90/10	10CBMAA1LN	10CBMAA3LN	10CBMAA5LN
80/20	20CBMAA1LN	20CBMAA3LN	20CBMAA5LN

Stability of hydrogels in water. The sample containing 10 mol% of CBMAA-3 and 3 wt% of LNs (10CBMAA3LN) (Table 1) was chosen to evaluate the stability of hydrogels in water. The weights of 25 freshly prepared hydrogel samples of 10CBMAA3LN were determined and they were immersed in deionised water to swell for 1, 2, 3, 4 and 6 days. Samples were kept under constant shaking conditions and the water was replaced every 12 hours. After the predetermined time intervals five samples were removed from water and dried *in vacuo* to constant weight. The ratio of masses of dried samples to initial masses of freshly prepared samples was determined.

Swelling properties of hydrogels. The equilibrium water content of hydrogels was determined gravimetrically. At least five samples of each composition of hydrogels were immersed in deionised water for swelling to equilibrium at a constant temperature of 25 °C. The mass of the hydrogels was determined every 12 h displaying no increase in mass after 5 days. Thus the swollen mass was taken as the mass after 6 days of swelling. The swollen samples were weighed and dried at ambient temperature *in vacuo* to constant weight (6 days). The equilibrium water content of the hydrogels was determined as:

$$\mathrm{EWC} = \frac{m_s - m_d}{m_d}$$

where m_s and m_d are the mass of swollen and dried hydrogels, respectively.

Mechanical properties of hydrogels. For the mechanical characterisation rod-shaped hydrogels ($d = 4$ mm, $l = 70$ mm) were used. Tensile tests of as-prepared hydrogels were carried out at room temperature using a universal tensile tester equipped with a 500 N load cell at a crosshead speed of 20 mm min^{-1}. At least five specimens were tested for each sample. The elongation at break and Young's modulus in the range of 5–10% strain were evaluated.

Additionally, for the visual demonstration of mechanical properties, such as elongation and compression, 10CBMAA3LN hydrogels (Table 1) were prepared in two different colours and dimensions. Blue ($d = 4$ mm, $l = 35$ mm) and orange ($d = 10$, $l = 10$ mm) coloured hydrogels were prepared by adding toluidine blue or methyl red to the polymerisation mixtures.

Self-healing properties. For the demonstration of self-healing properties of these hydrogels the composition of

10CBMAA3LN (Table 1) was selected. Hydrogel rods were prepared in two different colours by addition of toluidine blue or methyl red and dimensions ($d = 10$ mm, $l = 15$ mm or $d = 4$ mm, $l = 35$ mm) similar to the procedure described above. The rods were cut with a knife and allowed to self-heal by keeping the cut surfaces in contact for 5 minutes at ambient temperature, without the addition of any reagents.

Results and discussion

CBMA-3 was selected (Scheme 1) since it has been shown to confer unmatched resistance to fouling of hydrogels when introduced as a comonomer in chemically cross-linked hydrogels.[31] With the aim of achieving improved mechanical and self-healing properties, nanocomposite hydrogels with different molar concentrations of zwitterionic comonomer and LNs were prepared (Table 1). All hydrogels were robust and tough. FTIR-ATR unambiguously shows the success of the copolymerisation (Fig. 1). The increase in the amount of zwitterionic comonomer was evidenced by the concomitant increase in the intensity of amide bands at 1640 cm^{-1} and 1535 cm^{-1}, and the carboxyl band at 1600 cm^{-1} arising from the CBMAA-3 added.

Since the ability of biomaterials to prevent protein fouling is critical for several possible applications, we performed a test to confirm the antifouling characteristics of the newly presented hydrogels. For this purpose we used 10% foetal bovine serum and measured the amount of protein adsorbed (25 °C) by the hydrogels by UV-Vis spectroscopy (refer to the ESI† for a detailed experimental description and discussion). Briefly, while the addition of LNs for physical cross-linking of poly(HEMA) (HEMA1LN) resulted in an increase of fouling compared to chemical cross-linking in poly(HEMA) hydrogels, further increases in the concentration of LNs, from 1 wt% to 3 and 5 wt% only marginally increased the fouling. However, an addition of 5 mol% of CBMAA-3 was enough to cause a reduction in fouling of 70%.

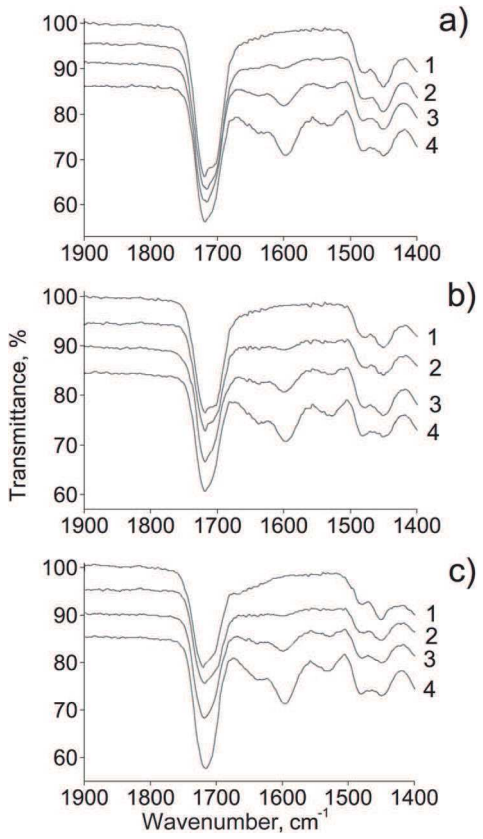

Fig. 1 Amidic region of the FTIR-ATR spectra of hydrogels of poly(HEMA) and poly(HEMA-*co*-CBMAA-3) containing (a) 1 wt% of LN, (b) 3 wt% of LN, and (c) 5 wt% of LN. Curves 1–4 show increasing concentrations of CBMAA comonomers: (1) pure poly(HEMA), (2) 5 mol% CBMAA-3, (3) 10 mol% CBMAA-3, and (4) 20 mol% CBMAA-3.

Further increases in the ratio of CBMAA-3 in the polymerisation feed helped suppress the fouling even further, resulting in a 95% decrease for 20CBMAA1LN demonstrating the much acclaimed non-fouling properties of carboxybetaines.

The long-term stability in aqueous media is a major challenge for physically cross-linked hydrogels and an important criterion for their applicability. The physical nature of the cross-linking could lead to leaching of nanoparticles or polymer chains, thus assessment of their stability is essential. The six-day stability in water of 10CBMAA3LN hydrogels was evaluated by the gel ratio as the ratio of masses of dried hydrogels after washing in water for 1, 2, 3, 4 or 6 days to the masses of freshly prepared hydrogels (Fig. 2a). The gel ratio of the hydrogel before the stability test was determined to be 0.2. No significant changes were observed even after 6 days of immersion in water, clearly indicating the stability of the material (Fig. 2a).

The swelling behaviour and water content are very important properties of hydrogels for bioapplications. A high water content, close to that of natural tissues, is essential for cell growth and proliferation.[46] The EWC of poly(HEMA) and poly(HEMA-*co*-CBMAA-3) hydrogels was determined gravimetrically. While poly(HEMA) can only bind water *via* hydrogen bonding with its hydroxyl groups, poly(carboxybetaine)s can bind water more strongly *via* electrostatic interactions. The newly presented material displayed a very high water uptake capacity. As expected, the EWC dramatically increases with the addition of the zwitterionic comonomer to the polymerisation feed (Fig. 2b). A 15% increase in the water uptake capability of hydrogels was observed with the addition of only 5 mol% of CBMAA-3 to the polymerisation feed. A further increment in the CBMAA-3 concentration to 10 mol% led to a significant fivefold increase in the amount of water in the hydrogel, reaching a value of EWC of 27.7 ± 2.0 for 10CBMAA1LN, 24.2 ± 0.2 for 10CBMAA3LN, and 23.0 ± 0.7 for 10CBMAA5LN. The addition of 20 mol% of CBMAA-3 to the polymerisation feed resulted in EWCs of 295.0 ± 10.0 for 20CBMAA1LN, 39.0 ± 2.2 for 20CBMAA3LN and 38.0 ± 7.0 for 20CBMAA5LN, *i.e.* water uptake by hydrogels is 60, 8 and 7 times more than pure poly(HEMA) respectively.

A less significant decrease in water uptake capability was observed with increasing nanoparticle concentration. This behaviour can be explained by the clay platelets acting as effective cross-linking agents. The increase of cross-linking points results in a denser network structure and shorter interlinked polymer chains, restricting a higher water uptake.

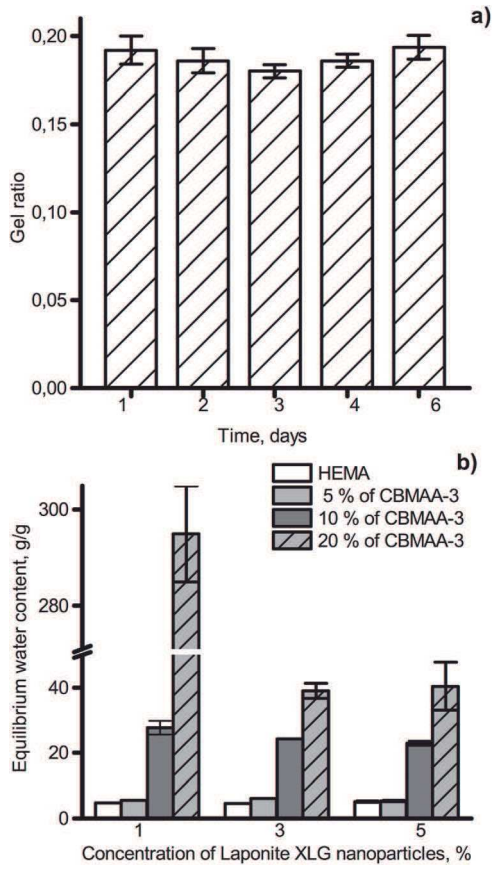

Fig. 2 (a) Assessment of the stability of 10CBMAA3LN hydrogels in water, by measuring the gel ratio as the ratio of mass of dried hydrogel to original mass after immersion in water for a specified time. The theoretical ratio corresponding to the polymerisation mixture is 0.20. (b) The equilibrium water content (EWC) of hydrogels, defined as the ratio between the mass of absorbed water after reaching the equilibrium and the mass of dried hydrogels.

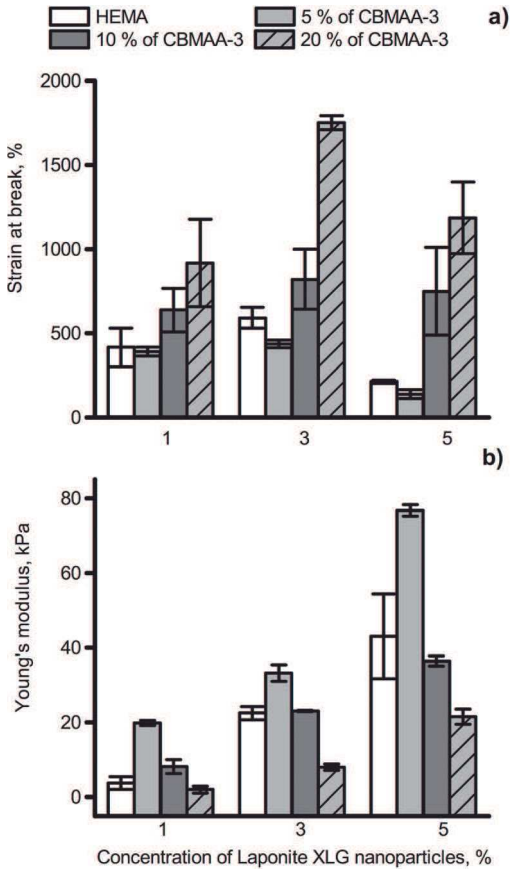

Fig. 3 Mechanical properties of hydrogels under tensile testing (500 N load cell, crosshead speed 20 mm min^{-1}). (a) Elongation at break and (b) Young's modulus.

Mechanically, all hydrogels containing zwitterionic comonomers were robust and tough, withstanding high degrees of various deformations (Fig. 4a). In order to evaluate the mechanical resistance the elongation at break and Young's modulus of poly(HEMA) and poly(HEMA-*co*-CBMAA-3) hydrogels were determined (Fig. 3). The addition of 5 mol% of zwitterionic comonomer resulted in materials with similar tensile behaviour to poly(HEMA) hydrogels resulting in elongations at break as high as 390 ± 28% for 5CBMAA1LN, 436 ± 21% for 5CBMAA3LN and 140 ± 25% for 5CBMAA5LN (Fig. 3a). However, the Young's moduli increased twofold compared to poly(HEMA) hydrogels corresponding to 19.9 ± 0.7 kPa, 33.3 ± 2.2 kPa and 76.7 ± 1.5 kPa for 1, 3 and 5 wt% of LNs respectively (Fig. 3b). Further increases of CBMAA-3 concentration in the polymerisation feed such as 10 and 20 mol% led to a sharp increase of elongation at break of the material. A remarkable strain at break as high as 1800 ± 42% was achieved by the 20CBMAA3LN hydrogel (Fig. 3a).

As expected, an increase in the concentration of nanoparticles leads to higher Young's moduli. Since the nanoparticles are acting as physical cross-linkers, the increase in their concentration in the polymerisation feed leads to an increase in the number of cross-linking points resulting in tougher hydrogels. However, the dependence of the elongation at break on the concentration of nanoparticles is not linear and achieves its maximum at 3 wt% of LNs for the entire range of CBMAA-3 concentrations. The low elongation at break for hydrogels containing only 1 wt% of LNs can be explained by the interaction between long polymer chains with sparsely scattered nanoparticles not being strong enough to withstand a high applied load. Consequently, a higher concentration of LNs (such as 5 wt%) led to an increase in the number of cross-linking points, enhancing the interaction between polymer chains and nanoparticles. However, the shorter length of the polymer segments between cross-linking points restricts greater elongation.

Additionally, 10CBMAA3LN hydrogel rods coloured in yellow and blue were prepared for a visual demonstration of their ability to return to their initial shape after an applied deformation (Fig. 4a).

The hydrogel rods were able to resist high levels of various deformations such as compression and elongation and quickly recover the initial shape.

Furthermore, all the presented hydrogels containing zwitterionic comonomers were able to very rapidly self-heal without the use of any healing agent or harsh conditions. Only keeping the cut surfaces in contact at room temperature for 5 min was

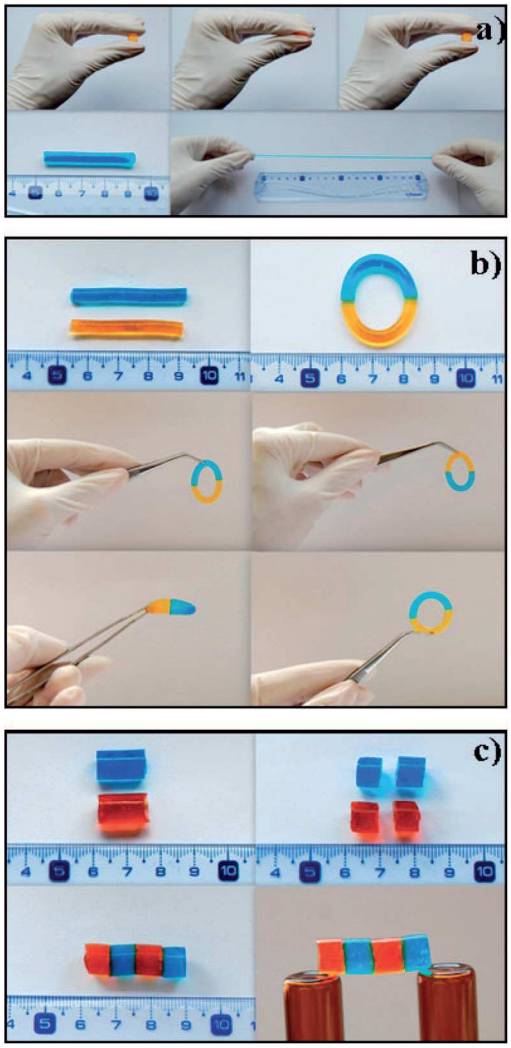

Fig. 4 (a) Mechanical resistance of 10CBMAA3LN hydrogels to different type of deformations. Self-healing of 10CBMAA3LN hydrogels: (b) hydrogel ring healed from two separate hydrogel rods and (c) hydrogel rod healed from four pieces.

sufficient for the hydrogels to heal. Fig. 4b shows the healed ring obtained from two separate hydrogel rods. The ring was mechanically stable and resistant to handling. Another demonstration of self-healing was performed with hydrogel rods of a larger diameter ($d = 10$, $l = 15$ mm) (Fig. 4c). The two differently coloured hydrogels were cut into half and brought into contact in alternating order of colours for 5 minutes at room temperature. The healed rod was placed on two platforms in order to show that the healed joints can withstand the load of the rod's weight without breaking. Even shorter healing times were observed with an increasing content of CBMAA-3. In contrast, no healing was observed in bare poly(HEMA) hydrogels.

Conclusion

Novel self-healing poly(HEMA-*co*-CBMAA-3) nanocomposite hydrogels with antifouling characteristics were synthesised. The cross-linking *via* Laponite nanoparticles endowed self-healing properties without the need for a healing agent or special conditions, excellent mechanical resistance, very high elongation and an extremely high water uptake capacity. Importantly, even hydrogels with higher molar contents of CBMAA-3 and higher degrees of swelling showed good mechanical properties and elongations at break as high as 1800%. Small molar ratios of the zwitterionic monomers rapidly increase the swelling while the mechanical properties remain well within the requirements for potential applications, such as tissue engineering. A wide range of properties, such as the degree of swelling from 5 to 300, elongation at break from 150 to 1800%, and Young's modulus from 4 to 80 kPa, are accessible. The obtained poly(HEMA-*co*-CBMAA-3) hydrogels can therefore be easily tuned by variation of the zwitterionic comonomer and nanoparticle concentrations.

The ease of functionalisation with bioreceptors of carboxybetaine moieties combined with the exceptional mechanical and self-healing properties brought about by the Laponite nanoparticles make these new materials a highly promising platform for biomedical applications. This work paves the way for the design of hydrogels mimicking the properties of natural tissues.

Acknowledgements

This work was supported by KAN 200520804, Grant Agency of the Czech Republic 13-00939S and by Czech Science Foundation (GACR) under Contracts no. P205/12/1702, P106/12/1451, P205-12-1702, P205-12-G118, and P106-12-451.

Notes and references

1 N. A. Peppas, P. Bures, W. Leobandung and H. Ichikawa, *Eur. J. Pharm. Biopharm.*, 2000, **50**, 27–46.
2 N. A. Peppas, J. Z. Hilt, A. Khademhosseini and R. Langer, *Adv. Mater.*, 2006, **18**, 1345–1360.
3 A. S. Hoffman, *Adv. Drug Delivery Rev.*, 2002, **54**, 3–12.
4 B. Rolando, *Hydrogels. Biological Properties And Applications*, Springer, 2009.
5 O. Wichterle and D. Lim, *Nature*, 1960, **185**, 117–118.
6 H. Studenovská, M. Šlouf and F. Rypáček, *J. Mater. Sci.: Mater. Med.*, 2007, **19**, 615–621.
7 D. F. Williams, *Biomaterials*, 2008, **29**, 2941–2953.
8 C. Rodriguez-Emmenegger, O. A. Avramenko, E. Brynda, J. Skvor and A. B. Alles, *Biosens. Bioelectron.*, 2011, **26**, 4545–4551.
9 Š. Kubinová, D. Horák, N. Kozubenko, V. Vaněček, V. Proks, J. Price, G. Cocks and E. Syková, *Biomaterials*, 2010, **31**, 5966–5975.
10 S. Atzet, S. Curtin, P. Trinh, S. Bryant and B. Ratner, *Biomacromolecules*, 2008, **9**, 3370–3377.
11 A. Hejčl, P. Lesný, M. Přádný, J. Šedý, J. Zámečník, P. Jendelová, J. Michálek and E. Syková, *J. Mater. Sci.: Mater. Med.*, 2009, **20**, 1571–1577.
12 P. Lesný, J. De Croos, M. Prádný, J. Vacík, J. Michálek, S. Woerly and E. Syková, *J. Chem. Neuroanat.*, 2002, **23**, 243–247.

13 E. Brynda, N. A. Cepalova and M. Štol, *J. Biomed. Mater. Res.*, 1984, **18**, 685–693.
14 M. L. W. Knetsch, Y. B. J. Aldenhoff and L. H. Koole, *Biomaterials*, 2006, **27**, 2813–2819.
15 B. D. Ratner, *Biomaterials*, 2007, **28**, 5144–5147.
16 T. Riedel, Z. Riedelová-Reicheltová, P. Májek, C. Rodriguez-Emmenegger, M. Houska, J. E. Dyr and E. Brynda, *Langmuir*, 2013, **29**, 3388–3397.
17 B. Wehrle-Haller, *Curr. Opin. Cell Biol.*, 2012, **24**, 116–124.
18 B. Wehrle-Haller, *Curr. Opin. Cell Biol.*, 2012, **24**, 569–581.
19 Q. Shao, Y. He, A. D. White and S. Jiang, *J. Phys. Chem. B*, 2010, **114**, 16625–16631.
20 J. C. Hower, M. T. Bernards, S. Chen, H.-K. Tsao, Y.-J. Sheng and S. Jiang, *J. Phys. Chem. B*, 2008, **113**, 197–201.
21 R. E. Holmlin, X. Chen, R. G. Chapman, S. Takayama and G. M. Whitesides, *Langmuir*, 2001, **17**, 2841–2850.
22 E. Ostuni, R. G. Chapman, R. E. Holmlin, S. Takayama and G. M. Whitesides, *Langmuir*, 2001, **17**, 5605–5620.
23 C. Rodriguez Emmenegger, E. Brynda, T. Riedel, Z. Sedlakova, M. Houska and A. B. Alles, *Langmuir*, 2009, **25**, 6328–6333.
24 C. Rodriguez-Emmenegger, B. V. Schmidt, Z. Sedlakova, V. Subr, A. B. Alles, E. Brynda and C. Barner-Kowollik, *Macromol. Rapid Commun.*, 2011, **32**, 958–965.
25 C. Rodriguez-Emmenegger, E. Hasan, O. Pop-Georgievski, M. Houska, E. Brynda and A. B. Alles, *Macromol. Biosci.*, 2012, **12**, 525–532.
26 C. Rodriguez-Emmenegger, O. Kylián, M. Houska, E. Brynda, A. Artemenko, J. Kousal, A. B. Alles and H. Biederman, *Biomacromolecules*, 2011, **12**, 1058–1066.
27 U. Edlund, C. Rodriguez-Emmenegger, E. Brynda and A.-C. Albersson, *Polym. Chem.*, 2012, **3**, 2920–2927.
28 S. Kudaibergenov, W. Jaeger and A. Laschewsky, in *Supramolecular Polymers Polymeric Betains Oligomers*, Springer, Berlin Heidelberg, 2006, pp. 157–224.
29 C. Rodriguez-Emmenegger, E. Brynda, T. Riedel, M. Houska, V. Subr, A. B. Alles, E. Hasan, J. E. Gautrot and W. T. Huck, *Macromol. Rapid Commun.*, 2011, **32**, 952–957.
30 C. Rodriguez-Emmenegger, M. Houska, A. B. Alles and E. Brynda, *Macromol. Biosci.*, 2012, **12**, 1413–1422.
31 N. Y. Kostina, C. Rodriguez-Emmenegger, M. Houska, E. Brynda and J. Michálek, *Biomacromolecules*, 2012, **13**, 4164–4170.
32 Z. Zhang, T. Chao, L. Liu, G. Cheng, B. D. Ratner and S. Jiang, *J. Biomater. Sci., Polym. Ed.*, 2009, **20**, 1845–1859.
33 L. Carr, G. Cheng, H. Xue and S. Jiang, *Langmuir*, 2010, **26**, 14793–14798.
34 M. B. Huglin and J. M. Rego, *Polymer*, 1991, **32**, 3354–3358.
35 Z. Zhang, T. Chao and S. Jiang, *J. Phys. Chem. B*, 2008, **112**, 5327–5332.
36 C. Rodriguez-Emmenegger, E. Brynda, T. Riedel, Z. Sedlakova, M. Houska and A. B. Alles, *Langmuir*, 2009, **25**, 6328–6333.
37 L. R. Carr, H. Xue and S. Jiang, *Biomaterials*, 2011, **32**, 961–968.
38 C.-W. Chang, A. van Spreeuwel, C. Zhang and S. Varghese, *Soft Matter*, 2010, **6**, 5157–5164.
39 K. Haraguchi and T. Takehisa, *Adv. Mater.*, 2002, **14**, 1120–1124.
40 Y. Tanaka, J. P. Gong and Y. Osada, *Prog. Polym. Sci.*, 2005, **30**, 1–9.
41 K. Haraguchi, *Polym. J.*, 2011, **43**, 223–241.
42 K. Haraguchi, K. Uyama and H. Tanimoto, *Macromol. Rapid Commun.*, 2011, **32**, 1253–1258.
43 Q. Wang, J. L. Mynar, M. Yoshida, E. Lee, M. Lee, K. Okuro, K. Kinbara and T. Aida, *Nature*, 2010, **463**, 339–343.
44 K. Haraguchi, T. Takehisa and M. Ebato, *Biomacromolecules*, 2006, **7**, 3267–3275.
45 S. Kalasin and M. M. Santore, *Colloids Surf., B*, 2009, **73**, 229–236.
46 J. L. Drury and D. J. Mooney, *Biomaterials*, 2003, **24**, 4337–4351.

Electronic Supplementary Material (ESI) for Journal of Materials Chemistry B

Supporting Information

for Journal of Materials Chemistry B,

Novel self-healing nanocomposite hydrogels based on antifouling poly(carboxybetaine) with superior mechanical properties

Nina Yu. Kostina, Cesar Rodriguez-Emmenegger, Andres de los Santos Pereira, Shahriar Sharifi, Jiří Michálek, Dirk W. Grijpma

Synthesis of (3-methacryloylamino-propyl)-(2-carboxy-ethyl)-dimethylammonium (carboxybetaine methacrylamide, CBMAA-3) monomer

The carboxybetaine methacrylamide (CBMAA-3) monomer was synthesised as reported earlier[1] (see Scheme 1). Briefly, DMAPM (17 g, 100 mmol) was dissolved in 100 mL of dry THF and cooled to 0 ^{o}C. Subsequently, β-propiolactone (9 g, 125 mmol) was dissolved in 30 mL of dry THF for each monomer and added dropwise under nitrogen for 3 h. The reaction was allowed to proceed for 24 h at 4 ^{o}C. The white precipitate was filtered-off and subsequently washed with dry THF and ether. The product was dried under high vacuum. The structure of the monomer was confirmed by ^{1}H- and ^{13}C-NMR.

Characterisation: ^{1}H- and ^{13}C-NMR

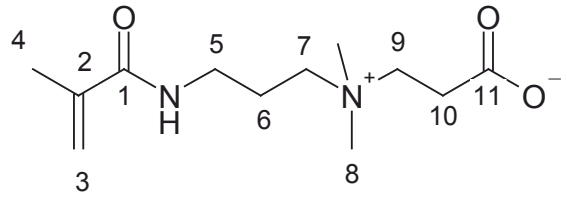

^{1}H NMR (400 MHz, D2O): δ = 1.907 (s, 3H, H^{4}), 1.912-2.09 (m, 2H, H^{6}), 2.64 (t, 2H, H^{10}, J$_{9,10}$ =7.7Hz), 3.06 (s, 6H, H^{8}), 3.29-3.37(m, 4H, H^{5}, H^{7}), 3.53 (t, 2H, H^{9}, J$_{9,10}$ = 7.7 Hz) 5.45-5.46 (m, 1H, H^{3trans}), 5.69-5.70 (m, 1H, H^{3cis}).

^{13}C NMR (100 MHz, D$_2$O): δ = 17.68 (C^{4}),22.35 (C^{6}), 30.82 (C^{10}), 36.31 (C^{5}), 50.62 (C^{8}), 61.30 (C^{7}), 62.05 (C^{9}), 121.44 (C^{3}), 138.92(C^{2}), 172.16 (C^{1}), 176.66 (C^{11}).

Protein Fouling test

In our previous work, we investigated the resistance to non-specific protein adsorption achieved on poly(HEMA) hydrogels when increasing amounts of zwitterionic comonomers were added.[2] All the hydrogels containing zwitterionic comonomers showed an unprecedented reduction of fouling from full blood plasma. In the present work we explore a new type of hydrogels synthesised by copolymerisation of HEMA and CBMAA-3 and physically cross-linked by Laponite XLG. In order to confirm that the material presented herein also possesses antifouling properties, we evaluated the non-specific protein adsorption from a 10 % foetal bovine serum (FBS) solution by UV-Vis spectroscopy.

Hydrogel rods of 2.5 cm length and 0.5 cm diameter were swollen in PBS at 25ºC to equilibrium and then were immersed in 4 mL of 10% FBS. The samples were gently shaken in 10% FBS during 1 hour at room temperature and then removed. UV spectra of FBS before (blank) and after incubating the hydrogel (both diluted 1:4 in PBS) were recorded using a Hitachi U-1900 spectrophotometer in the region λ = 600-200 nm using a 1 cm cuvette (Figure S1).

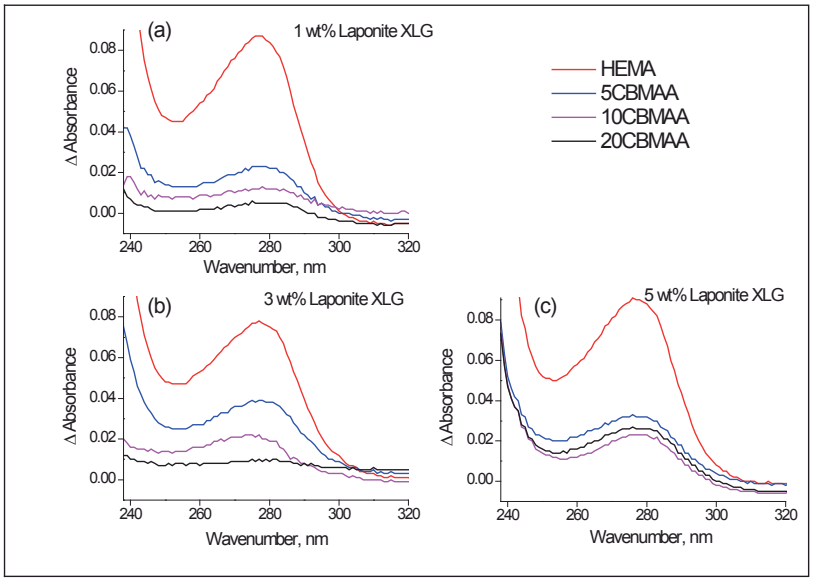

Fig. S1 UV-Vis absorbance spectra of FBS (after subtraction of the blank) after incubating hydrogels with 1% (a), 3% (b) and 5% (c) Laponite XLG.

Protein fouling was estimated from the difference in intensity of the protein absorbance[3] peak at λ = 277 nm by subtracting the spectra of solution contacted with the hydrogels from the blank spectrum. The protein fouling was expressed as the relative amount of adsorbed protein (%) taking the hydrogel with HEMA1LN as the reference. For the determination of the influence of Laponite XLG on the fouling of hydrogels, the fouling on a chemically cross-linked poly(HEMA) hydrogel, without Laponite XLG, was also measured (HEMA0LN). For the purpose of this comparison, HEMA was polymerised in the presence of 80 wt% of water and 0.5 wt% of ethylene glycol dimethacrylate, initiated by ammonium persulfate (APS) and *N*,*N*,*N*′,*N*′-tetramethylethylenediamine (TEMED).

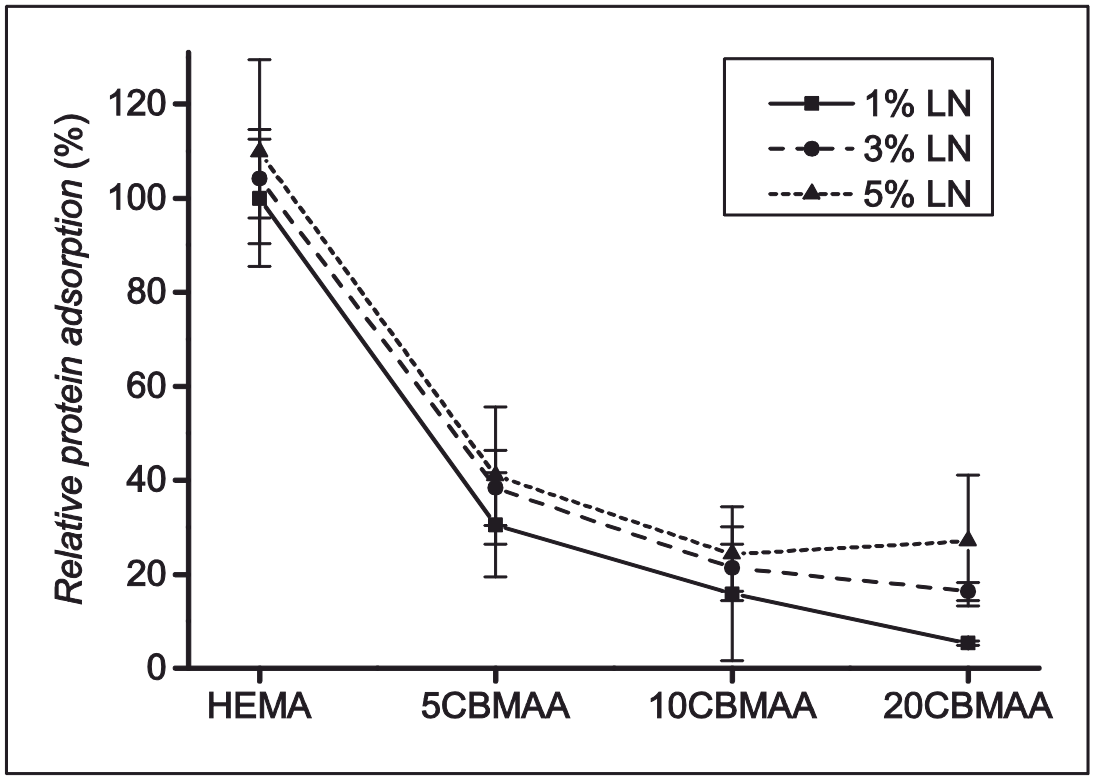

Fig. S2 Non-specific protein adsorption on hydrogels from 10 % FBS, measured by UV-Vis Spectroscopy.

The fouling for HEMA0LN amounted to about 60 % of the fouling observed on the physically cross-linked poly(HEMA) with 1% Laponite XLG and without zwitterionic comonomer (HEMA1LN). Further increases in the amount of Laponite XLG (HEMA3LN and HEMA5LN) caused only a minor increase in the fouling (Fig. S2). However, with the

addition of only 5 mol% of CBMAA-3 comonomer to the polymerisation feed, a dramatic reductions in the fouling (60 to 70 %) are achieved regardless the concentration of Laponite. A subsequent increase in the ratio of CBMAA-3 to 10 mol% further reduced the fouling by 85 %, 80 % and 75 % (Fig. S2) for hydrogels with 1, 3 and 5 wt% of Laponite XLG respectively. Remarkably, for hydrogels containing 20 mol% of CBMAA-3 and 1 wt% of nanoparticles (20CBMAA1LN), a suppression of more than 95 % of the fouling is attained. These results confirm the antifouling characteristics of the newly presented materials, with a trend similar to what has been previously reported.[2]

References

1. C. Rodriguez-Emmenegger, B. V. Schmidt, Z. Sedlakova, V. Subr, A. B. Alles, E. Brynda and C. Barner-Kowollik, *Macromolecular rapid communications*, 2011, **32**, 958-965.
2. N. Y. Kostina, C. Rodriguez-Emmenegger, M. Houska, E. Brynda and J. Michálek, *Biomacromolecules*, 2012, **13**, 4164-4170.
3. E. Brynda, J. Drobník, J. Vacík and J. Kálal, *Journal of Biomedical Materials Research*, 1978, **12**, 55-65.

Appendix 5

Biodegradable zwitterionic functionalizable scaffolds with gyroid pore architecture for tissue engineering

Macromolecular Bioscience, (under review)

DOI: 10.1002/mabi.

Full Paper

Biodegradable Zwitterionic Functionalizable Scaffolds with Gyroid Pore Architecture for Tissue Engineering [a]

Nina Yu. Kostina, Sebastien Blanquer, Ognen Pop-Georgievski, Anita Höcherl, Dirk W. Gripma, Jiří Michálek, Cesar Rodriguez-Emmenegger*

_____

N. Yu. Kostina, Dr. O. Pop-Georgievski, Dr. A. Höcherl, Dr. J. Michálek, Dr. Cesar Rodriguez-Emmenegger
Institute of Macromolecular Chemistry, Academy of Sciences of the Czech Republic, v.v.i., Heyrovsky sq.2, Prague 162 06, Czech Republic
E-mail: rodriguez@imc.cas.cz

Dr. S. Blanquer, Prof. Dr. D. W. Grijpma
MIRA Institute for Biomedical Technology and Technical Medicine, Department of Biomaterials Science and Technology, Faculty of Science and Technology, University of Twente, P.O. Box 217, 7500 AE Enschede, The Netherlands

Prof. Dr. D. W. Grijpma
W.J. Kolff Institute, Department of Biomedical Engineering, University Medical Center Groningen, University of Groningen, Antonius Deusinglaan 1, 9713 AV Groningen, The Netherlands
_____

[a] **Supporting Information** is available online from the Wiley Online Library or from the author.

ABSTRACT.

Designed hydrogels with gyroid pore architecture based on tri-block-copolymer consisting of biodegradable poly(D,L-lactide) (PDLLA) blocks and hydrophilic poly(ethylene glycol) (PEG) block and nonfouling zwitterionic carboxybetaine methacrylamide (CBMAA-3) were fabricated by stereolithography. Synthesized hydrogels were characterized by infrared and X-ray photoelectron spectroscopy (FTIR-ATR and XPS). By addition of the zwitterionic comonomer to the polymerization feed significant increase in the equilibrium water content of hydrogels, up to 700%, was achieved. Hydrogels were challenged with the solution of fluorescein isothiocyanate labeled bovine serum albumin (BSA-FITC) and showed suppression of non-specific interaction with protein. Finally, carboxyl groups of hydrogels bearing CBMAA-3 were exploited for immobilization of BSA-FITC, used as a model protein. The homogeneous protein immobilization across the hydrogel pores was confirmed by laser scanning confocal microscopy (LSCM). No protein immobilization was observed on the hydrogels without addition of CBMAA-3, due to deficiency of functional groups.

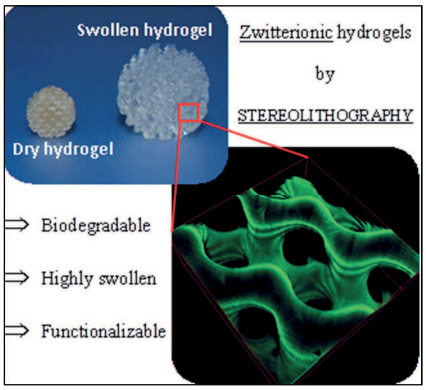

1. Introduction

A deficiency in available tissue and organ donors for transplantation gave rise to consideration for development of artificial material as a potential alternative to natural tissues.[1] Nowadays, the main concern of tissue engineering and regenerative medicine focuses on the fabrication of the scaffold that can replace damaged or lost tissues providing active support and signals for cells' growth and new tissue formation.[1-3] The successful implantation admittedly depends on a precise design of the properties scaffold in accordance to the tissue that needs to be replaced.[4, 5]

In the light of challenges of the scaffold design several important criteria must be attained. Firstly, the scaffold must possess sufficient water content, high porosity, large surface area, and at the same time be mechanically stable in the operative conditions.[6] Biodegradability is another highly sought property which allows to avoid undesirable postoperative surgery after implantation.[7-9] It is desirable to gain control over degradation rate coinciding with new tissue formation, in order not to lose the supportive function of the scaffold or not to inhibit tissue regeneration.[10]

The initial cell attachment to the surface of scaffold is essential precondition for the effective cellular functions, such as proliferation, differentiation and new tissue formation. One of the ubiquitous approaches to induce specific cell attachment is to decorate the surface of the scaffold with biological cues, such as peptides, or proteins interacting with integrin receptors of the cell.[11, 12] However, this approach becomes very challenging for real application when the decorated scaffold is implanted in vivo. In general the contact of the artificial scaffold with complex biological media, such as blood plasma or other bodily fluids induce non-specific protein adsorption, i.e. fouling, leading to irreversible changes in the properties of the material.[13, 14] This adverse effect not only can cause strong inflammatory responses but also mask the bioactive molecules, cues, immobilized on the material to support

specific interactions with cells. In order to prevent this risk the scaffold should fully suppress any non-specific interactions proceeding at the interface in complex biological fluid.[6, 13-19]

Cell motility is another very important aspect in the process of a new tissue formation. Cell migration is controlled by a complex set of mechanisms that are affected not only by extra- and intracellular signaling, but also by surrounding of extracellular environment.[20] For example, scaffold microstructure, such as porosity, pore size and shape, specific surface area, interconnectivity, have been shown to significantly affect cell adhesion, growth and differentiation and to control the bioactivity of scaffold used for in vivo regeneration of various tissues, such as skin, cartilage, bone and peripheral nerves.[20-24] In general, cell migration is limited within scaffold with too small pores (≤ 20 nm) and can result in the formation of cellular capsule around the edges of the scaffold resulting in resistance of fluid diffusion and risk of necrotic region appearance within the scaffold.[25] Enlarging the pore size will enhance the fluid flow and cell migration, but at same time will decrease in specific surface area which may limit cells attachment.[26] Additionally, interconnectivity and permeability of pores are essential for unrestricted fluid flow through the pore space and ensures diffusion of nutrients, waste products and cytokines through the scaffolds.[27]

Nowadays there are several techniques for preparation of porous polymeric scaffold, namely solvent casting, fibril networking and phase separation.[28] However, it is very difficult to gain control over the internal architecture and interconnectivity by using these techniques and often scaffolds result in inhomogeneous structures with irregular pore sizes and pore size distributions, poor pore interconnectivity and inferior mechanical properties.[29] Alternatively, the advances in solid freeform fabrication significantly improved the ability of production of the scaffolds with precise geometry and internal morphology. Stereolithography is known as one of the most developed computer-aided rapid prototyping technique for construction of complex three-dimensional scaffolds with respect to the freedom of structure exterior and

interior design with the highest accuracy. This technique is using a layer-by-layer approach that is based on spatially controlled solidification of liquid-based resins by photopolymerization.[27, 30-32] Stereolithography allows the fabrication of structures with designed shape and pore geometry from a computer-aided design (CAD) file or others 3D drawing computer software, which can be described using mathematical equations, or even be derived from scanning data of (clinical) imaging technologies such as magnetic resonance imaging(MRI), or tomography techniques.[30]

Latterly hydrogels have been considered as very perspective candidates for soft tissue engineering due to their highly swollen tree-dimensional environment, viscoelastic mechanical properties, and structural similarity to macromolecular-based components of the body. In particular poly(ethylene glycol) (PEG) is one of the widely used nontoxic, hydrophilic and biocompatible polymer for the preparation of hydrogels. Additionally, recently PEG based resins were utilized in stereolithography for the preparation of hydrogels with complex architecture introducing new avenues in the engineering design of soft tissue scaffolds.[31, 33, 34] However, even if for many years PEG based materials and coatings were considered to be the best alternative for the reduction of non-specific protein adsorption, recent studies showed that this persuasion is correct only in the case if the protein fouling is tested in single protein solution. It has been shown by Riedel et.al. that the exposure of PEG based surfaces to a blood plasma resulting in non-specific adsorption of certain nine proteins that can mediate the subsequent adsorption of other proteins and components from the media.[35] This discovery is ruling out the possibility to use purely PEG-based materials in the applications with blood contact.

Recently, our group has introduced preparation of nonfouling hydrogels by copolymerization of 2-hydroxyethyl methacrylate with zwitterionic carboxybetaines.[6, 18] Polymers based on zwitterionic carboxy betaines are known to be able to completely suppress

fouling from complex biological media, such as saliva, urine, cerebrospinal liquid, blood plasma and whole blood.[15, 17, 36] The addition of only a few percent (up to 10%) of zwitterionic carboxybetaines to the polymerization mixture led to a hydrogels with (i) dramatic increase in equilibrium water content preserving good mechanical properties, (ii) available functional groups and (iii) an unprecedented reduction and even suppression of fouling from undiluted blood plasma.[6]

Taking advantage of the unique properties of nonfouling zwitterionic poly(carboxybetaine)s and technique for fabrication of scaffolds with designed architecture, such as stereolithography, herein we introduce a functionalizable biodegradable zwitterionic hydrogels based on nonfouling poly(carboxybetaine methacrylamide) (CBMAA-3) and tri-block-copolymer consisting of degradable block - poly(D,L-lactide) (PDLLA) and hydrophilic block - poly(ethylen glycol) PEG. Prepared hydrogels possess complex gyroid pore architecture, high wettability and available functional groups arising from CBMAA-3. The successful copolymerization was confirmed by infrared spectroscopy with attenuated total reflectance (FTIR-ATR) and X-ray photoelectron spectroscopy (XPS). Hydrogels were functionalized with bovine serum albumin (BSA), as a model protein.

2. Experimental Section

2.1. Materials

3,6-Dimethyl-1,4-dioxane-2,5-dione (D,L-lactide), poly(ethylene glycol) (PEG) (average M_n=4,000), tin(II) 2-ethylhexanoate ($St(Oct)_2$) (92.5-100%), methacrylic anhydride (MAAH) (94%), triethylamine (TEA) (≥99%), N-[3-(dimethylamino)propyl]methacrylamide (99%), N-hydroxysulfosuccinimide sodium salt (sulfoNHS) (≥98%), N-(3-dimethylaminopropyl)-N′-ethylcarbodiimide hydrochloride (EDC), Bovine serum albumin–fluorescein isothiocyanate conjugate (BSA-FITC) were purchased from Sigma Aldrich. β-Propiolactone was purchased

from Serva electrophoresis GmbH. Lucirin TPO-L (ethyl-2,4,6-trimethylbenzoyl phenylphosphinate) was a granted by BASF (Germany). Phenol red was supplied by Riedel de Haën.

Isopropanol, dichloromethane, diethyl ether, chloroform, tetrahydrofuran, and methanol were purchased from Lachner. Tetrahydrofuran (anhydrous THF, ≥99.9%), diethyl ether (anhydrous, ≥99.7) and phosphate-buffered saline (PBS, pH 7.4) were from Sigma-Aldrich.

2.2. Synthesis of MA-PDLLA-PEG-PDLLA-MA macromer

The synthesis of MA-PDLLA-PEG-PDLLA-MA macromer (**Scheme 1**) consisted of two-step reaction, in which the PDLLA-PEG-PDLLA oligomer produced was subsequently functionalized with MAAH.

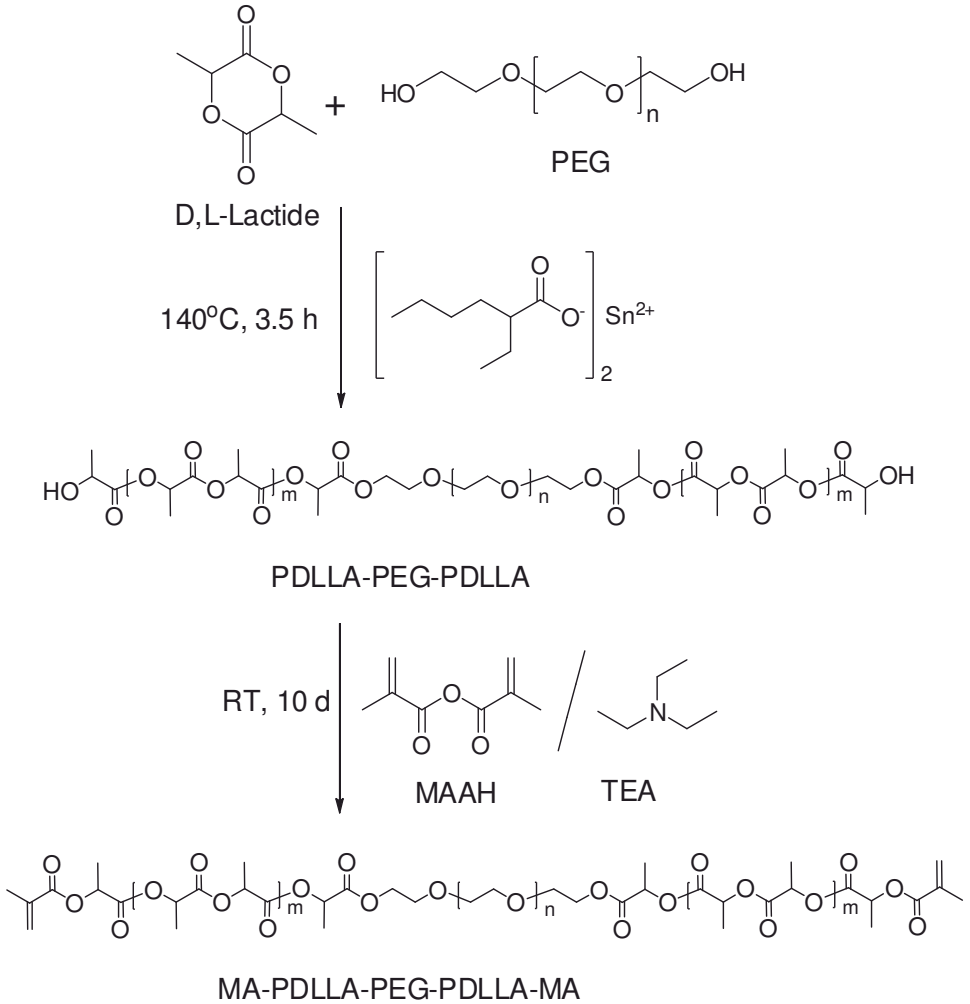

Scheme 1. Synthesis of PDLLA-PEG-PDLLA oligomer and MA-PDLLA-PEG-PDLLA-MA macromer.

2.2.1. Synthesis of PDLLA-PEG-PDLLA oligomer

PDLLA-PEG-PDLLA was synthetized by ring opening polymerization of D,L-lactide initiated from the terminal hydroxyl groups of PEG catalyzed by $St(Oct)_2$ (Scheme 1).[37] The targeted molecular weight of the oligomers was between 4500 and 5000 g mol^{-1}. Firstly, PEG was molten and dried in a three-necked flask, under vacuum and magnetic stirring, at 120˚C for 10 h. Then calculated amount of D,L-lactide and $Sn(Oct)_2$ was added under the flow of argon; the molar ratio of D,L-lactide/$Sn(Oct)_2$ was 400/1. Reaction carried out for 2 h at 120˚C and then the temperature was elevated up to 140˚C and reaction was allowed to proceed for 1.5 h more. Then PDLLA-PEG-PDLLA was precipitated in isopropanol and subsequently filtrated and dried in vacuum.

2.2.2. Synthesis of MA-PDLLA-PEG-PDLLA-MA macromer

Oligomer was functionalized with methacrylate groups by reaction of the terminal hydroxyl groups of the PDLLA-PEG-PDLLA oligomer with MAAH (Scheme 1). Solutions of PDLLA-PEG-PDLLA (C=0.25 g ml^{-1}) and MAAH (C=0.2 g ml^{-1}) in dry DCM were prepared in separate flasks and purged with argon for 20 min. Then TEA (18 ml) was injected into the solution of oligomer under argon. The solution of MAAH was added to the solution of oligomer and TEA by dropping funnel. Reaction was allowed to proceed for 10 days, with continues stirring. The formed MA-PDLLA-PEG-PDLLA-MA was precipitated into diethyl ether, and purified by dissolving in chloroform and precipitating one more time into diethyl ether.

2.3. Synthesis of carboxybetaine methacrylamide (3-Methacryloylamino-propyl)-(2-carboxy-ethyl)-dimethyl-ammonium) (CBMAA-3)

CBMAA-3 was synthesized by a modified procedure reported earlier (**Scheme 2**).[38] (The synthetic procedure is described in the ESI).

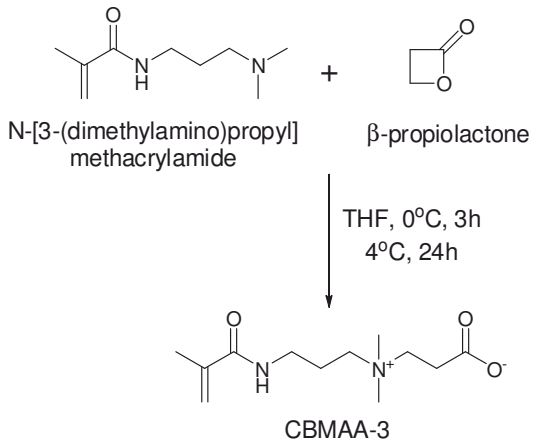

Scheme 2. Synthesis of CBMAA-3.

2.4. Formation of stereolithography resin and building of hydrogel structures

In order to prepare a liquid photopolymerizable resin for use in stereolithography, the MA-PDLLA-PEG-PDLLA-MA macromer, CBMMA-3 monomer in different weight ratios (**Table 1**) and phenol red dye were dissolved in Mili-Q water. Lucirin TPO-L (visible light photo-initiator) was dissolved in DMSO. Then, both solutions were mixed and stirred at room temperature until clear liquid resin was formed. The final resin composition was: 30 wt% of macromer and monomer mixture (Table 1), 4.95 wt% of Lucirin TPO-L, 0.05 wt% of phenol red, 50 wt% of water and 15 wt% of DMSO.

The formulated resins were used to prepare biodegradable hydrogel structures. Using a Perfactory Mini Multilens stereolithography apparatus (Envision-Tec, Germany), non-porous hydrogel films and hydrogels with gyroid pore architecture were prepared. The structures were designed using Rhinoceros 3D (McNeel Europe) and K3DSurf computer software as described elsewhere.[39]

Table 1. The composition of formulations of hydrogels with different weight ratio of macromer to monomer

Hydrogels abbreviation	MA-PDLLA-PEG-PDLLA-MA / CBMAA-3, wt%
0% CBMAA-3	100 / 0
10% CBMAA-3	90 / 10
20% CBMAA-3	80 / 20

The stereolithography apparatus (SLA) is equipped with a digital micro-mirror device that enables projections of 1280×1024 pixels, each measuring 32×32 μm^2. Using a build platform step height of 25 μm, layers of resin were sequentially photo-crosslinked by exposure to a pixel pattern of blue light (wavelength 400–550 nm, peak intensity at 440 nm). The fabrication of the hydrogel structures was carried out by exposing the photopolymerizable resin to light intensities of 10 mW cm^{-2}. The curing time per 25 μm thick layer was evaluated from the working curves obtained for each type of resin formulation. After photo-polymerization, the obtained structures were washed with acetone (1 day), water (2 days), acetone (1 day) to remove remained soluble compounds and dried at ambient conditions for 1 day and in vacuum until constant weight.

2.5. Immobilization of BSA-FITC via EDC/sulfoNHS chemistry

BSA-FITC was covalently immobilized on MA-PDLLA-PEG-PDLLA-MA-*co*-poly(CBMAA-3) hydrogels via an EDC/sulfoNHS reaction. Hydrogel structures of each formulation (0% CBMAA-3, 10% CBMAA-3 and 20% CBMAA-3) firstly were swollen in water and then placed individually in the solution of EDC (C=0.522 M) and sulfoNHS (C=0.115 M) in water for 2 h at room temperature under shaking conditions. Then hydrogels were washed three times with water, allowing at least 20 min for each wash. Activated hydrogels then were placed to PBS for 1 h. After incubation each sample was paced into 4 ml of fresh PBS solution and 2 ml of stock-solution of BSA-FITC (C=3.33 mg ml^{-1}) were added. The reaction was allowed to proceed in dark for 2 h at room temperature and then for 12 h at 4˚C. Finally, the hydrogels were washed and stored in PBS overnight, and confocal imagining was performed on the next day.

In order to prove the absence of non-specific adsorption of BSA-FITC on the hydrogels, blank experiments were performed. Hydrogels of each formulation were swollen in PBS

solution and then contacted with solution of BSA-FITC in the identical way as described above for hydrogels after activation with EDC/sulfo-NHS.

2.6. Characterization of oligomer, macromere and hydrogels

2.6.1. Proton nuclear magnetic resonance (^{1}HNMR)

^{1}HNMR spectra of reaction products were recorded on Bruker DPX 300 and utilized to determine conversion of D,L-lactide, chemical structure, molecular weight of PDLLA-PEG-PDLLA and degree of functionalization with MAAH. $CDCl_3$ was used as a solvent.

2.6.2. Fourier transform infrared spectroscopy with attenuated total reflectance (FTIR-ATR)

The chemical structure of synthesized PDLL-PEG-PDLLA oligomer and poly(MA-PDLLA-PEG-PDLLA-MA-co-CBMAA-3) hydrogels were characterized by FTIR-ATR. Spectra were recorded using an FTIR Thermo Nicolet Nexus 670 spectrometer equipped with a Specac Golden Gate attachment and diamond reflection prism.

2.6.3. X-ray photoelectron spectroscopy (XPS)

To confirm successful copolymerization of macromer MA-PDLLA-PEG-PDLLA-MA and CBMAA-3 XPS measurements were carried out with a K-Alpha+ spectrometer (ThermoFisher Scientific). The samples were analyzed using a micro-focused, monochromated Al Kα X-ray source (400 µm spot size). The kinetic energy of the electrons was measured using a 180º hemispherical energy analyzer operated in the constant analyzer energy mode (CAE) at 200 eV and 50 eV pass energy for survey and high resolution spectra. Data acquisition and processing were performed using Thermo Advantage software. The XPS spectra were fitted with one or more Voigt profiles (binding energy (BE) uncertainty: ±0.2 eV). The analyzer transmission function, Scofield sensitivity factors, and effective attenuation lengths (EALs) for photoelectrons were applied for quantification. EALs were calculated using the standard TPP-2M formalism. All spectra were referenced to the C 1s

peak of hydrocarbons at 285.0 eV BE controlled by means of the well-known photoelectron peaks of PET and metallic Cu, Ag, and Au.

2.6.4. Swelling properties of hydrogels

The equilibrium water content (EWC) of hydrogels was determined gravimetrically. Five samples of each composition of hydrogels were immersed in deionized water for swelling to equilibrium for five days, and the mass of the swollen samples was determined (m_s). Subsequently, the samples were dried in vacuum at ambient temperature to constant weight and the mass of dry hydrogels (m_d) was determined. The equilibrium water content was calculated as:

$$EWC(\%) = \frac{m_s - m_d}{m_d} * 100\% \text{ (Equation 1)}$$

2.6.5. Laser scanning confocal microscopy (LSCM)

Hydrogels with immobilized BSA-FITC were visualized using the Olympus multiphoton LSCM with FV10-ASW viewer soft-ware (Olympus, Japan). Images were recorded using a 4X-air objective and a 488 nm laser for excitation of FITC. 3D reconstructed image was obtained by stacking 20 LSCM xy-scans at 0.5 μm intervals using ImageJ software.

3. Results and Discussion

In this study we report a preparation of novel type of zwitterionic, functionalizable and biodegradable hydrogels with gyroid pore architecture. These hydrogels were prepared by copolymerization of biodegradable macromer (MA-PDLLA-PEG-PDLLA-MA) with nonfouling zwitterionic monomer (CBMAA-3) utilizing stereolithography for precise design of architecture. The successful copolymerization was confirmed by FTIR-ATR and XPS analysis.

Poly(MA-PDLLA-PEG-PDLLA-MA-co-CBMAA-3) hydrogels showed unprecedented increase in swelling ratio and antifouling properties. Finally, BSA-FITC, as a model protein, was successfully immobilized through carboxylic groups of zwitterionic hydrogels via

EDC/sulfoNHS reaction, while no immobilized BSA was observed on the hydrogels without CBMAA-3 copolymer (0% CBMAA-3) lacking of functional groups.

3.1. Synthesis of PDLLA-PEG-PDLLA oligomer and MA-PDLLA-PEG-PDLLA-MA macromer

The tri-block-copolymer PDLLA-PEG-PDLLA was synthesized by ring-opening polymerization of D,L-lactide, initiated by the hydroxyl terminal groups of the PEG chain (Scheme 1). The chemical structure of synthesized oligomer was confirmed by FTIR-ATR and ^{1}HNMR. The FTIR-ATR spectra of PDLLA-PEG-PDLLA shows a clear ester band raised at 1750 cm^{-1} confirming copolymerization of PEG and D,L-lactide (Figure S1). On the ^{1}HNMR spectra a peak at δ 4.2–4.3 ppm, corresponding to methene protons of the PEG connected to PDLLA could be discerned proving the structure of PDLLA-PEG-PDLLA (Figure S2 and FigureS3).

The conversion of D,L-lactide was determine from ^{1}HNMR spectra of reaction mixture of the synthesis of oligomer (Figure S2). Protons of the methyl groups present in D,L-lactide are shifted from δ 1.67–1.61 to δ 1.60–1.37 ppm while the cycle is opened. The conversion was calculated as a ratio of the integral of shifted peaks (δ 1.60–1.37 ppm) to the sum of integrals of shifted peaks and peaks of residual D,L-lactide (δ 1.67–1.61 ppm) and was equal to 93%.

The average degree of polymerization of the PDLLA blocks was accounted as m=4 by the correlation of the respective areas of the peaks corresponding to protons of methylene groups of PEG (1 in Figure S3) and protons of methyl lactyl units (4 and 6 in FigureS3), taking into account that the average degree of polymerization of PEG is n=83. From the values of n and m, number average molecular weight of PDLLA-PEG-PDLLA oligomer M_n=5250 g mol^{-1} was calculated.

The hydroxyl end groups of the synthesized PDLLA-PEG-PDLLA oligomer were reacted with MAAH to obtain MA-PDLLA-PEG-PDLLA-MA macromers (Scheme 1). The

incorporation of methacrylate groups to PDLLA-PEG-PDLLA was confirmed by the appearance of three peaks in the ^{1}HNMR spectra of the macromer: at δ 6.14 (6*), δ 5.58 (6) and δ 1.90 ppm (7), corresponding to the=CH2 (6*, 6) and –CH3 (7) of the methacrylate groups (FigureS4). The degree of functionalization was determined by correlation the integrals of the peaks corresponding to the methylene protons of the methacrylate group (δ 6.14 and 5.58 ppm) with those of the methylene protons of PEG (δ 3.92-3.22 ppm). A degree of functionalization of 100% was achieved.

3.2. Preparation and characterization of hydrogels

For the fabrication of hydrogels with designed architecture, photopolymerizable resins based on MA-PDLLA-PEG-PDLLA-MA with different weight ratio of CBMAA-3 were prepared (Table 1). Stereolithography is using a layer-by-layer approach that is based on spatially controlled crosslinking of liquid-based resins by photopolymerization. The thickness of a solidified layer (cure depth, C_d) is controlled by the light irradiation dose E (mJ cm^{-2}). A plot of the C_d versus the natural logarithm of the energy ln(E) is known as a working curve and can be described by the following equation:

$$C_d = D_p \ln\left(\frac{E}{E_c}\right) \quad \text{(Equation 2)}$$

From intercept and slope of working curve the critical energy E_c (mJ cm^{-2}), which represents the minimum energy level required for crosslinking the resin, and penetration depth D_p (μm), which describes the penetration depth of light into the resin, can be determined, respectively. The critical exposure and penetration depth are very important parameters and must be evaluated for each resin formulation before scaffold fabrication to prevent the failing of interlayer bonding or inaccuracies in the architecture.[33, 39]

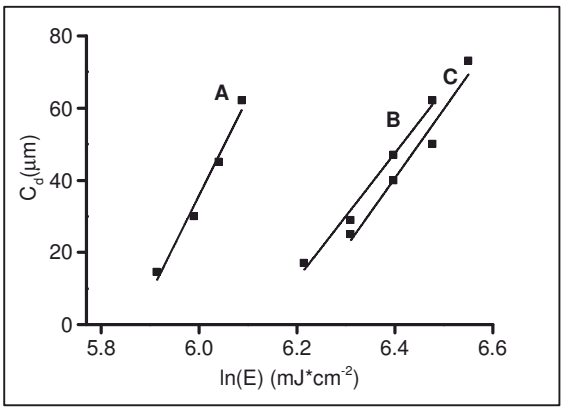

Figure 1.Stereolithographic working curves for (A) 0% CBMAA-3, (B) 10% CBMAA-3 and (C) 20% CBMAA-3 resins.

Working curves for all resin compositions (Table 1) were obtained by varying the light exposure at the resin surface (E) and measuring the resulting cure depths (C_d) of the resins (**Figure 1**). The 0.05wt% of dye was added to the each formulation for better control over the layer thickness. The required curing time per 25 µm thick layer was calculated as 40 s for 0% CBMAA-3, 54 s for 10% CBMAA-3, and 57 s for 20% CBMAA-3 resins at a light intensity of 10 mW cm^{-2}.

Non-porous films and hydrogels with gyroid pore architecture were fabricated by stereolithography utilizing resins containing different amount of zwitterionic comonomer CBMAA-3. All hydrogel structures were soft and highly flexible, their shape and structure precisely matched their design. The chemical structure of hydrogels was confirmed by FTIR-ATR (**Figure 2**). The increase in the amount of zwitterionic comonomer was evidenced by the concomitant increase in the intensity of amide bands at 1650 cm^{-1} and 1535 cm^{-1}, and the carboxyl band at 1600 cm^{-1} arising from the CBMAA-3 added to the resin formulation.

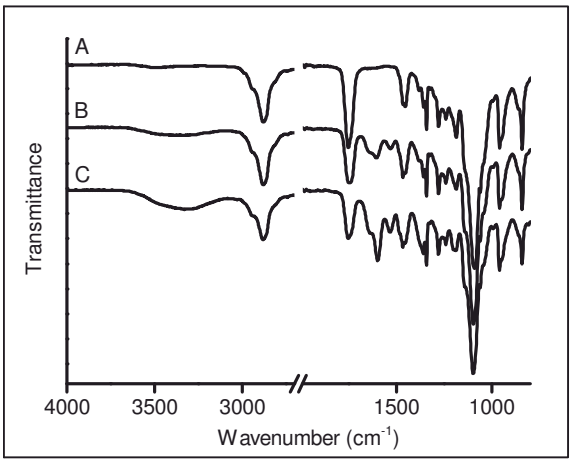

Figure 2. FTIR-ATR spectra of hydrogels prepared from different formulations of resin: (A) 0% CBMAA-3, (B) 10% CBMAA-3 and (C) 20% CBMAA-3.

In addition, the composition of hydrogels was confirmed by XPS. **Figure 3** reports the high resolution core level C 1s and N 1s of the bulk poly(CBMAA-3) material and 0% CBMAA-3, 10% CBMAA-3, and 20% CBMAA-3 hydrogels.

The core level C 1s spectra of poly(CBMAA) bulk material is characterized by a C—C contribution at 285.0 eV, which is accompanied by contributions at 285.6±0.1 eV, 286.2±0.2 eV, 287.9±0.1 eV and 288.3±0.1 eV arising from the secondary chemical shift, i.e. the effect of the ester group on the tertiary carbon atom in the CH_3—C*—C(=O)—NH structure, the C—N^+ moieties, the amide group C(=O)—NH and the carboxylic (O—C=O) group. The N 1s spectrum is characterized by contributions at about 399.5±0.1 eV and 402.5±0.1 eV of amides and charged quaternary ammonium groups, respectively.

The 0% CBMAA-3 hydrogel show the contributions characteristic for the lactide and ethylene oxide monomers as well as the methacrylate groups that did not react during the photo-curing reaction. The contributions centered at 284.5±0.1 eV, 285.0 eV, 286.3±0.2 eV, 287.0±0.2 eV, and 289.0±0.5 eV arising from the C=C, C—C, C—O—C, O—C*—C(=O)O, and ester O—C=O group, respectively. The N 1s spectrum of 0% CBMAA-3 completely lacks nitrogen (amides and charged quaternary ammonium groups) contributions.

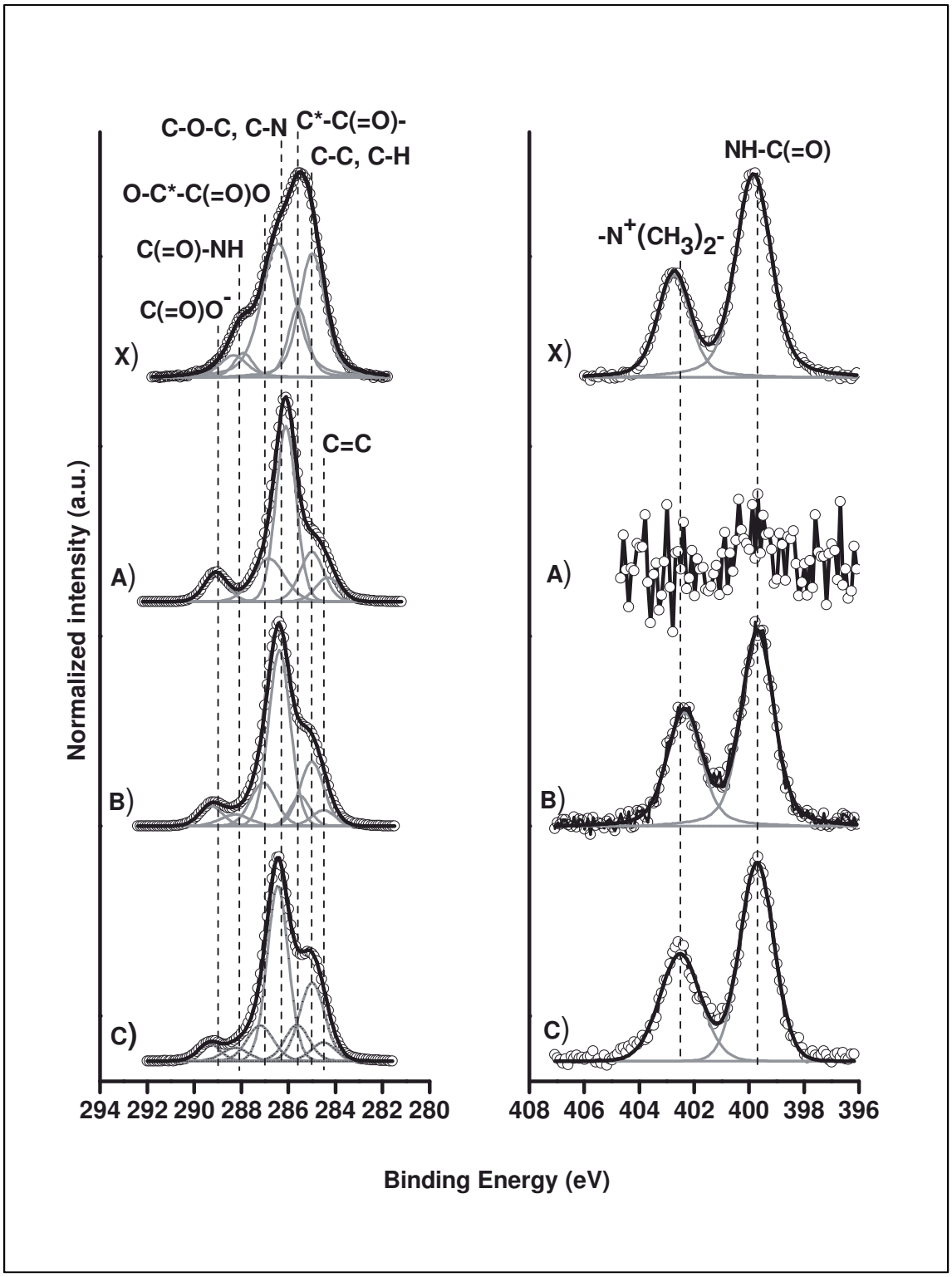

Figure 3. High resolution C 1s (left) and N 1s (right) XPS spectra of (X) poly(CBMAA), (A) 0%CBMAA-3, (B) 10%CBMAA-3, and (C) 20%CBMAA dry hydrogels.

The incorporation of CBMAA-3 monomer units into the MA-PDLLA-PEO-PDLLA-MA structure is clearly observed in the high resolution C 1s and N 1s spectra of the 10% CBMAA-3 and 20% CBMAA-3 hydrogels. The presence of CBMAA-3 can be verified

by the rise of the contributions of C—C (at 285.0 eV), CH_3—C*—C(=O)—NH (at 285.6±0.1 eV), the C—N^+ moieties (which strongly overlap with the O—C*—C(=O)O contributions of PDLLA at 286.3±0.2 eV) and the C(=O)—NH group (at 288.1±0.2 eV) within the C 1s spectra, as well as the occurrence of contributions arising from amide (at 399.7±0.1 eV) and charged quaternary ammonium groups (at 402.5±0.1 eV) in the high resolution N 1s spectra. The increase of CBMAA-3 in the polymerization feed from 10 to 20% lead to increase of the nitrogen content from 1.3 at.% to 2.8 at.%.

The swelling behavior and water uptake capability are essential parameters of scaffolds for tissue engineering. Highly wetted scaffolds provide a good environment for cell grows and proliferation. However, all natural tissues possess different water content depending on the tissue function and it is at high importance for the designing of the scaffold to have a simple tool which allows tuning this property in order to match the value of water content of desired tissue. For that we utilized the copolymerization of macromer MA-PDLLA-PEG-PDLLA-MA with zwitterionic comonomer CBMAA-3 as the tool to tailor the swelling properties of the hydrogels. It was shown previously that hydrogels with addition of CBMAA-3 will bind more and stronger water via electrostatic interactions.[6, 18] As expected, an increase in amount of CBMAA-3 in the polymerization resin lead to a dramatic increase of equilibrium water content (EWC) of hydrogels (**Figure 4**). A 50% increase was observed with addition of only 10% of CBMAA-3 to the polymerization feed. A further increment in the CBMAA-3 concentration to 20% led to an unprecedented increase of hydrogel water content, reaching the value of EWC of 700%. Therefore, the adjustment of the zwitterionic CBMAA-3 concentration is allowing to finely tune the swelling properties of the hydrogels in order to match them with desired tissues.

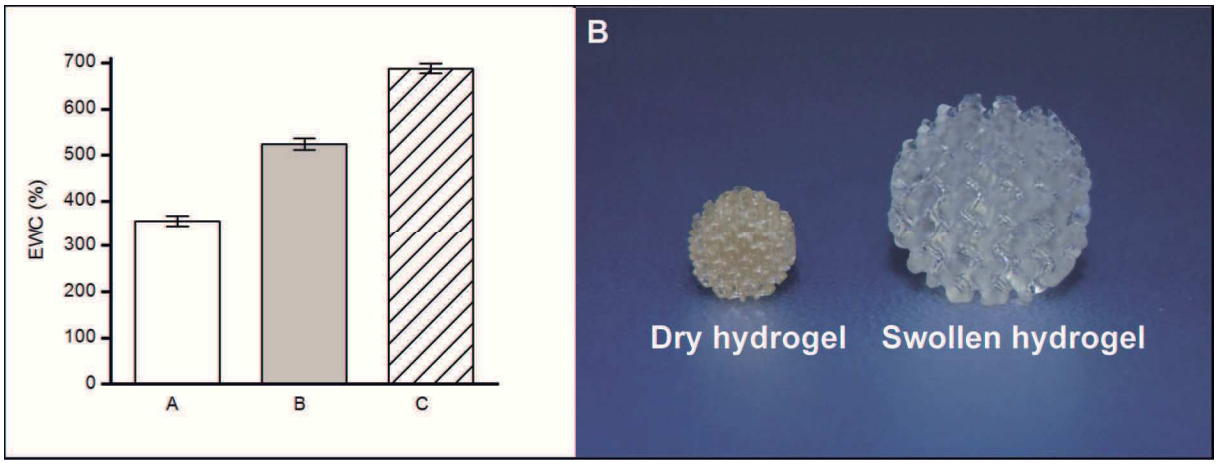

Figure 4. The equilibrium water content (EWC) of hydrogels (A) 0% CBMAA-3, (B) 10% CBMAA-3, and (C) 20% CBMAA-3, defined as the ratio between the mass of absorbed water after reaching the equilibrium and the mass of dried hydrogels (left). The photograph shows dry and swollen hydrogel of 10% CBMAA-3 (right).

3.3. Protein immobilization on the hydrogel surface

One of the main goals of the material for tissue engineering is to actively promote the tissue formation and/or regeneration. A widely used approach to induce specific cell adhesion is to immobilize biomolecules, such as peptides or proteins, on the surface of the scaffold to interact with integrin receptors of the cell. However, this approach meets considerable challenges when the material of the scaffold lacks of the available groups that can be easily functionalized. Typically, aggressive pre-treatments of the surface such as activation with plasma or other oxidative agents are required for this type of material in order to access functionality. Concurrently, during and upon the immobilization of biological cues any non-specific interactions that can occur at the interface between protein solution and the surface of the scaffold must be suppressed.

Initially, in order to prove the absence of non-specific protein adsorption, prepared hydrogels were challenged with the solution of fluorescein isothiocyanate labelled BSA (BSA-FITC) for 14 h and subsequently analyzed by LSCM (**A-C in the Figure 5**). No fluorescence was observed during the scanning of all hydrogels (0%, 10% and 20% CBMAA-

3) with 488 nm laser for excitation of FITC proving the absence of non-specific albumin adsorption on hydrogels (A-C in the Figure 5).

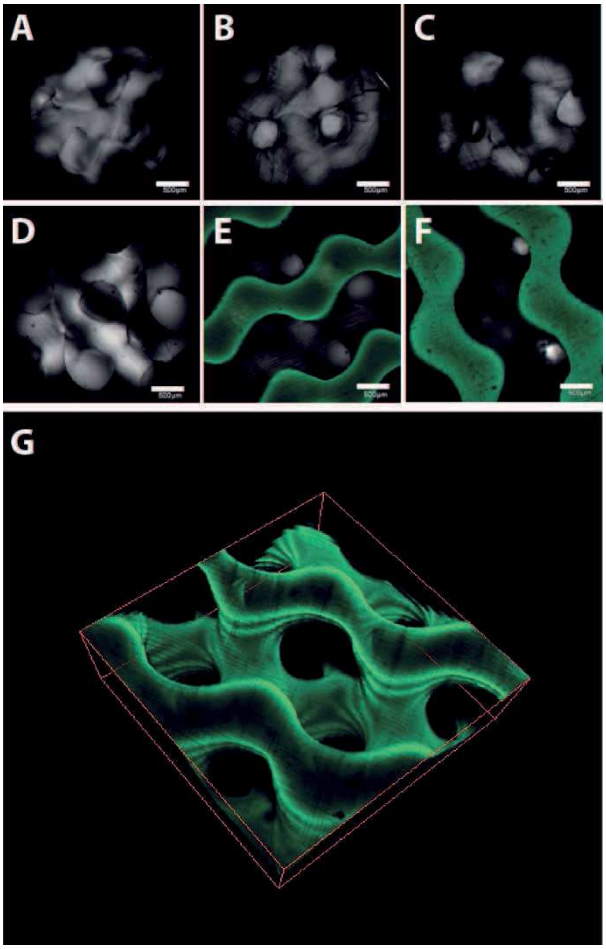

Figure 5. Confocal images D, E and F of the 0% CBMAA, 10% CBMAA and 20% CBMAA hydrogels, respectively, after immobilization of BSA-FITC via EDC/sulfoNHS chemistry. Confocal imagies A, B and C represent blank experiments for 0% CBMAA, 10% CBMAA and 20% CBMAA hydrogels, respectively, i.e. hydrogels were in contact with solution of BSA-FITC without functionalization by EDC/sulfoNHS. Image G represent 3D reconstruction of 20 confocal scans of 10% CBMAA hydrogels with immobilized BSA-FITC.

BSA-FITC was utilized as a model protein in order to demonstrate the ability of zwitterionic hydrogels to be functionalized with proteins or peptides. BSA-FITC immobilization on the hydrogels of 0, 10 and 20% of CBMAA-3 content was performed via EDC/sulfoNHS mediated reaction (D-E, F in the Figure 5). As expected, no BSA immobilization was observed on the hydrogel without any carboxybetaine addition (0% CBMAA-3) (D in the Figure 5) due to the lack of functional groups on the MA-PDLLA-PEG-PDLLA-MA chains. Addition of zwitterionic comonomer to the polymerization feed

resulted in material possessing easily functionalizable carboxyl groups arising from carboxybetaine moieties. Images E and F in the Figure 5 demonstrate the successful immobilization of BSA-FITC on the hydrogels containing 10% and 20% of CBMAA-3, respectively, by strong fluorescent emission upon laser excitation. Image G in the Figure 5 is a three dimensional reconstruction of 20 confocal scans of 10% CBMAA-3 hydrogel. It represents absolute homogeneity of immobilized BSA-FITC within hydrogel pore surface.

4. Conclusions

Taking an advantage of stereolithographic technique for the preparation of finely designed scaffolds for tissue engineering and nonfouling properties of zwitterionic carboxybetaine monomers herein we present a preparation of zwitterionic, biodegradable and functionalizable hydrogels with gyroid pore architecture. Biodegradable macromer MA-PDLLA-PEG-PDLLA-MA and zwitterionic monomer CBMAA-3 were synthesized and their chemical structure was confirmed by FTIR-ATR and ^{1}HNMR. For the hydrogels fabrication the formulations of photopolymerizable resins consisting of different amount of CBMAA-3 (0wt%, 10wt% and 20wt%) were optimized and required curing time for the crosslinking of 25 μm layer were determined from working curves accessed for each formulation.

Hydrogels with different ratio of macromer and zwitterionic monomer were synthesized by stereolithography and successful copolymerization was confirmed by FTIR-ATR and XPS. Prepared hydrogel structures were soft and highly flexible, their shape and structure precisely matched their design. The addition of CBMAA-3 comonomer dramaticaly incresed the water content of hydroges, EWC=700% at 20% of CBMAA-3 content.

Zwitterionic hydrogels possess carboxyl group arising from CBMAA-3 that were exploited for immobilization of BSA-FITC. However, prior protein immobilization, we challenged all hydrogels with BSA-FITC solution to prove the absence of non-specific BSA adsorption. All hydrogel were able to withstand BSA-FITS fouling evidencing by LSCM. BSA-FITC

immobilization on the hydrogels was mediated by EDC/sulfoNHS reaction and analyzed by LSCM. No BSA immobilization was observed on the hydrogel without addition of carboxybetaine monomer (0% CBMAA-3) due to deficiency of functional groups on the MA-PDLLA-PEG-PDLLA-MA chains. Hydrogels containing 10% and 20% of CBMAA-3 demonstrate successful immobilization of BSA-FITC. Moreover, the reconstruction of 20 LSCM scans showed that BSA-FITC immobilization was homogeneous across the pores of hydrogels.

The unique pore architecture, biodegradability, antifouling properties endowed to the prepared hydrogels in combination with the availability of functional groups exploitable for covalent immobilization of cell-binding biomolecules make the presented scaffold a highly promising material for tissue engineering applications.

Supporting Information

Supporting Information is available from the Wiley Online Library.

Acknowledgements: This work was supported by the Grant Agency of the Czech Republic (GACR) under contracts No. 13-00939S and No. 15-09368Y and the project “BIOCEV – Biotechnology and Biomedicine Centre of the Academy of Sciences and Charles University” (CZ.1.05/1.1.00/02.0109).

Received: Month XX, XXXX; Revised: Month XX, XXXX; Published online:

DOI: 10.1002/mabi.

Keywords: Hydrogels, zwitterionic, stereolithography, gyrod pore structure, biodegradable.

References

[1] B. D. Ratner, A. S. Hoffman, F. J. Schoen, J. E. Lemons, "*Biomaterials Science: An Introduction to Materials in Medicine, Second Edition "*, Elsevier Academic Press, 2004.
[2] N. Huebsch, D. J. Mooney, *Nature* **2009**, *462*, 426.
[3] N. A. Peppas, J. Z. Hilt, A. Khademhosseini, R. Langer, *Advanced Materials* **2006**, *18*, 1345.

[4] B. V. Slaughter, S. S. Khurshid, O. Z. Fisher, A. Khademhosseini, N. A. Peppas, *Advanced Materials* **2009**, *21*, 3307.
[5] Drury, J., *Biomaterials* **2003**, *24*, 4337.
[6] N. Y. Kostina, C. Rodriguez-Emmenegger, M. Houska, E. Brynda, J. Michálek, *Biomacromolecules* **2012**, *13*, 4164.
[7] J. H. Kim, C. H. Park, O.-J. Lee, J.-M. Lee, J. W. Kim, Y. H. Park, C. S. Ki, *Journal of Biomedical Materials Research Part A* **2012**, *100A*, 3287.
[8] D. Kai, S. S. Liow, X. J. Loh, *Mater Sci Eng C Mater Biol Appl* **2014**, *45*, 659.
[9] L. S. Nair, C. T. Laurencin, *Progress in Polymer Science* **2007**, *32*, 762.
[10] J. Zhu, R. E. Marchant, *Expert Rev Med Devices* **2011**, *8*, 607.
[11] B. Wehrle-Haller, *Current Opinion in Cell Biology* **2012**, *24*, 116.
[12] R. W. Sands, D. J. Mooney, *Current Opinion in Biotechnology* **2007**, *18*, 448.
[13] C. Blaszykowski, S. Sheikh, M. Thompson, *Chemical Society Reviews* **2012**, *41*, 5599.
[14] C. Rodriguez Emmenegger, E. Brynda, T. Riedel, Z. Sedlakova, M. Houska, A. B. Alles, *Langmuir* **2009**, *25*, 6328.
[15] C. Rodriguez-Emmenegger, E. Brynda, T. Riedel, M. Houska, V. Subr, A. B. Alles, E. Hasan, J. E. Gautrot, W. T. Huck, *Macromolecular rapid communications* **2011**, *32*, 952.
[16] C. Rodriguez-Emmenegger, A. Jäger, E. Jäger, P. Stepanek, A. B. Alles, S. S. Guterres, A. R. Pohlmann, E. Brynda, *Colloids and Surfaces B: Biointerfaces* **2011**, *83*, 376.
[17] C. Rodriguez-Emmenegger, M. Houska, A. B. Alles, E. Brynda, *Macromolecular Bioscience* **2012**, *12*, 1413.
[18] N. Y. Kostina, S. Sharifi, A. de los Santos Pereira, J. Michalek, D. W. Grijpma, C. Rodriguez-Emmenegger, *Journal of Materials Chemistry B* **2013**, *1*, 5644.
[19] C. Blaszykowski, S. Sheikh, M. Thompson, *Trends in Biotechnology* **2014**, *32*, 61.
[20] B. A. C. Harley, H.-D. Kim, M. H. Zaman, I. V. Yannas, D. A. Lauffenburger, L. J. Gibson, *Biophysical Journal* **2008**, *95*, 4013.
[21] V. Karageorgiou, D. Kaplan, *Biomaterials* **2005**, *26*, 5474.
[22] F. J. O'Brien, B. A. Harley, I. V. Yannas, L. J. Gibson, *Biomaterials* **2005**, *26*, 433.
[23] Q. Zhang, H. Lu, N. Kawazoe, G. Chen, *Acta Biomaterialia* **2014**, *10*, 2005.
[24] M. Madaghiele, L. Salvatore, A. Sannino, "4 - Tailoring the pore structure of foam scaffolds for nerve regeneration", in *Biomedical Foams for Tissue Engineering Applications*, P.A. Netti, Ed., Woodhead Publishing, 2014, p. 101.
[25] C. M. Murphy, M. G. Haugh, F. J. O'Brien, *Biomaterials* **2010**, *31*, 461.
[26] T. M. Freyman, I. V. Yannas, L. J. Gibson, *Progress in Materials Science* **2001**, *46*, 273.
[27] F. P. Melchels, A. M. Barradas, C. A. van Blitterswijk, J. de Boer, J. Feijen, D. W. Grijpma, *Acta Biomaterialia* **2010**, *6*, 4208.
[28] J. C. Ashworth, S. M. Best, R. E. Cameron, *Materials Technology* **2014**, *29*, 281.
[29] G. Antonio, R. Teresa, D. S. Roberto, A. Luigi, *Journal of Applied Biomaterials & Biomechanics* **2009**, *7*, 141.
[30] F. P. Melchels, J. Feijen, D. W. Grijpma, *Biomaterials* **2010**, *31*, 6121.
[31] S. A. Skoog, P. L. Goering, R. J. Narayan, *J Mater Sci: Mater Med* **2014**, *25*, 845.
[32] S. B. G. Blanquer, S. P. Haimi, A. A. Poot, D. W. Grijpma, *Macromolecular Symposia* **2013**, *334*, 75.
[33] T. M. Seck, F. P. Melchels, J. Feijen, D. W. Grijpma, *Journal of controlled release : official journal of the Controlled Release Society* **2010**, *148*, 34.
[34] B. Dhariwala, E. Hunt, T. Boland, *TISSUE ENGINEERING* **2004**, *10*, 1316.
[35] T. Riedel, Z. Riedelová-Reicheltová, P. Májek, C. Rodriguez-Emmenegger, M. Houska, J. E. Dyr, E. Brynda, *Langmuir* **2013**, *29*, 3388.
[36] F. Surman, T. Riedel, M. Bruns, N. Y. Kostina, Z. Sedláková, C. Rodriguez-Emmenegger, *Macromolecular Bioscience* **2015**, *15*, 636.
[37] D. Cohn, A. Hotovely-Salomon, *Polymer* **2005**, *46*, 2068.

[38] C. Rodriguez-Emmenegger, B. V. Schmidt, Z. Sedlakova, V. Subr, A. B. Alles, E. Brynda, C. Barner-Kowollik, *Macromolecular rapid communications* **2011**, *32*, 958.
[39] F. P. W. Melchels, J. Feijen, D. W. Grijpma, *Biomaterials* **2009**, *30*, 3801.

Zwitterionic biodegradable hydrogels with gyroid pore architecture were fabricated by stereolithography. The addition of zwitterionic carboxybetaine to the polymerization resins resulted in hydrogels with improved swelling and functional groups. All hydrogels showed suppression of fouling from albumin solution. Albumin was immobilized on the zwitterionic hydrogels while no protein immobilization was observed on the hydrogels without any addition of carboxybetaine monomer.

Nina Yu. Kostina, Sebastien Blanquer, Ognen Pop-Georgievski, Anita Höcherl, Dirk W. Gripma, Jiří Michálek, Cesar Rodriguez-Emmenegger*

Biodegradable Zwitterionic Functionalizable Scaffolds with Gyroid Pore Architecture for Tissue Engineering

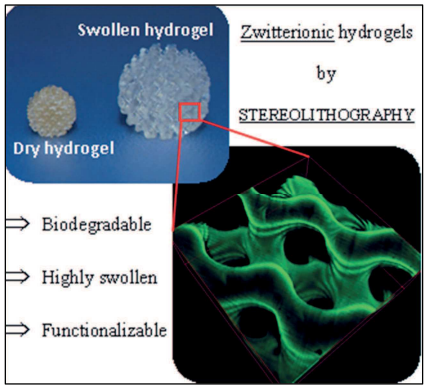

Supporting Information

for *Macromol. Biosci.*, DOI: 10.1002/mabi.2015#####

Biodegradable Zwitterionic Functionalizable Scaffolds with Gyroid Pore Architecture for Tissue Engineering

Nina Yu. Kostina, Sebastien Blanquer, Ognen Pop-Georgievski, Anita Höcherl, Dirk W. Gripma, Jiří Michálek, Cesar Rodriguez-Emmenegger*

N. Yu. Kostina, Dr. O. Pop-Georgievski, Dr. J. Michálek, Dr. Cesar Rodriguez-Emmenegger
Institute of Macromolecular Chemistry, Academy of Sciences of the Czech Republic, v.v.i., Heyrovsky sq.2, Prague 162 06, Czech Republic
E-mail: rodriguez@imc.cas.cz
Dr. S. Blanquer, Prof. Dr. D. W. Grijpma
MIRA Institute for Biomedical Technology and Technical Medicine, Department of Biomaterials Science and Technology, Faculty of Science and Technology, University of Twente, P.O. Box 217, 7500 AE Enschede, The Netherlands
Prof. Dr. D. W. Grijpma
W.J. Kolff Institute, Department of Biomedical Engineering, University Medical Center Groningen, University of Groningen, Antonius Deusinglaan 1, 9713 AV Groningen, The Netherlands

Materials and Methods

Synthesis of carboxybetaine methacrylamide (3-Methacryloylamino-propyl)-(2-carboxy-ethyl)-dimethyl-ammonium) (CBMAA-3)

Dimethylaminopropyl methacrylamide (7.8 g, 55 mmol) was dissolved in 100 mL of anhydrous THF and cooled to –20˚C. A pinch of DPPH was added as inhibitor. Subsequently, β-propiolactone (5.0 g, 69 mmol) was dissolved in 40 mL of THF and added dropwise under nitrogen atmosphere. The reaction was allowed to proceed for 24 h at 4˚C. The white precipitate was washed with dry THF and ether and dried under vacuum. Prior to polymerization, DPPH was removed by reprecipitation from methanol solution by addition of THF to yield 19.4 g (yield: 80 %).

Additional Results and Discussion

Synthesis of PDLLA-PEG-PDLLA oligomer and MA-PDLLA-PEG-PDLLA-MA macromer

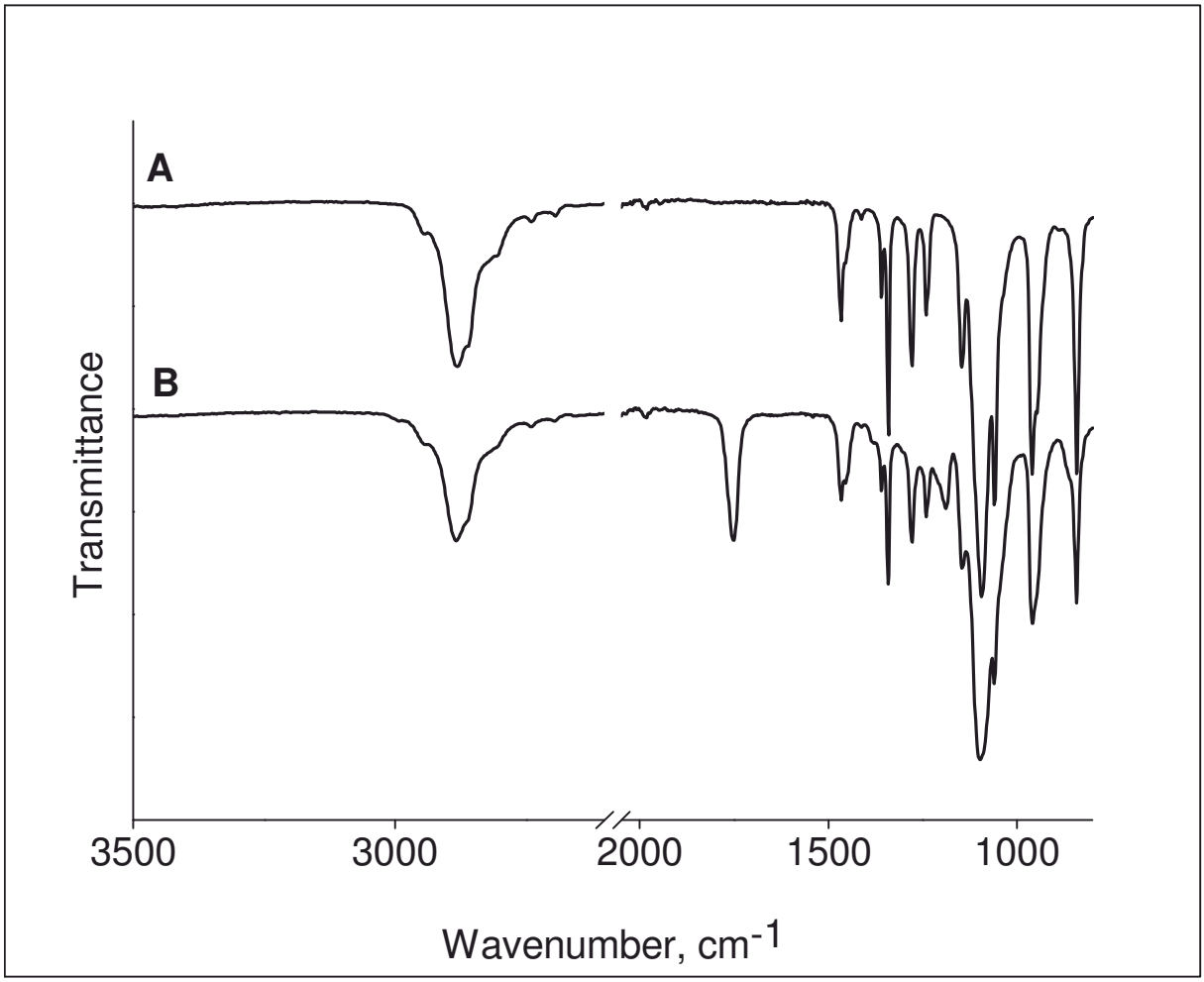

Figure S1. FTIR-ATR spectra of (A) PEG and (B) PDLLA-PEG-PDLLA

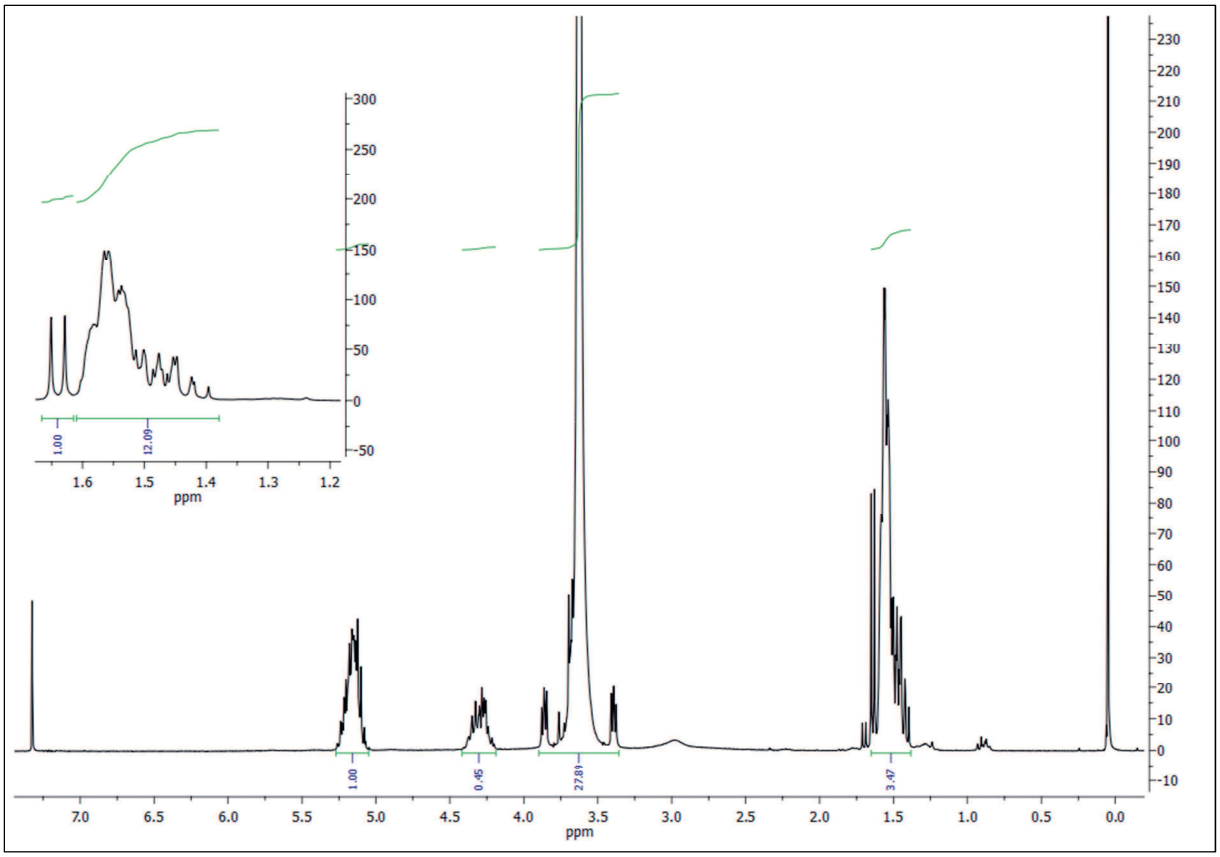

Figure S2. [1]HNMR spectra of reaction mixture of the synthesis of PDLLA-PEG-PDLLA after 3.5 h.

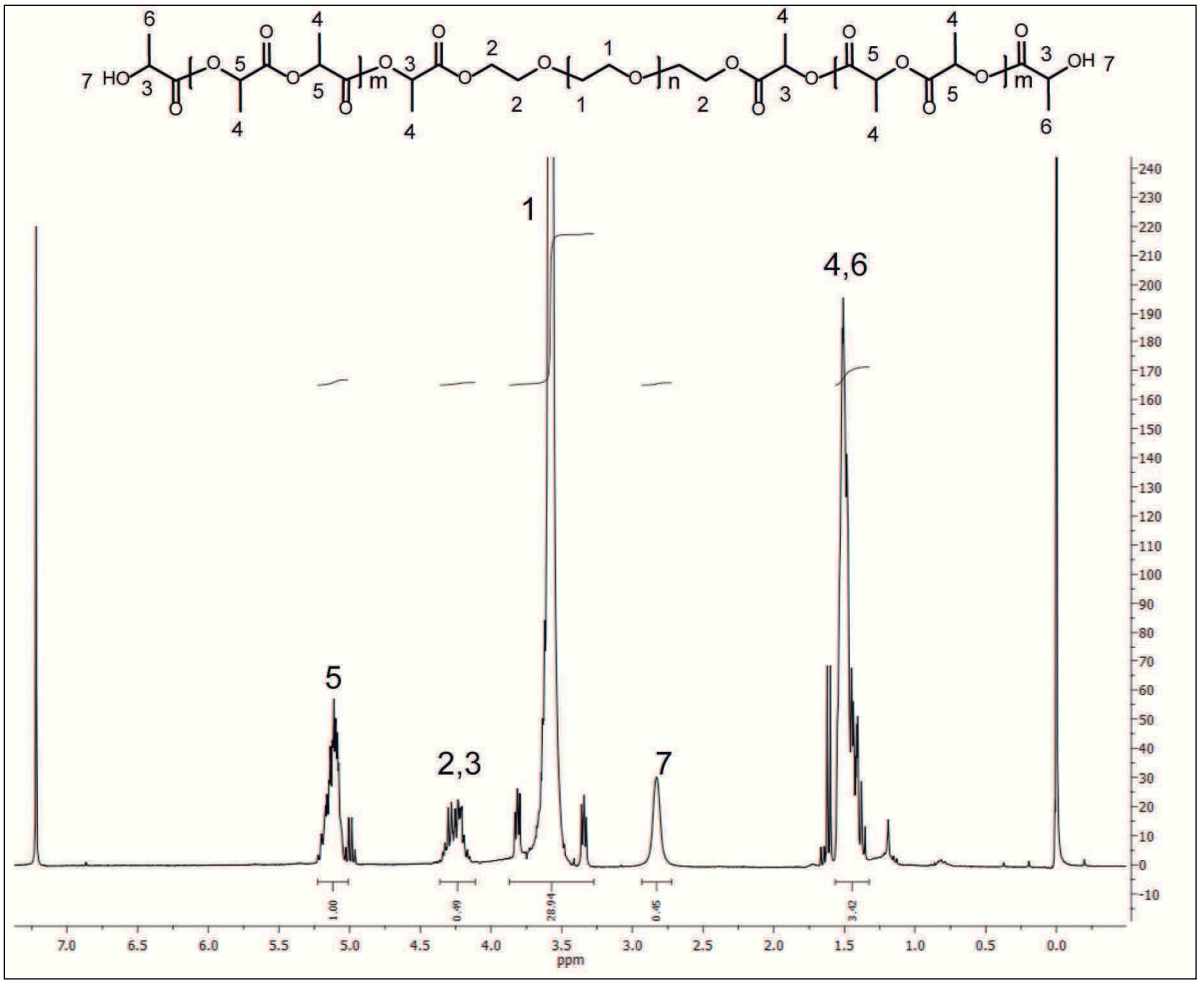

Figure S3. [1]HNMR spectra of PDLLA-PEG-PDLLA.

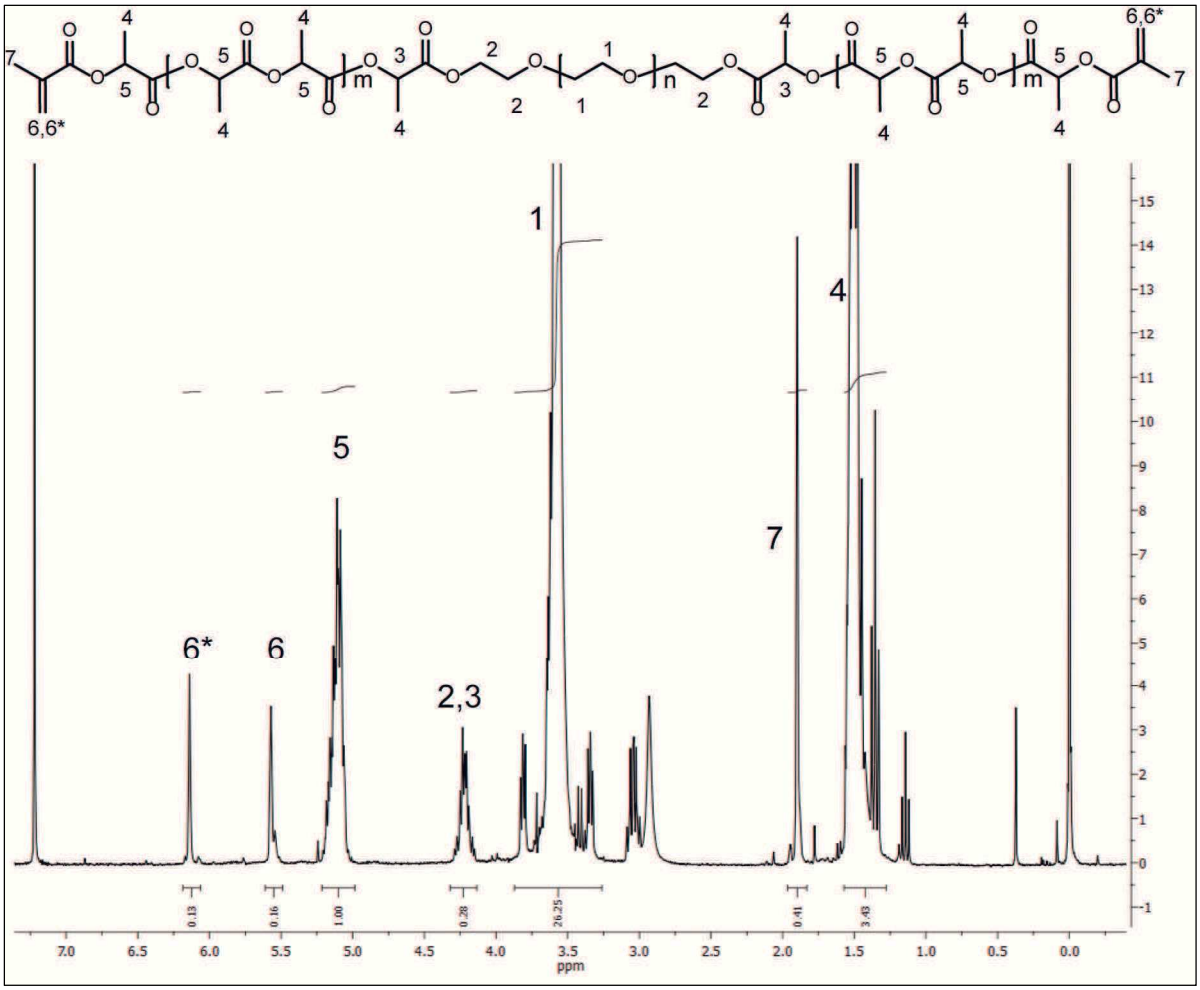

Figure S4. [1]HNMR spectra of MA-PDLLA-PEG-PDLLA-MA.

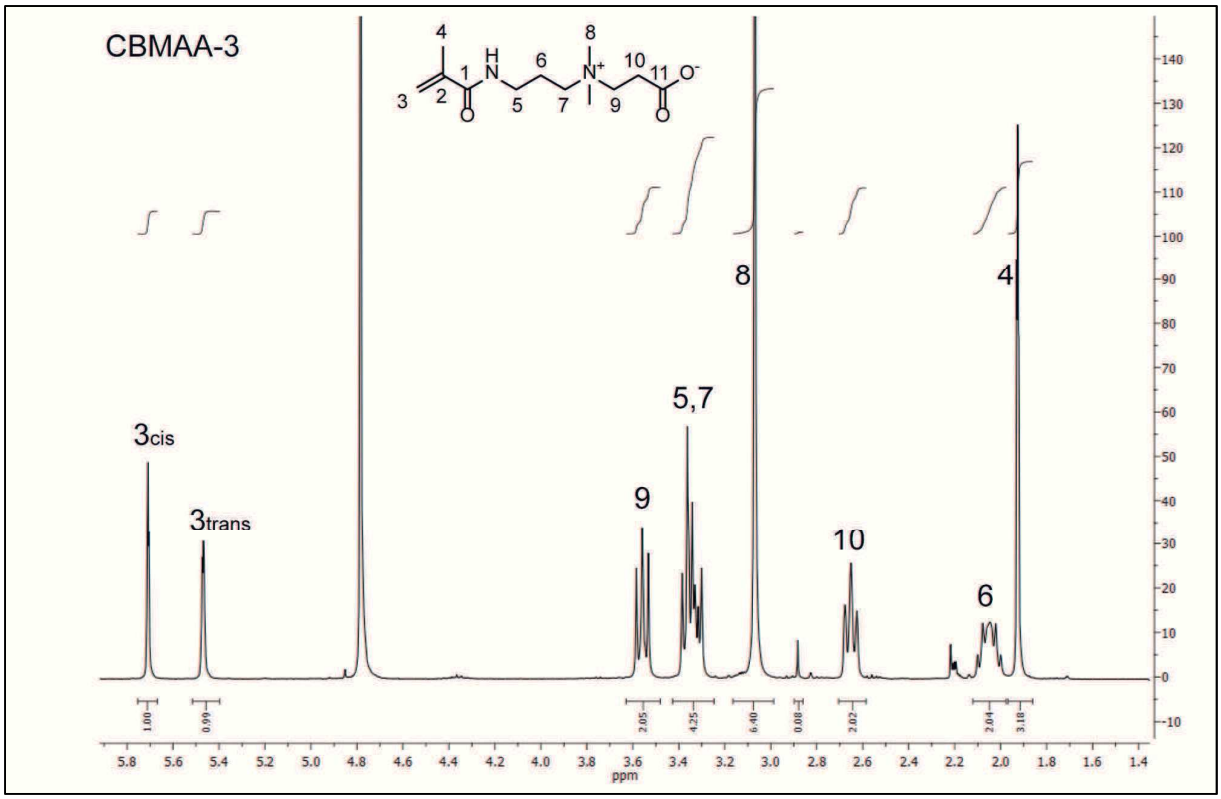

Figure S5. [1]HNMR spectra of CBMAA-3.

Appendix 6

Non-fouling biodegradable poly(ε-caprolactone) nanofibers for tissue engineering

Macromolecular Bioscience, 2015, DOI: 10.1002/mabi.201500252

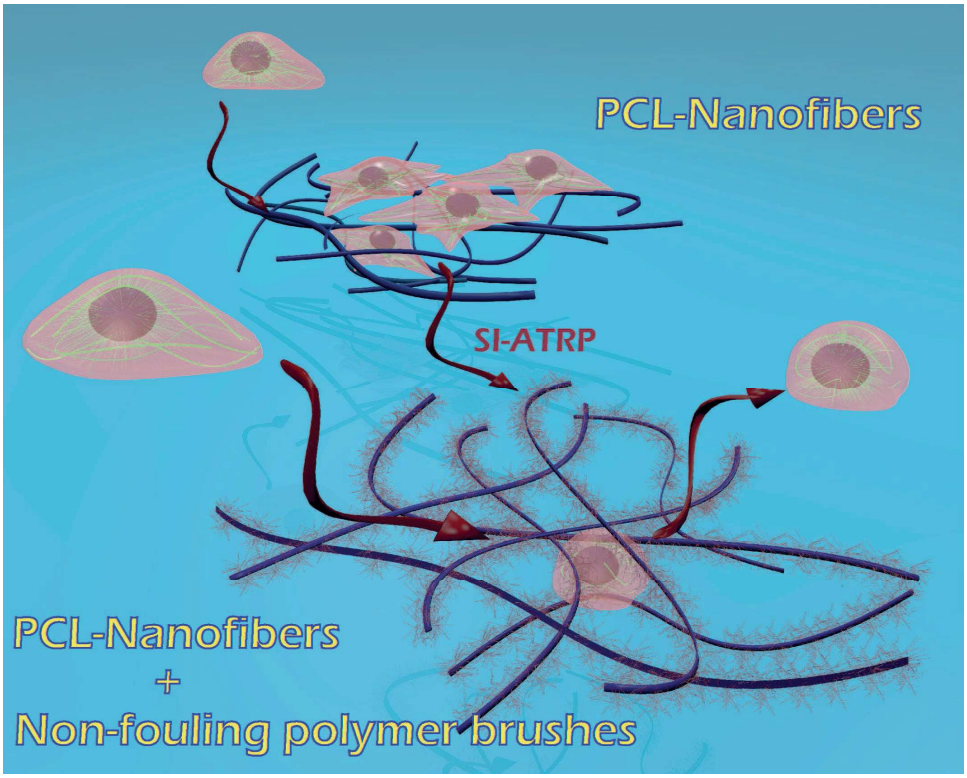

Non-Fouling Biodegradable Poly(ε-caprolactone) Nanofibers for Tissue Engineering[a]

Nina Yu. Kostina, Ognen Pop-Georgievski, Michael Bachmann, Neda Neykova, Michael Bruns, Jiří Michálek, Martin Bastmeyer,* Cesar Rodriguez-Emmenegger*

Poly(ε-caprolactone) (PCL) nanofibers are very attractive materials for tissue engineering (TE) due to their degradability and structural similarity to the extracellular matrix (ECM). However, upon exposure to biological media, their surface is rapidly fouled by proteins and cells, which may lead to inflammation and foreign body reaction. In this study, an approach for the modification of PCL nanofibers to prevent protein fouling from biological fluids and subsequent cell adhesion is introduced. A biomimetic polydopamine (PDA) layer was deposited on the surface of the PCL nanofibers and four types of antifouling polymer brushes were grown by surface-initiated atom transfer radical polymerization (SI-ATRP) from initiator moieties covalently attached to the PDA layer. Cell adhesion was assessed with mouse embryonic fibroblasts (MEFs). MEFs rapidly adhered and formed cell–matrix adhesions (CMAs) with PCL and PCL-PDA nanofibers. Importantly, the nanofibers modified with antifouling polymer brushes were able to suppress non-specific protein adsorption and thereby cell adhesion.

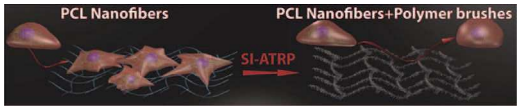

Dr. C. Rodriguez-Emmenegger, N. Yu. Kostina, Dr. O. Pop-Georgievski, Dr. J. Michálek
Institute of Macromolecular Chemistry, Academy of Sciences of the Czech Republic, v.v.i., Heyrovsky sq.2, Prague 162 06, Czech Republic
E-mail: rodriguez@imc.cas.cz
Prof. M. Bastmeyer, Dr. M. Bachmann
Zoological Institute, Cell and Neurobiology, Karlsruhe Institute of Technology (KIT), Haid-und-Neu-Straße 9, Karlsruhe 76131, Germany
E-mail: martin.bastmeyer@kit.edu
Prof. M. Bastmeyer
Institute for Functional Interfaces (IFG) Karlsruhe Institute of Technology (KIT), Hermann-von-Helmholtz-Platz 1, Eggenstein-Leopoldshafen 76344, Germany
Dr. N. Neykova
Institute of Physics, Academy of Sciences of the Czech Republic, Cukrovarnicka 10, Prague 16253, Czech Republic
Faculty of Nuclear Science and Physical Engineering, Czech Technical University in Prague, Trojanova 13, Prague 12000, Czech Republic
Dr. M. Bruns
Institute for Applied Materials (IAM) and Karlsruhe Nano Micro Facility (KNMF), Karlsruhe Institute of Technology (KIT), Hermann-von-Helmholtz-Platz 1, Eggenstein-Leopoldshafen 76344, Germany

[a]**Supporting Information** is available from the Wiley Online Library or from the author.

1. Introduction

Tissue engineering emerges as a potential solution for the increased need of tissues and organs for transplantation by promoting de novo tissue formation and recovery of function.[1,2] This interdisciplinary field aims at replacing lost or damaged tissues by using tissues formed by growing human cells on or within biomaterial scaffolds.[3] The design of scaffolds for tissue engineering plays a central role in the success of the implantation and its properties have to be tuned in accordance with the features of the tissue that needs to be replaced.[2,4–6] Recently, electrospun nanofibers have gained wide recognition in the field for the engineering of soft tissues due to the combination of their intrinsic properties such as elasticity, high porosity, large surface area, and presence of fibril structures. This enables them to mimic the morphology of native extracellular matrix (ECM) and thus provide not only sufficient mechanical support,[7] but also unrestricted transport of nutrients/oxygen and excreted products for cell growth and differentiation.

Biodegradability is another highly sought-after property to avoid undesirable postoperative surgery after implantation.[8–11] Synthetic degradable polymers, in particular polyesters and polycarbonates undergoing enzymatic or hydrolytic degradation, are generally preferred over natural polymers due to their uniformity and the ability to tailor their properties for specific applications.[8,9] Conceivably, poly(ε-caprolactone) (PCL) is one of the most attractive degradable polymers due to the ease of synthesis, low cost, good mechanical properties, and possibility to finely tune its degradation rate by adjustment of the molecular weight and crystallinity.[9,11] The degradation of PCL proceeds by hydrolytic scission without strongly affecting the pH of the surrounding fluids.[12]

The unique features of the PCL nanofibrous meshes make them very attractive as scaffolds for tissue engineering applications.[13–15] However, their extensive use in tissue engineering is limited by the requirements for the biomaterial to actively promote the tissue formation and/or regeneration. A conceivable approach is to decorate the surface of the nanofibers with biological cues, such as peptides or proteins interacting with integrin receptors of the cell mimicking the extracellular matrix–cell signaling pathways.[16–19] However, this approach faces considerable challenges when PCL is in contact with biological media. Upon contact with biological fluids, the surface of PCL is rapidly coated by proteins.[20] Protein fouling is an ubiquitous problem affecting the surface of most (bio) materials, which not only masks the bioactive molecules previously immobilized on the material surface but also can induce a series of adverse effects, such as the inflammatory response, complement, and platelet activation. This may lead to thrombus formation and facilitates the attachment of nosocomial pathogens.[21–28] Therefore, the successful use of PCL nanofibers can only be conceived if their surface is engineered to completely prevent any non-specific interactions, i.e., prevent the fouling. Currently, few strategies have been utilized to address this problem for nanofibers; (i) the electrospinning of blends of PLA with an amphiphilic triblock terpolymer containing oligo(ethylenglycol) side chains, (ii) to modify the surface of the fibers by clicking zwitterionic groups such as sulfobetaines, and (iii) the electrospinning of catechol-conjugated PEG and thiolated PLGA (PLGA-SH) followed by post-cross-linking via catechol–thiol reactions and catechol–catechol conjugation.[15,29,30] In most of these studies, the resistance to protein fouling was assessed only by challenging the fibers with serum albumin, which is not a sufficient test for proving the resistance to complex biological media.[25,31,32] The antifouling and rarely achieved non-fouling properties must be demonstrated by the ability of the material surface to resist fouling from multi-component protein solutions such as serum and plasma, as well as by its aptitude to completely passivate the surface of the nanofibers preventing cell adhesion.[32,33]

To date, only highly dense polymer brushes prepared by surface-initiated radical polymerizations have been able to meet the challenges associated with the prevention of fouling and cell adhesion.[25,31–39] The unmatched resistance to fouling of polymer brushes has been associated with (i) the entropic penalty that proteins have to overcome to adsorb at the surfaces and (ii) the association with water. Usually, the latter has been correlated with the wettability of the surface,[40] however, conflicting studies[31,33] have shown that a high wettability does not necessarily lead to resistance to fouling, while structuring of water in the vicinity of the surface seems to play a more important role.[41] From the vast list of polymer brushes grown to date, only few have resulted in an important reduction of fouling from real biological fluids. In particular, carboxybetaine acrylamide (CBAA),[31] *N*-(2-hydroxypropyl) methacrylamide (HPMA),[33] oligo(ethylene glycol) methyl ether methacrylate (MeOEGMA),[37] and oligo(ethylene glycol) methacrylate (HOEGMA)[32] grafted by surface-initiated radical polymerizations have demonstrated complete suppression of fouling from various biological fluids and thereby prevented cell adhesion on various substrates[42] over periods of time which are significant for biomedical applications.[36,37,43–46] For instance, poly(HPMA) brushes showed full resistance to blood plasma even after two years of immersion in buffer.[33] Furthermore, the above-mentioned brushes have been proven to be nonthrombogenic in vitro and able to withstand the adhesion of cellular blood components (erythrocytes, leukocytes, and platelets) and fibroblasts in agreement with their excellent resistance to protein adsorption.[24,38] Moreover, the exposure of these brushes to an environmental strain of *Pseudomonas aeruginosa* resulted in no biofilm formation while single cell force spectroscopy with *Yersinia pseudotuberculosis*

Macromolecular Journals

Macromol. Biosci. **2015,** DOI: 10.1002/mabi.201500252

showed that the bacterium exerted minimal adhesion forces to the surface (100 times weaker than directly on Teflon or glass), proving their unmatched ability to resist bacterial adhesion and colonization.[23,47]

Even though antifouling polymer brushes represent the best alternative to prevent fouling, their growth from inert three-dimensional substrates is not exempt from challenges. Surface-initiated polymerization of polymer brushes is often limited by the absence or availability of functional groups on the material surface onto which initiator molecules can be immobilized. Typically, aggressive pre-treatments of the surface such as activation with plasma or other oxidative agents are required.[48] Recently, poly(dopamine) films have been introduced as a way to create functional adlayers.[49–52] PDA films mimic the ability of marine mussels to adhere underwater utilizing their byssal threads. It has been shown that this strong adhesion is achieved by the coexistence of catechol (of 3,4-dihydroxy-l-phenylalanine (DOPA)) and amine groups (of lysine) in the *Mytilus edulis* foot protein 5, a major adhesive precursor protein present in the mussel foot.[50,53–55] In a similar fashion, PDA films adhere to virtually any solid material[38,44,49,52,56,57] irrespective of their surface energy and shape via molecular interactions ranging from van der Waals forces to formation of covalent bonds. The amine groups present within the PDA layer can be exploited for the facile immobilization of initiators as well as moieties enabling photo- or thermally triggered grafting reactions.[38,44,49,58,59] However, polymer brushes in a good thermodynamic solvent exert strong pulling forces to their anchoring points due to osmotic pressure. Therefore, a successful grafting from PDA required very strong adhesion to the substrate as well as excellent stability. PDA films have been shown to possess a remarkable stability in aqueous media even under harsh pH conditions.[60] In addition, grafting polymer brushes from PDA has been shown not to compromise its stability, resulting in films able to perform for more than 4 months.[60,61]

Herein, we introduce a novel route for the modification of PCL nanofibers with antifouling polymer brushes, which enables them to resist protein fouling and completely prevent non-specific cell adhesion. This was achieved by the formation of an adlayer of PDA on the surface of the electrospun PCL nanofibers. This adlayer was further functionalized with 2-bromoisobutyryl groups (an ATRP initiator) subsequently exploited for the growing of polymer brushes based on MeOEGMA, HOEGMA, HPMA, and CBAA via SI-ATRP. The modified fibers were characterized by X-ray photoelectron spectroscopy (XPS) and scanning electron microscopy (SEM). The absence of non-specific protein adsorption from fetal bovine serum (FBS) and cell culture media (CM) was assessed on a model system by surface plasmon resonance (SPR). The nanofibers were challenged by placing them in contact with mouse embryonic fibroblasts (MEFs). The fibroblasts rapidly colonized and formed cell–matrix adhesions (CMAs) on pristine PCL and PCL-PDA nanofibers as determined by fluorescence microscopy. However, all nanofibers modified with polymer brushes were able to fully suppress cell adhesion because non-specific protein adsorption was prevented.

2. Experimental Section

2.1. Materials

Poly(ε-caprolactone) (PCL) nanofibers were purchased from Nanovia Ltd, Czech Republic. Dopamine · HCl (98.5%), CuCl, CuBr, $CuBr_2$, triethylamine (TEA), 2,2′-dipyridyl (BiPy), 2-bromo-2-methylpropionyl bromide (BIBB), 1,4,8,11-tetramethyl-1,4,8,11-tetraazacyclotetradecane (Me_4Cyclam), methacryloyl chloride, 1-aminopropan-2-ol, sodium carbonate, oligo(ethylene glycol) methyl ether methacrylate $\overline{M}_n$ 300 (MeOEGMA), oligo(ethylene glycol) methacrylate $\overline{M}_n$ 526 (HOEGMA), *N*,*N*-dimethylformamide (99.5%), fetal bovine serum (FBS), and phosphate-buffered saline (PBS), pH 7.4, were obtained from Sigma–Aldrich, Czech Republic. *N*-[3-(dimethylamino) propyl] acrylamide (DMAPA, 98%) and β-propiolactone (90%) were from TCI Europe and Serva Electrophoresis GmbH, respectively. HCl (37%) was purchased from Roth. Ethanol (96%), methanol (99.5%), acetone, and hexane were obtained from Lachner, Czech Republic. Tetrahydrofuran (THF, 99.5% extra dry) was purchased from Acros Organics, Czech Republic. All materials, reagents, and solvents were used as received.

The monomers *N*-(2-hydroxypropyl) methacrylamide (HPMA) and (3-acryloylaminopropyl)(2-carboxyethyl) dimethylammonium (carboxybetaine acrylamide, CBAA) were synthesized according to the literature procedures (see the Supporting Information).[31,37]

Dulbecco's Modified Eagle Medium (DMEM), F12 Nutrient Mixture Kaighn's Modification (F12), goat-anti mouse Alexa Fluor 647 antibodies, L-glutamine, Penicillin–Streptomycin, phalloidin Alexa Fluor 568, phosphate-buffered saline (PBS), and trypsin/EDTA were purchased from life technologies. Fetal bovine serum (FBS) was purchased from GE Healthcare, USA. 4-(2-hydroxyethyl)-1-piperazineethane-sulfonic acid (HEPES) and TritonX-100 were purchased from Roth. 4′,6-diamidino-2-phenylindole (DAPI), mowiol, and paraform-aldehyde (PFA) were purchased from Sigma–Aldrich, Germany. Antibodies against mouse paxillin were purchased from BD Biosciences, USA.

2.2. Modification of PCL-Nanofibers

2.2.1. Formation of PDA Film on the Surface of Nanofibers (PCL-PDA)

Dopamine hydrochloride was dissolved in 10 mM Tris buffer (pH 8.5) to a concentration of 2 mg · mL^{-1}. The deposition/polymerization of PDA on the surface of the nanofibers was performed in open glass dishes and under controlled stirring that provided a continuous supply of oxygen through the air–solution interface. The PCL nanofibers were fixed in vertical position to ensure a constant stream of the reactive solution and to minimize microparticle sedimentation.

After 3 h of polymerization, the coated PCL nanofibers (PCL-PDA) were rinsed with water, sonicated in water for 15 min to remove residual dopamine monomer, and lyophilized overnight.

2.2.2. Immobilization of ATRP Initiator on the Surface of PCL-PDA Nanofibers (PCL-PDA-Br)

The initiator (BIBB) was covalently attached to the PDA anchoring layer by acylation to hydroxy- and amino- groups present at the surface of PDA.[44] PLC-PDA nanofibers were immersed in a solution of TEA in dry hexane (0.18 M, 20 mL) at 0 °C and shaken for 30 min. A solution of BIBB in dry hexane (0.32 M, 10 mL) was added. After 15 min, the fibers were removed from the reaction solution and washed with hexane, acetone, ethanol, and immersed in Milli-Q water for 2 d. Water was changed every 5 h. Then PCL-PDA-Br nanofibers were freeze-dried for the following modification.

2.2.3. Polymerization of MeOEGMA From the Surface of Nanofibers

The polymerization was carried out according to a modified procedure reported earlier.[62] The solution of MeOEGMA (13.65 g, 45.5 mmol) in water (12 mL) was degassed by bubbling Ar for 1 h. The solid compounds $CuBr_2$ (41.1 mg, 0.18 mmol), CuBr (129 mg, 0.9 mmol), BiPy (374.4 mg, 2.4 mmol), were separately degassed by six cycles of vacuum–Ar and dissolved by adding previously degassed methanol (12 mL). Subsequently, the catalyst solution was transferred to the monomer solution. The polymerization mixture was transferred under Ar atmosphere to the reactors containing the PCL-PDA-Br nanofibers and the polymerization was allowed to proceed for 30 min at 30 °C. The fibers coated with poly(MeOEGMA) (PCL-PDA-poly(MeOEGMA)) were subsequently washed with ethanol (4 h) and Mili-Q water for 2 d. Finally, the PCL-PDA-poly(MeOEGMA) nanofibers were freeze-dried.

2.2.4. Polymerization of HOEGMA From the Surface of Nanofibers

The polymerization was carried out according to a modified procedure reported earlier.[37] The solution of HOEGMA (10 g, 19 mmol), $CuBr_2$ (8.1 mg, 0.036 mmol), and BiPy (144.8 mg, 0.928 mmol) in water (10 mL) was degassed by bubbling Ar for 1 h. Then, the CuCl (37 mg, 0.37 mmol) was added to the polymerization solution and mixed for 30 min. The polymerization mixture was transferred under Ar atmosphere to the reactors containing the PCL-PDA-Br nanofibers. The polymerization was allowed to proceed for 30 min at 30 °C. The fibers coated with poly(HOEGMA) (PCL-PDA-poly(HOEGMA) were washed subsequently in ethanol and Mili-Q water for 2 d. Finally, the PCL-PDA-poly(HOEGMA) nanofibers were freeze-dried.

2.2.5. Polymerization of HPMA and CBAA From the Surface of Nanofibers

The polymerization was carried out according to a modified procedure reported earlier.[37] Briefly, a mixture of ethanol (7 mL) and water (3 mL) was degassed using six freeze–pump–thaw cycles and transferred to a Schlenk tube containing CuBr (19.1 mg, 0.133 mmol), $CuBr_2$ (5.9 mg, 0.026 mmol), and Me_4Cyclam (40.9 mg, 0.16 mmol). The blue solution of the catalyst was added to the monomer HPMA (953 mg, 6.8 mmol) or CBAA (1500 mg, 6.7 mmol). Finally, the polymerization solution was transferred to the reactor containing the PCL-PDA-Br nanofibers. Reaction proceeded for 2 h at 30 °C. The fibers coated with poly(HPMA) (PCL-PDA-poly(HPMA)) or poly(CBAA) (PCL-PDA-poly(CBAA)) were washed subsequently with ethanol (4 h) and Mili-Q water for 2 d with periodic water change. Finally, the PCL-PDA-poly(HPMA) and PCL-PDA-poly(CBAA) nanofibers were freeze-dried.

2.3. Model Experiments

2.3.1. Thickness of Polymer Brushes

To assess the thickness of the prepared polymer brushes, a model system on silicon wafers, treated in the same way as PCL nanofibrous meshes, was utilized. The referenced samples consisted of silicon substrates polished on one side (CZ, orientation <100>, B-doped, resistivity 5–20 Ω cm, Siegert Consulting e.K, Germany) bearing a 50 nm thick SiO_2 overlayer. The bare substrates were cut into 1.2×1.2 cm^2 pieces, and were subsequently cleaned by sonication in methanol for 15 min and deionized water for 15 min and finally treated by plasma (25 W, Plasma Cleaner/Sterilizer, Harrick, USA) for 5 min just before the immobilization of PDA layer. The deposition of PDA layer and immobilization of ATRP initiator were performed in an identical method, as described for PCL nanofibrous meshes. In order to accurately estimate the thickness of the polymer brushes grown from PCL nanofibers, the silicon wafers with deposited PDA layer and immobilized ATRP initiator were placed together with nanofibers in the same reactor. After polymerization, the Si substrates were washed with ethanol and Milli-Q water and the thickness of polymer brushes was measured by spectroscopic ellipsometry.

2.3.2. Protein Fouling Experiment

Protein fouling after contact with 10% FBS and cell culture media (CM) containing 10% of FBS was assessed by SPR. For this, polymer brushes were grown from initiator immobilized on PDA on gold-coated SPR chips. The SPR chips were rinsed with ethanol and water, blow dried with nitrogen, and cleaned with UV-ozone cleaner (Jelight) for 15 min. The deposition of PDA, immobilization of ATRP initiator, polymerization of poly(MeOEGMA), poly(HOEGMA), poly(HPMA), and poly(CBAA) were performed identically as described for the nanofibrous meshes and the referenced samples. The polymerization time was adjusted for each monomer to obtain brushes with thickness of 20 nm: poly(MeOEGMA): 15 min, poly-(HOEGMA): 12 min, poly(CBAA): 1.5 h, and poly(HPMA): 2 h. This is necessary to be able to perform SPR measurements.

2.4. Characterization Techniques

2.4.1. Scanning Electron Microscopy (SEM)

The morphology of the nanofibers was obtained by an ultra-high-resolution field emission scanning electron microscope

Macromolecular Journals

Macromol. Biosci. **2015,** DOI: 10.1002/mabi.201500252

(FE-SEM, MAIA3, Tescan Orsay Holding). The images were taken at low accelerating voltages of the primary electrons of 3–5 kV. An in-lens detector was used to image the investigated surface. All samples were in their pristine (natural) state without any conductive coating.

2.4.2. X-Ray Photoelectron Spectroscopy (XPS)

X-ray photoelectron spectroscopy measurements were performed using a K-Alpha XPS spectrometer (Thermo Fisher Scientific, East Grinstead, UK). All of the samples were analyzed using a microfocused, monochromated Al Kα X-ray source (400 μm spot size). The kinetic energy of the electrons was measured by a 180° hemispherical energy analyzer operated in the constant analyzer energy mode (CAE) at 50 eV pass energy for elemental and high-resolution spectra. Data acquisition and processing using the Thermo Avantage software are described elsewhere.[63] The spectra were fitted with one or more Voigt profiles (binding energy uncertainty: +/−0.2 eV). The analyzer transmission function, Scofield sensitivity factors,[64] and effective attenuation lengths (EALs) for photoelectrons were applied for quantification. EALs were calculated using the standard TPP-2M formalism.[65] All spectra were referenced to the C1s peak of hydrocarbon at 285.0 eV binding energy which was controlled by means of the well-known photoelectron peaks of metallic Cu, Ag, and Au.

2.4.3. Spectroscopic Ellipsometry (SE)

The measurements were performed using Variable Angle Spectroscopic Imaging Auto-Nulling Ellipsometer EP^3-SE (Nanofilm Technologies GmbH, Germany) in the wavelength range of $\lambda = 399–811$ nm (source Xe-arc lamp, wavelength step ≈10 nm) at an angle of incidence AOI = 70° in air at room temperature. For assessing the uniformity of the modifications, all samples were measured at three points. The obtained SE spectra were fitted with multilayer models in the EP^3-SE analysis software. The thickness and refractive index of polymer layers were obtained from simultaneous fitting the obtained ellipsometric data using Cauchy relationship model. Due to the low penetration depth of light, the gold layer was modeled as bulk gold using predefined EP^3-SE dispersion function. The optical dispersion functions of silicon, silicon dioxide, and PDA were taken from earlier studies.[49,66]

2.4.4. Infrared Reflection Absorption Spectroscopy (IRRAS)

The infrared spectra of the dry polymer brushes grown from SPR chips with initiator attached to PDA films (thickness of 10.5 ± 1.1 nm) were recorded using a Thermo Nicolet NEXUS 870 FTIR Spectrometer equipped with a deuterated triglycine sulfate thermoelectric-cooled detector, and a Smart SAGA grazing angle (80°, p-polarization) reflection spectroscopy accessory (Thermo Fisher Scientific). The measurement chamber was continuously purged with dry air. The spectra (512 scans per spectrum at a resolution of 2 cm^{-1}) are reported as $-\log(R/R_0)$, where R is the reflectance of the sample and R_0 is the reflectance of initiator-PDA layers on gold.

2.5. Biological Studies

2.5.1. Cell Culture

Mouse embryonic fibroblasts (MEFs) were kindly provided by Clemens Franz, KIT, Germany. MEF cells were cultured in DMEM + 10% v/v FBS at 37 °C in a humidified atmosphere of 5% CO_2.

2.5.2. Cell Adhesion Studies via Live Imaging and Immunostaining

The original and modified nanofibers were incubated in PBS for 12 h. Prior to cell seeding, the substrates were placed in six-well culture plates containing imaging medium (F12 culture medium, 25 mM Hepes, 2 mM l-glutamine, 1% v/v penicillin/streptomycin and 10% v/v FBS). Trypsinized cells were resuspended in imaging medium and 150 000 cells were seeded onto each substrate. Imaging was performed on a Zeiss ApoTome Imager Z1 microscope with a 40×/0.75 Zeiss water immersion objective in hourly intervals. Subsequently, cells were fixed after 7 or 24 h with 4% w/v paraformaldehyde in PBS at ambient temperature for 10 min and permeabilized by washing three times with PBS containing 0.1% v/v Triton X-100. The samples were incubated for 1 h at ambient temperature with primary antibodies (mouse anti-paxillin). Incubation with secondary antibodies (goat anti-mouse Alexa 647), phalloidin Alexa 568, and 4′,6-diamidino-2-phenylindole (DAPI) was also performed for 1 h at room temperature. After each incubation step, the samples were washed three times with PBS-Triton. The samples were mounted on glass slides by covering them with Mowiol and cover slips, and imaged using 5×/0.25 or 10×/0.3 Zeiss objectives. Images were acquired in ApoTome mode to obtain optical sections of the samples and to increase resolution in the axial direction. Cell size was assessed by Particle Analysis using ImageJ (NIH, Maryland, USA).

3. Results and Discussion

In this study, we report a new approach for the modification of PCL nanofibers by growing antifouling polymer brushes to prevent protein fouling from biological fluids and non-specific cell adhesion. In order to generate functional groups for the effective immobilization of ATRP initiator, a multifunctional biomimetic layer of PDA was deposited on the nanofibers surface (PCL-PDA) (Scheme 1).

Subsequently, ATRP initiator was immobilized to the hydroxy- and amino- groups present at the surface of PDA.[49] Polymer brushes of MeOEGMA, HOEGMA, HPMA, and CBAA were grown from the activated PCL-PDA-Br meshes utilizing SI-ATRP, which allows good control over the polymer brush properties while maintaining the surface confinement of the polymer chains. The selection of these four polymer brushes is based on our previous studies, in which they displayed excellent resistance to fouling from blood plasma, several bodily fluids, FBS, bacterial adhesion.[24,32,38,39,47] The resistance to protein

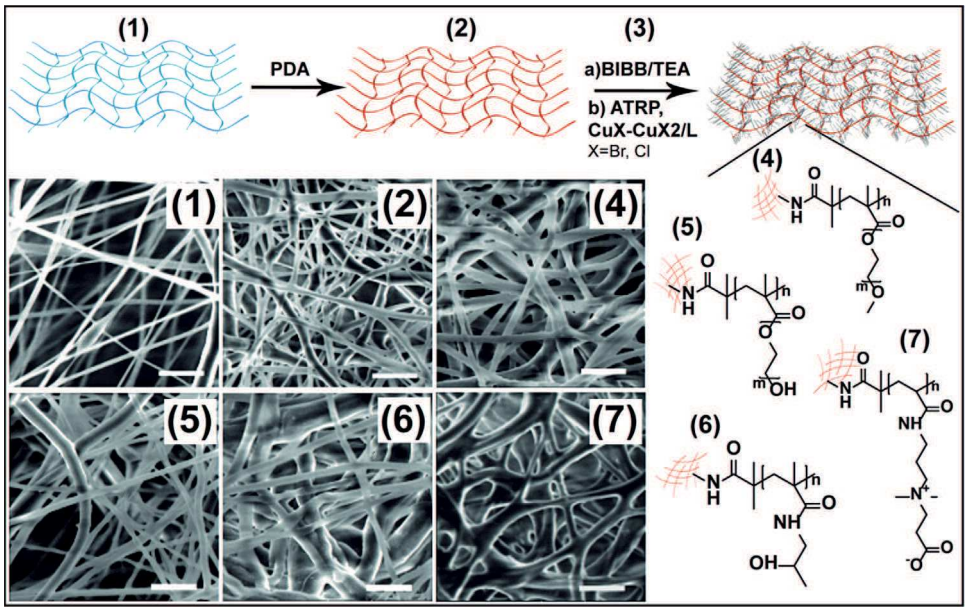

Scheme 1. The sequence of modification of PCL nanofibers and corresponding SEM images of (1) bare PCL, (2) PCL-PDA, (4) PCL-PDA-poly(MeOEGMA), (5) PCL-PDA-poly(HOEGMA), (6) PCL-PDA-poly(HPMA), and (7) PCL-PDA-poly(CBAA) nanofibers. Images were acquired at 20.0 kx magnification. Scale bar equals 2 μm.

fouling was evaluated by SPR on a model system while cell adhesion was studied by seeding of MEFs on the pristine and modified nanofibers.

3.1. Modification of Nanofibers

A PDA layer was deposited on the surface of PCL nanofibers (Scheme 1). The successful deposition of PDA layer was confirmed by XPS analysis. An increase of the contribution at 285.0 eV, corresponding to sp^2 and sp^3 carbon species, is clearly observed in the C 1s spectrum (Figure 1). Concomitantly, in the N 1s spectra of PCL-PDA we observed the appearance of a peak at 400.1 eV assigned to the predominant secondary amine groups of indole, nonprotonated and protonated primary amine, and imine functionalities of PDA (Figure 1).[24] The SEM images clearly show that the morphology of the fibers was preserved after the PDA polymerization. The PDA layer perfectly matched the morphology of the bare fibers (Scheme 1) while no PDA aggregates could be observed. The presence of these aggregates would impair the complex interpenetrating architecture of the PCL mesh and could give rise to instability of the subsequent polymer brush layers.[49,67]

The ATRP initiator was acylated to the residual amine and catechol groups of the PDA layer (Scheme 1). The immobilization of BIBB is evidenced by the appearance of pronounced peaks at 70.2 and 71.2 eV in Br 3d high-resolution XPS spectra corresponding to [Br–C] bonds (Figure S1). [23,68]

Polymer brushes based on MeOEGMA, HOEGMA, HPMA, and CBAA were grown from the initiator molecules immobilized on PCL-PDA nanofibers by SI-ATRP (Scheme 1). The monomers were chosen for the fabrication of brushes due to their excellent resistance to protein fouling and their ability to passivate surfaces against cell adhesion.[31,32,38] In light of the challenges for measuring the thickness of the brushes grown from nanofibers, we utilized a simple two-dimensional model system. Silicon wafers coated with PDA layer and immobilized initiator were placed together with nanofibers in the same reactor during polymerization. The thicknesses of polymer brushes grown by SI-ATRP were assessed by SE (Table 1). The thickness of the brushes was in the range of 20–46 nm which is typically sufficient to prevent fouling.[32,44]

The composition of the polymer brushes on PCL-PDA nanofibers was confirmed by XPS. Analysis of the C 1s spectra of PCL-PDA-poly(MeOEGMA) and PCL-PDA-poly(HOEGMA) brushes shows a strong increase of the contribution at 286.4 eV assigned to [C–O] bonds of the oligo(ethylene glycol) side chains of the brush and a decrease of the signal at 285.0 eV (Figure 1).[38]

The absence of any contributions characteristic of PDA in the high-resolution N 1s spectra confirms the complete coverage of the PLC-PDA-Br surfaces with thick polymer brushes of poly(MeOEGMA) and poly(HOEGMA). The XPS spectra of poly(HPMA) brushes displayed characteristic contributions at 287.8 eV in the C 1s spectrum and the significant narrowing of the peak at 400.0 eV in N 1s spectrum confirming the presence of the [O=C–N] groups

Macromolecular Journals
Macromol. Biosci. **2015,** DOI: 10.1002/mabi.201500252

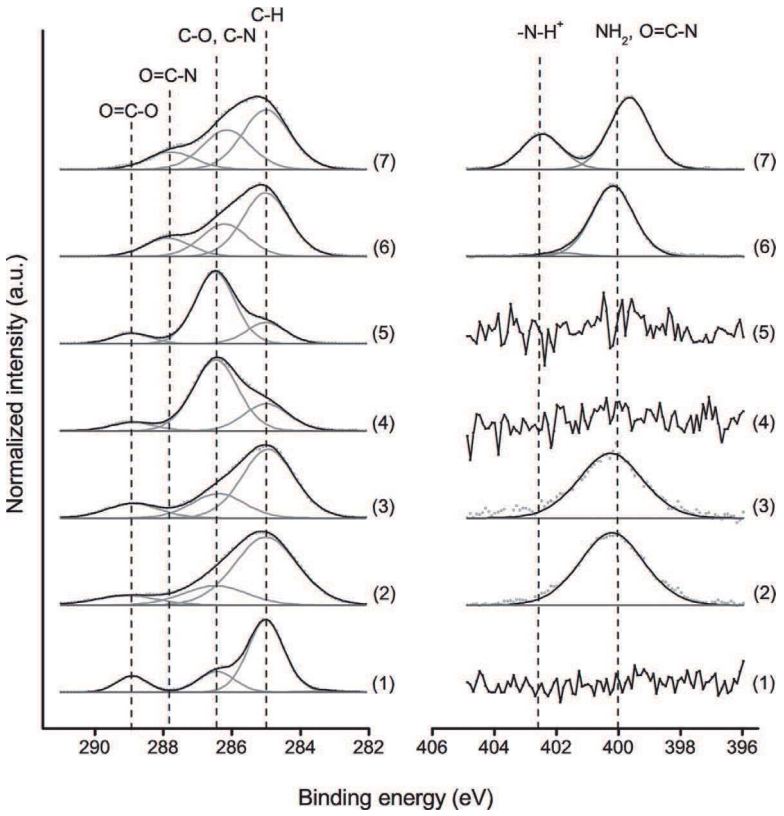

Figure 1. C 1s and N 1s high-resolution XPS spectra of nanofibers; (1) bare PCL, (2) PDA-modified (PCL-PDA), (3) PCL-PDA with immobilized ATRP initiator (PCL-PDA-Br), (4) PCL-PDA-poly(MeOEGMA), (5) PCL-PDA-poly(HOEGMA), (6) PCL-PDA-poly(HPMA), and (7) PCL-PDA-poly(CBAA).

(Figure 1). The C 1s spectrum of PCL-PDA-poly(CBAA) is characterized by a peak at 287.8 eV from the amide functionality (Figure 1).[24] Moreover, the N 1s spectrum of PCL-PDA-poly(CBAA) nanofibers shows a pronounced signal at 402.7 eV characteristic of the quaternary amine [$-N^+(CH_3)_2-$] species of the zwitterionic side chain of the polymer brushes (Figure 1).[24] The absence of XPS spectral features characteristic for the PDA and PCL mesh indicate that the outermost surface of the fibers is modified with a thick confluent polymer brush layer similar to the one observed in the SE measurements on the model systems.

Table 1. The thickness of polymer brushes determined by SE on a model system.

Polymer brush	Thickness [nm]
Poly(MeOEGMA)	46.2 ± 2.5
Poly(HOEGMA)	41.5 ± 2.7
Poly(HPMA)	40.0 ± 2.2
Poly(CBAA)	24.3 ± 1.7

The SEM analysis showed that the polymerization was confined to the surface of the nanofibers, increasing their diameter while the morphology of the individual fibers and the highly interpenetrating porous structure of the mesh were not altered (Scheme 1).

3.2. Protein Fouling

Cell adhesion to artificial materials is usually mediated by a pre-adsorbed layer of proteins, which is formed by the irreversible adsorption from complex biological media present in cell culture. In order to determine the protein adsorption from biological fluids used in cell adhesion studies, a model system analogous to the PCL-PDA-(non-fouling polymer brushes) nanofibers was used. The gold-coated SPR chips were covered with PDA anchoring layer to which ATRP initiator was immobilized. Polymer brushes of MeOEGMA, HOEGMA, HPMA, and CBAA were synthesized in an identical way as was described for PCL nanofibers, but the thicknesses of the brushes were tuned to approximately 20 nm to enable use of SPR for the assessment of fouling. Due to the evanescent nature of the electromagnetic field exploited for SPR, thicker brushes would result in insufficient sensitivity and loss of linearity.[69] The dry thicknesses of PDA layers (10.5 ± 1.1 nm) and polymer brushes of MeOEGMA (17.4 ± 0.4 nm), HOEGMA (18.1 ± 0.7 nm), HPMA (17.5 ± 0.8 nm), and CBAA (17.6 ± 1.8 nm) were determined by SE. The chemical composition of the polymer brushes on the SPR chips was determined by IRRAS (Figure 2). The spectra show four characteristic regions having their origin in (1) the O–H and N–H stretching modes, (2) C–H stretching modes of alkyl and ether moieties of the polymers, (3) the C═O and NH modes arising from the ester and secondary amide bonds of methacrylate (poly(MeOEGMA) and poly(HOEGMA)), and methacrylamide (poly(HPMA)) and acrylamide (poly(CBAA)) polymers, respectively, and (4) the different scissoring, wagging, twisting, stretching, rocking, as well as skeletal vibrations from different conformers of the EO and alkyl subunits.[37,43,44,70] The broad bands above 3200 cm^{-1} arise from the H-bonded hydroxyl of poly(HOEGMA) and poly(HPMA), as well as residual water molecules throughout the polymer films. These bands overlap with the contributions from the stretching modes of free and hydrogen-bonded amines of PDA and secondary amides of poly(CBAA) and poly(HPMA).

Macromol. Biosci. **2015,** DOI: 10.1002/mabi.201500252

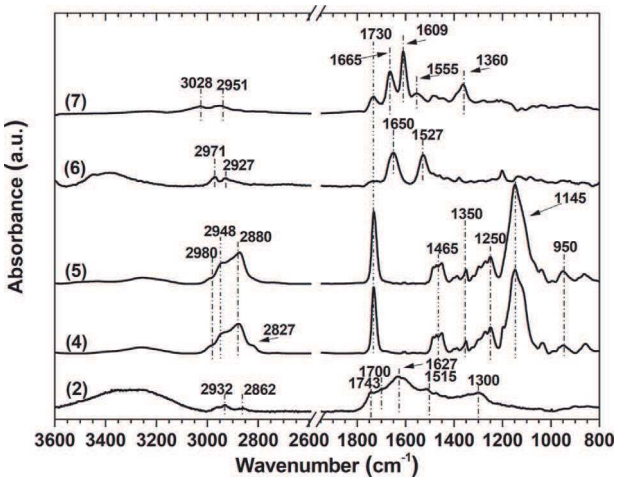

Figure 2. IRRAS spectra of (2) PDA, (4) poly(MeOEGMA), (5) poly(HOEGMA), (6) poly(HPMA), and (7) poly(CBAA). The spectra of the polymer brushes were acquired against initiator-PDA background.

In the C–H region, the spectrum of the PDA anchor exhibits bands at 2932 and 2862 cm^{-1} originating from the alkyl chains of dopamine units that did not undergo cyclization[44,56,57,71] and TRIS molecules which might be incorporated in the covalent structure of PDA[72,73] during the course of the polymerization reaction.

In the same region, the spectra of polymer brushes of poly(HOEGMA) and poly(MeOEGMA) (Figure 2) are dominated by bands at 2948 and 2880 cm^{-1} characteristic of the asymmetric and symmetric CH_2 stretching vibrations of the ethylene oxide side chains, respectively. The latter band overlapped the contributions arising from the CH_3 symmetric stretching modes, whereas the corresponding CH_3 asymmetric stretching modes gave rise to a weak and broad shoulder at 2980 cm^{-1}. The spectrum of poly(MeOEGMA) is characterized by an additional band at 2827 cm^{-1} which is specific for the methoxy terminating group (OCH_3) of the side chains. In the same region, the spectrum of poly(HPMA) is characterized by two broad features at 2971 and 2927 cm^{-1} stemming from different CH_3 and CH_2 stretching vibrations of the polymer backbone and the N-(2-hydroxypropyl) side chains. The spectrum of poly(CBAA) shows a distinctive band at 3028 cm^{-1} arising from the asymmetric stretching modes of CH_3 attached to the quaternary nitrogen of the zwitterionic group.[74]

Below 2000 cm^{-1}, the PDA spectrum shows a broad-band structure with many overlapping modes (C=O stretching vibration (1743 and 1700 cm^{-1} of hydrogen-bonded and free quinone groups respectively), C=C aromatic ring vibrations of the different PDA subunits (1627, 1607, 1585, and 1436 cm^{-1}), C=N pyrrole ring stretching vibrations (1515 cm^{-1}), C–O stretching (1300 cm^{-1}), etc.).[75] The spectra of poly(MeOEGMA) and poly(HOEGMA) brushes exhibit a strong peak at 1730 cm^{-1} arising from the ester carbonyl. In the same spectral region, poly(CBAA) brushes display an amide I band at 1665 cm^{-1}, a dominant peak of ionized carboxyl (COO^-) at 1609 cm^{-1} (asymmetric stretching), and an amide II band at 1555 cm^{-1}.[37,74] The amide I and II bands in the spectrum of poly(HPMA) brushes appear at 1650 and 1527 cm^{-1}, respectively.

In the fingerprint region (below 1500 cm^{-1}), poly(MeOEGMA) and poly(HOEGMA) brushes are characterized by a family of bands having their origin in CH_2 scissoring (≈1465 cm^{-1}), wagging (≈1350 cm^{-1}), twisting (≈1250 cm^{-1}), and rocking (≈950 cm^{-1}) modes. The strongest band in the spectra of poly(MeOEGMA) and poly(HOEGMA) brushes at 1145 cm^{-1} is assigned to the C–O–C stretching vibrations of OEG. The spectrum of poly(CBAA) brushes is dominated by a band at 1360 cm^{-1} originating from the symmetric stretching mode of COO^-. All spectra show weak contributions of asymmetric and symmetric C–CH_3 deformation vibrations at about 1450 and 1380 cm^{-1}. The IRRAS findings verified the successful polymerization and proved the covalent structure of the polymer brushes grown from the activated PDA anchor layer by SI-ATRP.

Protein fouling from complex and highly fouling biological media, i.e., FBS (10%) and CM, was monitored in situ by SPR (Figure 3, Figure S2). In order to be able to utilize this technique, the brushes needed to be grown from gold-coated SPR chips. It is important to note that we have previously shown that this model bears high resemblance to brushes grown on other more complex systems.[20,37]

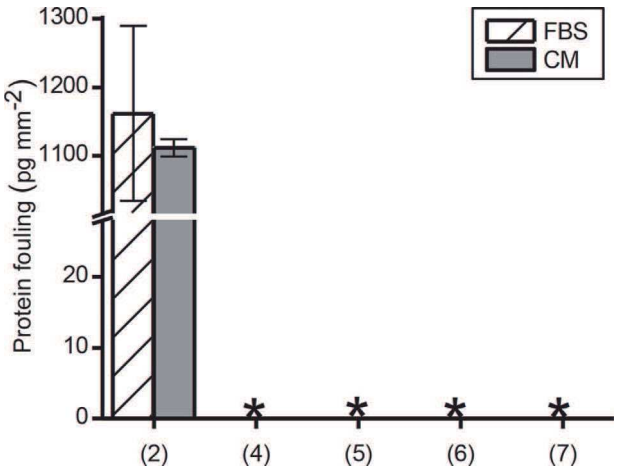

Figure 3. Protein fouling from 10% FBS solution and cell culture media (CM) on (2) bare PDA layer and polymer brushes of (4) MeOEGMA, (5) HOEGMA, (6) HPMA, and (7) CBAA grown from PDA determined by SPR. (*)—fouling below the limit of the SPR detection of 3 pg · mm^{-2}. The fouling from 10% FBS on bare PCL was determined 950 pg · mm^{-2}.[20]

Macromolecular Journals

Macromol. Biosci. **2015,** DOI: 10.1002/mabi.201500252

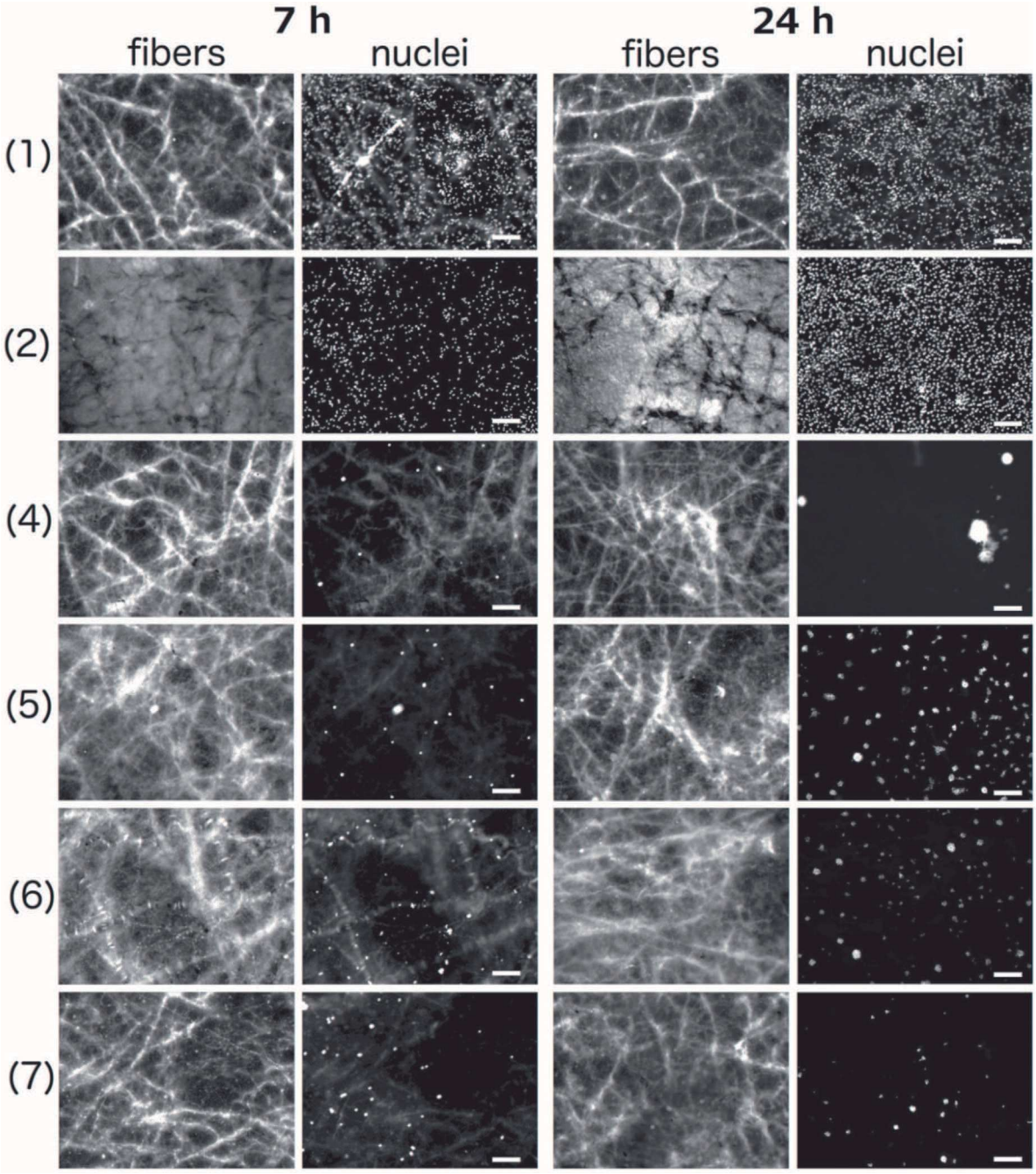

Figure 4. Cell adhesion on (1) PCL, (2) PCL-PDA, (4) PCL-PDA-poly(MeOEGMA), (5) PCL-PDA-poly(HOEGMA), (6) PCL-PDA-poly(HPMA), and (7) PCL-PDA-poly(CBAA) nanofibers after 7 and 24 h (scale bar 200 μm). Fibers are visualized by their autofluorescence after excitation at 488 nm, cell nuclei by staining with DAPI and 405 nm excitation. It should be noted that low number of cells on nanofibers with polymer brushes (4–7) required higher excitation energy to visualize them. Therefore, in some cases the autofluorescence of the fibers is visible in the 405 nm channel.

Upon contact with FBS and CM, very large protein fouling (1162 and 1112 pg · mm^{-2}) was observed on PDA-coated gold surfaces in agreement with our previous findings. On the other hand, after contact with 10% FBS and CM, no fouling could be detected on any of the surfaces modified with polymer brushes using an SPR with a detection limit 3 pg · mm^{-2}, thus proving the excellent resistance to fouling of these brushes grown from PDA.

In previous studies, it has been shown that poly(CBAA) displays a stronger association with water via ionized

Macromol. Biosci. **2015,** DOI: 10.1002/mabi.201500252

groups compared to the other brushes presented in this work. However, the resistance to fouling of all the brushes suggests that non-fouling properties are mediated by more complex mechanisms than simple hydration or wettability.

3.3. Cell Adhesion Experiments

The passivation of the nanofibers against cell adhesion was assessed by seeding MEFs on PCL, PCL-PDA, and the nanofibrous meshes bearing the selected polymer brushes (PCL-PDA-poly(MeOEGMA), PCL-PDA-poly(HOEGMA), PCL-PDA-poly(HPMA), and PCL-PDA-poly(CBAA)). The nanofibers were incubated with MEF cells for 7 and 24 h at 37 °C, cultivated in cell culture medium with 10% v/v FBS, to probe the cell adhesion behavior. The cells on the samples were fixed and stained for paxillin (marker of cell–matrix adhesions, CMAs), actin (marker of cytoskeleton), and cell nuclei. Microscopic images reveal that after 7 h cells adhered in high numbers throughout the PCL and PCL-PDA nanofibrous meshes (Figure 4, Figure S3). Furthermore, three-dimensional high-resolution reconstructions of ApoTome optical sections (Figure 5) show that they were even able to penetrate the porous PCL nanofibrous mesh and to grow three-dimensionally. The fibroblasts adapted their shape to the nanofibers and made preferential contact with them. This, together with distinct paxillin-positive clusters, indicates that cells were able to establish functional, signaling-competent CMAs which truly mimicked cell–matrix interactions. The average cell size was estimated using particle analysis by ImageJ software. The cell size on PCL nanofibers averaged over the whole population of cells shown in Figure 5 was 530 μm^2. This value is in accordance to published measurements for cells adhering to environments with discontinues in the ECM.[76]

These observations indicate that the fibroblasts were able to use the non-specifically adsorbed protein deposits on PCL and PCL-PDA as a substitute for extracellular matrix. Importantly, the behavior of fibroblasts on PCL meshes modified with polymer brushes was in sharp contrast to pristine PCL and PDA-PCL. Namely, after 7 h cells did not adhere on any of the nanofibers modified with antifouling polymer brushes (Figure 4, Figure S3). The polymer brushes minimize the cell–surface interactions.

Only after 24 h could some fibroblasts be detected among the modified nanofibers. However, close examination of ApoTome optical sections (Figure 5) shows that the fibroblasts did not adhere to the nanofibers but rather stuck to each other. The fibroblasts acquired a roundish shape, organizing themselves in non-spread cell clusters that were only entrapped among the polymer-brush-modified fibers. Paxillin accumulated in the cytoplasm and no clear colocalization between paxillin and fibers was observed, indicating that cells failed to establish CMAs. It is worth noting that fibroblasts like NIH 3T3 cells used in this work preferably adhere to ECM and avoid forming colonies in

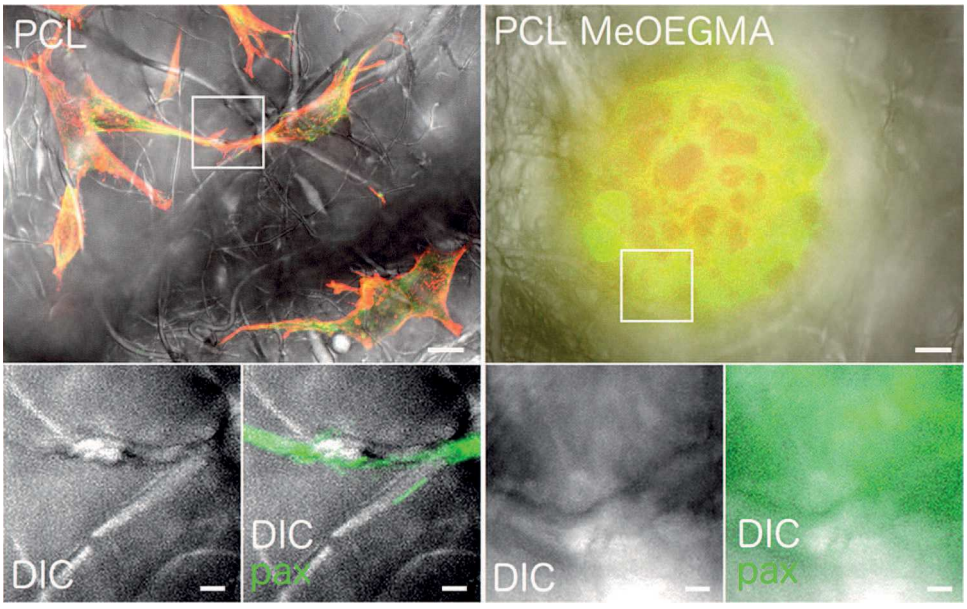

Figure 5. ApoTome optical sections of a three-dimensional image stack at high magnification for cells on PCL and PCL-PDA-poly(MeOEGMA) nanofibers after 24 h. An overview (upper row) shows that the cells adapt their shape to PCL but not to PCL-PDA-MeOGMA nanofibers. Actin (red) indicates cell shape, paxillin (green) cell–matrix adhesions (CMAs) while nanofibers are shown in grayscale. Zoom in of the white boxes (lower row) show clear colocalization for paxillin (green) and PCL (grayscale) but not for paxillin and PCL-PDA-MeOEGMA (garyscale). Scale bars equal 10 μm in first upper row and 2 μm—in lower row.

Macromolecular Journals
Macromol. Biosci. **2015,** DOI: 10.1002/mabi.201500252

physiological situations.[77] As shown above, proteins from the culture media do not adhere to the interfaces modified with brushes. Accordingly, this lack of surface adsorbed proteins is believed to be the reason preventing the formation of CMAs on the nanofibers modified with brushes, leading to the inability of the cells to adhere, spread, and proliferate on the nanofibers modified with polymer brushes (Figure 5). Since all the studied brushes fully prevented the adsorption of proteins from culture media, no important differences among them were observed.

Therefore, all polymer brushes tested showed a remarkable passivation against cell adhesion. Although demonstrated only on PCL nanofibers, the presented surface modification approach, utilizing a substrate-independent PDA anchor layer and SI-ATRP of non-fouling polymer brushes, can be envisioned as a promising route for the modification of other materials being used as vascular grafts or wound dressing, as well as anti-adhesive barriers capable of preventing blood coagulation and tissue adhesion.

4. Conclusion

A new route to passivate the surface of the nanofibers was introduced. Antifouling polymer brushes of MeOEGMA, HOEGMA, HPMA, and CBAA were grown by SI-ATRP from initiators covalently bonded to an ad-layer of PDA. The facile deposition of the PDA layer accounted for the maintenance of the morphology of the fibers. All of the brushes displayed an excellent resistance to protein fouling from complex biological fluids as assessed on a model system using SPR. The resistance to non-specific cell adhesion was evaluated by challenging the fibers with fibroblasts. Fibroblast rapidly adhered to pristine PCL and PDA-coated nanofibers. Microscopic examinations showed that adhered cells on PCL and PCL-PDA nanofibers were well spread, elongated along the fibers, and were connected to them via cell–matrix interactions as evidenced by the large number of focal contacts. On the other hand, cell adhesion was greatly suppressed on all of the fibers modified with antifouling brushes.

The few cells observed on the fibers modified with brushes were only entrapped into the three-dimensional mesh of nanofibers and failed to create any cell–matrix contacts, demonstrating that cells neither adhered nor spread on the nanofibers, thus proving the passivation provided by the brushes grown on PCL.

The unique non-fouling properties endowed to the PCL nanofibers in combination with the availability of functional groups exploitable for covalent immobilization of cell-binding biomolecules make the presented scaffolds a highly promising material for tissue engineering applications.

Acknowledgements: This work was supported by the Grant Agency of the Czech Republic (GACR) under contract No. 15-09368Y and the project "BIOCEV – Biotechnology and Biomedicine Centre of the Academy of Sciences and Charles University" (CZ.1.05/1.1.00/02.0109). N. N. acknowledges the support from the Ministry of Education, Youth and Sports of the Czech Republic (SGS No. 10/297/OHK4/3T/14LH13178). Mi. Ba. acknowledges funding by the Karlsruhe School of Optics and Photonics (KSOP). A. Kuzmyn is acknowledged for his help in the preliminary polymerization work.

Received: July 3, 2015; Revised: September 15, 2015; Published online: January 01, 2015; DOI: 10.1002/mabi.201500252

Keywords: antifouling; cell adhesion; nanofibers; polymer brushes; surface-initiated atom transfer radical polymerization (SI-ATRP)

[1] N. Huebsch, D. J. Mooney, *Nature* **2009**, *462*, 426.
[2] N. A. Peppas, J. Z. Hilt, A. Khademhosseini, R. Langer, *Adv. Mater.* **2006**, *18*, 1345.
[3] B. V. Slaughter, S. S. Khurshid, O. Z. Fisher, A. Khademhosseini, N. A. Peppas, *Adv. Mat.* **2009**, *21*, 3307.
[4] J. Drury, *Biomaterials* **2003**, *24*, 4337.
[5] B. D. Ratner, A. S. Hoffman, F. J. Schoen, J. E. Lemons, *"Biomaterials Science: An Introduction to Materials in Medicine, Second Edition"*, *Elsevier Academic Press*, San Diego, California, U.S.A. **2004**.
[6] T. J. Sill, H. A. von Recum, *Biomaterials* **2008**, *29*, 1989.
[7] A. Arinstein, E. Zussman, *J. Polym. Sci., Part B: Polym. Phys.* **2011**, *49*, 691.
[8] L. S. Nair, C. T. Laurencin, *Prog. Polym. Sci.* **2007**, *32*, 762.
[9] Y. Dong, S. Liao, M. Ngiam, C. K. Chan, S. Ramakrishna, *Tissue Eng., Part B* **2009**, *15*, 333.
[10] J. H. Kim, C. H. Park, O.-J. Lee, J.-M. Lee, J. W. Kim, Y. H. Park, C. S. Ki, *J. Biomed. Mater. Res., Part A* **2012**, *100A*, 3287.
[11] D. Kai, S. S. Liow, X. J. Loh, *Mater. Sci. Eng., C* **2014**, *45*, 659.
[12] H.-J. Sung, C. Meredith, C. Johnson, Z. S. Galis, *Biomaterials* **2004**, *25*, 5735.
[13] J. Širc, R. Hobzová, N. Kostina, M. Munzarová, M. Juklíčková, M. Lhotka, Š. Kubinová, A. Zajícová, J. Michálek, *J. Nanomater.* **2012**, 2012, 1.
[14] Y. Zhu, M. F. Leong, W. F. Ong, M. B. Chan-Park, K. S. Chian, *Biomaterials* **2007**, *28*, 861.
[15] H. S. Kim, H. O. Ham, Y. J. Son, P. B. Messersmith, H. S. Yoo, *J. Mater. Chem. B* **2013**, *1*, 3940.
[16] B. Wehrle-Haller, M. Bastmeyer, *"Chapter 18 - Intracellular signaling and perception of neuronal scaffold through integrins and their adapter proteins"*, in *Progress in Brain Research*, B. W .-H. Alexander Dityatev, P. Asla, Eds., Elsevier, Amsterdam, the Netherlands **2014**, p. 443.
[17] B. Wehrle-Haller, *Curr. Opin. Cell Biol.* **2012**, *24*, 116.
[18] B. Wehrle-Haller, *Curr. Opin. Cell Biol.* **2012**, *24*, 569.
[19] R. W. Sands, D. J. Mooney, *Curr. Opin. Biotechnol.* **2007**, *18*, 448.
[20] C. Rodriguez-Emmenegger, A. Jäger, E. Jäger, P. Stepanek, A. B. Alles, S. S. Guterres, A. R. Pohlmann, E. Brynda, *Colloids Surf., B* **2011**, *83*, 376.
[21] B. D. Ratner, *Biomaterials* **2007**, *28*, 5144.
[22] J. Zhu, *Biomaterials* **2010**, *31*, 4639.
[23] C. Rodriguez-Emmenegger, S. Janel, A. de los Santos Pereira, M. Bruns, F. Lafont, *Polym. Chem.* **2015**, *6*, 5740.

[24] F. Surman, T. Riedel, M. Bruns, N. Y. Kostina, Z. Sedláková, C. Rodriguez-Emmenegger, *Macromol. Biosci.* **2015**, *15*, 636.
[25] C. Blaszykowski, S. Sheikh, M. Thompson, *Chem. Soc. Rev.* **2012**, *41*, 5599.
[26] M. Krishnamoorthy, S. Hakobyan, M. Ramstedt, J. E. Gautrot, *Chem. Rev.* **2014**, *114*, 10976.
[27] S. R. Meyers, M. W. Grinstaff, *Chem. Rev.* **2012**, *112*, 1615.
[28] C. Blaszykowski, S. Sheikh, M. Thompson, *Trends Biotechnol.* **2014**, *32*, 61.
[29] J. Huang, D. Wang, Y. Lu, M. Li, W. Xu, *RSC Adv.* **2013**, *3*, 20922.
[30] Y. Cho, D. Cho, J. H. Park, M. W. Frey, C. K. Ober, Y. L. Joo, *Biomacromolecules* **2012**, *13*, 1606.
[31] C. Rodriguez Emmenegger, E. Brynda, T. Riedel, Z. Sedlakova, M. Houska, A. B. Alles, *Langmuir* **2009**, *25*, 6328.
[32] C. Rodriguez-Emmenegger, M. Houska, A. B. Alles, E. Brynda, *Macromol. Biosci.* **2012**, *12*, 1413.
[33] C. Rodriguez-Emmenegger, E. Brynda, T. Riedel, M. Houska, V. Subr, A. B. Alles, E. Hasan, J. E. Gautrot, W. T. Huck, *Macromol. Rapid Commun.* **2011**, *32*, 952.
[34] A. de los Santos Pereira, T. Riedel, E. Brynda, C. Rodriguez-Emmenegger, *Sens. Actuators, B* **2014**, *202*, 1313.
[35] M. Zamfir, C. Rodriguez-Emmenegger, S. Bauer, L. Barner, A. Rosenhahn, C. Barner-Kowollik, *J. Mater. Chem. B* **2013**, *1*, 6027.
[36] M. Vorobii, A. de los Santos Pereira, O. Pop-Georgievski, N. Y. Kostina, C. Rodriguez-Emmenegger, V. Percec, *Polym. Chem.* **2015**, *6*, 4210.
[37] C. Rodriguez-Emmenegger, O. Kylián, M. Houska, E. Brynda, A. Artemenko, J. Kousal, A. B. Alles, H. Biederman, *Biomacromolecules* **2011**, *12*, 1058.
[38] C. Rodriguez-Emmenegger, C. M. Preuss, B. Yameen, O. Pop-Georgievski, M. Bachmann, J. O. Mueller, M. Bruns, A. S. Goldmann, M. Bastmeyer, C. Barner-Kowollik, *Adv. Mater.* **2013**, *25*, 6123.
[39] T. Tischer, C. Rodriguez-Emmenegger, V. Trouillet, A. Welle, V. Schueler, J. O. Mueller, A. S. Goldmann, E. Brynda, C. Barner-Kowollik, *Adv. Mater.* **2014**, *26*, 4087.
[40] S. Chen, L. Li, C. Zhao, J. Zheng, *Polymer* **2010**, *29*, 5283.
[41] N. M. Pawlowska, H. Fritzsche, C. Blaszykowski, S. Sheikh, M. Vezvaie, M. Thompson, *Langmuir* **2014**, *30*, 1199.
[42] A. de los Santos Pereira, N. Y. Kostina, M. Bruns, C. Rodriguez-Emmenegger, C. Barner-Kowollik, *Langmuir* **2015**, *31*, 5899.
[43] C. Rodriguez-Emmenegger, E. Hasan, O. Pop-Georgievski, M. Houska, E. Brynda, A. B. Alles, *Macromol. Biosci.* **2012**, *12*, 525.
[44] O. Pop-Georgievski, C. Rodriguez-Emmenegger, A. de los Santos Pereira, V. Proks, E. Brynda, F. Rypáček, *J. Mater. Chem. B* **2013**, *1*, 2859.
[45] N. Y. Kostina, C. Rodriguez-Emmenegger, M. Houska, E. Brynda, J. Michálek, *Biomacromolecules* **2012**, *13*, 4164.
[46] N. Y. Kostina, S. Sharifi, A. de los Santos Pereira, J. Michálek, D. W. Grijpma, C. Rodriguez-Emmenegger, *J. Mater. Chem. B* **2013**, *1*, 5644.
[47] C. Rodriguez-Emmenegger, A. Decker, F. Surman, C. M. Preuss, Z. Sedlakova, N. Zydziak, C. Barner-Kowollik, T. Schwartz, L. Barner, *RSC Adv.* **2014**, *4*, 64781.
[48] R. Barbey, L. Lavanant, D. Paripovic, N. Schüwer, C. Sugnaux, S. Tugulu, H.-A. Klok, *Chem. Rev.* **2009**, *109*, 5437.
[49] O. Pop-Georgievski, S. Popelka, M. Houska, D. Chvostová, V. Proks, F. Rypáček, *Biomacromolecules* **2011**, *12*, 3232.
[50] H. Lee, S. M. Dellatore, W. M. Miller, P. B. Messersmith, *Science* **2007**, *318*, 426.
[51] B. H. Kim, D. H. Lee, J. Y. Kim, D. O. Shin, H. Y. Jeong, S. Hong, J. M. Yun, C. M. Koo, H. Lee, S. O. Kim, *Adv. Mater.* **2011**, *23*, 5618.
[52] B. S. Lee, J. K. Lee, W.-J. Kim, Y. H. Jung, S. J. Sim, J. Lee, I. S. Choi, *Biomacromolecules* **2007**, *8*, 744.
[53] K. Numata, P. J. Baker, *Biomacromolecules* **2014**, *15*, 3206.
[54] M. Yu, T. J. Deming, *Macromolecules* **1998**, *31*, 4739.
[55] J. H. Waite, N. H. Andersen, S. Jewhurst, C. Sun, *J. Adhes.* **2005**, *81*, 297.
[56] O. Pop-Georgievski, N. Neykova, V. Proks, J. Houdkova, E. Ukraintsev, J. Zemek, A. Kromka, F. Rypaček, *Thin Solid Films* **2013**, *543*, 180.
[57] O. Pop-Georgievski, D. Verreault, M.-O. Diesner, V. Proks, S. Heissler, F. Rypáček, P. Koelsch, *Langmuir* **2012**, *28*, 14273.
[58] M. Kaupp, A. S. Quick, C. Rodriguez-Emmenegger, A. Welle, V. Trouillet, O. Pop-Georgievski, M. Wegener, C. Barner-Kowollik, *Adv. Funct. Mater.* **2014**, *24*, 5649.
[59] V. Proks, J. Jaroš, O. Pop-Georgievski, J. Kučka, Š. Popelka, P. Dvořák, A. Hampl, F. Rypáček, *Macromol. Biosci.* **2012**, *12*, 1232.
[60] H. Wei, J. Ren, B. Han, L. Xu, L. Han, L. Jia, *Colloids Surf., B* **2013**, *110*, 22.
[61] D. Zheng, K. G. Neoh, Z. Shi, E. T. Kang, *J. Colloid Interface Sci.* **2013**, *406*, 238.
[62] A. Kuzmyn, A. de los Santos Pereira, O. Pop-Georgievski, M. Bruns, E. Brynda, C. Rodriguez-Emmenegger, *Polym. Chem.* **2014**, *5*, 4124.
[63] K. L. Parry, A. G. Shard, R. D. Short, R. G. White, J. D. Whittle, A. Wright, *Surf. Interface Anal.* **2006**, *38*, 1497.
[64] J. H. Scofield, *J. Electron Spectrosc. Relat. Phenom.* **1976**, *8*, 129.
[65] S. Tanuma, C. J. Powell, D. R. Penn, *Surf. Interface Anal.* **1994**, *21*, 165.
[66] C. M. Herzinger, B. Johs, W. A. McGahan, J. A. Woollam, W. Paulson, *J. Appl. Phys.* **1998**, *83*, 3323.
[67] O. Pop-Georgievski, D. Kubies, J. Zemek, N. Neykova, R. Demianchuk, E. M. Chanova, M. Slouf, M. Houska, F. Rypacek, *Beilstein J. Nanotechnol.* **2015**, *6*, 617.
[68] B. Yameen, N. Zydziak, S. M. Weidner, M. Bruns, C. Barner-Kowollik, *Macromolecules* **2013**, *46*, 2606.
[69] J. Homola, *Chem. Rev.* **2008**, *108*, 462.
[70] C. Rodriguez-Emmenegger, O. A. Avramenko, E. Brynda, J. Skvor, A. Bologna Alles, *Biosens. Bioelectron.* **2011**, *26*, 4545.
[71] F. Binns, J. A. G. King, S. N. Mishra, A. Percival, N. C. Robson, G. A. Swan, A. Waggott, *J. Chem. Soc. C* **1970**, *15*, 2063.
[72] N. F. Della Vecchia, A. Luchini, A. Napolitano, G. D'Errico, G. Vitiello, N. Szekely, M. d'Ischia, L. Paduano, *Langmuir* **2014**, *30*, 9811.
[73] N. F. Della Vecchia, R. Avolio, M. Alfè, M. E. Errico, A. Napolitano, M. d'Ischia, *Adv. Funct. Mater.* **2013**, *23*, 1331.
[74] J.-J. Max, C. Chapados, *J. Phys. Chem. A* **2004**, *108*, 3324.
[75] S. A. Centeno, J. Shamir, *J. Mol. Struct.* **2008**, *873*, 149.
[76] D. Lehnert, B. Wehrle-Haller, C. David, U. Weiland, C. Ballestrem, B. A. Imhof, M. Bastmeyer, *J. Cell Sci.* **2004**, *117*, 41.
[77] T. D. Pollard, W. C. Earnshaw, "*Cell Biology*", Saunders elsevier, Philadelphia, U.S.A. **2008**.

Macromol. Biosci. **2015,** DOI: 10.1002/mabi.201500252

Supporting Information

for *Macromol. Biosci.*, DOI: 10.1002/mabi.201500252

Non-fouling Biodegradable Poly(ε-caprolactone) Nanofibers for Tissue Engineering

Nina Yu. Kostina, Ognen Pop-Georgievski, Michael Bachmann, Neda Neykova, Michael Bruns, Jiří Michálek, Martin Bastmeyer,* Cesar Rodriguez-Emmenegger*

———

N. Yu. Kostina, Dr. O. Pop-Georgievski, Dr. J. Michálek, Dr. Cesar Rodriguez-Emmenegger
Institute of Macromolecular Chemistry, Academy of Sciences of the Czech Republic, v.v.i., Heyrovsky sq.2, Prague 162 06, Czech Republic
E-mail: rodriguez@imc.cas.cz
Dr. M. Bachmann, Prof. M. Bastmeyer
Zoological Institute, Cell and Neurobiology, Karlsruhe Institute of Technology (KIT), Haid-und-Neu-Straße 9, Karlsruhe 76131, Germany
E-mail: martin.bastmeyer@kit.edu
Prof. M. Bastmeyer
Institute for Functional Interfaces (IFG) Karlsruhe Institute of Technology (KIT), Hermann-von-Helmholtz-Platz 1, Eggenstein-Leopoldshafen 76344, Germany
N. Neykova
Institute of Physics, Academy of Sciences of the Czech Republic, Cukrovarnicka 10, Prague 16253, Czech Republic
Faculty of Nuclear Science and Physical Engineering, Czech Technical University in Prague, Trojanova 13, Prague 12000, Czech Republic
Dr. M. Bruns
Institute for Applied Materials (IAM) and Karlsruhe Nano Micro Facility (KNMF), Karlsruhe Institute of Technology (KIT), Hermann-von-Helmholtz-Platz 1, Eggenstein-Leopoldshafen 76344, Germany

———

Materials and Methods

Synthesis of N-(hydroxypropyl) Methacrylamide (HPMA)

N-(hydroxypropyl) methacrylamide (HPMA) was synthesized by the modified reaction of methacryloyl chloride with 1-aminopropan-2-ol in dichloromethane in the presence of sodium carbonate.[1]

Synthesis of (3-Acryloylamino-propyl)-(2-carboxy-ethyl)-dimethyl-ammonium (CBAA)

(3-Acryloylamino-propyl)-(2-carboxy-ethyl)-dimethyl-ammonium (CBAA) was synthesized by the modified procedure published earlier.[2] DMAPA (7.8 g, 55 mmol) was dissolved in 100 mL of anhydrous THF and cooled to 0°C. A pinch of diphenylpicryl hydrazyl (DPPH) was added as inhibitor. Subsequently, β-propiolactone (5.0 g, 69 mmol) was dissolved in 40 mL of THF and added dropwise under nitrogen. The reaction was allowed to proceed for 24 h at 4°C. The white precipitate was washed with dry THF and ether. The product was dried under high vacuum. Prior to polymerization DPPH was removed by reprecipitation from methanol by THF to yield 19.4 g (yield: 80 %)

^{1}H NMR (Bruker 250 MHz in D_2O: 6.32 (t, 1H, CHH=CH), 6.2 (t, 1H, CHH=CH), 5.87 (t, 1H, CHH=CH), 3.66 (t, 2H, N-CH_2-CH_2-COO), 3.48 (m, 4H, NH-CH_2-CH_2-CH_2), 3.17(s, 6H, N-$(CH_3)_2$), 2.75 (t, 2H, CH_2-COO)

Surface Plasmon Resonance

A custom-built SPR instrument (Institute of Photonics and Electronics, Academy of Sciences of the Czech Republic, Prague) based on the Kretschmann geometry of the attenuated total reflection method and spectral interrogation was used. The protein fouling from 10 % FBS and cell culture media (CM) was measured as the difference between the baselines in phosphate buffered saline (PBS) before and after the injection of the tested samples. The sensor response was calibrated to the mass deposited at the surface of bound molecules. According to a calibration made by Fourier-transform infrared grazing angle specular reflectance, a shift of 1 nm corresponds to a change in the deposited protein mass of 150 $pg \cdot mm^{-2}$.

Additional Results and Discussion

Br 3d High Resolution XPS Spectra

In order to grow polymer brushes from PCL-PDA nanofibers, 2-bromo isobutyryl bromide (BIBB), ATRP initiator, was acylated to residual amine groups of the PDA layer. The successful immobilization of BIBB is evidenced by the appearance of dominating peaks at 70.2 eV and 71.2 eV in Br 3d high resolution XPS spectra corresponding to [Br-C] bonds (Figure S1).[3, 4]

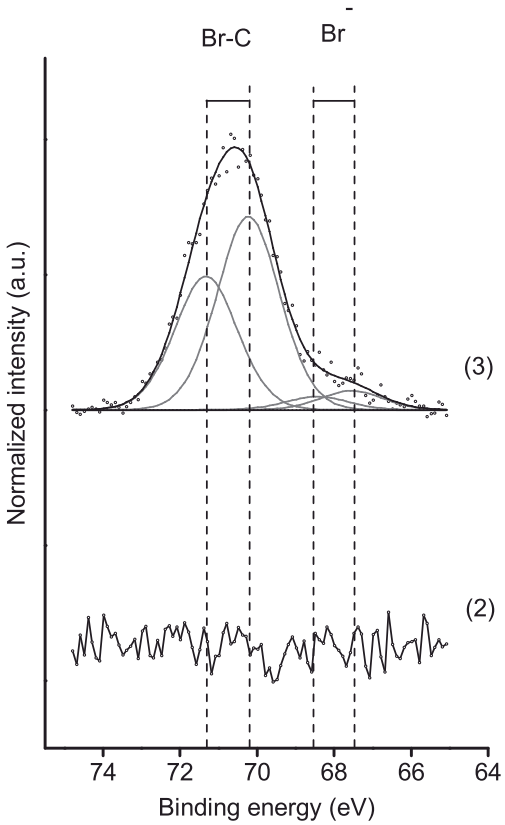

Figure S1. Br 3d high resolution XPS spectra of (2) PCL-PDA and (3) PCL-PDA-Br nanofibers

SPR Sensograms

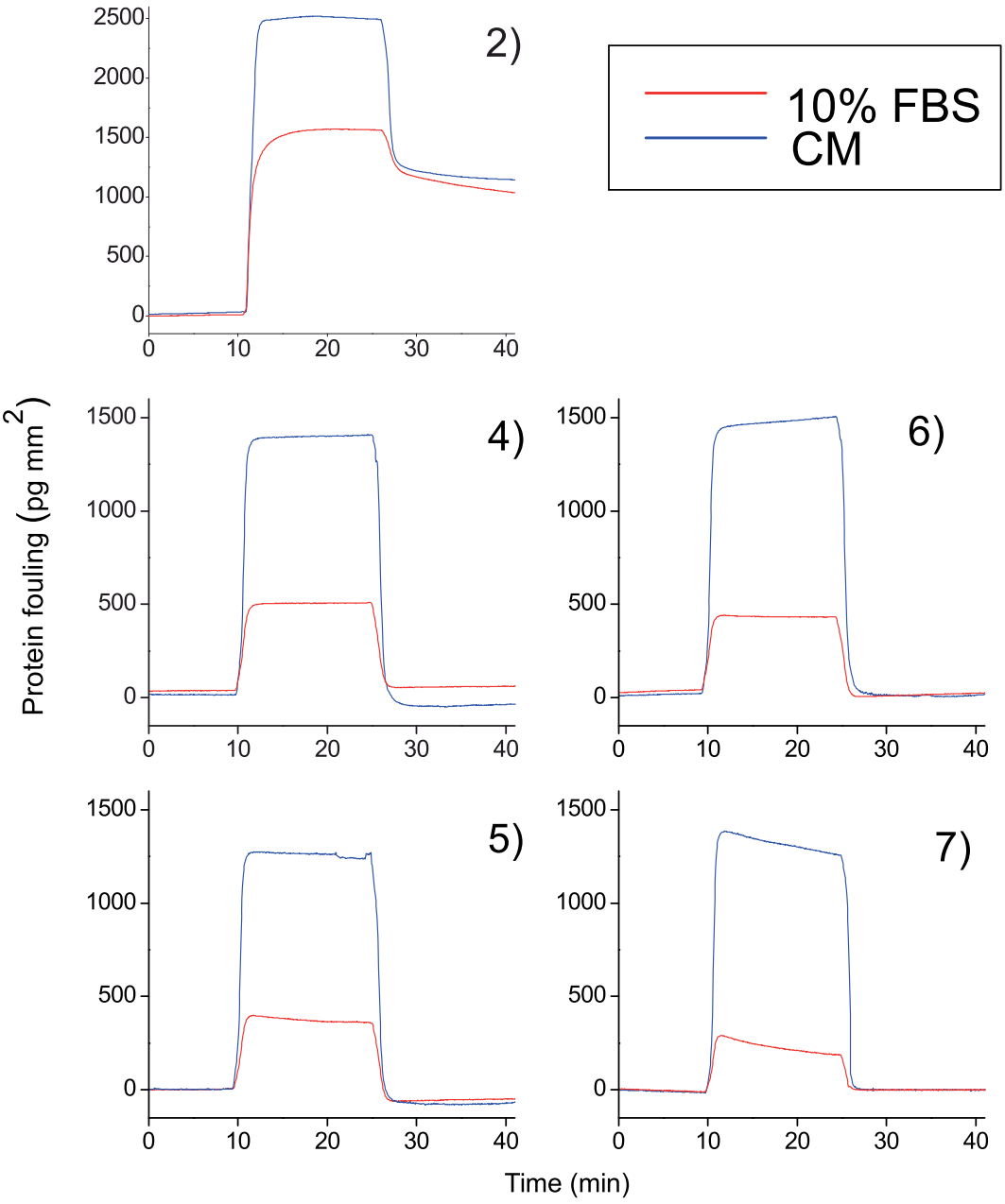

Figure S2. Adsorption of proteins from 10 % FBS and CM on a gold sensor surface coated with (2) PDA, (4) PDA-poly(MeOEGMA), (5) PDA-poly(HOEGMA), (6) PDA-poly(HPMA) and (7) PDA-poly(CBAA). Merely the same fouling was observed on bare gold, PCL and PDA surfaces.

Table S1. The protein fouling of PDA and polymer brushes determined by SPR on a model system

Surface	**Protein fouling [pg mm^{-2}]**	
	FBS	**CM**
PDA	1162 ± 128	1112 ± 13
Poly(MeOEGMA)	0	0
Poly(HOEGMA)	0	0
Poly(HPMA)	0	0
Poly(CBAA)	0	0

Cell adhesion experiment

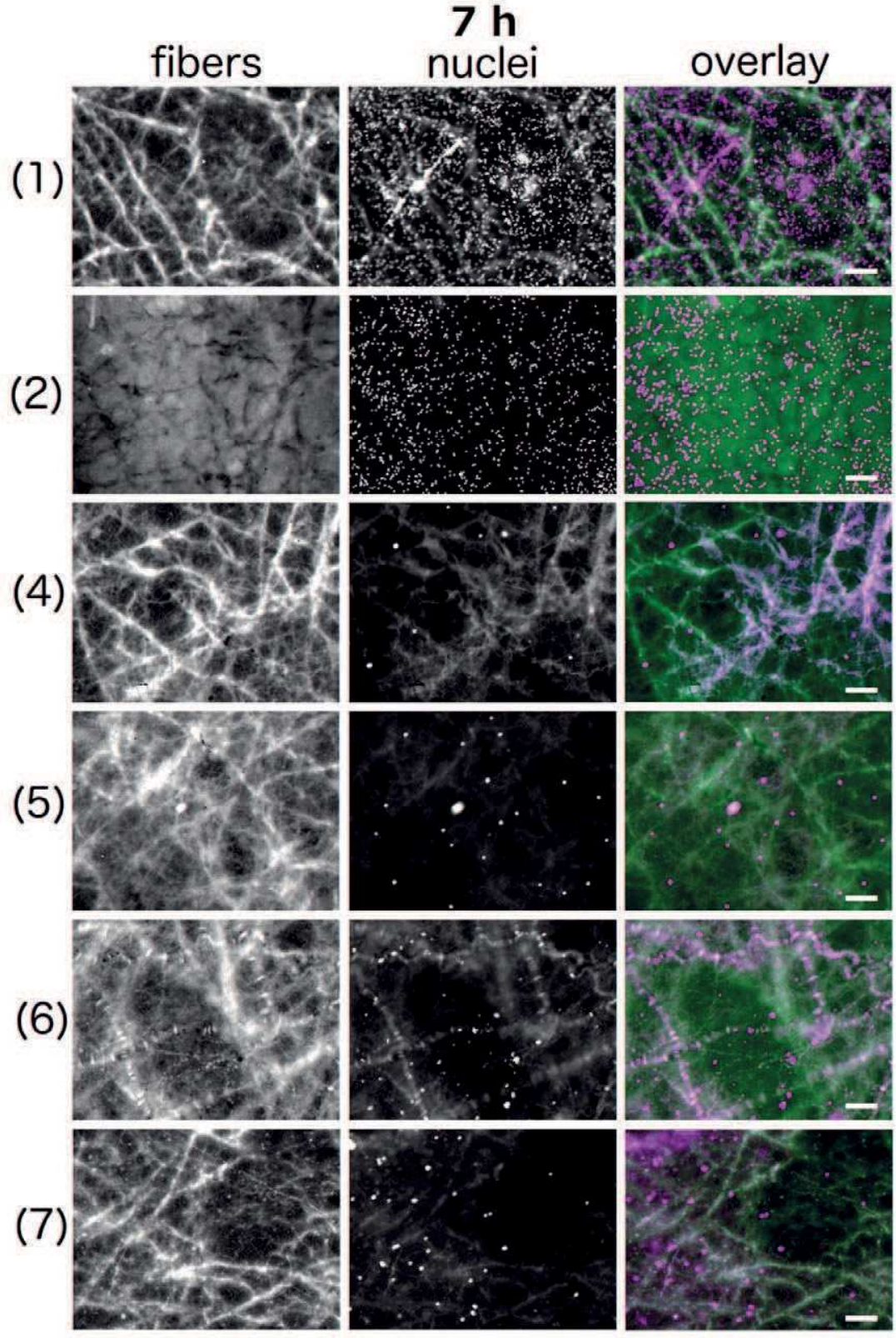

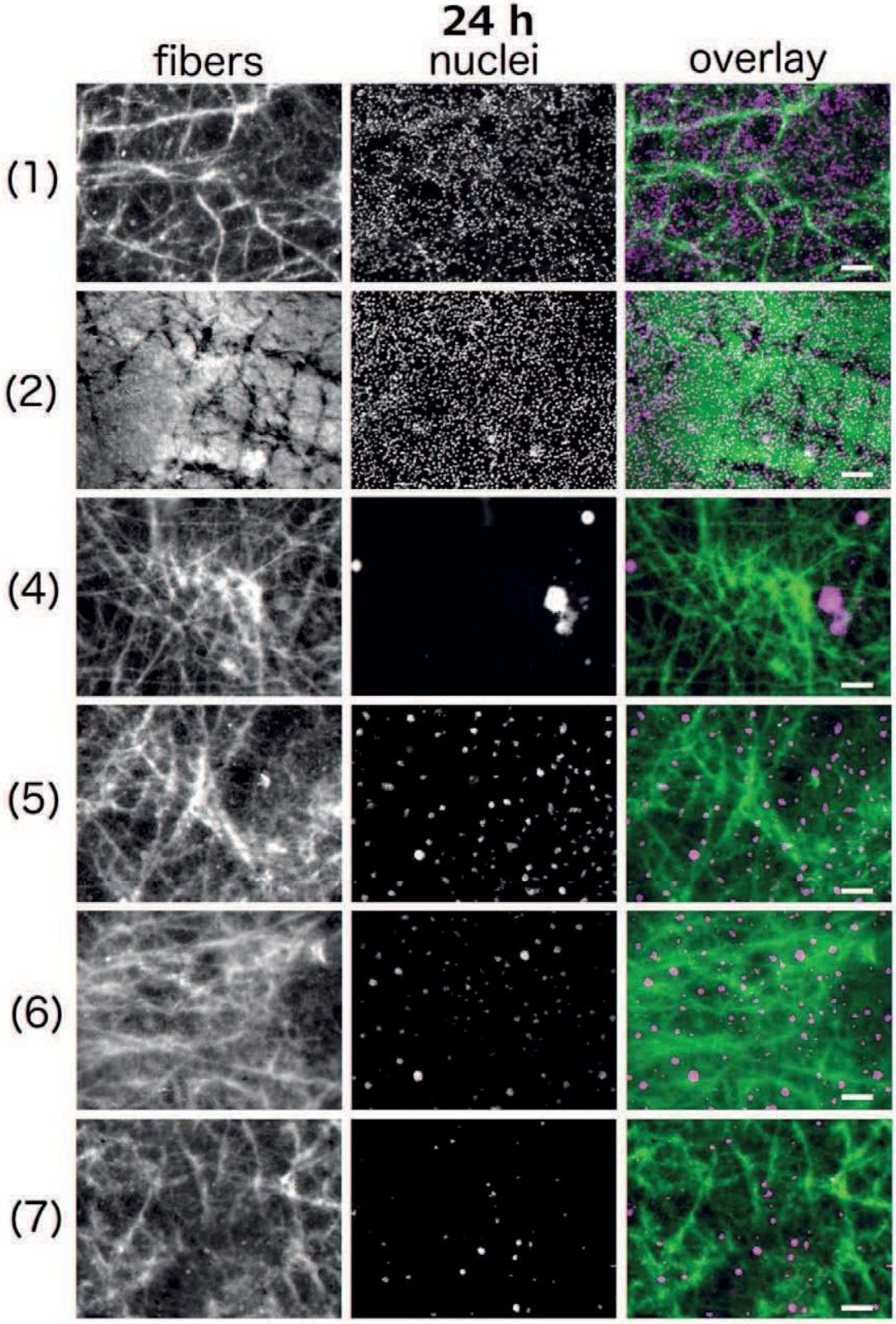
24 h
fibers
nuclei
overlay
(1)
(2)
(4)
(5)
(6)
(7)

Figure S3. Cell adhesion on (1) PCL, (2) PCL-PDA, (4) PCL-PDA-poly(MeOEGMA), (5) PCL-PDA-poly(HOEGMA), (6) PCL-PDA-poly(HPMA) and (7) PCL-PDA-poly(CBAA) nanofibers after 7 and 24 h (scale bar 200 μm). Fibers (green) are visualized by their autofluorescence after excitation at 488 nm, cell nuclei (magenta) by staining with DAPI and 405 nm excitation. Please note that low number of cells on nanofibers with polymer brushes (4 – 7) required higher excitation energy to visualize them. Therefore, in some cases autofluorescence of fibers is visible in the 405 nm channel.

References

[1] C. Rodriguez-Emmenegger, E. Brynda, T. Riedel, M. Houska, V. Subr, A. B. Alles, E. Hasan, J. E. Gautrot, W. T. Huck, *Macromol. Rapid Commun.* **2011**, *32*, 952.
[2] C. Rodriguez Emmenegger, E. Brynda, T. Riedel, Z. Sedlakova, M. Houska, A. B. Alles, *Langmuir* **2009**, *25*, 6328.
[3] B. Yameen, N. Zydziak, S. M. Weidner, M. Bruns, C. Barner-Kowollik, *Macromolecules* **2013**, *46*, 2606.
[4] C. Rodriguez-Emmenegger, S. Janel, A. de los Santos Pereira, M. Bruns, F. Lafont, *Polym. Chem.* **2015**, DOI:10.1039/c5py00197h.